

St Petersburg University

Manuscript copyright

Aleksandra Vladimirovna Paderina

**Pt(II) complexes based on alkynylphosphonium ligands  
with different conjugated  $\pi$ -systems: synthesis and photophysical properties**

Thesis for the degree  
of Candidate of Chemical Sciences

1.4.1. Inorganic Chemistry

*Translation from Russian*

**Academic supervisor:**  
Doctor of Science in Chemistry,  
Professor  
Elena V. Grachova

Saint Petersburg  
2024

## TABLE OF CONTENTS

INTRODUCTION.....	4
CHAPTER 1. LITERATURE REVIEW .....	11
1.1. The nature of Pt(II) complexes' excited states .....	11
1.1.1. Metal-centered excited states (MC) .....	14
1.1.2. Metal-to-ligand charge-transfer excited states (MLCT) .....	15
1.1.3. Ligand-to-ligand charge-transfer excited states (LLCT) .....	18
1.1.4. Ligand-centered excited states (LC) .....	21
1.1.5. Intraligand charge-transfer excited states (ILCT).....	26
1.2. Features of platinum(II) complexes photophysics, caused by aggregation .....	29
1.3. Alkynyl Pt(II) complexes .....	33
1.3.1. Bis-alkynyl complexes .....	34
1.3.2. Mono-alkynyl complexes .....	35
1.4. Phosphonium-based systems of “donor-linker-acceptor” type .....	37
CHAPTER 2. RESULTS AND DISCUSSION.....	40
2.1. Selection of research objects .....	40
2.2. Pt(II) complexes synthesis.....	41
2.2.1. Bis-alkynyl Pt(II) complexes with ancillary N <sup>N</sup> ligand .....	41
2.2.2. Bis-alkynyl Pt(II) complexes with ancillary PPh <sub>3</sub> and cyanide ligands .....	45
2.2.3. Mono-alkynyl Pt(II) complexes with ancillary C <sup>N</sup> N ligand.....	48
2.2.4. Mono-alkynyl Pt(II) complexes with ancillary N <sup>N</sup> N ligand .....	51
2.2.5. Mono-alkynyl Pt(II) complexes with ancillary C <sup>N</sup> C ligand.....	52
2.3. Photophysical properties of Pt(II) complexes .....	56
2.3.1. Bis-alkynyl Pt(II) complexes with N <sup>N</sup> ancillary ligand .....	56

2.3.2. Bis-alkynyl Pt(II) complexes with ancillary phosphine and cyanide ligands ..	68
2.3.3. Mono-alkynyl Pt(II) complexes with ancillary C <sup>N</sup> N and N <sup>N</sup> N ligands ..	76
2.3.4. Mono-alkynyl Pt(II) complexes with C <sup>N</sup> C ancillary ligand .....	85
CHAPTER 3. EXPERIMENTAL SECTION .....	89
3.1. Materials and instruments .....	89
3.2. Synthesis of bis-alkynyl Pt(II) complexes with ancillary N <sup>N</sup> ligand .....	91
3.3. Synthesis of bis-alkynyl Pt(II) complexes with ancillary phosphine and cyanide ligands .....	94
3.4. Synthesis of mono-alkynyl Pt(II) complexes with ancillary C <sup>N</sup> N ligand .....	97
3.5. Synthesis of Pt(II) mono-alkynyl complexes with ancillary N <sup>N</sup> N ligand .....	99
3.6. Synthesis of Pt(II) mono-alkynyl complexes with ancillary N <sup>N</sup> N ligand ...	102
CONCLUSION .....	104
LIST OF ABBREVIATIONS .....	107
ACKNOWLEDGEMENTS .....	109
REFERENCES .....	110
SUPPORTING INFORMATION .....	133

## INTRODUCTION

### **The relevance of the field of research and the degree of its development.**

One of the key tasks of modern organometallic chemistry is the design of new functional materials based on luminescent transition metal complexes. At the moment, the main driving force of research in this direction is the application of such complexes as a light-emitting layer in organic light-emitting diodes (OLEDs) [1]. OLEDs are the recognized next-generation electroluminescent devices exhibiting high color quality, low fabrication cost, low power consumption, and a wide range of applications from displays to lighting devices. However, the organic fluorophores currently used for OLED fabrication have rather low maximum energy efficiency value, namely 25%. The solution to this problem may be the use of transition metal phosphorescent complexes. They attract great attention of researchers because of their ability to convert the incoming electrical energy into outgoing light energy almost completely, i.e. up to 100%. This increases the energy efficiency of light-emitting devices and solves the problem of energy losses in the use of electricity.

One of the most promising metal-organic luminophores are platinum(II) complexes. Due to the strong spin-orbit interaction between the metal and its coordination environment, these compounds have high emission quantum yield. The introduction of acceptor substituents to the periphery of the coordination sphere of the platinum complex leads to the formation of donor-acceptor complexes with intramolecular charge transfer. This allows to change the emission color in a controlled way by varying the distance between the highest occupied and lowest unoccupied molecular orbitals of the organometallic system. Also, the intrinsic fluorescent properties of the ligand can contribute to the formation of a unique system with double singlet-triplet emission. Currently, the interest of researchers is shifting from traditional organic acceptor functional groups (carbonyl-, cyano-, fluorine-containing groups) to organometallic groups containing boron, oxygen, sulfur, and phosphorus [2]. For example, simple methylation of a phosphine group yields positively charged phosphonium salts that are effective electron acceptor groups [3]. However, these molecules, despite their

pronounced acceptor properties, are unexpectedly rarely used as ligands for the synthesis of coordination compounds. Nevertheless, some successful examples of using the above phosphorus-containing groups for the design and synthesis of donor-acceptor molecules with intramolecular charge transfer have been presented in the literature. This has inspired us to propose their possible use for the synthesis of platinum(II) donor-acceptor complexes [4].

Besides their obvious applications in OLED devices, such platinum(II) donor-acceptor complexes can also be used as sensors, photocatalysts, molecular probes, and molecular thermometers, which opens up a wide range of applications in a wide variety of practical fields [5].

**The purpose and tasks of the thesis.** The aim of this work was to develop a synthetic methodology for mono- and bis-alkynyl platinum(II) complexes based on alkynylphosphonium ligands with different conjugated  $\pi$ -systems, as well as to establish the regularity of the influence of peripheral modification and extent of  $\pi$ -system of alkynylphosphonium ligand with internal charge transfer on the photophysical properties of the obtained Pt(II) complexes.

To achieve the goal, the following tasks were set:

- 1) Synthesis of alkynylphosphonium ligands with different conjugated  $\pi$ -system;
- 2) Synthesis of bis-alkynyl and mono-alkynyl platinum(II) complexes with various ancillary ligands and varying alkynylphosphonium ligands;
- 3) Characterization of the composition and structure of the obtained platinum(II) complexes by a set of physicochemical methods: nuclear magnetic resonance (NMR) spectroscopy, mass spectrometry, single-crystal X-ray diffraction analysis, infrared (IR) spectroscopy, elemental analysis.
- 4) Study of photophysical characteristics of the obtained platinum(II) complexes: measurement of absorption spectra, emission spectra, excited state lifetimes and luminescence quantum yields in solution and solid phase;
- 5) Establishment of correlation between photophysical properties and composition/structure of the obtained platinum(II) complexes.

**The scientific novelty of the work** lies in optimization of the synthetic methodology and obtaining platinum(II) complexes with donor-linker-acceptor systems based on phosphonium salts with controllable photophysical properties. The influence of the length of the ligand linker on the emission properties of the obtained compounds has been demonstrated, and the trends in the luminescence of alkynylphosphonium complexes of platinum(II) with the use of various additional ligands have been shown.

**Theoretical and practical significance of the work** lies in the development of methods for the synthesis of platinum(II) complexes bearing a charged phosphonium fragment at the periphery of the ligand environment. The introduction of the phosphonium group allowed us to obtain the first example of bright luminescence in trans-phosphine-alkynyl complexes of Pt(II) in the solid phase. The dependence of the photophysical properties of terpyridine complexes of platinum(II) in the solid phase on the size of the counterion was also shown for the first time.

The obtained alkynylphosphonium platinum compounds based on bipyridine show *stimuli-responsive* properties, which can potentially be used in both sensing and anti-counterfeiting applications. The water solubility of these systems allowed our colleagues to incorporate these complexes into nanoparticles for bioimaging. Also, the above compounds exhibit pronounced two-photon absorption and two-photon emission, which can be utilized in the field of nonlinear optics.

**Methodology and research methods.** The composition and structure of the obtained compounds were determined by a set of modern physicochemical methods: polynuclear ( $^1\text{H}$ ,  $^{31}\text{P}\{\text{H}\}$ ,  $^{19}\text{F}\{\text{H}\}$ ) NMR spectroscopy and two-dimensional  $^1\text{H}$ - $^1\text{H}$  COSY NMR spectroscopy; high-resolution electrospray ionization mass spectrometry in positive mode (ESI+), IR spectroscopy and elemental analysis. For some compounds it was possible to obtain single crystals suitable for studies by single-crystal X-ray diffraction analysis (XRD).

The optical and photophysical properties of the obtained compounds were characterized using UV-vis spectroscopy in solution and luminescence spectroscopy both in solution and in the solid phase. Excited state lifetimes and luminescence quantum

yields were also measured in both aerated and deaerated solution and in the solid phase. The nonlinear optical properties were investigated using a femtosecond laser.

**Structure and content of the work.** The thesis consists of five parts: introduction, literature review, results and discussion, experimental part and conclusions. The introduction includes the relevance of the study and the degree of its development, the purpose and tasks of the work. Further in the same section the scientific novelty, theoretical and practical significance of the work are disclosed, after that, the research methodology, the degree of reliability and approbation of the results are described. The introduction concludes with a list of publications, main findings of the dissertation to be defended and the main scientific results. The section "Literature Review" is divided into four semantic parts. The first one is devoted to the description of the nature of excited states of platinum, and the second one considers the peculiarities of photophysical properties of platinum(II) complexes associated with aggregation. The third and fourth parts summarize the information on platinum(II) alkynyl complexes and donor-linker-acceptor systems, respectively. There are two parts in the "Results and Discussion" section: the first one describes the synthesis of the target complexes and the second one analyzes their photophysical properties in detail. The section "Experimental part" contains details of experimental techniques, spectral data and other details of the conducted studies. All figures, tables, and compounds are numbered sequentially.

**Degree of reliability and approbation of the research.** The main findings to be defended were presented and discussed at the following conferences: XXIII International Chernyaev conference on chemistry, analytics and technology of platinum metals 3.10.2022–7.10.2022 (oral presentation), the All-Russian conference on natural sciences and humanities with international participation "SPbSU Science-2022" 21.11.2022 (poster presentation), International scientific conference of students, postgraduates and young scientists "Lomonosov-2023" 10.04.2023–21.04.2023 (oral presentation, III class diploma), International scientific conference of students, postgraduates and young scientists "Lomonosov-2024" 12.04.2023–26.04.2023 (oral presentation, awardee diploma), First All-Russian Conference on Luminescence «LUMOS-2024» 23.04.2024–

26.04.2024 (poster presentation), XIII International Conference on Chemistry for Young Scientists "Mendeleev 2024" 2.09.2024–6.09.2024 (oral presentation).

The work was carried out with the financial support of the Russian Science Foundation №21-13-00052, №22-23-00287, №24-13-00024.

Based on the dissertation materials, 4 articles were published in journals indexed in the WoS and Scopus databases, as well as abstracts of 6 reports at national and international scientific conferences.

#### **Articles published based on the results of the dissertation:**

1. Petrovskii S. et al. Homoleptic Alkynylphosphonium Au(I) Complexes as Push–Pull Phosphorescent Emitters // *Inorg. Chem.* 2023. Vol. 62, № 13. P. 5123–5133.

2. Paderina A. et al. Alkynylphosphonium Pt(II) Complexes: Synthesis, Characterization, and Features of Photophysical Properties in Solution and in the Solid State // *Inorg. Chem.* 2023. Vol. 62, № 44. P. 18056–18068.

3. Paderina A. et al. Aggregation game: changing solid-state emission using different counterions in mono-alkynylphosphonium Pt(II) complexes // *Inorg. Chem.* 2024, Vol. 63, № 38, P. 17548–17560.

4. Paderina A. et al. Cationic or neutral: dependance of photophysical properties of bis-alkynylphosphonium Pt(II) complexes on ancillary ligand // *Chemistry – A European Journal*, 2024, Vol. 30, № 58, P. e202402242.

#### **Main findings of the dissertation to be defended:**

1. Introduction of “donor-linker-acceptor” systems, namely alkynylphosphonium salts as ligands into platinum(II) complexes allows to vary the photophysical properties of the target compounds by changing the linker length.

2. The presence of a positively charged acceptor phosphonium fragment on the periphery of the ligand environment requires significant modifications of synthesis techniques due to the problem of "counterion migration".

3. The phosphonium fragment introduced into the ligand not only enhances the nonlinear optical properties (two-photon absorption and emission) of bis-alkynylphosphonium complexes of Pt(II) in the cis-configuration, but also contributes to the *stimuli-responsive* properties.

4. In the case of bis-alkynylphosphonium compounds in the trans configuration of  $[\text{Pt}(\text{P}_i)_2(\text{PPh}_3)_2]\text{OTf}_2$  and  $[\text{Pt}(\text{P}_i)_2(\text{CN})_2]$  composition, the improved conjugation between the two ligands plays an important role in determining the photophysical properties and leads to a dominant ligand-centered emission.

5. Charged mono-alkynylphosphonium Pt(II) complexes with ancillary tridentate ligands are more likely to exhibit aggregation effects than bis-alkynylphosphonium analogs. For these systems, the luminescence character is determined by packing and metallophilic interactions in the solid phase.

6. The presence of a naphthyl linker in the alkynylphosphonium ligand is a determinant of the nature of luminescence for alkynylphosphonium complexes in solution, regardless of the nature of the ancillary ligands.

#### **Main scientific results:**

1. Four alkynylphosphonium ligands with different linkers were synthesized [6].

2. Six series of alkynylphosphonium Pt(II) complexes (overall 27 compounds) were synthesized. We have classified compounds in the following way:

- (1) Bis-alkynylphosphonium Pt(II) complexes based on 4,4'-di-tertbutyl-2,2'-bipyridine in *cis*-configuration [7];
- (2) Bis-alkynylphosphonium Pt(II) complexes with ancillary triphenylphosphine and cyanide ligands in *trans*-configuration [8];
- (3) Mono-alkynylphosphonium Pt(II) complexes based on tridentate  $\text{N}^{\wedge}\text{N}^{\wedge}\text{N}$  (2,2':6',2''-terpyridine), cyclometallated  $\text{C}^{\wedge}\text{N}^{\wedge}\text{N}$  (6-phenyl-2,2'-bipyridine) and  $\text{C}^{\wedge}\text{N}^{\wedge}\text{C}$  (2,6-diphenylpyridine) ligands [9].

3. The ligand-located charged phosphonium group influence on the Cu-catalyzed chloride-alkyne metathesis reaction was investigated. The optimization of the corresponding synthetic methods was carried out.

4. The obtained complexes were characterized by a full set of modern physicochemical methods, including polynuclear ( $^1\text{H}$ ,  $^{31}\text{P}\{\text{H}\}$ ,  $^{19}\text{F}\{\text{H}\}$ ) NMR spectroscopy and two-dimensional  $^1\text{H}$ - $^1\text{H}$  COSY; NMR spectroscopy; high-resolution electrospray ionization mass spectrometry in positive mode, IR spectroscopy and

elemental analysis. The structures of seven compounds were established by single-crystal X-ray diffraction analysis.

5. The photophysical properties were characterized using UV-vis spectroscopy in solution and luminescence spectroscopy in both solution and solid phase. The excited state lifetimes and luminescence quantum yields were also measured in both aerated and deaerated solution and in the solid phase, and the stimuli-responsive and nonlinear optical properties of the obtained compounds were investigated.

6. It is shown that the introduction of alkynylphosphonium ligands into the coordination environment of the platinum(II) metal center has a positive effect on the emission characteristics of the obtained complexes. Thus, systems in *cis*-configuration acquire *stimuli-responsive* and nonlinear optical properties, and compounds in *trans*-configuration show previously undescribed bright luminescence in the solid state. The dependence of the photophysical properties in the solid state on the size of the counterion is also shown for the first time using terpyridine alkynylphosphonium Pt(II) compounds as an example. In addition, changing the linker allows a controlled change in the luminescence wavelength.

The personal contribution of the dissertant consists in the collection and analysis of literature data, participation in setting the goal, setting the objectives, scaling the synthesis of alkynylphosphonium ligands, optimizing and carrying out the synthesis of platinum(II) complexes, preparation of samples for physicochemical methods of analysis, solving and refining the data of single-crystal X-ray diffraction analysis, carrying out photophysical measurements in solution and solid state, as well as interpretation of all the obtained results. Preparation of publication materials, writing of draft versions of articles and preparation of reports at scientific conferences were also performed by the dissertant independently.

## CHAPTER 1. LITERATURE REVIEW

Platinum(II) coordination compounds have attracted the interest of many researchers largely due to their rich luminescent properties. They find applications in a wide range of fields, from bio-visualization [10], OLED devices [11,12] and light-emitting electrochemical cells [13] to chemosensing [14] and non-linear optics [15]. Recent works prove the possibility of using platinum(II) complexes in anti-counterfeiting applications [16], pressure sensors [17] and even in memory devices [18]. The possibility of fine-tuning the luminescent characteristics of these compounds is provided by the rational choice of ligands included in the coordination sphere. The square-planar geometry of platinum(II) complexes favors the formation of metallophilic interactions and  $\pi$ -stacking, which also directly affect the emission properties [19].

This thesis is devoted to platinum(II) compounds with donor-acceptor ligands based on alkynylphosphonium salts. In the first subsection of the literature review, the nature of the emission states of platinum(II) complexes and the ways of their variation upon introduction of different ligands are given. The second subsection is devoted to the peculiarities of photophysical properties of square-planar Pt(II) coordination compounds associated with aggregation. Further, the advantages of introducing alkynyl ligands into the Pt(II) coordination sphere, the influence of such ligands on the photophysical properties of the obtained compounds and potential applications of platinum(II) alkynyl complexes are discussed. Finally, the last subsection of the literature review presents data on luminescent systems with charge transfer containing phosphonium fragments and discusses the possibility of their application as ligands for the creation of coordination compounds.

### 1.1. The nature of Pt(II) complexes' excited states

Platinum lies in group 10 of the Mendeleev Periodic System of Chemical Elements and is a transitional element of the third row. The most important oxidation state of platinum is +2, which corresponds to the electronic configuration  $d^8$ . Pt(II) complexes in most cases have a square planar configuration (Figure 1), which directly affects the photophysical properties of these compounds. Thus, the square planar geometry is easily

subjected to various non-radiative pathways of luminescence deactivation, such as the formation of exciplexes, interaction with the solvent, reversible coordination and some others [20–23].

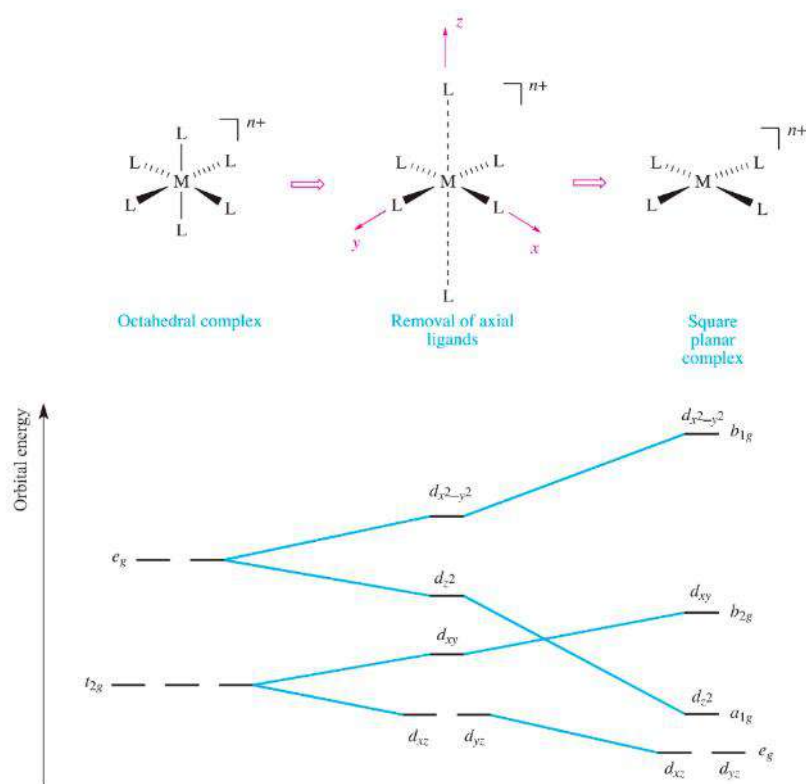


Figure 1. Ligand field-splitting diagram for metal d orbitals in octahedral and square planar complexes [24].

Moreover, the high-energy  $d_{x^2-y^2}$  orbital has antibonding character, and when excited by ultraviolet radiation, is able to accept an electron from lower-lying orbitals. Thus, the transition of the molecule to the excited state is accompanied by a significant distortion of the structure and an increase in the length of metal-ligand bonds. This is reflected on the potential energy surface diagram (Figure 2a), where the excited state energy minimum is markedly displaced compared to the ground state. Such an arrangement of energy levels has an extremely negative effect on the possibility of luminescence due to the thermal accessibility of the isoenergetic point where internal or intercombination conversion to the ground state occurs. As a consequence, platinum(II) complexes with simple inorganic ligands, such as  $\text{Pt}(\text{NH}_3)_4^{2+}$ ,  $\text{PtCl}_4^{2-}$ , *etc.*, do not exhibit emission in solutions or are extremely low-intensity metal-centered (MC) emitters. The

rate constant of non-radiative decay for such complexes are very large, and small radiative decay rate constants of Laporte forbidden d-d transitions further aggravate the situation. In the solid state, excited-state structural distortion of Pt(II) complexes is inhibited, and in some cases luminescence becomes possible [25–27].

The introduction of more complex organic ligands into the coordination sphere of the platinum(II) metal center leads to the additional excited states involving the ligand. In many cases they have lower energy than the d-d excited states, but the latter can be accessible at room temperature (see Figure 2b,  $\Delta E$  is comparable to  $kT$ ) and effectively redirect the relaxation along the non-radiative pathway [19]. To avoid this it is necessary to achieve a large  $\Delta E$  value, which can be realized either by lowering the energy of the emitting state or by raising the energy of the d-d state to practically inaccessible values. The introduction of strong-field ligands is the possible solution to this problem, which is discussed in detail in the following subsections.

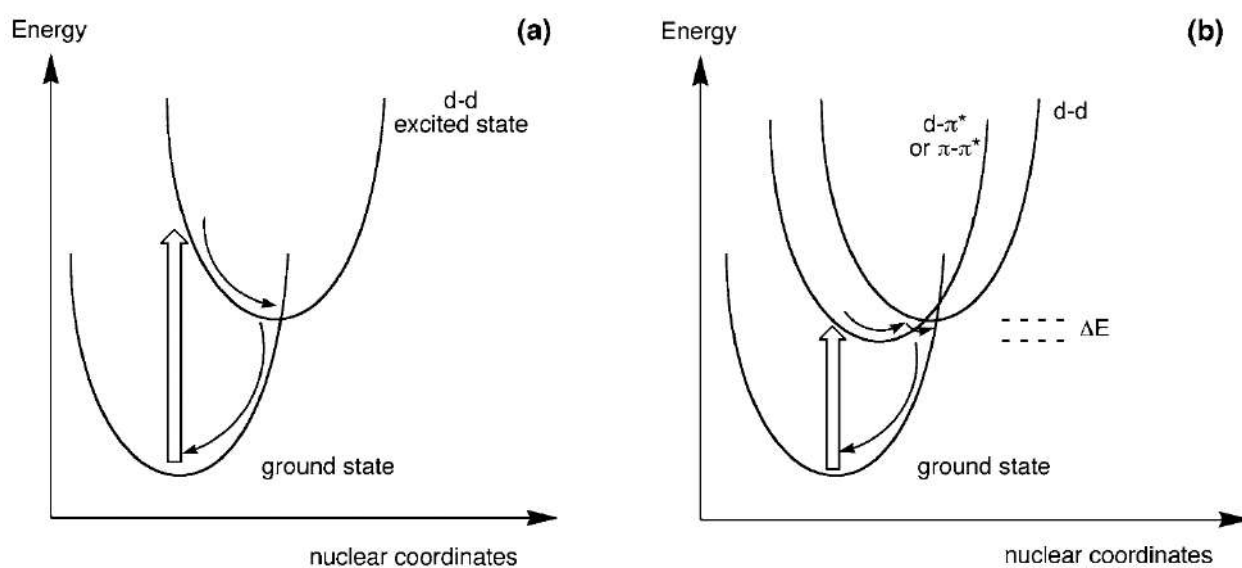


Figure 2. Pt(II) complex potential energy surface diagram with d-d excited states (a) and additional d- $\pi^*$  and  $\pi$ - $\pi^*$  excited states (b). Thick arrows represent absorption, thin ones – vibrational relaxation and non-radiative decay [19].

As mentioned above, additional excited states appear when organic ligands are coordinated to platinum(II). Thus, the complete list of the most frequently occurring excited states of Pt(II) complexes is as follows:

- Metal-centered, MC;

- Metal-to-ligand charge-transfer, MLCT ( $d-\pi^*$ );
- Ligand-to-ligand charge-transfer, LLCT;
- Ligand-centered, LC ( $\pi-\pi^*$  or  $n-\pi^*$ );
- Intra-ligand charge-transfer, ILCT.
- Metal/metal-to-ligand charge-transfer, MMLCT.

Next, we will look at a few examples for each case.

### 1.1.1. Metal-centered excited states (MC)

As discussed earlier, the metal-centered emission caused by d-d transitions in the metal center has low intensity and is extremely rare. It is characterized by broad structureless Gaussian-shaped bands that appear only in the solid state and at low temperature, e.g., in frozen solutions. At the same time, cooling of the solid phase does not lead to a significant shift of the luminescence band maximum, affecting only the width of the band itself. This is due to the cooling out of thermally excited low-frequency stretching and bending modes associated with the distortion of the  $^3MC$  excited state [27,28].

Miskowski et al. [27] have synthesized complexes **1–6** based on the bidentate diamine ligands with ancillary chloride ligands (Figure 3a). These compounds feature orange luminescence with broad structureless band both in frozen solutions and the solid state. At lower temperature the emission maximum is slightly red-shifted due to the narrowing of the band (Figure 3b). These complexes do not exhibit any vibronic structure even at 10K. Based on the above, the authors conclude that the emission has metal-centered nature. Interestingly, complex **5** exists in two crystalline modifications, yellow and red, and the MC type of emission appears only in the yellow one. The second modification is discussed in subsection 1.2.

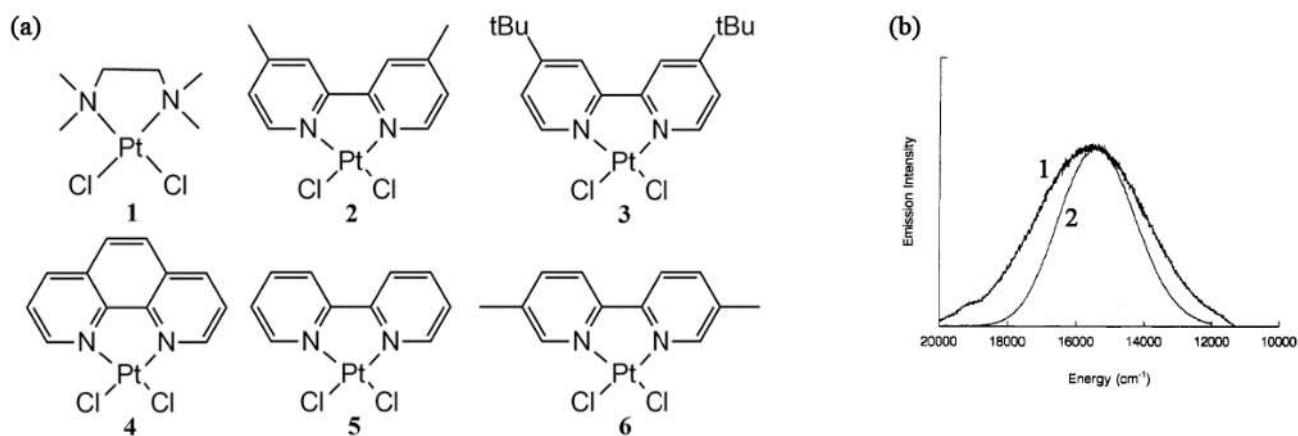


Figure 3. (a) Compounds 1–6; (b) luminescence spectra of complex 2 at 300 K (1) and 10 K (2) [27].

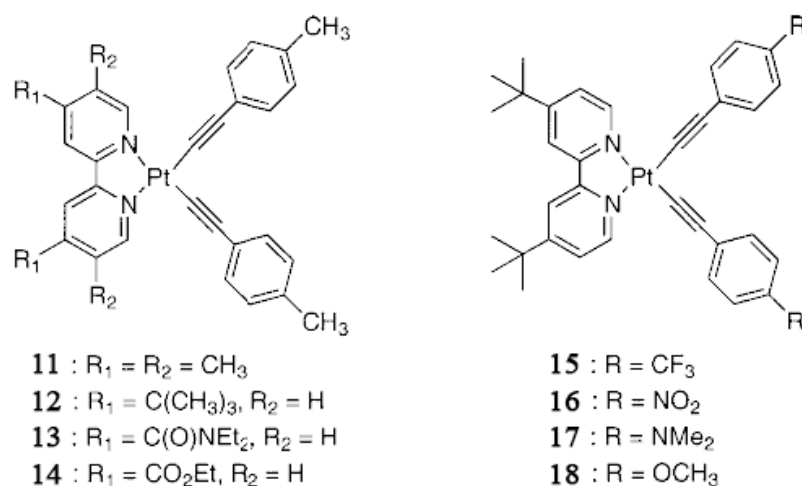
### 1.1.2. Metal-to-ligand charge-transfer excited states (MLCT)

Upon introduction of complex organic ligands into the coordination sphere of platinum(II) complexes, new excited states appear. One of them, the low-lying MLCT transition is characteristic of systems with acceptor ligands providing  $\pi^*$  or  $\sigma^*$  orbitals with low energy [29]. Such an emission can be formally considered as intramolecular electron transfer from metal to ligand with concomitant irradiation [30]. The distinctive feature of the MLCT luminescence are broad, structureless bands, which are partially resolved upon freezing the solutions [31]. Also, complexes with charge transfer can exhibit so-called solvatochromism, a reversible spectrum change caused by a solvent polarity change. This happens due to the different polarity of the ground and excited states. The excited state, which is more polar than the ground state, is more stable in polar solvents, which reduces both excitation and emission energies. Such a phenomenon is called positive solvatochromism. On the contrary, if the excited state is less polar than the ground state, a hypsochromic shift of emission and absorption maxima is observed, and this is called negative solvatochromism [32,33]. However, for MLCT emitters, solvatochromism is usually weakly manifested in the luminescence spectra, being reflected only in the absorption spectra [34].

Polypyridine systems, such as 2,2'-bipyridine, 9,10-phenanthroline, 2,2':6',2''-terpyridine *etc.* were one of the first acceptor ligands used for MLCT-emitting Pt(II) complexes construction [21,35].

Terpyridine complexes of general formula  $[\text{Pt}(\text{terpy})\text{X}]^+$ ,  $\text{X} = \text{Cl}$  (**7**),  $\text{NCS}$  (**8**),  $\text{OMe}$  (**9**),  $\text{OH}$  (**10**) were studied in the work [36]. The authors point out the obvious advantages of systems based on 2,2':6',2''-terpyridine (terpy), namely its stereochemical rigidity that helps to avoid  $\text{D}_{2d}$  distortions, the presence of low-lying orbitals due to the conjugated  $\pi$ -system, and the easy substitution of an ancillary ligand. Chloride complex **7** is non-luminescent in the room temperature solution. However, complexes **8–10** feature broad structureless bands, typical for MLCT transition, under the same conditions. The authors note that excimer emission was excluded due to the lack of concentration dependence (see subsection 1.2 for details). They also admit the possibility of the ligand-to-ligand charge transfer presence, but the absence of spectral changes when changing the solvent indicates the minimal participation of such a state. The absence of solvatochromism additionally confirms the presence of the MLCT excited state, since this state is not characterized by a large dipole moment.

A comparative study of the photophysical properties of bipyridine Pt(II) complexes with ancillary alkynyl ligands was carried out in Ref. [37]. The authors investigated two series of compounds, **11–14** and **15–18** (Scheme 1), varying substituents with different donor and acceptor strengths in both bipyridine and alkynyl ligands.



Scheme 1. Complexes **11–14** and **15–18** [37].

All studied in this work compounds demonstrated broad structureless phosphorescent emission bands in dichloromethane solutions. Comparison of complexes **11–14** revealed a gradual increase in the emission maximum in this series. From the

authors' point of view, the bathochromic shift indicates MLCT (Pt→diimine) photoluminescence, because its energy decreases with the decrease in the energy of the lowest unoccupied molecular orbital (LUMO) localized on the chelating acceptor ligand. Complexes **15** and **18** also exhibit emission from the MLCT state. Based on the obtained results, authors conclude that the electronic and vibronic characteristics of the Pt→diimine MLCT states in studied complexes and the Re→diimine states in compounds such as [(diimine)Re<sup>I</sup>(CO)<sub>3</sub>(L)] are very similar.

With the development of quantum-chemical calculations, “pure” assignments of luminescence bands to specific types are becoming increasingly rare in the literature. Consider, for example, compounds **19–21** (Figure 4a), based on C<sup>∧</sup>C<sup>∧</sup>N ligand with ancillary  $\gamma$ -picoline (**19**) or different N-heterocyclic carbenes, NHC (**20**, **21**) from Ref. [38]. Despite the completely different nature of the ancillary ligands, these complexes exhibit nearly identical emission spectra in solution (Figure 4b). They show already familiar to us broad structureless bands in the yellow region of the spectrum without pronounced vibronic splitting. The authors conclude that this shape of the spectra indicates a large contribution of the MLCT state to the luminescence and a negligible contribution of additional ligands. However, further calculations show that the luminescence character in these complexes is more correctly described by the mixed MLCT/ILCT type, where ILCT is localized on the tridentate ligand.

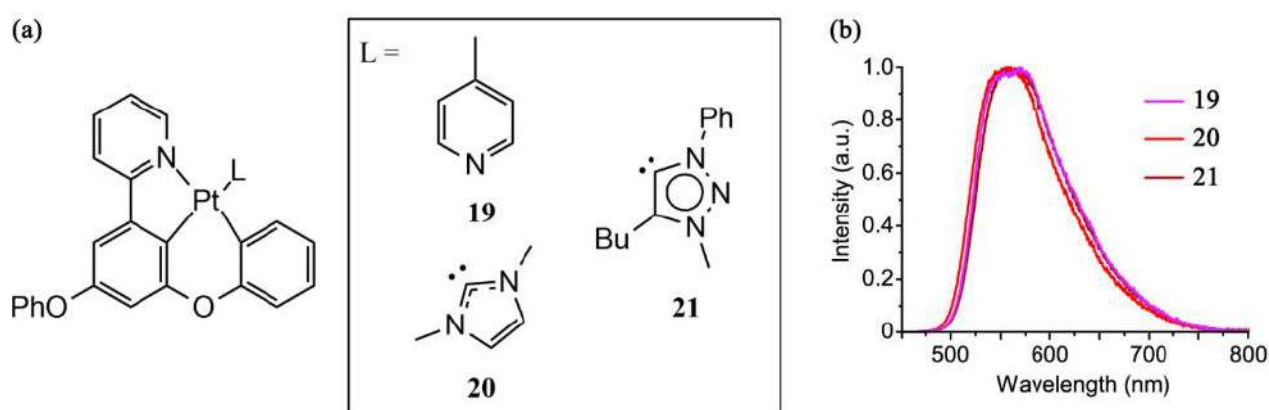
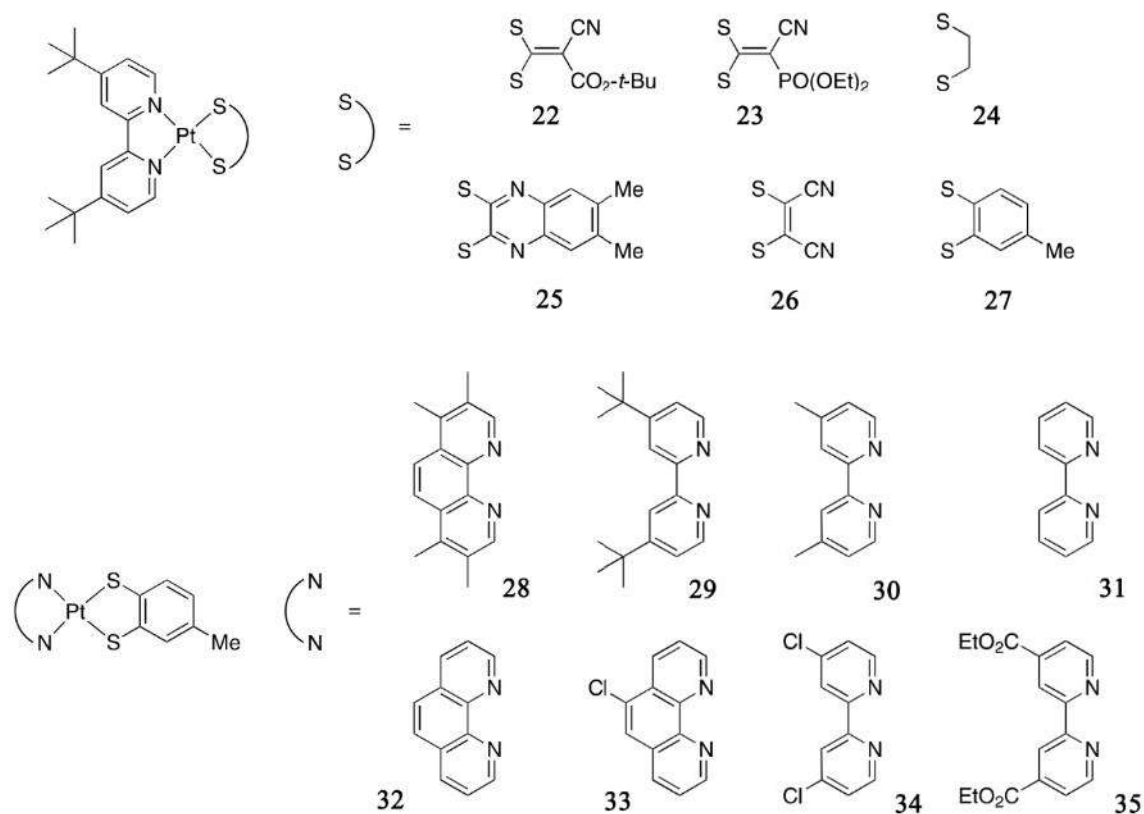


Figure 4. (a) Complexes **19–21**; (b) Emission spectra of complexes **19–21** in acetone (**19**) and MeCN (**20,21**) solutions [38].

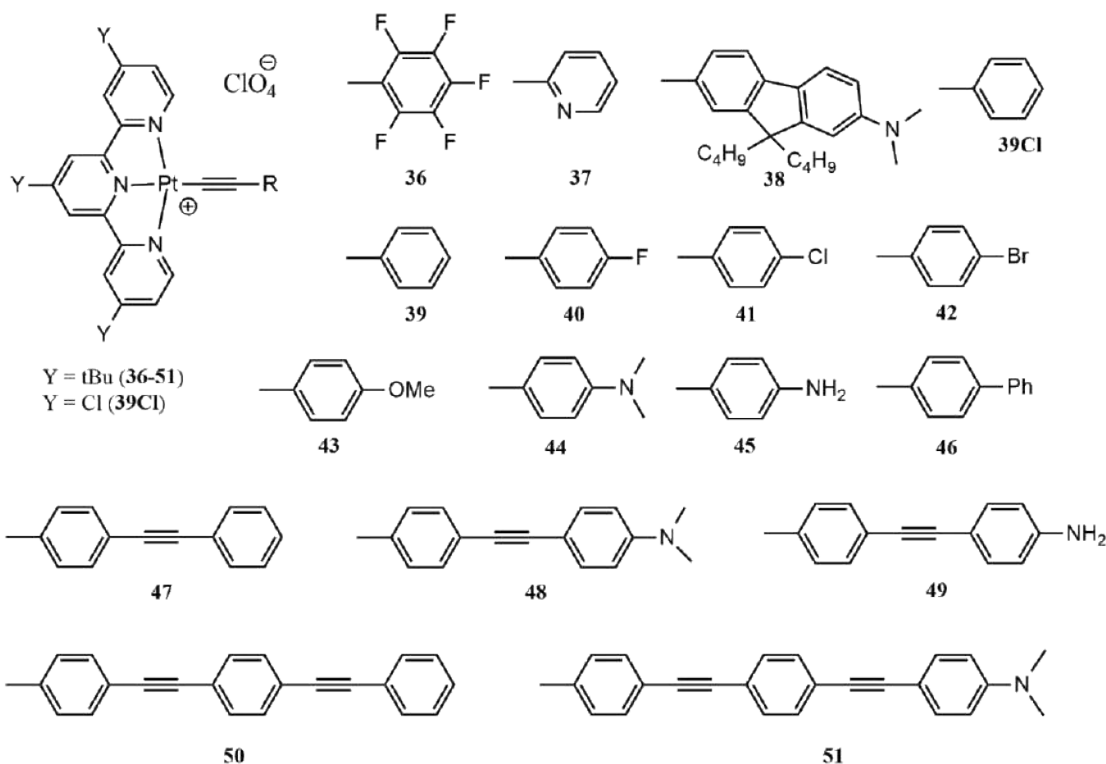
### 1.1.3. Ligand-to-ligand charge-transfer excited states (LLCT)

In case when coordination environment of metal center contains both oxidizable ligand and another reducible ligand, a new low-energy ligand-to-ligand charge-transfer excited state may appear. The metal in this case acts as a conductor of interaction between the ligand-donor and ligand-acceptor. The former ones can be anions, such as halides, thiolates and carbanions. The latter ones can be, for example, porphyrins or polypyridines [29,39]. Monomeric complexes with any type of charge transfer tend to exhibit broad structureless luminescence bands, partially resolved upon cooling, but in the case of LLCT type the emission energy depends on the nature of two ligands simultaneously. Also in this case solvatochromic properties can be more pronounced.

One of the most comprehensive early works [40] considers two series of platinum(II) complexes bearing diimine and dithiolate ligands. In the first series six different dithiolates are varied (**22–27**), while in the second series different diimines are used (**28–35**, Scheme 2). Comparing these two series, the authors provide evidence for the presence of LLCT character in all the studied compounds. All 13 complexes exhibit broad structureless luminescence bands in solution with sufficiently high quantum yields that cut off MC states. The wavelength of the emission maximum for the studied compounds depends on both the nature of the diimine and the nature of the dithiolate ligands. Thus, upon introduction stronger electron-accepting N<sup>N</sup> ligands, a gradual bathochromic shift is observed in the series **28-35**. This is indicative of an excited state involving charge transfer to the diimine, because the introduction of acceptor substituents into this fragment should lower the LUMO energy. The influence of different dithiolate ligands can be seen in series **22-27** as a bathochromic shift from 590 (**22**) to 720 nm (**27**). This means that the nature of the dithiolate ligand affects the energy of the highest occupied molecular orbital (HOMO), and emissive transitions have LLCT nature.

Scheme 2. Complexes **22–35** [40].

Terpyridine derivatives also can exhibit luminescence with ligand-to-ligand charge transfer. An article [41] described 16 compounds (**36–51**, Scheme 3) possessing an LLCT-type excited state and exhibiting broad structureless emission bands, with energies depending markedly on the nature of the ligands. The energy of the LLCT state, as in the previous case, is affected by two factors at once. One of them is the HOMO energy, which is located on the arylalkynyl ligand and increases with the introduction of electron-donating groups, increasing  $\pi$ -conjugation and chain length of this ligand. The second factor is the energy of the LUMO localized on terpyridine, which decreases when the electron-donating tert-butyl (tBu) is replaced by the electron-accepting Cl.

Scheme 3. Complexes **36–51** [41].

Taking into account this arrangement of the frontier orbitals, several experimental observations can be successfully explained. First, the emission energy increases with increasing electron-donating properties of para-substituents in complexes **39–46**. Second, the luminescence wavelength increases with the elongation of the  $\pi$ -conjugated linker in the arylalkynyl ligand (complexes **39**, **47**, **50**). Finally, for compounds **39** and **39Cl** containing the same alkynyl ligands but different substituents in the terpyridine moiety, the emission energy experiences a bathochromic shift when the electron-donating tert-butyl (tBu) is replaced by the electron-accepting Cl.

As mentioned above, with the development of quantum-chemical calculations, the “pure” assignment of certain bands is becoming less and less common. In Ref. [42], the emission properties of complexes **52–62** based on substituted o-phenanthroline with various arylalkynyl ligands were compared (Figure 5a). All the obtained systems were luminescent in solution, exhibiting structureless bands at room temperature (Figure 5b) and bands with weak vibronic splitting at 77 K. The emission maximum wavelength for complexes with electron-deficient substituents was shorter than for systems with electron-donating functional groups.

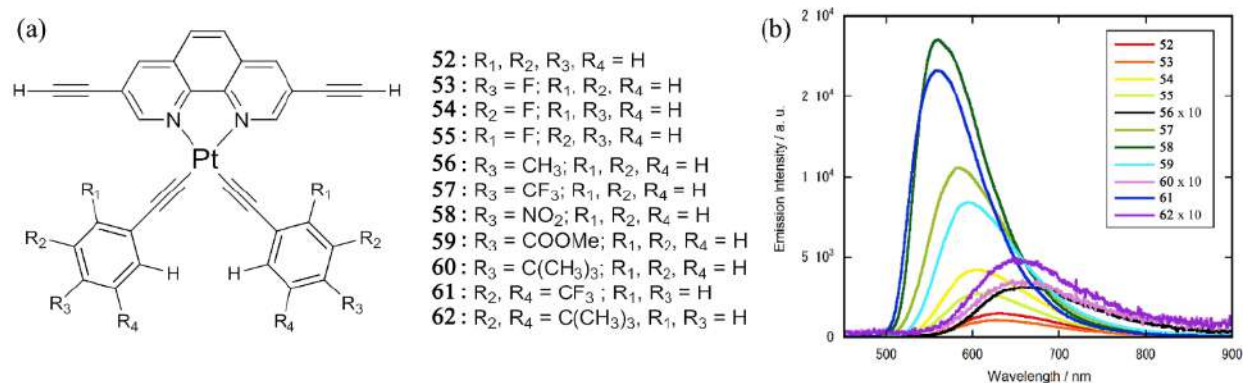


Figure 5. (a) Complexes **52–62**; (b) emission spectra of complexes **52–62**,  $\text{CH}_2\text{Cl}_2$ , 298K.

Methods of time-dependent density functional theory (TD-DFT) were used for quantum-chemical calculations of complexes **52–62**. These calculations showed that the nature of the excited state is LLCT with an admixture of the MLCT. The authors also found that the emission transition energy in compounds **52–62** correlates linearly with the energy difference between the excited triplet state and the ground singlet state. Such correlation, according to the authors, proves that the calculated orbitals reflect the position of the real ones in these systems.

#### 1.1.4. Ligand-centered excited states (LC)

Almost any organic phosphor attached to a metal center is theoretically capable of demonstrating the ligand-centered emission type. There are systems where this type of charge transfer is easily determined due to the similarity of the emission spectrum of the free ligand and the complex based on it, for example, in Refs. [43,44]. However, in the case of platinum(II) complexes, this is rare because of the strong spin-orbit coupling characteristic for the third row transition metals. The strong spin-orbit coupling favors the intersystem crossing due to the heavy atom effect. As a consequence, LC fluorescence does not appear, switching to the triplet LC state [45]. This, ligand-centered emission in aerated solutions is rather weakly pronounced. A distinctive feature of this luminescence is a rather well pronounced vibronic splitting of the emission spectra even at room temperature. When the temperature is lowered, the spectra are even more clearly resolved.

Also, the excited state lifetimes for ligand-centered luminescence are usually higher than for charge transfer complexes [19,29].

In Ref. [46], a pyrene fragment was introduced into the coordination environment of platinum(II) (Figure 6a). The luminescence of complex **63** was nearly not observed in aerated solution, increasing in intensity during degassing and showing structured bands. The excited state lifetimes of this compound were almost forty times higher than those of the model complex with a phenylalkynyl ligand exhibiting MLCT-type luminescence.

When freezing a solution of compound **63** in a mixture of alcohols, an increase in vibronic coupling was observed (Figure 6b), which additionally confirmed the LC-type excited state localized on the pyrene fragment.

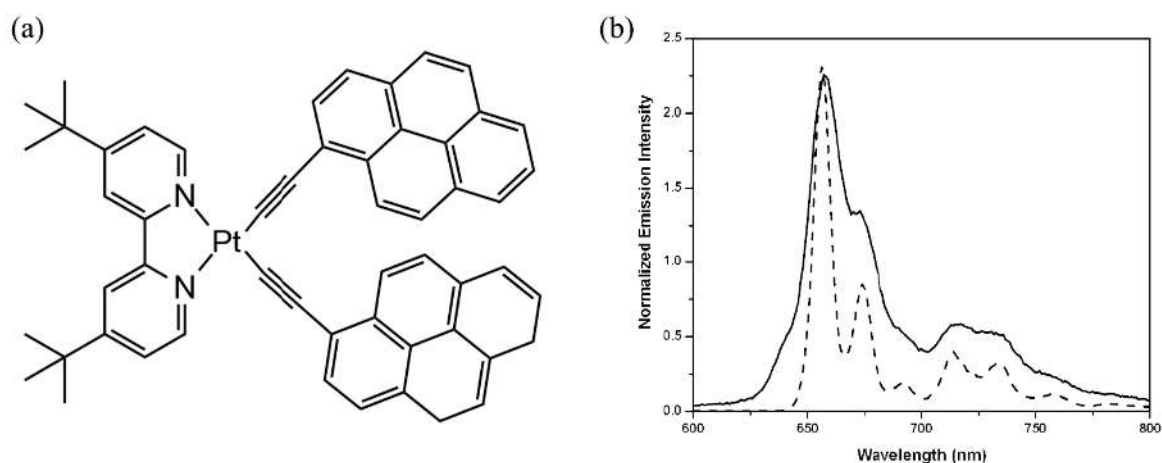


Figure 6. (a) Complex **63**; (b) emission spectra of complex **63** at 298K, solid line, and 77K, dashed line. Solvent: EtOH/MeOH 4:1,  $\lambda_{\text{ex}} = 480$  nm [46].

As mentioned earlier, the introduction of complex organic ligands into Pt(II) complexes leads to the appearance of several potentially active excited states. The authors of the study [47] suggest that a rational choice of ligands for *cis*-bis-alkynyl platinum systems and the solvent for the photophysical experiment can promote both the appearance of “pure” MLCT and LC transitions and their close arrangement with possible switching from one state to another. The latter was demonstrated by them on the example of complex **64** (Figure 7a).

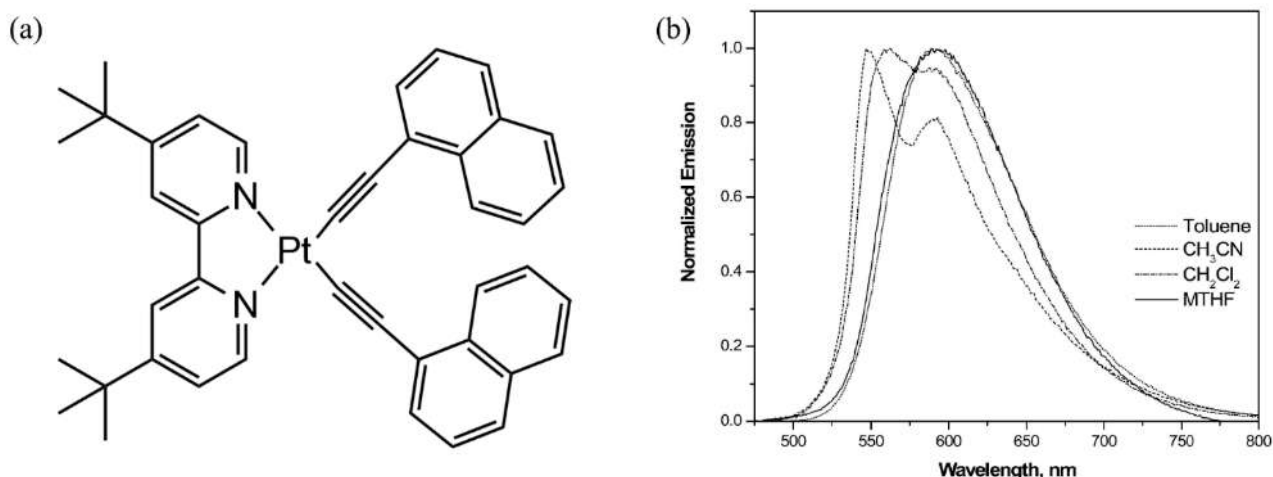


Figure 7. (a) Complex **64**; (b) emission spectra of complex **64** at 298 K in  $\text{CH}_3\text{CN}$ , MTHF,  $\text{CH}_2\text{Cl}_2$  and toluene [47].

The emission spectra profile of the obtained compound looks differently in different solvents (Figure 7b). Thus, the luminescence of compound **64** in 2-methyltetrahydrofuran (MTHF) and toluene exhibits broad structureless bands of MLCT nature. The other extreme case, namely emission in acetonitrile, exhibits pronounced vibronic splitting, indicating the LC nature of the excited state. The luminescence of complex **64** in dichloromethane looks like something average between the above two states. Based on the obtained data, the authors conclude that the studied compound has close in energy MLCT and LC states localized on the alkyne ligand, switching to each other depending on external conditions, in this case, the polarity of the solvent.

Another known chromophore, namely a pyridyl-functionalized coumarin derivative, was introduced into acetylacetonate platinum complexes **65** and **66** in [48] (Figure 8a).

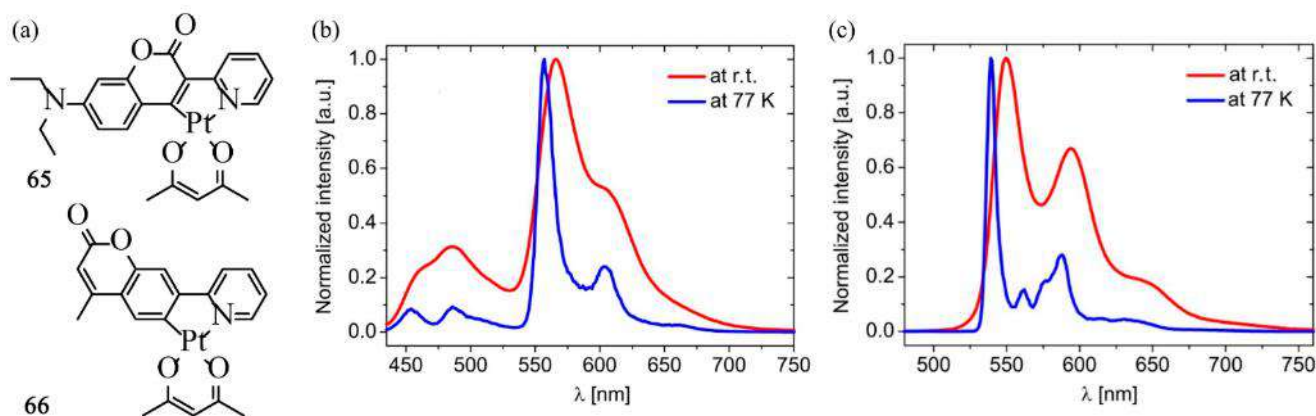


Figure 8. (a) Complexes **65** и **66**; (b), (c) emission spectra of **65** and **66** respectively at 298 K ( $\text{CH}_2\text{Cl}_2$ ) and 77 K (MTHF) [48].

Complex 66, unlike the corresponding free ligand, has a high luminescence quantum yield and exhibits emission bands with vibronic splitting (Figure 8b). As expected for the LC excited state, this splitting is enhanced upon cooling to 77 K. Interestingly, similar in structure and chromophore fragment, complex **65** possesses the so-called double emission – simultaneously existing fluorescent and phosphorescent emission bands. Apparently, for this compound the rate of intercombination conversion is comparable to the rate of singlet-singlet radiative relaxation.

The ligand-centered luminescence has one important advantage over charge-transfer emission in the context of emitter applications for OLED devices. This advantage is the reduced half-width of the emission band, which is important for obtaining the pure colors required for electroluminescent devices. Blue-colored phosphors are particularly valuable, and the Ref. [47] addresses these two problems. The authors synthesized two trans-NHC platinum(II) complexes **67** and **68** (Figure 9a) based on butadiene ligands. It is known that complexes of this structure usually exhibit LC luminescence, and functionalization of alkynyl ligands will thus affect it. Figure 9b shows the emission spectra of the obtained compounds in tetrahydrofuran (THF) and polymethylmethacrylate (PMMA) films at room temperature.

In both cases, the luminescence is attributed to the ligand-centered character based on the pronounced vibronic splitting and the data of previous works on similar systems. The magnitude of the vibronic splitting corresponds to the vibration frequency of the  $\text{C}\equiv\text{C}$

bond, and the FWHM of the 0-0 transition band is only 10 nm ( $589\text{ cm}^{-1}$ ) or 14 nm ( $596\text{ cm}^{-1}$ ) for complexes **67** and **68**, respectively. Despite the structural similarity of the studied systems, doping of PMMA films with complexes **67** and **68** leads to different results. The quantum yield of luminescence of complex **68** nearly does not change during the transition from solution to polymer matrix. At the same time, when PMMA films are doped with complex **67**, there is a sharp increase in quantum yield compared to solution (from 0.25% to 57%). As a rule, in compounds of similar structure MC states lie only slightly higher in energy than LC states. The similarity of the photophysical characteristics of complex **68** in solution and PMMA matrix, however, indicates that the metal-centered state is not accessible due to the relatively low energy of the ligand-centered state. In contrast, in the case of complex **67**, which possesses a higher energy LC state, non-radiative relaxation in solution is possible due to the presence of a thermally accessible MC state. In addition, in PMMA films, the rigidity of the polymer matrix does not favor MC relaxation because it prevents excited-state distortion of the complex structure.

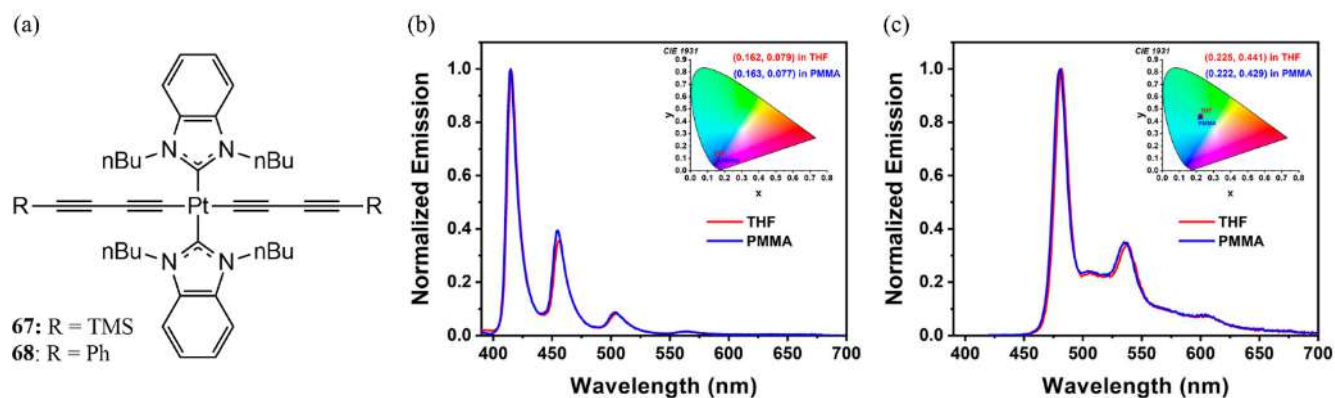


Figure 9. (a) Complexes **67** and **68**; (b), (c) emission spectra of complexes **67** and **68** respectively (THF solution and PMMA films) [49].

Upon cooling to 77 K, the emission spectra of complexes **67** and **68** in MTHF solutions narrow even more dramatically, which further indicates the LC character of the excited state. The FWHM of the 0-0 transition bands decrease to 4 and 8 nm, respectively. The authors conclude that the emission CIE color coordinates of complex **67** are close to

the standard CIE color coordinates of pure blue, and due to the high quantum yields, this compound can be successfully used to fabricate a blue OLED device.

### 1.1.5. Intraligand charge-transfer excited states (ILCT)

If both donor and acceptor fragments are present in the structure of the coordinated ligand, intraligand charge transfer can occur. Like the abovementioned types of charge transfer, it is characterized by broad structureless emission bands exposed to solvatochromism. The excited state lifetimes for such type of luminescence will be generally higher than for complexes with the MLCT type. This can be explained by a relatively small change in geometry at intraligand charge transfer, because it nearly does not affect the metal center. Also, the ILCT state is characterized by increased resistance to quenching due to the formation of exciplexes. Formally, this quenching occurs due to the attack by Lewis bases of the free coordination vacancy on the metal, and is facilitated in the case of MLCT states, increasing the electrophilicity of the metal center in the excited state. In the case of intraligand charge transfer, the electrophilicity of the donor moiety within the ligand is enhanced. The ILCT excited state is usually close in energy to or mixed with other excited states present in the complex [19,29].

The first example in this section will demonstrate that the ILCT excited state, like the MLCT state, can be energetically close to the intraligand state and “switch” depending on external conditions. Complex **69** based on tridentate N<sup>^</sup>C<sup>^</sup>N ligand with 4-(dimethylamino)phenyl substituent in the fourth position was considered in Ref. [50] (Figure 10a). Its emission appears as a broad structureless band in dichloromethane solution and is not affected by concentration quenching. As suggested by the authors, the introduction of an electron-donating amino group as a substituent increases the energy of the 4-(dimethylamino)phenyl substituent to such an extent that a separate molecular orbital localized on this fragment appears. As a result, the LC character of the excited state changes to ILCT. Interestingly, the ILCT and LC excited states appear to be close in energy, and the emission type changes with a gradual change in solvent polarity from acetonitrile to carbon tetrachloride (Figure 10b). The stability to the formation of excimers in dichloromethane is explained by the fact that the excited state with intraligand

charge transfer will have a low affinity for unexcited molecules playing the role of Lewis base. The resistance to excimer formation in DCM solutions is rationalized by the low affinity of ILCT excited state to non-excited molecules, acting as Lewis bases.

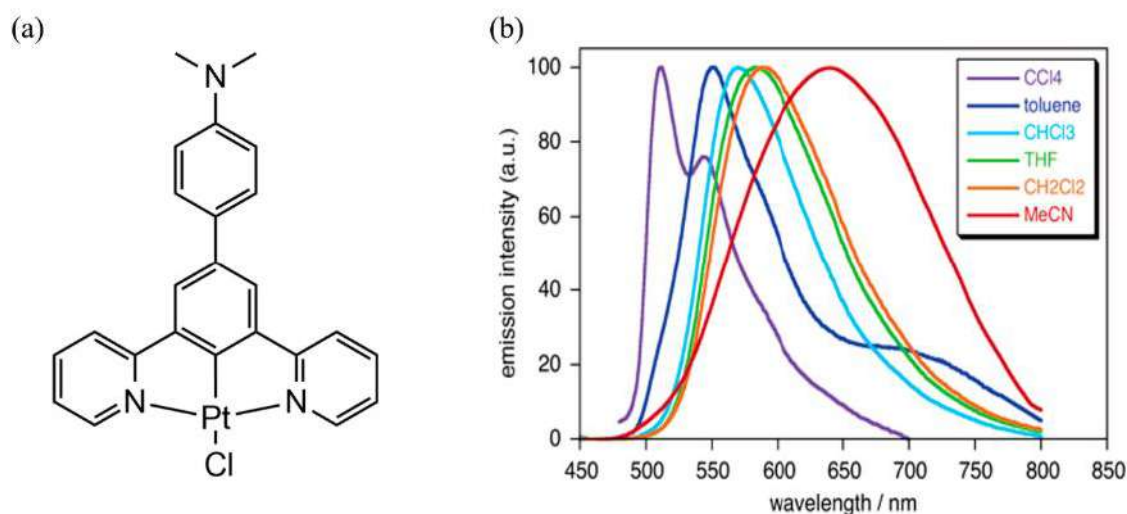


Figure 10. (a) Complex **69**; (b) emission spectra of complex **69** at 298K in  $\text{CCl}_4$ , toluene,  $\text{CHCl}_3$ , THF,  $\text{CH}_2\text{Cl}_2$  and  $\text{CH}_3\text{CN}$  solutions [50].

Similar behavior was shown by the complex **70** based on tetradentate ligand (Figure 11a), described in Ref. [51]. Authors used this ligand due to its bulkiness, inhibiting aggregation process. Also, its structure contains both donating and accepting fragments, and this favors intraligand charge transfer. Indeed, complex **70** exhibited a broad structureless luminescence band in dichloromethane solution (Figure 11b). Upon changing the solvent to a more polar one, the hypsochromic shift occurred, together with gradual emergence of vibronic coupling. Thus, authors have concluded that there are two energetically close LC/MLCT and ILCT/MLCT states in complex **70**. This was also proved by the quantum-chemical calculations.

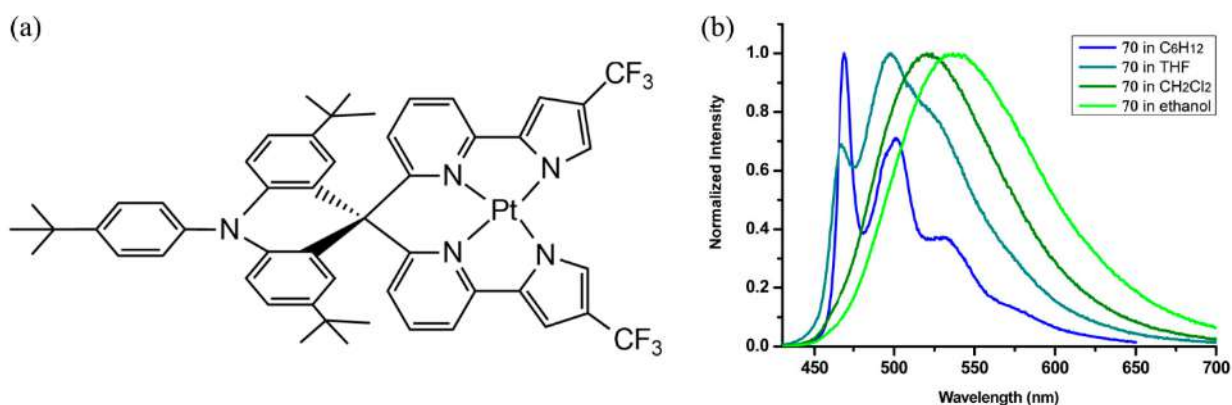


Figure 11. (a) Complex **70**; (b) emission spectra of complex **70** at 298K in cyclohexane, THF,  $\text{CH}_2\text{Cl}_2$  and ethanol [51].

Chloride complexes **71–73** based on cyclometallating 6,6'-substituted 2,2'-bipyridine bearing additional ester group in fifth position (Figure 12a), demonstrate even more complicated behavior [52]. This work has shown that exactly the ester accepting group provides substantial changes of complexes' emission properties. Authors compare complex **71** and the isostructural analog without ester group and point at the change of the nature of the excited states from MLCT to the mixed ILCT/LC/MLCT type with dominating ILCT state. The luminescence spectra reflect this, featuring bathochromic shift (Figure 12b). Interestingly, the introduction of donor methoxy group in the phenyl fragments, located in the 6 and 6' positions of the bipyridine ligand (complex **73**) leads to the prevalent LC state with decreasing of the MLCT contribution. This is the reason why the luminescence spectrum of complex **73** is hypsochromically shifted compared to the others and has vibronic splitting.

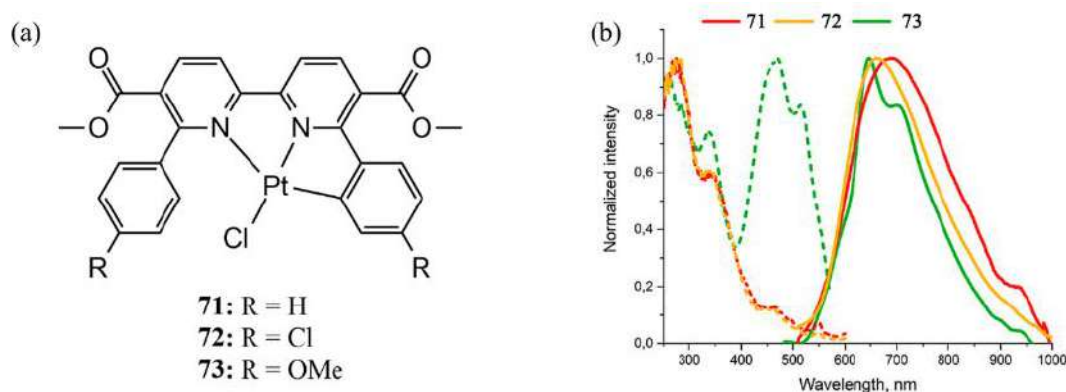


Figure 12. (a) Complexes **71–73**; (b) excitation and emission spectra of complexes **71–73** at 298K in  $\text{CH}_2\text{Cl}_2$  [52].

## 1.2. Features of platinum(II) complexes photophysics, caused by aggregation

As it was already mentioned before, Pt(II) complexes with organic ligands can demonstrate various excited states upon ultraviolet (UV) irradiation. These states are MLCT, ILCT, LLCT and LC (Figure 13a). However, this list is incomplete without special excited state, emerging due to the aggregation. The distinctive feature of square-planar complexes is their ability to form weak metal-metal and/or ligand-ligand interactions between closely located molecules. Metallophilic interactions appear due to the filled  $d_z^2$  orbitals of Pt(II) complexes, which are perpendicular to the plane of the molecule and lie energetically lower than HOMO. These orbitals can interact both with solvent molecules and with other molecules of the same complex.

Considering a simplified molecular orbital diagram for a Pt-Pt dimer in comparison with the same diagram for a monomer (Figure 13b), we can see that their HOMO and LUMO are different. The formation of the dimer destabilizes the filled  $d_z^2$  orbitals, and the nature of the HOMO changes from  $d\pi(\text{ligand})$  or  $d_z^2$  to  $\sigma^*$  (i.e. to  $d_z^2 \cdots d_z^2$ ). Thus, a new excited state called metal/metal-to-ligand charge transfer (MMLCT) is formed [53–55]. This state usually has a lower transition energy than the excited states of monomeric compounds.

This phenomenon was discovered recently, and the early works on it, in most cases, investigated only photophysical properties of the solid [54,56,57]. We have already seen the Ref. [27], and complex 5 with two different forms, “yellow” and “red”. The packing of this complex in the red form favors exclusively metallophilic interactions. The emission spectrum shows a broad structureless band in the red region of the spectrum, narrowing and experiencing a bathochromic shift upon cooling. This is the hallmark of MMLCT-type luminescence. The bathochromic shift at low temperatures occurs due to the reduction of the metal-to-metal bond due to the contraction of the whole unit cell upon cooling [54,56].

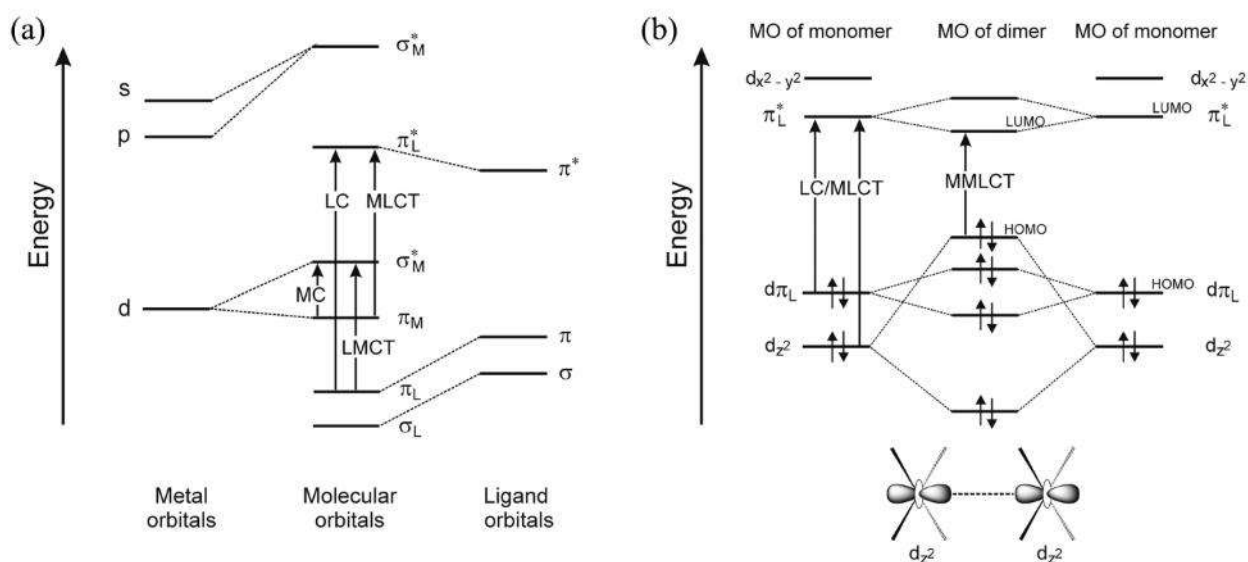


Figure 13. (a) Simplified molecular orbitals (MO) diagram of metallocomplex with transitions of the excited states; (b) simplified MO diagram for two interacting Pt(II) complexes [10].

In 2002, a classic paper by Yam [58], was published, devoted to aggregation due to metallophilic interactions in solution. The authors synthesized complexes **74** and **75** based on terpyridine ligands with additional diinyl ligands (Figure 14a). Complex **74** exists in two crystalline forms, dark green and red. The first is an infinite almost linear chain with short Pt $\cdots$ Pt contacts (3.388 Å). The second exhibits dimeric packing, with alternating metal-to-metal bond lengths of 3.394 and 3.648 Å. Complex **75**, as expected, does not show metallophilic interactions due to sterically loaded tert-butyl substituents in the terpyridine ligand preventing aggregation.

When complex **74** is dissolved in acetonitrile, a yellow solution with an absorption spectrum typical for monomeric Pt(II) compounds is formed. However, upon increasing the diethyl ether content in the solution of the complex of constant concentration up to 80%, a significant change in the optical and photophysical properties occurred (Figure 14b, c). The obtained solutions remained stable for more than two hours and no precipitation was observed. The change in the color of the solution and the appearance of luminescence at about 800 nm, according to the authors, was caused by the aggregates

formation in solution. Compound **74** is insoluble in diethyl ether, and the addition of the so-called “bad solvent” leads to aggregation by reducing the solubility.

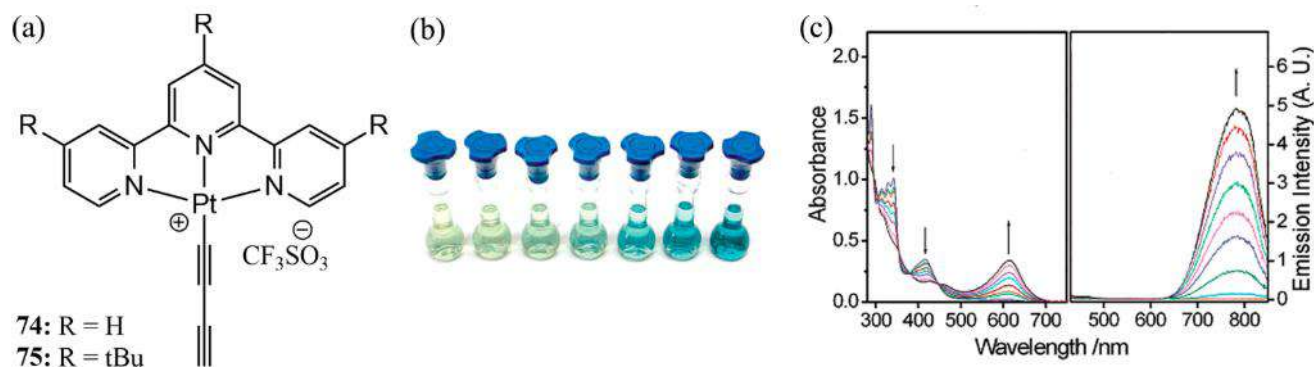


Figure 14. (a) Complexes **74** and **75**; (b) photographs of complex **74** solutions with different concentration of Et<sub>2</sub>O; (c) changes in UV-vis and emission spectra of complex **74** at 298 K in acetonitrile solutions with different Et<sub>2</sub>O concentration [58].

It is important to realize that the energy of MMLCT transitions strongly depends on the metal-metal distance. This means that there is a fundamental possibility to control the optical and photophysical properties of such compounds by changing the distance between metal atoms [59]. The introduction of bridging ligands or spacer ligands makes it possible to vary the color of platinum complexes: when platinum metal centers are connected by short bridges, a bathochromic shift of absorption and emission spectra is observed, and when they are distant in space, the properties of monomers are manifested. For example, the substitution of monodentate phosphine in platinum(II) complexes by bridged polydentate ones with a significant change in photophysical properties has been described in [60–62]. These complexes and their emission spectra are shown in Figure 15.

In some cases, aggregates with metallophilic interactions can break down and re-form, and this affects the complexes' optical and photophysical properties. This phenomenon can appear in the presence of mechanochromic response (change of luminescence under mechanical action), vapochromic response (the same when treated with solvent vapor), and other so-called *stimuli-responsive* properties [63–68].

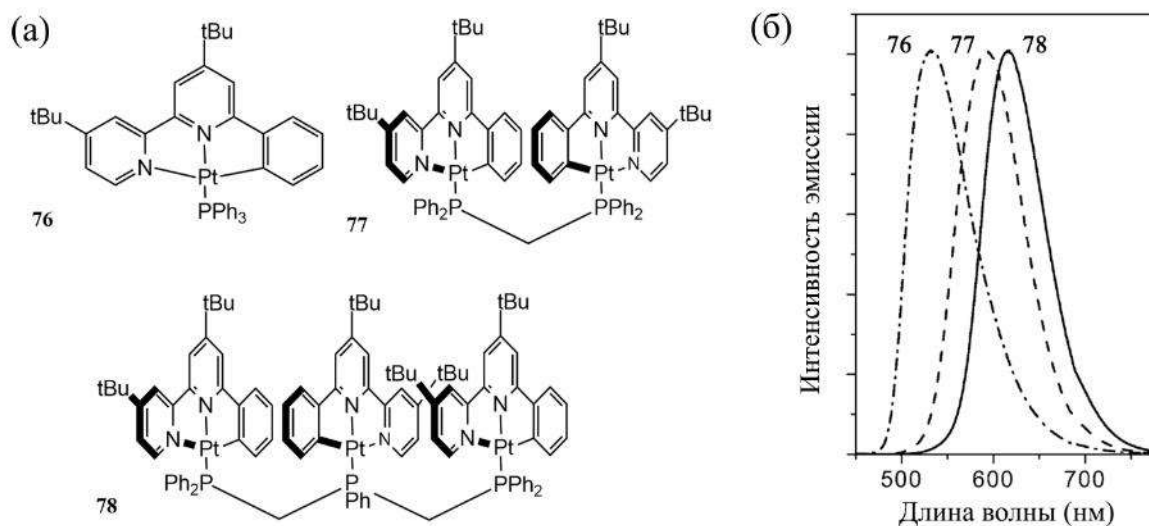


Figure 15. (a) Complexes **76**, **77** and **78**; (b) solid-state emission spectra of complexes **76**, **77** and **78**, r.t. [61]

In Ref. [68], neutral tert-butylisocyanide complexes of platinum(II) **79** and **80** with additional cyclometallating ligands based on phenylpyridine were synthesized and characterized (Figure 16a). The studied complexes can form aggregates at high concentrations in solution. It is reflected in the appearance of an additional band in the red region of the absorption and emission spectra. Complexes **79** and **80** tend to form pseudopolymorphs with different solvents, forming different 1D chains due to metallophilic and  $\pi$ - $\pi$  interactions in the solid state. Varying the length of these contacts entails a change in luminescence from greenish-yellow to red. Complexes **79** and **80** exhibit a wide range of *stimuli-responsive* properties, among them vapochromism, solvatochromism, thermochromism and mechanochromism (Figure 16b, c). Apparently, the vapochromic and solvatochromic effects appear due to the presence of cavities in the crystal structures that can be reversibly occupied by solvent molecules, leading to rearrangement of the entire unit cell. Grinding the powders of compounds **79** and **80** strongly affects the packing of molecules in the solid phase, causing a transition to orange emission and loss of crystallinity.

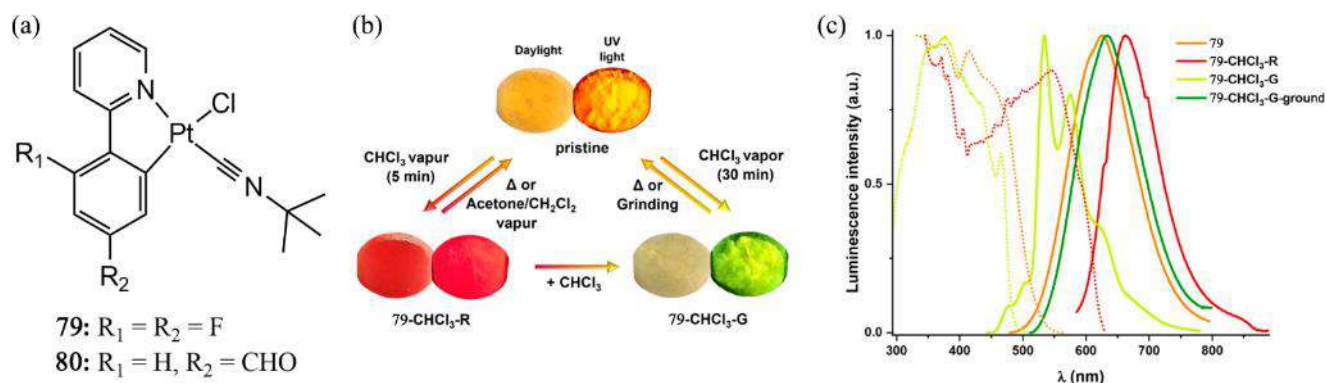


Figure 16. (a) Complexes **79** and **80**; (b) photographs of complex **79** under different conditions; (c) excitation and emission spectra of complex **79** in the solid state at 298 K (**79-CHCl<sub>3</sub>-G-ground** – form of **79-CHCl<sub>3</sub>-G** after grinding) [68].

The phenomenon of platinum(II) complexes aggregation is a powerful tool to influence the photophysical properties of the target compounds. This thesis, however, does not aim to address this topic in detail and refers the curious reader to several comprehensive reviews [10,59,69–72].

### 1.3. Alkynyl Pt(II) complexes

As mentioned in subsection 1.1, to enhance the luminescent properties of platinum(II) complexes, it is necessary to introduce strong-field ligands that increase the energy of metal-centered excited states. One of the most common approaches today is the introduction of  $\sigma$ -donor alkynyl ligands. These molecules offer several advantages, among them the relatively easy functionalization and simple introduction into the Pt(II) coordination sphere through copper-catalyzed substitution of chloride for alkyne. In addition, in the interaction of  $p\pi(C\equiv C)$  and  $d\pi(Pt)$  orbitals,  $\pi$ -donor properties of the alkynyl ligand lead to destabilization of the HOMO of the corresponding platinum complex, lowering the energy of the luminescent excited states [19,73]. Besides, alkynyl ligands do not prevent the formation of metallophilic interactions, and this allows us to vary the emissive properties in the bulk. The introduction alkynyl ligands carrying a luminescent fragment at the periphery can yield of compounds with dual emission or the manifestation of LC excited states. Finally, alkynyl ligands can also react after

coordination on the platinum moiety [74,75], opening up additional possibilities for the variation of photophysical properties due to post-synthetic modification.

It is not surprising that since the first alkynyl complexes of platinum were obtained, dating back to 1994 [76], this area has attracted so much research interest. Taking into account the huge number of works and being limited in scope, we will only give a brief overview of the state of affairs in this field to date.

### 1.3.1. Bis-alkynyl complexes

In this chapter, we will divide bis-alkynyl Pt(II) complexes into *cis*- and *trans*-derivatives. The former are more common, because studies of such compounds began with diimine-containing Pt(II) complexes. As discussed above, the luminescent properties of square-planar complexes can deteriorate due to structural distortion of the excited state, and bidentate ligands allow to overcome this. In addition, the introduction of diimine ligands is a relatively simple process. Several early works investigating the emission states of *cis*-bis-alkynyl platinum(II) complexes are reviewed in the Ref. [19]. It includes, among others, the papers [37] and [46] already reviewed in subsection 1.1. Authors conclude that the introduction of different alkynyl ligands allows one to achieve a large variation in the excited states and luminescence wavelengths of bis-alkynyl platinum complexes.

Platinum bis-alkynyl complexes in both *cis*- and *trans*-configurations can be used to obtain various heterometallic compounds. The review [77] describes more than 170 such compounds and supramolecular aggregates with unusual topology. For example, in [78], it was shown that the luminescence of platinum-cadmium systems depends on the configuration of the initial Pt(II) complex: *cis*- systems have more hypsochromic luminescence than *trans*- compounds. Another example of supramolecular structure based on *bis*-alkynyl platinum(II) complexes is given in [79]. The formation of platinum-silver clusters of complex topology allowed authors to obtain red luminescence originating from the  $[\text{Pt}_2\text{Ag}_4 \rightarrow \text{RC}\equiv\text{C}^-]$  state.

Some bis-alkynyl platinum(II) complexes have found applications in prototype OLED devices, as indicated in the review [80]. One of them is a *trans*-phenylalkynyl

complex with additional NHC ligands [81]. It showed quite high quantum efficiency as a dopant in the emissive layer, but proved to be unstable to burnout. The photophysical properties of other alkynyl-carbene complexes of Pt(II) and their application in photoluminescent devices are reviewed in Ref. [82].

Platinum(II) bis-alkynyl complexes often exhibit *stimuli-responsive* properties applicable in many fields, from sensing to memory devices. A review [83] provides examples of such systems. The papers [84,85], mentioned in the review describe unusual photochromic *cis*- and *trans*-alkynyl platinum compounds capable of reversible cyclization at the periphery of the ligand environment upon irradiation with ultraviolet radiation of different wavelengths. The authors suggest that these compounds can serve as photoswitches, for instance, in memory devices. Another interesting example of vapochromic properties of *cis*-bis-alkynyl platinum(II) complexes is presented in [63]. Functionalized by a BR<sub>3</sub> group on the periphery of the ligand environment, this *cis*-alkynyl Pt(II) complex demonstrates a color change of luminescence in the solid state upon treatment with vapors of both polar and nonpolar solvents. The authors emphasize that, in contrast to numerous literature examples, vapochromism in this system is not caused by changes in the lengths of weak contacts, but by local interactions of solvent molecules with the complex, leading to changes in the energy of different excited states.

### 1.3.2. Mono-alkynyl complexes

Compared to complexes based on mono- and bidentate ligands, compounds with tridentate ligands allow to achieve greater rigidity of the coordination environment of the platinum metal center. This allows to avoid torsional deformations of the excited state favoring the non-radiative relaxation. Thus, terpyridine-based ligands are able to fix the planar geometry of the metalcenter. However, the bite angle of tridentate ligands is not ideally sized for the Pt(II) ion, which reduces the strength of this ligand and lowers the energy of the metal-centered states. The introduction of an additional strong-field ligand helps to overcome this, and alkynyl ligands are ideal candidates for this task [19,73].

One of the first examples of luminescent platinum(II) mono-alkynyl complexes is given by Yam [86]. In this work, several systems based on terpyridine ligand were

synthesized. It was shown that the emission state energy decreases with increasing electron-donor properties of the alkynyl ligand. This work gave rise to numerous studies of terpyridine complexes of platinum(II) with various alkynyl ligands. Among them, the study of aggregation effects in solutions, already familiar to us from the article [58] and the preparation of low-molecular-weight gels [87,88] and pH-sensitive compounds [89–93] were carried out.

An excellent review [94] on the application of metal complexes in biosensing, bioimaging and theranostics discusses, among others, terpyridine complexes of Pt(II) with additional alkynyl ligands for luminescent bioimaging of lysosomes in living cells and G-quadruplex sensing, which can be used to detect cancers and neurological disorders. Finally, mono-alkynyl platinum(II) complexes based on N<sup>^</sup>N<sup>^</sup>N ligands are widely used for self-assembly of supramolecular functional materials due to their propensity for metallophilic interactions [95].

Mono-alkynyl platinum complexes are not limited to N<sup>^</sup>N<sup>^</sup>N derivatives. Cyclometallation, or the attachment of a polydentate ligand to a metal via a metal-carbon covalent bond and the usual coordination bonds for the remaining sites, represents a powerful tool for creating luminescent complexes. Such pincer ligands have an important advantage relative to terpyridine ligands: they are much stronger  $\sigma$ -donors due to the “C<sup>-</sup>” moiety and are therefore stronger field ligands. The  $\pi$ -acceptor character is secured by coordinated pyridine moieties. In this way it is possible to increase the energy of metal-centered states and enhance the luminescence of cyclometallated systems [73].

A nice review [96] considers mono-alkynyl platinum(II) compounds with C<sup>^</sup>N<sup>^</sup>N, N<sup>^</sup>C<sup>^</sup>N and C<sup>^</sup>N<sup>^</sup>C ligands. The brightest emission properties are characteristic of N<sup>^</sup>C<sup>^</sup>N systems, which is apparently associated with the shortening of the Pt-C bond in the cyclometallating fragment and the resulting increase in the energy of d-d transitions. The least intense emission is characteristic of C<sup>^</sup>N<sup>^</sup>C systems: thus, the only described in the literature monoalkynyl complexes based on 2,6-diphenylpyridine do not emit in solution and have only very weak luminescence in the solid state [97]. In this context, we cannot help but mention the computational work [98], which utilized DFT/TD-DFT approaches to investigate the different luminescence efficiencies in various

cyclometallated systems. The absence of luminescence of the cyclometallated C<sup>^</sup>N<sup>^</sup>C complex was explained by a strong distortion of the excited state structure.

Cyclometallated mono-alkynyl platinum(II) complexes have found applications in a wide variety of fields. These include OLED devices [12,18,99,100], organic field-effect transistor, OFET [101,102], nonlinear optics [103–105], triplet photosensitization [106,107] and sensing to various metal ions [108–110].

Thus, we have reviewed some modern studies on Pt(II) alkynyl complexes and have shown that the variation of alkynyl ligands allows fine-tuning of the luminescence of these systems. To our knowledge, no data on the photophysical properties of platinum(II) alkynyl compounds bearing phosphonium moieties at the periphery of the ligand environment have been reported in the literature to date. The properties of phosphonium-containing “donor-linker-acceptor” systems and their potential applicability as ligands are discussed in subsection 1.4.

#### **1.4. Phosphonium-based systems of “donor-linker-acceptor” type**

Charged organic molecular chromophores possess a wide range of photophysical and electrochemical properties suitable for a variety of applications. One important subclass of these compounds consists of systems with intramolecular charge transfer, also known as push-pull systems or donor-linker-acceptor or D- $\pi$ -A systems. The latter name fully reflects the structure of these molecules carrying functional groups with positive mesomeric or inductive effects (e.g., –OR, –NH<sub>2</sub>, –OH or –NR<sub>2</sub>), i.e., donor groups, and acceptor moieties with negative mesomeric or inductive effects (например, –CHO, –NO<sub>2</sub>, –CN). These parts are combined into a single molecule via a  $\pi$ -conjugated linker. An important feature of such compounds is the possibility to control the luminescent properties by changing all three fragments, both donor and acceptor, and the linker [111].

Until recently, the field of molecular chromophores with intramolecular charge transfer was traditionally represented by nitrogen- and oxygen-containing compounds. However, phosphorus-containing compounds are currently receiving more and more attention. Phosphorus is very convenient for the construction of organometallic compounds due to the electronegativity values close to carbon and possible simple

transition from the trivalent state to the quaternary and pentavalent state. Thus, alkylation of organic phosphines leads to the formation of alkynylphosphonium cations, which have strong acceptor properties and are suitable for the construction of “donor-linker-acceptor” systems. The most important feature is that the electronic properties of the phosphonium cation and the degree of electron density delocalization can be finely tuned by modification of the phosphorus-bound radicals.

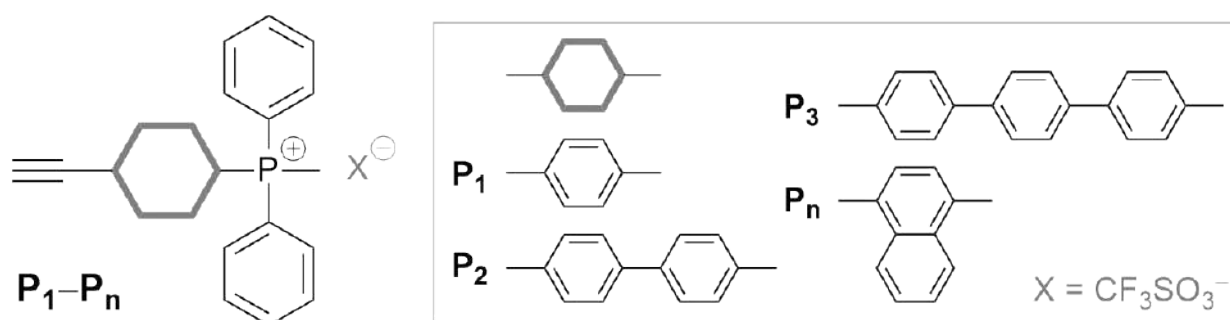
Methods of synthesis and some properties of cationic organophosphorus chromophores with intramolecular charge transfer are discussed in the review [2]. The study of these compounds began in 1991 with a molecule bearing a phosphonium cation and a borate anion joined by a diphenylene linker [112]. This molecule exhibited values of the first hyperpolarizability (a value characterizing the nonlinear optical activity of a single chromophore molecule) comparable to para-nitroaniline, which made it suitable for generation of the second optical harmonics. The solvatochromic and nonlinear-optical properties of such systems were subsequently studied in the works [113–115]. More recently, studies on the use of “push-pull” molecules based on phosphonium salts as colorimetric and luminescent sensors for fluoride anion have appeared [116–118]. This topic was further developed in the works of Koshevoy's group, who demonstrated that the coupling of a phosphonium fragment with a strong electron donor by means of various linkers leads to the formation of systems with intramolecular charge transfer, possessing bright luminescence with quantum yields up to 95% and varying emission wavelengths [119,120]. These compounds are also capable of two-photon absorption with high efficiency.

It is known that phosphonium cation tends to localize in mitochondria, which is widely used in bioimaging applications [121]. Phosphonium fragments are also used to enhance the solubility and biocompatibility of hydrophobic organic compounds. Thus, in Ref. [122], a phosphonium-functionalized structure of BODIPY (boron-dipyrromethene) type was designed and used for cancer cell imaging.

To date, phosphonium salt-based donor-linker-acceptor systems have not been used as ligands for metal complexes. In 2022, our research group developed new

alkynylphosphonium “push-pull” derivatives with different  $\pi$ -conjugated  $\mathbf{P}_1$ – $\mathbf{P}_n$  linkers (Scheme 4) and applied them as ligands to create bis-alkynyl Au(I) complexes [6].

The non-coordinated phosphonium salts proved to be efficient emitters with fluorescence quantum yields up to 77%. After coordination to the gold(I) metalcenter, the luminescence exhibited a triplet character and experienced a bathochromic shift. Variation of the linker in the alkynylphosphonium ligands allowed a controlled change in the phosphorescence wavelength. Complexes with ligands  $\mathbf{P}_2$  and  $\mathbf{P}_3$  also showed an additional fluorescence band, which in the case of the latter complex had a high intensity. This resulted in white emission in DMSO solutions and PMMA films.



Scheme 4. Alkynylphosphonium ligands  $\mathbf{P}_1$ – $\mathbf{P}_n$ .

Thus, based on the literature data, we decided to investigate the coordination of the synthesized alkynylphosphonium ligands onto a platinum(II) metal center to obtain efficient triplet emitters with controllable photophysical characteristics.

## CHAPTER 2. RESULTS AND DISCUSSION

### 2.1. Selection of research objects

The literature review has revealed that alkynyl Pt(II) complexes are very promising research objects. The introduction of such a strong-field ligand enhances the emission characteristics, whereas the features of square-planar Pt(II) metal center allow additional change of the luminescence due to the aggregation effects.

Alkynylphosphonium salts  $\mathbf{P}_1\text{--}\mathbf{P}_n$  were chosen mainly because of their intersystem charge transfer ability, which leads to the bright luminescent properties both as pro-ligands and ligands for Au(I) complexes. Varying the linker, a controlled variation of the emission wavelength can be achieved. The acceptor phosphonium moiety is able to influence the position of the frontier orbitals, which also affects the luminescence characteristics. Finally, the introduction of a charged group at the periphery of the ligand environment requires the presence of a counterion, which can also be used to control the luminescent properties of the resulting systems predominantly in the solid state.

Bidentate ( $\text{N}^{\wedge}\text{N}$ ) 4,4'-di-tert-butyl-2,2'-bipyridine (**dtbpy**) and monodentate triphenylphosphine ( $\text{PPh}_3$ ) and cyanide (CN) ligands were used as ancillary ligands for the synthesis of bis-alkynyl complexes. In this way all possible variants of the geometry of bis-alkynyl complexes are covered: *cis*- and *trans*- in the case of complexes with dtbpy and  $\text{PPh}_3/\text{CN}$ , respectively. Also, the influence of charge on the properties of the obtained systems is evaluated.

The tridentate  $\text{N}^{\wedge}\text{N}^{\wedge}\text{N}$  2,2':6',2''-terpyridine (**terpy**) and the cyclometallating  $\text{C}^{\wedge}\text{N}^{\wedge}\text{N}$  and  $\text{C}^{\wedge}\text{N}^{\wedge}\text{C}$  ligands 6-phenyl-2,2'-bipyridine (**phbpy**) and 2,6-diphenylpyridine (**dphpy**) were used to synthesize more rigid structures of monoalkynyl Pt(II) complexes. This set of ancillary ligands allowed us to investigate all possible charge states in the case of monoalkynyl systems. Importantly, almost all of the above ancillary ligands are commercially available, which allows both to save time on their synthesis and to easily reproduce the synthesis according to the literature methodology if necessary.

Examples of platinum(II) complexes with  $\text{N}^{\wedge}\text{C}^{\wedge}\text{N}$  cyclometallating ligands, for example with 2,6-dipyridylbenzene (**dpbz**), exhibiting efficient luminescence are also

found in the literature. In this research work, attempts were made to synthesize these compounds, unfortunately, they were not successful. For more details on these systems, see subsection 2.2.4.

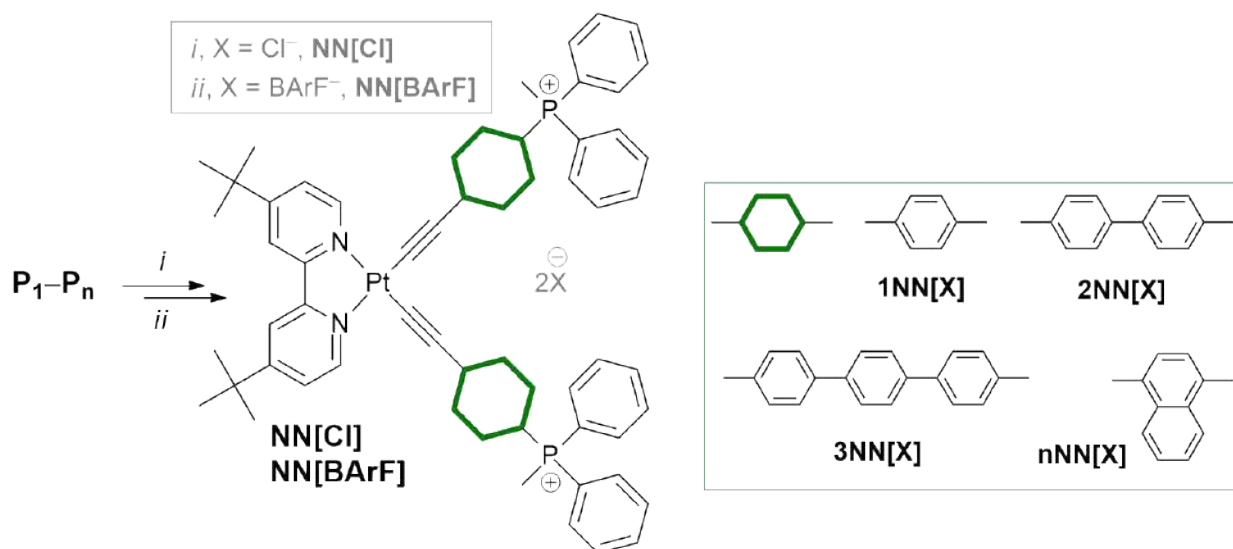
According to the research plan, Chapter 2 is divided into two semantic parts: synthesis (Section 2.2) and studies of the photophysical properties of the obtained compounds (Section 2.3). Each section is divided into subsections devoted to specific platinum(II) complexes.

## 2.2. Pt(II) complexes synthesis

The synthesis of various bis- and mono-alkynyl platinum(II) complexes is described in numerous literature sources. As a rule, chloride derivatives of platinum with appropriate ancillary ligands are used as starting compounds. The reaction takes place in organic solvents such as dichloromethane (DCM) or N,N-dimethylformamide (DMF) in the presence of various aliphatic amines as a base and copper(I) iodide as a catalyst. However, the presence of a charged phosphonium group at the periphery of the ligand environment requires modification of the literature techniques. Thus, this section is devoted to the synthesis of five different series of platinum(II) complexes and the proof of their composition and structure.

### 2.2.1. Bis-alkynyl Pt(II) complexes with ancillary N<sup>N</sup> ligand

In the present work, four platinum(II) complexes based on alkynylphosphonium ligands **P<sub>1</sub>–P<sub>n</sub>** with triflate counterion and ancillary diimine ligand **dtbpy** were synthesized. The latter ligand was chosen due to the presence in its structure of sterically demanding tert-butyl functional groups that prevent the aggregation of square-planar platinum(II) complexes and, consequently, improve the solubility of the target compounds (Scheme 5).



Scheme 5. Synthesis of **NN[Cl]** and **NN[BArF]** series. *i* = Pt(dtbpy)Cl<sub>2</sub>, CuI, DCM:Et<sub>3</sub>N=7:1, 18 h, r.t. Next step with crude product: DCM, TMAcI, 1 h, r.t.; *ii* = NaBArF, DCM, 1 h, r.t.

The first step involved copper-catalyzed substitution of chloride for alkyne according to the literature procedure [123,124]. The reaction mixture was separated by two-stage column chromatography (1: silica, CH<sub>2</sub>Cl<sub>2</sub> → acetone → CH<sub>2</sub>Cl<sub>2</sub> + 30% MeOH; 2: alumina, CH<sub>2</sub>Cl<sub>2</sub> + 50% acetone → CH<sub>2</sub>Cl<sub>2</sub> + 4% MeOH). A second column chromatography step was performed to remove the impurity of triethylammonium chloride, whose R<sub>f</sub>(retention factor) was very similar to the R<sub>f</sub> of the target complex when silica gel was used.

Based on the results of this synthesis, we expected to obtain triflate-containing platinum(II) complexes, but the main product of this reaction did not contain signals in the <sup>19</sup>F{H} NMR spectrum (Figure S1–S4). Apparently, in the reaction, the leaving chloride group, previously occupying a position in the inner coordination sphere of platinum(II), took over the role of the chloride anion, which was already in the outer sphere of the target complex. Further we will refer to this phenomenon as “counterion migration”. When further scaling up the synthesis, we also managed to isolate the triflate-containing fraction, which differed from the chloride-containing fraction only by the signal in the <sup>19</sup>F{H}NMR spectrum. The counterion distribution in the reaction mixture is random, and therefore the ratio of triflate- and chloride-containing fractions is not

reproduced during the synthesis. To overcome this disadvantage, an additional step was introduced: the reaction mixture was evaporated to dryness and redissolved in dichloromethane at the end of the first step. An excess of tetramethylammonium chloride (TMACl) was added to the resulting solution and the reaction mixture was stirred for one hour at room temperature. Further isolation proceeded according to the above scheme.

The reaction yields scaled on chloride-containing product, were 58-82%. These compounds were yellow solids, well-soluble in DCM and DMSO, slightly soluble in acetone, and insoluble in diethyl ether and hexane. Also, their interesting property is solubility in water.

The second-step metathesis of chloride anion to  $\text{BArF}^-$  afforded orange powders of  $\text{NN[BArF]}$  complexes, initially forming as a dry foam. The change of counterion improved solubility dramatically: target  $\text{NN[BArF]}$  complexes became well-soluble not only in DCM, DMSO and acetone, but also slightly soluble in  $\text{Et}_2\text{O}$ .

The complexes obtained were characterized by the polynuclear NMR spectroscopy,  $\text{ESI}^+$  mass-spectrometry and CHN analysis. Proton NMR spectra of all compounds were assigned using  $^1\text{H}^1\text{H}$  COSY experiment (Figs. S1–S8). The number of signals, their relative integral intensities and multiplicities, correspond to the proposed structures (Scheme 5). Complexes'  $^{31}\text{P}$  NMR spectra exhibit one singlet at ca. 21 ppm that is a characteristic chemical shift of  $\text{PPh}_2\text{Me}^+$  phosphonium fragment [125]. As it was stated before,  $^{19}\text{F}$  NMR spectra of compounds  $1\text{NN[Cl]}$ - $n\text{NN[Cl]}$  contain no signals. On the contrary,  $^{19}\text{F}$  NMR spectra of complexes **1–4** show one intensive signal of  $\text{BArF}^-$  anion at ca.  $-63$  ppm.  $\text{ESI}^+$  mass-spectra of series  $\text{NN[Cl]}$  and  $\text{NN[BArF]}$  exhibit one major signal of  $[\text{M}]^{2+}$ , fully matching predicted composition and isotopic distribution (Figs. S9–S10).  $\text{NN[BArF]}$  complexes also show characteristic bands for  $\text{C}\equiv\text{C}$  bonds in FTIR spectra (Figure S11) [126].

The structure of  $1\text{NN[Cl]}$  and  $2\text{NN[Cl]}$  complexes in the solid state was studied by single-crystal XRD. Figure 17 demonstrates the cationic part of the complex  $1\text{NN[Cl]}$  molecular structure. Figure S12 for  $2\text{NN[Cl]}$ , the table of crystallographic data and selected structural parameters (Tables S1, S2) can be found in the Appendix. Complexes  $1\text{NN[Cl]}$  and  $2\text{NN[Cl]}$  crystallize in a slightly distorted square-planar configuration,

usual for Pt(II) complexes. The coordination sphere of metalcenter is formed by the chelating **dtbpy** ligand and two alkynyl ligands coordinated through carbon of triple bond. The distances and angles of Pt(II) coordination environment fall in ranges presented in literature (see Table S2) [63,123,127–131].

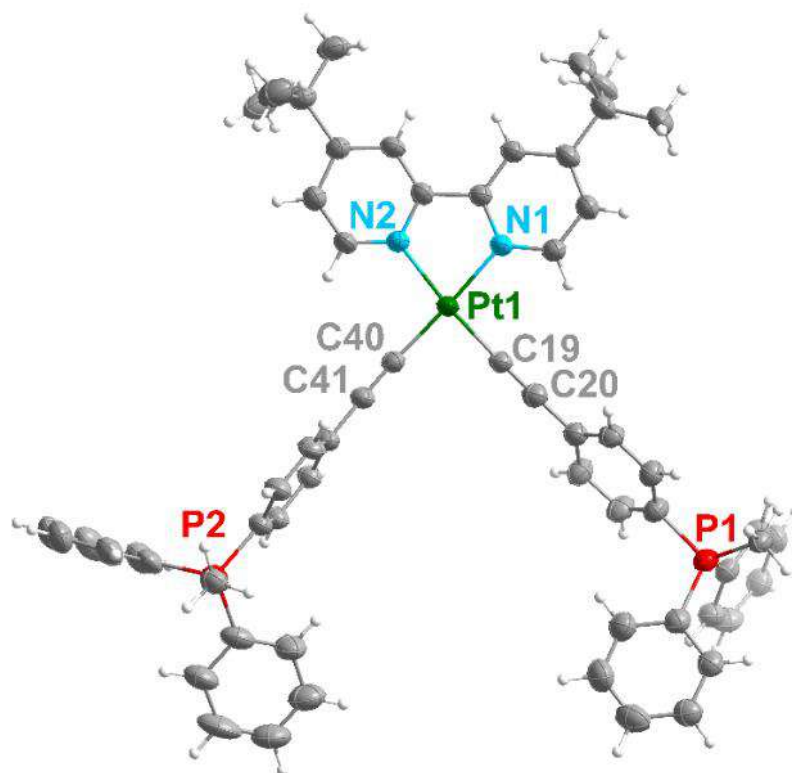


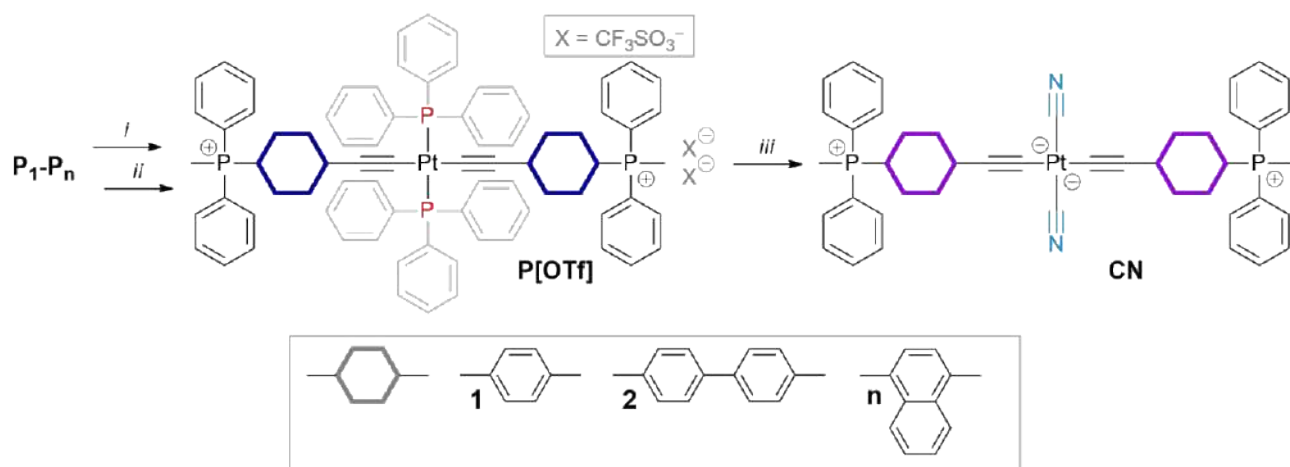
Figure 17. ORTEP view of **1NN[Cl]** molecular structure, the thermal ellipsoids are set at a 50% probability level. Counterions and solvent molecules are omitted for clarity.

Complex **1NN[Cl]** packs in a layered fashion. Each layer consists of **1NN** molecules, arranged tail-to-tail and forming a 3D zig-zag chain. Neither Pt–Pt metallophilic interactions, nor  $\pi\pi$  interactions are present in the structure. The packing behavior of **2NN[Cl]** is more complicated. The layers of this compound, consisting of tail-to-tail arranged molecules, form a herringbone macrostructure (Figure S13). Despite this fact, no weak interactions are present here. The solid-state structures of complex **1NN[Cl]** and **2NN[Cl]** correspond to the spectroscopic data. Moreover, these structural data additionally prove the absence of  $\text{CF}_3\text{SO}_3^-$  anion.

### 2.2.2. Bis-alkynyl Pt(II) complexes with ancillary PPh<sub>3</sub> and cyanide ligands

The next research objects are two series of bis-alkynyl Pt(II) complexes with *trans*-arrangement of triphenylphosphine and cyanide ligands. According to the literature, the *trans*-arrangement of acetylide ligands in the bis-alkynyl Pt(II) systems is more favorable for  $\pi$ -conjugation along the molecular axis [43,132,133]. In the case of alkynylphosphonium ligands **P<sub>i</sub>** this can promote emission characteristics of corresponding Pt(II) complexes. Starting from these series, we decided to abandon syntheses with the **P<sub>3</sub>** ligand carrying a terphenyl linker. The reason for this was the extremely labor-intensive synthesis of this alkynylphosphonium salt, as well as low yields in all reactions with its participation together with almost complete insolubility.

For the first series of *trans*-alkynyl Pt(II) complexes ancillary PPh<sub>3</sub> ligand was chosen. It is sufficiently air-stable and solid at room temperature. The synthesis was performed according to the modified literature method, [134] starting from the *cis*-[PtCl<sub>2</sub>(PPh<sub>3</sub>)<sub>2</sub>] precursor, in the CHCl<sub>3</sub>:Et<sub>3</sub>N 7:2 v/v mixture and using CuI as a catalyst (Scheme 6). As we have already discovered before [7,9], upon formation of alkynylphosphonium Pt(II) complexes, chloride anion can “migrate” from the Pt(II) precursor, leading to mixed counterionic composition. To avoid this, we have included second-stage metathesis with NaOTf. This reagent is more convenient than AgOTf because of its non-coordinating nature [135]. The resulting NaCl and the excess of NaOTf are easily removed by filtration of complexes' DCM solutions. The choice of triflate anion in this case was extremely convenient, since the complexes were purified from excess reagent and by-products of metathesis by simple filtration of the solution in dichloromethane, in contrast to metathesis to chloride anion, where column chromatography would have been required for purification. Complexes **1P[OTf]** – **nP[OTf]** are air-stable, soluble in CH<sub>2</sub>Cl<sub>2</sub> and DMSO, and sparingly soluble in chloroform, acetone and acetonitrile.



Scheme 6. Synthesis of **P[OTf]** and **CN** series. *i* =  $\text{cis-}[\text{Pt}(\text{PPh}_3)_2\text{Cl}_2]$ , 5 mol. %  $\text{CuI}$ ,  $\text{CHCl}_3:\text{Et}_3\text{N}=7:2$ , 24 h,  $35^\circ\text{C}$ ; *ii* =  $\text{NaOTf}$ ,  $\text{DCM}/\text{acetone}$ , 30 min, r.t.; *iii* = 4 eq  $\text{NaCN}$ ,  $\text{DCM}/\text{MeOH}$ , r.t.

Second series, featuring complexes **1CN–nCN**, was synthesized from the phosphine-alkynyl complexes **P[OTf]** using modified literature method [136]. It included stirring the precursor compounds **P[OTf]** with an excess of  $\text{NaCN}$  until formation of precipitate. Powders of creamy-white color corresponding to complexes **1CN** and **2CN** precipitated almost instantly, while for the complete reaction yielding compound **nCN** it took a day of stirring. Complexes **1CN–nCN** are neutral and have a zwitterionic nature. As we assume, this is the reason for their extremely low solubility: for instance, 1 mg of complex **2CN** needs ca. 30 ml of  $\text{DMSO}$  to dissolve completely. However, due to this fact, the separation of the pure compounds is rather straightforward.

Complexes of **P[OTf]** and **CN** series were fully characterized by polynuclear NMR spectroscopy,  $\text{ESI}^+$  mass-spectrometry, FTIR spectroscopy and elemental analysis. The multiplicities and integral intensities of complexes'  $^1\text{H}$  NMR spectra fully match the predicted ones (Scheme 6, Figs. S15–S17). The  $^{31}\text{P}\{\text{H}\}$  NMR spectra of **P[OTf]** series feature two signals: one singlet at ca. 21 ppm, corresponding to the phosphonium fragment, and second singlet at ca. 18 ppm with  $J_{\text{P-Pt}}$  coupling of ca. 2600 Hz, which is characteristic for the *trans*- location of  $\text{PPh}_3$  substituents. According to the published data [137,138], *cis*-location of  $\text{PR}_3$  ligands in  $\text{Pt}(\text{II})$  complexes results in larger  $J_{\text{P-Pt}}$  coupling values (ca. 3500 Hz). In the  $^{31}\text{P}\{\text{H}\}$  NMR spectra of **CN** complexes, the expected one

signal of phosphonium fragment is visible, confirming the full conversion of phosphine-alkynyl precursor (Figs. S18–S20).

Phosphine derivatives demonstrate one major signal in their ESI<sup>+</sup> mass-spectra (Fig. S21). This peak corresponds to the [M]<sup>2+</sup> molecular ion. For the cyanide series, the situation is much worse (Fig. S22). The low solubility together with zwitterionic nature leads to the low signals of corresponding molecular ions. For **1CN**, no signal of molecular ion was observed at all.

The FTIR spectra of all studied compounds (Fig. S23) exhibit an absorption band of C≡C bond in the expected region. For the phosphine derivatives, this absorption lies in the range of 2087–2107 cm<sup>-1</sup>, whereas for cyanide ones it is shifted to the 2075–2095 cm<sup>-1</sup>. This was already discussed in the literature [136], and was primarily attributed to a lesser electronic  $\pi$ -back donation from the metallocentre to the acetylide ligands, as the cyanide ligand is better  $\pi$ -acceptor than phosphine. Complexes of **CN** series also possess an additional signal of C≡N stretching band, located at 2104–2114 cm<sup>-1</sup>, which was also expected according to the published data [136,139,140].

For complexes **1P[OTf]** and **nP[OTf]**, single-crystal XRD studies were also performed. The key crystallographic data and selected structural parameters could be found in the Appendix (Table S3, S4). The crystal structures of both compounds confirm the *trans*-configuration, that was predicted on the basis of the <sup>31</sup>P{H} NMR spectra. The Pt(II) atom in both systems adopts slightly distorted square-planar geometry, whereas C–Pt–C and P–Pt–P fragments are ideally linear with corresponding angles of 180° (Figure 18). The bond lengths and angles lie in the range, reported in the literature for Pt(II) complexes with the same structural motif [141–144]. The packing of both **1P[OTf]** and **nP[OTf]** features no metallophilic or  $\pi$ -interactions, and the molecules are arranged in the layered fashion.

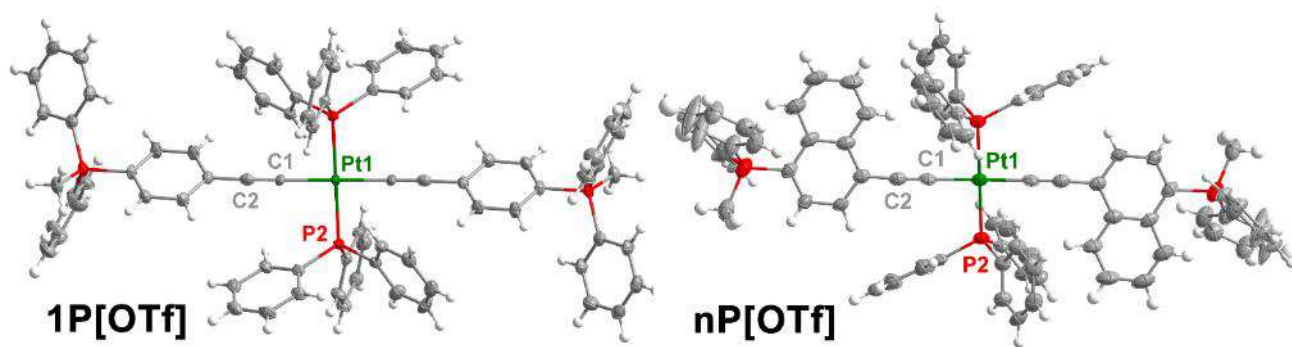
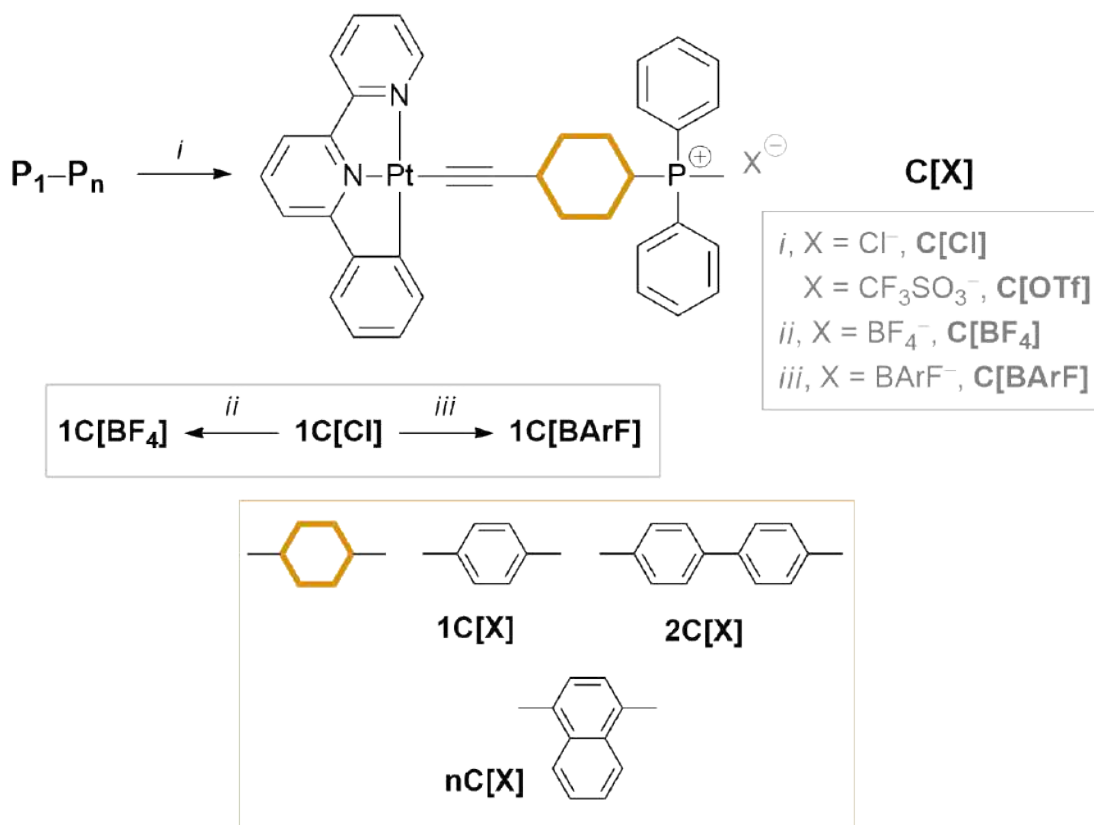


Figure 18. ORTEP view of **1P[OTf]** and **nP[OTf]** molecular structure, the thermal ellipsoids are set at a 50% probability level. Counterions and solvent molecules are omitted for clarity.

### 2.2.3. Mono-alkynyl Pt(II) complexes with ancillary C<sup>n</sup>N<sup>n</sup> ligand

Complexes with ancillary **phbpy** ligand were synthesized according to the modified literature method [145] starting from Pt(phbpy)Cl precursor via abovementioned copper-catalyzed substitution of chloride to alkyne (Scheme 7).



Scheme 7. Synthesis of **C[X]** series. *i* = Pt(phbpy)Cl, CuI, DCM:Et<sub>3</sub>N=7:2, 18 h, r.t.; *ii* = NaBF<sub>4</sub>, DCM/MeOH, 1 h, r.t.; *iii* = NaBArF, DCM/Et<sub>2</sub>O, 1 h, r.t.

The argon-purged solution of the platinum precursor and alkynylphosphonium ligand was loaded with 5 mol.% of copper iodide, followed by triethylamine. The reaction mixture was stirred at room temperature overnight. The reaction mixture was evaporated and purified with column chromatography using silica as adsorbent. As the starting materials contained different counterions, chloride in the platinum precursor and triflate anion in the alkynylphosphonium salt, we found two different Pt-containing fractions on the chromatography column. The resulting complexes **1C[Cl]** and **1C[OTf]** were dramatically different in color in the solid state: orange for chloride and dark-green for triflate species. This inspired us to investigate the influence of counterion on the emission properties of studied compounds. For this purpose, tetrafluoroborate- and BArF-containing complexes were obtained. These derivatives of **1C[X]** series were synthesized by adding to the solution of **1C[Cl]** in dichloromethane methanol solution of 5 eq NaBF<sub>4</sub> and diethyl ether solution of 1 eq NaBArF, respectively. After stirring for 1 hour at room temperature, the suspensions were filtered through celite, then evaporated, washed with hexane, and dried in vacuo.

All complexes of the **C[X]** series are readily soluble in DMSO, chloride derivatives are soluble in polar and weakly polar organic solvents (MeOH, MeCN, acetone and DCM), as well as in water. BArF-complexes form solutions in most common polar (methanol, acetonitrile, acetone) and less polar (dichloromethane, diethyl ether) organic solvents. **1C[BF<sub>4</sub>]** and **1C[OTf]** are soluble in MeOH and acetone.

All obtained complexes were characterized by the standard set of methods: polynuclear NMR spectroscopy, CHN analysis, FTIR spectroscopy and ESI<sup>+</sup> mass-spectrometry. <sup>1</sup>H, <sup>31</sup>P{H}, <sup>19</sup>F and <sup>1</sup>H<sup>1</sup>H COSY NMR spectra (Figures S25–S27) were used to confirm the solution structure and the type of counterion of studied compounds. The number of signals, their multiplicities and integral intensities correspond to the predicted from the structure ones (Scheme 7). Complexes' <sup>31</sup>P NMR spectra exhibit one singlet at ca. 21 ppm that is a characteristic chemical shift of PPh<sub>2</sub>Me<sup>+</sup> phosphonium fragment [125]. <sup>19</sup>F NMR spectra of chloride complexes contain no signals. On the contrary, <sup>19</sup>F NMR spectra of BArF complexes demonstrate intensive signals, corresponding to the different fluorine-containing counterions (Figure S28). The ESI<sup>+</sup>

mass-spectra of the Pt(II) complexes feature one intensive ion signal with the expected composition and isotopic distribution (Figure S29). Complexes **1C[Cl]**–**nC[Cl]** also show characteristic bands for C≡C bonds in FTIR spectra (Figure S30) [126].

Gas-phase diffusion in the MeOH/pentane systems allowed us to obtain the crystal structures of **2C[Cl]** and **3C[Cl]**, crystallographic data are listed in Table S1. However, the crystal of the former compound was of very poor quality, and can be only used as the image of the structural motif (Figure S31). In the **nC[Cl]** structure, the Pt(II) atom has a distorted square-planar coordination environment, which is governed by the **phbpy** ligand (Figure 19).

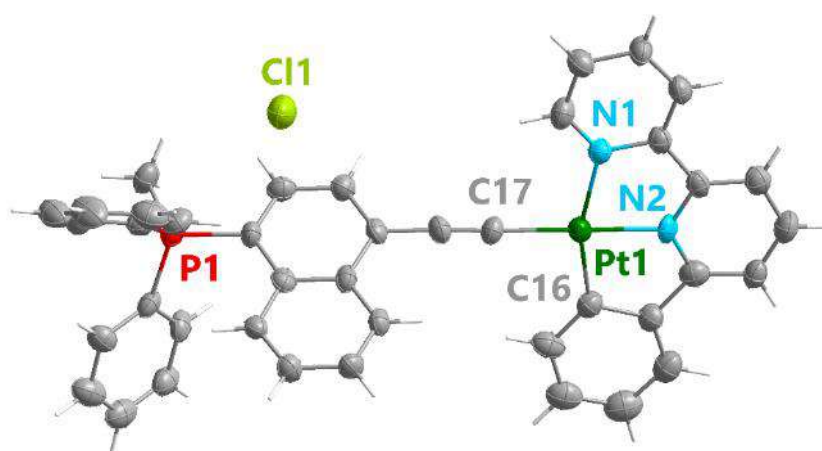


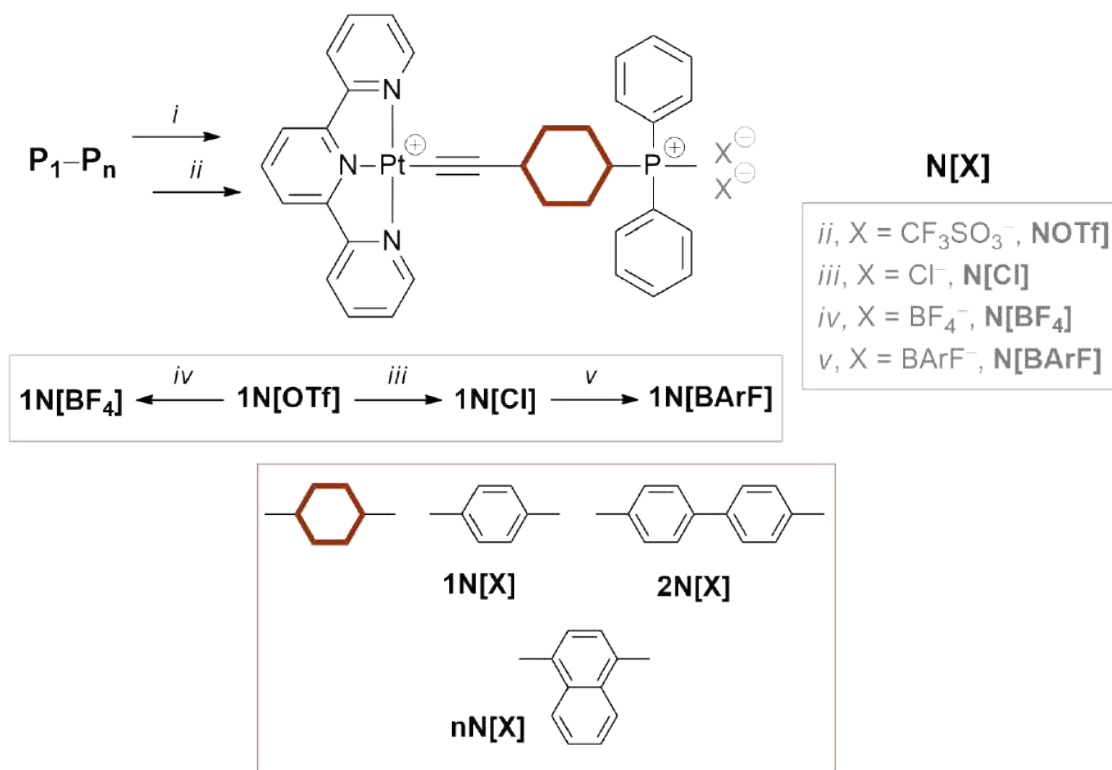
Figure 19. ORTEP view of **nC[Cl]** molecular structure, the thermal ellipsoids are set at a 50% probability level. Solvent molecules are omitted for clarity.

The overall packing of this complex is determined by the parallel-displaced  $\pi$  stacking, which is present both in naphthyl fragments and in the central pyridine rings of the **phbpy** ligands. As a result, the molecules are packed in a head-to-head (**phbpy**, distance between C<sup>^</sup>N<sup>^</sup>N planes is 3.376 Å) and tail-to-tail (naphthyl, distance between naphthyl planes is 3.372 Å) manner simultaneously, forming parallel layers (Figure S32).

Continuing the topic of synthesis of single-charged monoalkynyl complexes of platinum(II), we cannot but note the attempts to synthesize a series of alkynylphosphonium complexes with an additional N<sup>^</sup>C<sup>^</sup>N ligand 2,5-dipyridylbenzene. According to literature data, such complexes should have bright emission, but it was not possible to obtain such systems using alkynylphosphonium ligands. Schemes of the performed syntheses are shown in Fig. S33.

### 2.2.4. Mono-alkynyl Pt(II) complexes with ancillary N<sup>n</sup>N<sup>n</sup>N<sup>n</sup> ligand

Complexes of N[X] series were synthesized similar to the C[X] series (Scheme 8). However, we had to modify the literature method because of the solubility issues.



Scheme 8. Synthesis of N[X] series. *i* = [Pt(terpy)Cl]Cl, 5 mol. % CuI, MeOH:Et<sub>3</sub>N=7:2, 60 h, 55°C; *ii* = without purification, 2.3 eq AgOTf, 0°C, 1 h; *iii* = 5 eq. TEACl, acetone, 24 h; *iv* = 5 eq. NaBF<sub>4</sub>, acetone/MeOH, 24 h, r.t.; *v* = NaBArF, DXM/Et<sub>2</sub>O, 1 h, r.t.

We chose MeOH as a solvent because of the low solubility of [Pt(terpy)Cl]Cl in DCM, and stirred the reaction mixture for 60 hours at 55°C. The completion of the reaction was monitored with TLC chromatography. For these species, we were not able to separate different counterions using column chromatography. In order to get the complexes with pure anionic composition, we cooled the reaction mixture to the 0°C on the ice bath, added 2.3 equivalents of AgOTf and stirred the reaction mixture for 1 hour. The resulting precipitate of N[OTf] and AgCl was centrifuged, dissolved in acetone:MeOH 3:1 mixture and filtered through the celites, yielding pure N[OTf]. The synthesis of N[Cl] included stirring N[OTf] in acetone with an excess of

tetraethylammonium chloride. Tetrafluoroborate and BArF compounds **1N[X]** were synthesized similar to the **1C[X]** series (Scheme 8). However, for yielding the **1N[BF<sub>4</sub>]** complex the stirring was made for 24 h.

Complexes of the **N[X]** series have worse solubility compared to the **C[X]** series. They are well soluble in DMSO and methanol, chloride derivatives are also soluble in acetonitrile and water. The derivatives containing BArF<sup>-</sup> anions are expected to form solutions with almost all polar (methanol, acetonitrile, acetone) and less polar (dichloromethane, diethyl ether) organic solvents. **1N[OTf]** is well soluble in acetone, **1N[BF<sub>4</sub>]** in acetonitrile.

All obtained complexes were characterized by the standard set of methods: polynuclear NMR spectroscopy, CHN analysis, FTIR spectroscopy and ESI<sup>+</sup> mass-spectrometry. <sup>1</sup>H, <sup>31</sup>P{H}, <sup>19</sup>F and <sup>1</sup>H<sup>1</sup>H COSY NMR spectra (Figures S34–S36) were used to confirm the solution structure and the type of counterion of studied compounds. The number of signals, their multiplicities and integral intensities correspond to the predicted from the structure ones (Scheme 8). Complexes' <sup>31</sup>P NMR spectra exhibit one singlet at ca. 21 ppm that is a characteristic chemical shift of PPh<sub>2</sub>Me<sup>+</sup> phosphonium fragment [125]. <sup>19</sup>F NMR spectra of chloride complexes contain no signals. On the contrary, <sup>19</sup>F NMR spectra of BArF complexes demonstrate intensive signals, corresponding to the different fluorine-containing counterions (Figure S37). The ESI<sup>+</sup> mass-spectra of the Pt(II) complexes feature one intensive ion signal with the expected composition and isotopic distribution (Figure S38). Complexes **1N[Cl]–nN[Cl]** also show characteristic bands for C≡C bonds in FTIR spectra (Figure S39) [126]. The attempts to crystallize any of the **N[X]** series compounds were fruitless, as they formed either oily substances or crystalline powders, not suitable for single-crystal XRD studies.

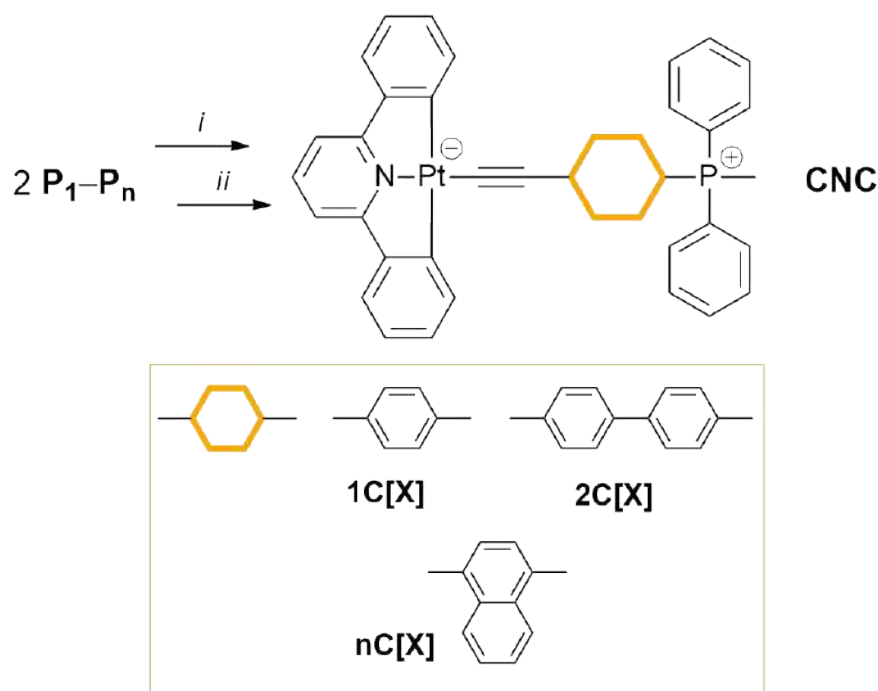
### 2.2.5. Mono-alkynyl Pt(II) complexes with ancillary C<sup>^</sup>N<sup>^</sup>C ligand

The synthesis of bis-cyclometallated Pt(II) complexes with ancillary 2,6-diphenylpyridine requires more complex synthetic protocol compared to another mono-alkynyl systems, studied in this work. Apparently, this is due to the formation of neutral

{Pt-CNC} fragment with low electrophilicity, which hampers the interaction between deprotonated alkynyl ligand with the metal center.

There is only one example of such complexes synthesis described in the literature [97]. We have developed modified literature method, which included reaction of 2 eq of corresponding alkynylphosphonium ligand with 10% excess of nBuLi solution at  $-50^{\circ}\text{C}$  for 30 min with subsequent addition of [Pt(dphpy)dmsO] (Scheme 9).

Due to the positive-charged phosphonium fragment on the periphery of the ligand environment, the target compounds have zwitter-ionic nature and do not possess negative charge, as their arylalkynyl analogues  $(\text{NBu}_4)[\text{Pt}(\text{CNC})(\text{C}\equiv\text{C}-\text{Ar})]$  do [97]. This also leads to the low insolubility of yielded compounds and simplifies the isolation and purification processes. Compared to the literature method, [97] higher yields were generally observed. Besides, our method involved less amount of alkynylphosphonium ligand (1:8 molar ratio of Pt(II) precursor to the alkyne in the literature *versus* 1:2 molar ratio in our method).



Scheme 9. Synthesis of **CNC** series. *i* = 10% excess nBuLi,  $-50^{\circ}\text{C}$ , 30 min; *ii* = [Pt(dphpy)dmsO], leave until reaches r.t., 18 h.

The identity of **CNC** series compounds was fully established by  $^1\text{H}$ ,  $^{31}\text{P}\{\text{H}\}$  and  $^1\text{H}-^1\text{H}$  COSY NMR experiments together with ESI+ mass-spectra, FTIR spectroscopy and CHN analysis (Figures S40–S43). For **1CNC**, single-crystal diffraction studies were

also conducted. In the  $^1\text{H}$  NMR spectra, which were interpreted using  $^1\text{H}$ - $^1\text{H}$  COSY experiment, all the integral intensities and multiplicities correspond to the proposed ones (Scheme 9).  $^{31}\text{P}\{\text{H}\}$  spectra demonstrate one signal at ca. 21 ppm, which is characteristic for the phosphonium group [146]. The ESI+ mass-spectra are dominated by two signals, corresponding to the  $[\text{M}+\text{H}]^+$  and  $[\text{M}+\text{MeOH}+\text{H}]^+$  fragments, as the studied systems are neutral. FTIR experiment shows the  $\text{C}\equiv\text{C}$  vibrations in the expected area (ca.  $2100\text{ cm}^{-1}$ ).

Complex **1CNC** was crystallized from the diluted acetone solution. The key crystallographic details and some selected bond angles and distances are summarized in the Tables S4, S5). Single-crystal XRD studies revealed the expected distorted square-planar configuration of the metal center (Figure 20). Among the four Pt(II) bonds, the Pt –  $\text{C}_{\text{aryl}}$  distances are nearly the same, whereas Pt – N and Pt –  $\text{C}_{\text{alkynyl}}$  are much shorter. The bond angle between  $\text{C}_{\text{aryl}} - \text{Pt} - \text{C}_{\text{aryl}}$  differs from ideal  $180^\circ$  by  $20^\circ$ , which is caused by the rigidity of the CNC ligand. The Pt – alkynyl part of the structure is slightly bent, and as we suppose, it can be induced by the bulky phosphonium fragment. Overall, the observed crystallographic parameters are in line with the reported experimental data of isostructural compounds [97]. The packing of **Pt1** demonstrates paired molecules in head-to-tail fashion, which is easily explained by zwitterionic nature of the compound (Fig. S44). These molecular “duets” form two layers, arranged in a “herringbone” manner. No weak interactions were found in the structure.

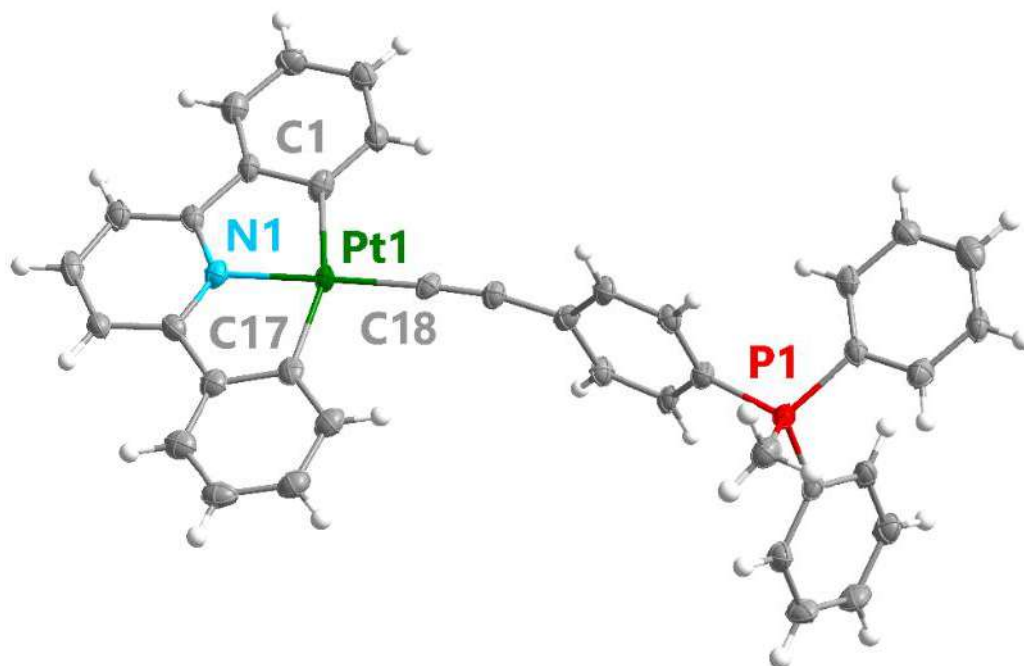


Figure 20. ORTEP view of **1CNC** molecular structures, the thermal ellipsoids are set at a 50% probability level. Counterions and solvent molecules are omitted for clarity.

## 2.3. Photophysical properties of Pt(II) complexes

### 2.3.1. Bis-alkynyl Pt(II) complexes with N<sup>N</sup> ancillary ligand

The study of NN[BArF] series' photophysics included both solution and solid state. The absorption spectra of NN[BArF] complexes in acetonitrile solution feature two bands (Figure 21, Table 1).

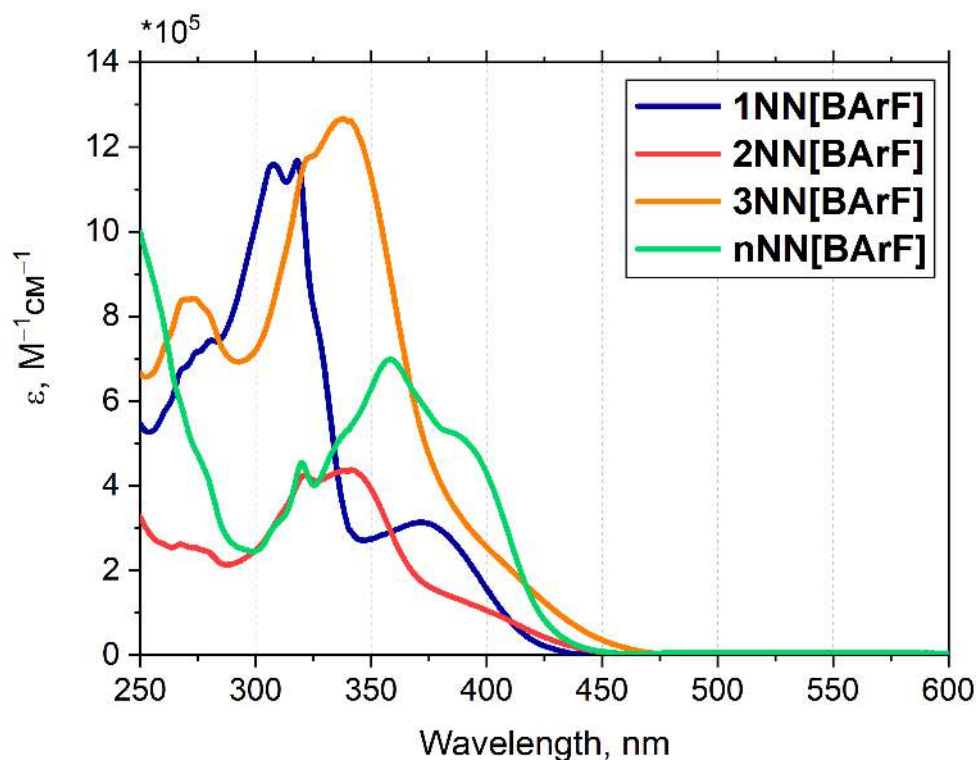


Figure 21. UV-vis spectra of NN[BArF] complexes, MeCN, r.t.

The absorption maxima of high-energetic ones lie in the range of 260–360 nm. These bands are usually assigned to  $\pi\pi^*$  ligand centered (LC) transitions of diimine ligand and arylalkynyl ligands [147–149]. However, in this case, the contribution of alkynylphosphonium ligand is more prominent than of **dtbpy**, as absorption spectra of complexes NN[BArF] mimic those of free **P<sub>1</sub>-P<sub>n</sub>** ligands [6]. The low-energy bands, lying in the range of 360–450 nm, presumably originate from metal-to-ligand charge transfer [21,148]. For spectra of complexes 2NN[BArF] and 3NN[BArF], it is hard to estimate the absorption maxima of low-energetic band, as they overlap with high-energetic bands. As a result, the MCLT transition in complex 3NN[BArF] is nearly invisible. Overall, the absorption bands of compounds NN[BArF] are similar to those for compounds with

neutral acetylide ligands, reported in literature, but have a more complex shape due to the presence of the phosphonium fragment [63,123,124,128].

Table 1. Optical and photophysical properties of **1NN[BArF]**–**nNN[BArF]** complexes in 1,2-dichloroethane solution, r.t.

Complex	$\lambda_{\text{abs}}$ , nm	$\lambda_{\text{em}}$ , nm	$\tau$ , ** ns		QY, * %	
			aerated	deaerated	aerated	deaerated
<b>1NN[BArF]</b>	307, 318, 372	503	115	172	3	4
<b>2NN[BArF]</b>	266, 321, 339, ~390	542	429	8258	2	13
<b>3NN[BArF]</b>	273, 323, 336, ~390	561	376	7462	2	10
<b>nNN[BArF]</b>	320, 350, 386	565	769	19259	<1	2

\*  $\lambda_{\text{ex}}$  365 nm. \*\*  $\lambda_{\text{ex}}$  351 nm

All obtained complexes demonstrate moderately intense emission in DCE solutions at room temperature (Figure 22). Emission maxima, as well as solution quantum yields and lifetimes, are summarized in Table 1. Emission spectra of complexes **1 NN[BArF]**–**3 NN[BArF]** feature broad, nearly structureless bands typical for MLCT (Figure 22). Upon the elongation of the linker from phenyl to terphenyl, the luminescence energy demonstrates bathochromic shift. We have also compared the obtained emission spectra to their isostructural analogues without phosphonium fragment, which were described early [124]. The comparison reveals that the introduction of electron-accepting functional group leads to a hypsochromic shift of emission in a pair of similar compounds. This is in line with other literature data, where electron-withdrawing ligands are reported to be commonly used for blue-shifting emission, as acceptor moiety lowers the HOMO, thus enlarging the HOMO–LUMO gap [128,147,150].

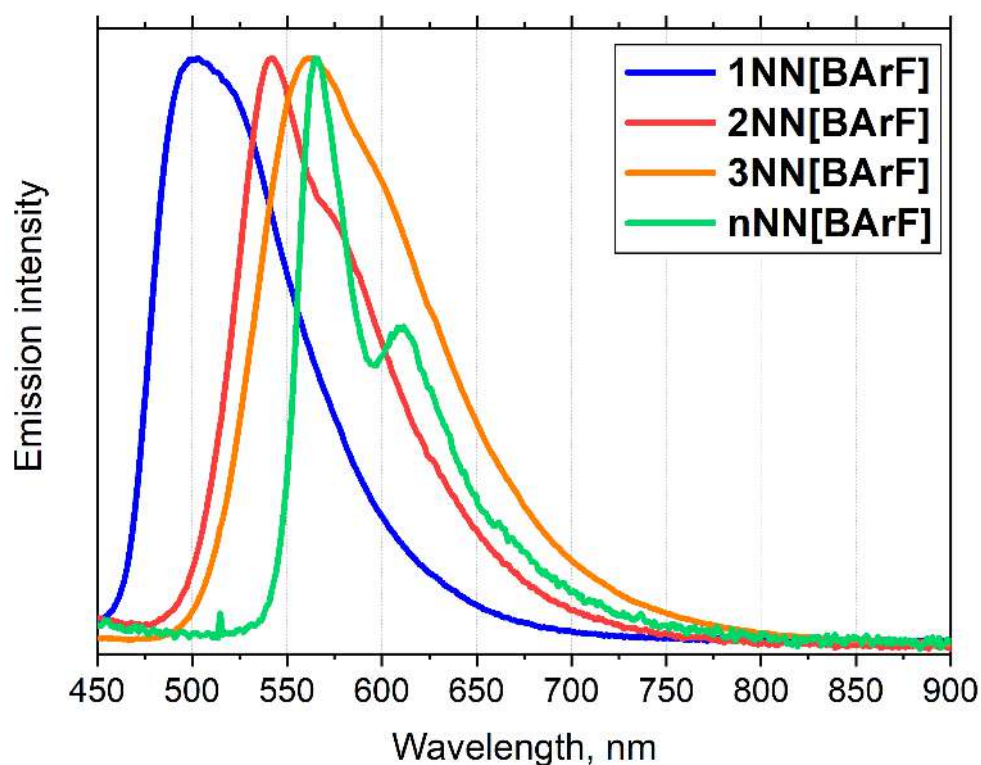


Figure 22. Normalized emission spectra of **NN[BArF]** complexes, 1,2-DCE, r.t.,  $\lambda_{\text{ex}}$  365 nm.

Complex **nNN[BArF]**, bearing naphthalene linker, which is similar to phenyl in length, nevertheless, demonstrates nearly the same  $\lambda_{\text{em}}$  as complex **3NN[BArF]**. This phenomenon is reported in the literature for D- $\pi$ -A type phosphonium salts with different  $\pi$ -conjugated linkers: the introduction of the polycyclic moieties into luminophore usually results in bathochromic shift [119]. The shape of the emission spectra for this compound is different compared to the other ones in this series. It has vibronic structure, and thus we attribute the luminescence to the  $^3\text{LC}$  type, localized in the naphthyl fragment. The vibronic progression of  $\sim 1300\text{ cm}^{-1}$ , characteristic for naphthalene, proves this hypothesis.

Upon deaeration, the luminescence intensity for complexes **2NN[BArF]**–**nNN[BArF]**, increases distinctly, implying the triplet origin of the emission state. The quantum yields in deaerated solutions reflect this trend and increase more than in eight times for **2NN[BArF]** and **3NN[BArF]** and twice for **nNN[BArF]** (Table 1). The lifetime values confirm the abovementioned statement about triplet emission, increasing upon deaeration from the nanosecond to microsecond ranges.

On the contrary, the luminescence intensity of complex **1NN[BArF]**, only slightly increases upon deaeration, and so do emission quantum yields and lifetimes. Moreover, the excited-state lifetime of complex **1NN[BArF]** in deaerated solution is substantially shorter than for other complexes in the series. One possible explanation for this can be a more pronounced MLCT character of emission in this complex. Upon the elongation of the linker, LC contribution to the emission is increasing along with the increase of the excited state lifetime values. Changing the polarity of the solvent does not show any significant effect on the optical and photophysical properties of compounds **NN[BArF]**, although some emission quenching is expectedly observed in a polar solvent (acetonitrile). This effect was studied in the literature for diimine Pt(II) complexes [21]. The interpretation of solution photophysical properties in **NN[BArF]** series is confirmed by TD-DFT quantum-chemical calculations.

Complexes **1NN[BArF]**–**nNN[BArF]** also demonstrate emission in the solid state (Figure 23, Table 1). At 292K, complexes show broad structureless emission spectra, typical for transitions with a significant contribution of charge transfer. Overall, at room temperature, the solid-state emission spectra of complexes **1NN[BArF]**, **2NN[BArF]** and **nNN[BArF]** are bathochromically shifted compared to solution spectra. According to the literature data, this is usually rationalized as the effect of Pt–Pt interactions present in the solid state [151–156], which was described in the chapter **Ошибка! Источник ссылки не найден.** The HOMO–LUMO transition in this case is a metal/metal-to-ligand charge transfer (MMLCT), and the emission is shifted bathochromically [64]. Complex **nNN[BArF]** has an additional band on the high-energy part of the spectrum, which could be attributed to the monomeric species, emerging from slightly ground sample. This effect will be discussed later. The behavior of complex **3NN[BArF]** is different, as its solid-state emission energy is nearly the same as that of the solution. The reasons for that will be also discussed below.

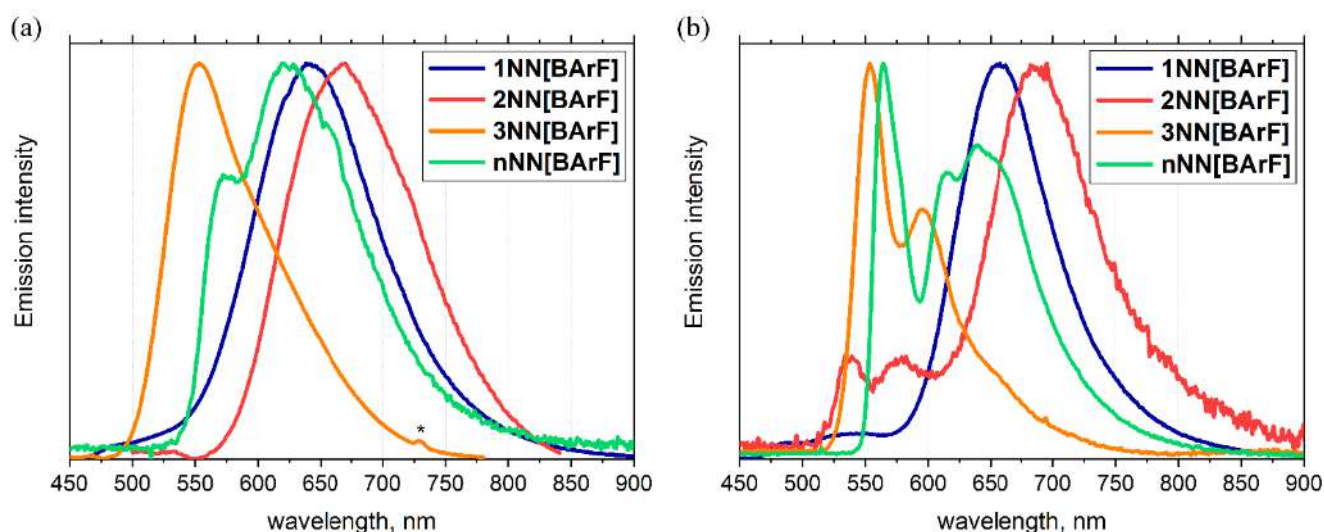


Figure 23. (a) Normalized solid-state emission spectra of **NN[BArF]** series, r.t.; (b) normalized solid-state emission spectra of **NN[BArF]** series, 77 K. An asterisk denotes an artifact of the optical system,  $\lambda_{\text{ex}}$  365 nm.

Upon cooling, emission of complex **1NN[BArF]** exhibits bathochromic shift that is also indicative of transitions of MMLCT nature. As the temperature decreases, the lattice shrinks, thus shortening the Pt–Pt distance. The Pt–Pt interaction strengthens, and the MMLCT excited state energy decreases, producing a red-shift of the photoluminescence [19]. Complex **3NN[BArF]** on the contrary, demonstrates no shift along with vibronic structuration of the emission spectrum upon cooling. This phenomenon, together with similarity of emission maxima in solution and solid state, points out the origin of emissive excited states to be LC (ligand-centered) rather than MLCT. It was already shown in the literature for Re(I) [157] and Pt(II) [16,37,158] complexes, and the remarkable increase of the excited state lifetimes (Table 2) support this hypothesis. However, the LC triplet emission might have an admixture of MLCT character, as the lifetime decay is biexponential.

Complexes **2NN[BArF]** and **nNN[BArF]** show more complicated behavior. In the spectra of compound **nNN[BArF]**, as was already mentioned above, two bands are present: one presumably attributed to  $^3\text{LC}$  of the monomer, and the second one, arising from  $^3\text{MMLCT}$  as result of Pt–Pt aggregates formation. For complex **2NN[BArF]**, the band of the monomer is only visible at 77 K, where its intensity drastically increases. As

a proof of this concept, we compared the emission maxima upon cooling. For the high-energy  $^3\text{LC}$  band, the hypsochromic shift together with vibronic structuration occurs upon lowering the temperature to 77 K, and the low-energy  $^3\text{MMLCT}$  band demonstrates bathochromic shift like for complex **1NN[BArF]**. For **2NN[BArF]** and **nNN[BArF]** the excited state lifetime values also increase drastically, and are fitted by the biexponential decay due to two different emission bands. It is interesting to note that in contrast to the solution, the complex **1NN[BArF]**, has the largest quantum yield in the solid state and the smallest in the solution.

Table 2. Photophysical properties of complexes **NN[BArF]** in frozen solutions at 77 K and in the solid state.

Complex	$\lambda_{em}$ [frozen solutions], nm	$\lambda_{em}$ [solid state], nm		$\tau$ [solid state], ns		QY [solid state, r.t.], %
		77 K	r.t.	77 K	r.t.	
<b>1NN[BArF]</b>	acetone: 460 DCE: 465, 611 MeCN: 468, 612	658	638	1076.33	691.67	27.1
<b>2NN[BArF]</b>	DCE: 517	538, 685	663	1190.37*	616.33	5.8
<b>3NN[BArF]</b>	DCE: 531	553	553	37059.36*	1426.0	1.5
<b>nNN[BArF]</b>	DCE: 556	564, 639	572, 628	59142.50*	3984.78*	6.1

\* Amplitude average lifetime  $\tau_{aver} = \sum A_i \tau_i$  was calculated according to published method [159].

To further investigate the emission properties of **NN[BArF]** complexes, measurements of luminescence spectra were made in frozen solutions at 77 K (Figure 24, Table 2). For the most peculiar one, namely complex **1NN[BArF]** the color of emission was varied depending on the solvent (MeCN, DCE and acetone were tested), as it is

shown in the Figure 24b. For other complexes, there was no change in luminescence color in different media, so results obtained only in DCE are discussed.

It has been found that inside of a series **1NN[BArF]**–**nNN[BArF]** the emission energy is shifted bathochromically depending on the linker length, similar to the solution at room temperature experiment (Figure 22). For all complexes, the blue shift of  $\lambda_{em}$  in frozen solvent is observed compared to the room temperature one. This phenomenon is usually rationalized by the hindered reorientation of solvent molecules at low temperatures, so the emission occurs from the unrelaxed state [160,161]. For all complexes, the vibronic resolution is also visible that is common for MLCT/LC excited states, and this phenomenon can be a result of temperature ‘switching’ of emissive state [37,76,162].

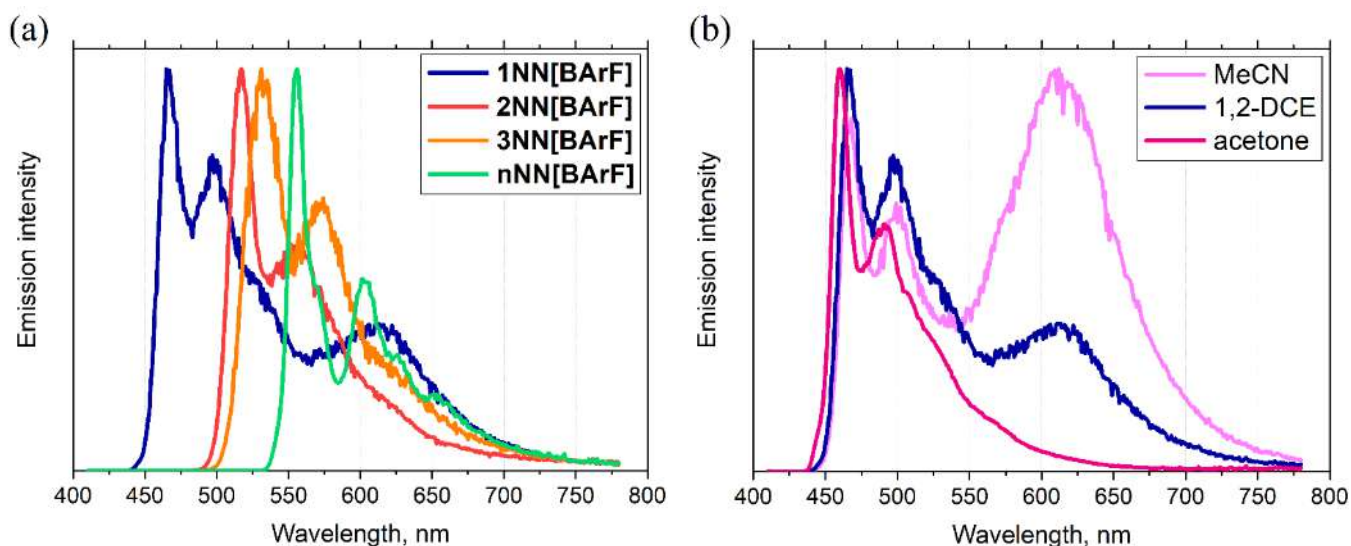


Figure 24. (a) Normalized emission spectra of **NN[BArF]** in frozen DCE, 77 K; (b) normalized emission spectra of **1 NN[BArF]** in different frozen solvents, 77 K;  $\lambda_{ex}$  365 nm

Complex **1NN[BArF]** showed different behavior, demonstrating two emission bands at low temperature frozen solutions (Figure 24b). The high energy (HE) band has vibronic resolution and nearly the same emission maximum for all solvents, while the low energy (LE) one is nearly invisible in acetone, emerges in DCE and drastically raises in acetonitrile. Surprisingly, the increase of this band does not correlate with the polarity of the solvent. We assume that due to the lower solubility under low temperature, the

aggregation process starts, and acetonitrile, being the most compact molecule among three examined, hinders this process to the minimum, thus the aggregation band is the most pronounced for it. The presence of the aggregation band only in complex **1NN[BArF]** can be explained by its sterical properties: other complexes, probably, are too bulky to form aggregates in the frozen solutions.

Summarizing the emission properties up, we can conclude that the nature of the excited state in **1NN[BArF]**–**nNN[BArF]** depends on the linker length and aggregation formation. The complex **1NN[BArF]** with “shortest” ligand demonstrates emission, originating mostly from MLCT state with admixture of LC in solution and MMLCT state in the bulk. Upon elongation of the linker, the emission state gradually changes to LC one, finishing at complex **nNN[BArF]**, and formation of Pt–Pt dimer is unfavourable for the complex **3NN[BArF]**. For the complex **nNN[BArF]**, both monomeric and aggregated species are present in the bulk state, probably because of bulky naphthyl fragment.

Pt(II) complexes are widely known to possess non-linear optical properties, such as two-photon induced emission (TPIE) [124,163]. The work of Melekhova et al., [124], dealing with alkynyl-biphenyl and alkynyl-terphenyl complexes of Pt(II), strongly resembling those described here, inspired us to investigate TPIE properties of complexes **1NN[BArF]**–**nNN[BArF]**. The theoretical framework and experimental protocol for these measurements can be found in the work of Melnikov et al. [164]. Two-photon emission spectra of compounds **1NN[BArF]**–**nNN[BArF]** (Figure 25) are shown in Fig. 3C. Comparing to the one-photon excited emission spectra (Figure 22), we can conclude that they are nearly identical. The two-photon absorption process was confirmed by a power-dependence experiment (Figure S45). Also, all complexes showed no sign of decomposition under the experimental conditions. Acetonitrile solutions of complexes **1NN[BArF]**–**nNN[BArF]** show two-photon absorption cross-section in the range of 20–400 GM, that is ten times more than reported in the literature for analogues to date [124,163,165,166]. Emission data for compounds **1–4** in MeCN solution are summarized in the Table S6 in Appendix.

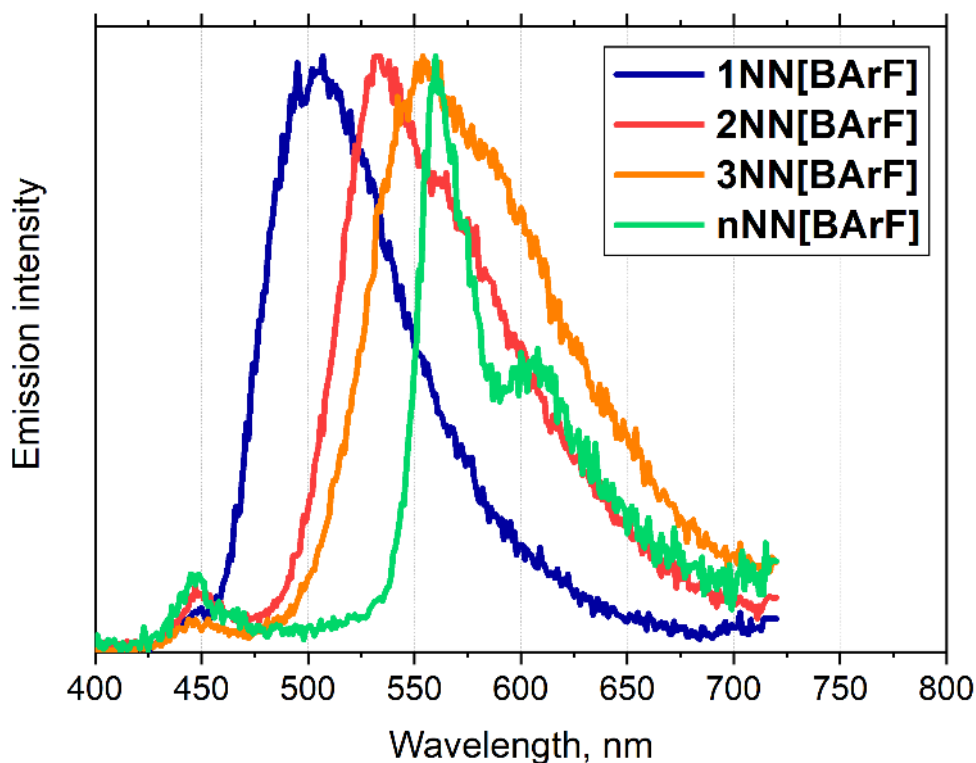


Figure 25. Normalized two-photon induced emission spectra of **NN[BArF]** series, MeCN, r.t.,  $\lambda_{\text{ex}}$  790 nm

The solid-state photophysical properties of **nNN[BArF]** together with realization of metallophilic interactions in **1NN[BArF]** inspired us to investigate *stimuli-responsive* properties of **NN[BArF]** series. To achieve this, we performed a series of experiments, measuring solid-state emission spectra after each one. Initially, the bulk, “as-obtained” crude solid was investigated. Then, it was ground in the mortar with pestle to break up the Pt–Pt aggregates, fumed with Et<sub>2</sub>O, and mixed with one drop of hexafluorobenzene. Emission spectra of all states and their CIE 1931 color coordinates are presented in Figure 26, and Figures S46, S47. Emission characteristics, including excited state lifetimes and quantum yields after grinding, are presented in Table S7 in Appendix.

Despite the fact that complexes **NN[BArF]** are completely amorphous both as bulk and ground powders, all recorded emission spectra clearly show the existence of *stimuli-responsive* properties in the studied systems. Solid-state <sup>3</sup>MMLCT emission of complex **1NN[BArF]** has orange color, visible to the naked eye. After grinding the aggregation is partly destroyed, as we see more intensive additional emission band at 503 nm, which coincides with emission band of solution, attributed to the “monomeric” emission (Figure

26). We assume that mechanical grinding leads to the partial destruction of Pt–Pt aggregates. However, for bulk powder of **1** NN[BArF], **2** NN[BArF] and **n** NN[BArF] the mechanical grinding even for 15 minutes is not enough to break up all the Pt–Pt aggregates (Figure S46). Fuming the ground powder of complex **1** NN[BArF] with diethyl ether, as well as dichloromethane, chloroform, methanol, acetonitrile and THF, results in the dramatic decrease of emission intensity of the high energy “monomeric” band, and similar trend is visible for the complexes **2** NN[BArF] and **4** NN[BArF] (Figure S46). We assume that exactly this band was becoming more pronounced in the 77 K solid-state emission spectra of **2** NN[BArF] (Figure 23b), as the setup of the emission measurement experiment could lead to the slight grinding of the sample.

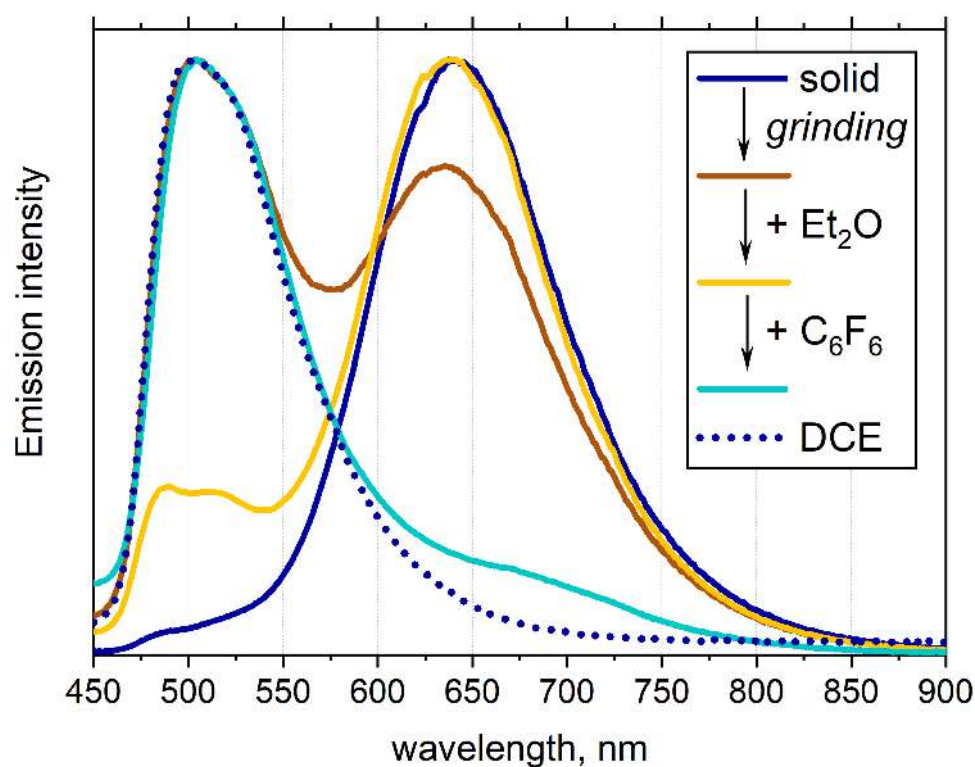


Figure 26. Normalized emission spectra of **1** NN[BArF] in *stimuli-responsive* experiments, r.t..  $\lambda_{\text{ex}}$  365 nm

The next step was an investigation of hexafluorobenzene influence, as there are several examples in the literature, showing the formation of so-called “reverse sandwich” complexes with  $\text{C}_6\text{F}_6$  with different from parent complexes emission [167,168]. The “reverse sandwich” compounds are based on non-covalent interactions and possess the charge distribution opposite to the classic sandwich species. Thus, the metal center in

such compounds acts as a nucleophile. Fuming of the abovementioned powder **1NN[BArF]** with hexafluorobenzene did not provide any changes, but mixing with only one drop of it resulted in the nearly disappeared low energy emission band of aggregate. This is similar to the earlier reported results on platinum complexes, [168], however, we did not need to co-crystallize the samples. The more pronounced effect compared to the literature spectra can be explained by very low, but existing, solubility of compound **1NN[BArF]** in  $C_6F_6$ . We assume that the mechanism of this phenomenon could be the same as for quenching of Au(I) complexes, as previously reported in the literature [169]. The addition of hexafluorobenzene impairs metallophilic interactions and thus quenches the Au–Au based emission. Similarly, Pt–Pt interaction in aggregates of **1NN[BArF]** и **2NN[BArF]** getting broken by  $C_6F_6$  and the “aggregation” emission band is also suppressed, while the “monomeric” one remains responsible for luminescence. Schematic representation of *stimuli-responsive* properties from the point of view of Pt–Pt aggregations formation and destruction are given in Figure 27.

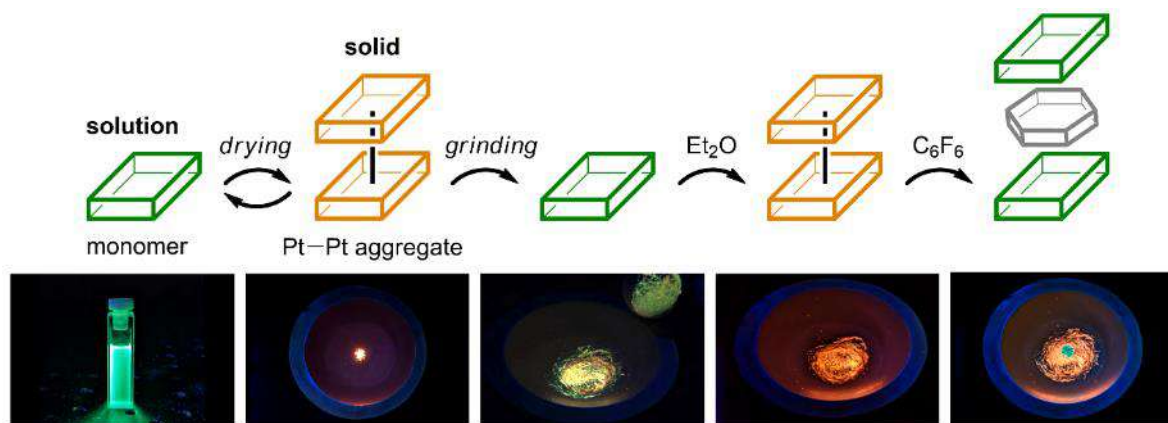


Figure 27. Schematic representation of *stimuli-responsive* properties of **1NN[BArF]** and photographs under UV irradiation (365 nm).

Referring to the complex **3NN[BArF]** that, as we believe, does not have Pt–Pt interactions in the “as-obtained” bulk sample, we observe the opposite behaviour. Its solid-state emission closely resembles that of DCE solution, and after grinding, surprisingly, the “aggregation” band of lower energy starts to emerge (Figure S48). Fuming with diethyl ether results in the increase of this band intensity. Further addition of  $C_6F_6$  at the first glance leads to the emission quenching. This is also true for complex

**nNN[BArF]**, however, the quenching is less distinct. This effect is reversible: after approx. 5 minutes from evaporation of  $C_6F_6$ , the emission shifts to the first, “as obtained” spectrum (Figures S48, S49).

Based on results of the experiment, we believe that aggregation process in complex **3NN[BArF]** needs some additional external energy, such as mechanical grinding [170,171]. The quenching upon the addition of  $C_6F_6$  to the complexes **3NN[BArF]** and **nNN[BArF]** could be the result of  $\pi$ -stacked non-emissive complex formation between arene moieties in alkynylphosphonium ligands and  $C_6F_6$ . Such a phenomenon was already described in the literature for various pyrenes [172,173]. This effect is less pronounced for complex **nNN[BArF]**, because its spectrum consists of “monomeric” LC and “aggregation” MMLCT bands. The first one is quenched because of the complex with  $C_6F_6$  formation, and the second becomes less pronounced due to the disaggregation process, giving rise to the “monomeric” one.

The study of photophysical properties of bis-alkynyl complexes of platinum(II) in *cis*-configuration has shown that for such systems the emission depends not only on the nature of alkynyl ligands, but also on aggregation effects. Changing the length or aromaticity of the linker, as expected, leads to a shift in luminescence in solution. This structure-property relationship can be further utilized to obtain emitters with given photophysical characteristics. The introduction of alkynylphosphonium fragment along with bulk tert-butyl groups in the diimine ligand leads to the appearance of *stimuli-responsive* properties and enhancement of nonlinear-optical properties of the obtained compounds. The obtained results were published in the first quartile journal ACS Inorganic Chemistry [7].

The **1NN[Cl]** complex obtained in this work was applied as a bioimaging agent by the group of A.R. Mustafina (Arbuzov Institute of Organic and Physical Chemistry, a separate structural subdivision of the Federal State Budgetary Institution of Science “Federal Research Center Kazan Scientific Center of the Russian Academy of Sciences”). Its interaction with silicon nanoparticles allowed to obtain a functional material possessing double emission due to the equilibrium of monomeric and aggregated forms

of the complex. The obtained nanomaterial showed greater specificity towards cancer cells than the complex itself [174].

### 2.3.2. Bis-alkynyl Pt(II) complexes with ancillary phosphine and cyanide ligands

In this chapter, we will consider *trans*-alkynylphosphonium Pt(II) complexes of **P[OTf]** and **CN** series together for comparison. UV-vis electronic spectra were measured at room temperature in MeCN for complexes **P[OTf]** and in DMSO for **CN** series (Figure 28). All optical and photophysical characteristics in solution are summarized in the Table 3. The former series of complexes possesses  $\lambda_{\max}$  in the range of 350–400 nm, with pronounced bathochromic shift along with the extension of the  $\pi$ -conjugated system in **1**→**2**→**n** sequence. The absorbance spectra of **P[OTf]** complexes are strongly resembling the corresponding ones of bis-alkynylphosphonium Au(I) complexes, which were also studied before in our group [6]. The electronic spectra of **P[OTf]** series are also demonstrating red shift compared to the free **P<sub>i</sub>** ligands because metal center participates in the conjugation through the C≡C bond [138,175].

The careful analysis of the literature reveals that in *trans*-alkynyl Pt(II) complexes with ancillary P(Ar)<sub>3</sub> ligand, the latter one participates in the conjugation. As a result, the LUMO is located not only at the alkynyl ligand but also at Pt(II) atom and the ancillary arylphosphine ligand [176,177]. However, our data, based on DFT calculations, points at the absence of conjugation between PPh<sub>3</sub> ligands and the rest of the system. With this in mind, and considering the abovementioned similarity between *trans*-Pt(II) and Au(I) bis-alkynylphosphonium complexes, we assign the absorbance band as ILCT with possible admixture of the MLCT state. Also, this assignment is often stated for *trans*-alkynyl Pt(II) complexes in the literature [178,179].

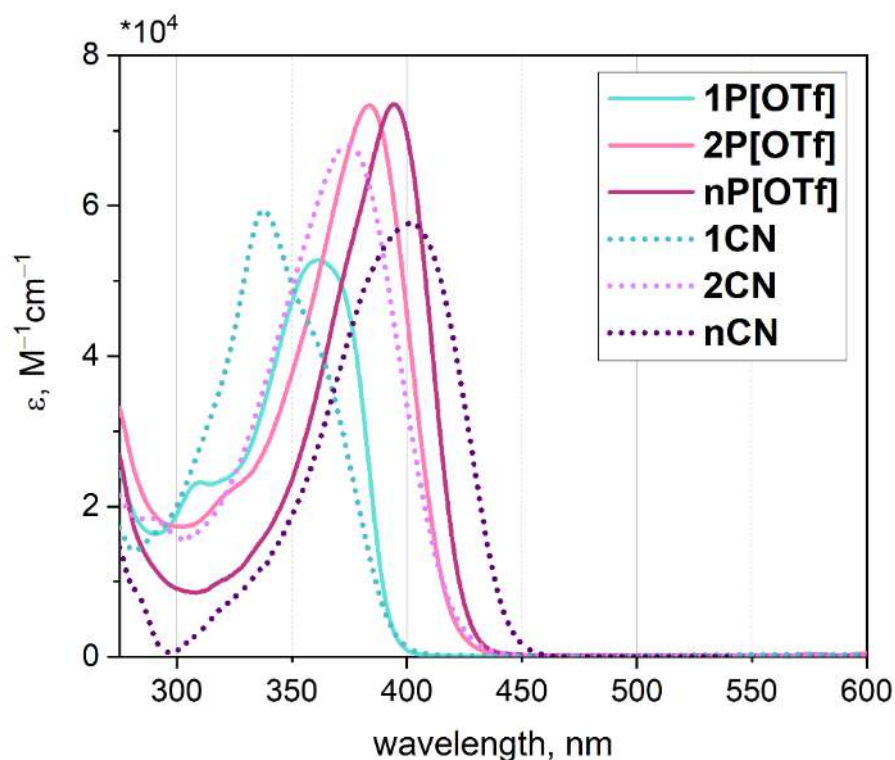


Figure 28. UV-vis spectra of **P[OTf]** and **CN** series, MeCN and DMSO respectively, r.t.

As for the second series, complexes **1CN–nCN** demonstrate similar behavior, as their UV-vis spectra consist of only one band. Pairwise compared to the series **1P–nP**, these complexes do not show an obvious trend. Thus,  $\lambda_{\text{abs}}$  of **1CN** is hypsochromically shifted, whereas for **2CN** it is much closer to that of **2P[OTf]**. The absorption maxima of the third derivative, **nCN**, is bathochromically shifted in comparison to **nP[OTf]**. Overall, the UV-vis spectra of cyanide derivatives differ from the phosphine ones more distinctly than it is stated in the literature, but the bathochromic shift upon elongation of the linker is even more pronounced [140]. The general tendency of emission bathochromic shift upon the elongation of the linker is also preserved, and becomes even more distinct in the **CN** series. Nevertheless, we also assign this absorption to the ILCT with admixture of MLCT character, bearing in mind that cyanide ligand is better  $\pi$ -acceptor than  $\text{PPh}_3$ , and thus can affect the HOMO and LUMO energy.

Table 3. Optical and photophysical properties of **P[OTf]** complexes in MeCN solution and **CN** series in DMSO solutions, r.t.

Complex	$\lambda_{\text{abs}}$ , nm	$\lambda_{\text{em}}$ , nm	$\tau$ , ** ns		QY, * %	
			aerated	deaerated	aerated	deaerated
<b>1P[OTf]</b>	361	—	—	—	—	—
<b>2P[OTf]</b>	384	—	—	—	—	—
<b>nP[OTf]</b>	395	—	—	—	—	—
<b>1CN</b>	338	487	382.6	2115.1	<1	3
<b>2CN</b>	375	451, 552	1.8, 544.1	1.8, 68951.1	<1	18
<b>3CN</b>	402	578	1270.7	87890.1	<1	22

Despite the favorable position of the absorption bands, the acetonitrile solutions of **P[OTf]** complexes are non-luminescent under UV excitation. Moreover, these compounds are unstable under the UV irradiation in solution, in contrast with the literature data, where several solution luminescent complexes of similar structures are reported [43,138,180]. After irradiating the solution of complexes with the UV flashlight with  $\lambda_{\text{ex}}$  of 365 nm for 1 minute, they decomposed to give completely different absorption spectra (Figure S50). That could be possibly explained by a very efficient ILCT/MLCT excited state, which can transfer the electron density from the formal donor (C≡C bond) to the alkynylphosphonium fragment, thus promoting the rupture of Pt–C bond.

After substituting the triphenylphosphine ligands to the cyanide ones, the resulting complexes **1CN–nCN** immediately light up, featuring weak emission in the aerated DMSO solutions at room temperature (Figure 29a). After deaeration, strong emission with a large Stokes shift becomes clearly visible (Figure 29b), indicating the triplet nature of the emission state. The lifetime values before and after deaeration also support this statement, increasing in Ar-filled solutions (Table 3). The interesting fact is that irradiating the solutions in the closed vials with 365 nm 10W flashlight also results in the increase of emission intensity. This is happening because the ground triplet state of molecular oxygen is excited to the singlet state upon irradiation and is no longer capable of phosphorescence quenching [181].

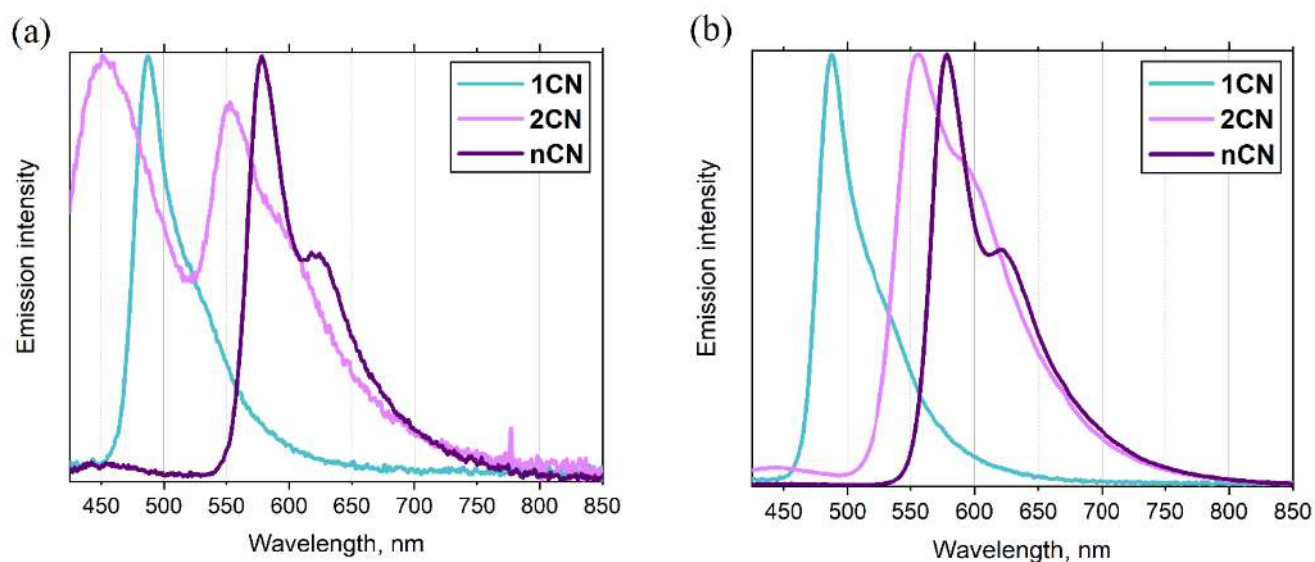


Figure 29. Normalized emission spectra of **CN** complexes in (a) aerated and (b) deaerated DMSO, r.t.;  $\lambda_{\text{ex}}$  365 nm

Complexes **1CN** and **2CN** feature slightly structured emission, green for the former and yellow for the latter. This bathochromic shift follows the common tendency of the  $\lambda_{\text{em}}$  increase upon the elongation of the  $\pi$ -conjugated linker, i.e. in **NN[BArF]** series. We assign these emissions to the  $^3\text{ILCT}$  with possible contribution of the  $^3\text{MLCT}$  state. Also, compound **2CN** demonstrates dual emission (Figure 29a) with the additional fluorescent band located at 451 nm. We have already observed similar dual emission in the bis-alkynylphosphonium Au(I) complexes [6]. The fluorescent nature of the additional band was proved by the lifetimes measurement together with intensity invariability upon deaeration.

The luminescence spectrum of complex **nCN** is again different from the other representatives. It features structured emission spectrum with a vibronic spacing of ca.  $1200\text{ cm}^{-1}$ , which is characteristic for the naphthalene fragment [182]. Comparing the emission band of naphthyl-containing derivative **nCN** with **nNN[BArF]**, we see that it has nearly the same  $\lambda_{\text{em}}$  value. Based on this fact, we set up a hypothesis about the determinative role of naphthyl-linked alkynylphosphonium ligand in the emission nature, leading to the dominating  $^3\text{LC}$  state.

For the sake of comparison, we have also measured frozen solutions for both series, assuming that at 77 K the phosphine derivatives will be more stable. The emission spectra in frozen 1,2-DCE and DMSO for **P[OTf]** and **CN** series respectively are shown in Figure 30, and the  $\lambda_{em}$  can be found in the Table 4. Upon freezing, the emission of cyanide complexes **1CN–3CN** exhibits hypsochromic shift. This is usual for the luminescence in the frozen solvents: at low temperature it occurs from the unrelaxed state because of the hindered solvent molecules reorientation. Also, the vibronic structuration is more pronounced at low temperature, indicative of “temperature switching” to the  $^3LC$  emission character.

As expected, complexes **P[OTf]** are luminescent in the frozen solutions (Figure 30). Their spectra are bathochromically shifted compared to the cyanide ones, except for **nP[OTf]**, which has nearly the same emission band as **nCN**. Based on this fact, we believe that complex **nP[OTf]** also emits from the  $^3LC$  excited state, localized on the naphthyl fragment. As for the compounds **1P[OTf]** and **2P[OTf]** the luminescence could be assigned to the  $^3LC$  luminescence with some MLCT admixture, as the ancillary ligands seem to change the spectra of these compounds slightly.

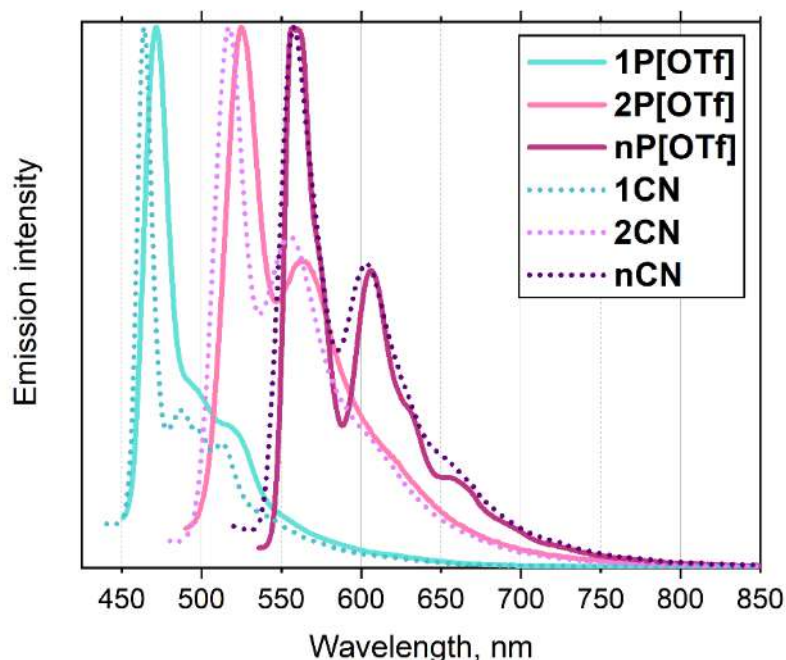


Figure 30. Normalized emission spectra of **P[OTf]** and **CN** series in frozen DCE and DMSO respectively, 77 K;  $\lambda_{ex}$  365 nm

The distinctive feature of **P[OTf]** complexes is their solid-state luminescence at room temperature. All emission characteristics are summarized in the Table 4. Interestingly, there is only one example of 298 K solid-state luminescent Pt(II) complexes of general formula *trans*-[Pt(C≡CAr)<sub>2</sub>(PAR<sub>3</sub>)<sub>2</sub>] reported in the literature [43]. Nolan et al. have synthesized Pt(II) complexes with polyaromatic ligands, namely hexa-peri-hexabenzocoronene (L2) and its uncyclised ethynyl-hexaphenylbenzene precursor (L1) (Figure S51). However, the Pt(II) orbitals' contribution to the excited states in *trans*-[Pt(L)<sub>2</sub>(PPh<sub>3</sub>)<sub>2</sub>] (L = L1, L2) was quite small. Thus, the reported in the work [43] compounds demonstrated fluorescence with a small additional phosphorescent band in the case of *trans*-[Pt(L1)<sub>2</sub>(PPh<sub>3</sub>)<sub>2</sub>]. In contrast with this data, complexes **P[OTf]** possess no fluorescence in their solid-state emission spectra (Figure 31a). The latter are dominated by sharp phosphorescent bands with slightly pronounced vibronic structure.

Table 4. Photophysical properties of complexes **1P–3P** and **1CN–3CN** in frozen solutions (1,2-DCE and DMSO correspondingly) at 77 K and in the solid state.

Complex	$\lambda_{em}$ [frozen solutions]*, nm	$\lambda_{em}$ [solid state], nm		$\tau^{aver}_{RT, **}$ ns	QY [solid state, r.t.], %
		77 K	r.t.		
<b>1P[OTf]</b>	472	474	475	14015.5	16
<b>2P[OTf]</b>	525	521	526	24171.7	3
<b>nP[OTf]</b>	558	573	570	41243.2	1
<b>1CN</b>	464	484	503, 526	289572.9	1
<b>2CN</b>	517	548	585	12453.8	1
<b>3CN</b>	558	586	–	–	–

\*  $\lambda_{exc}$  365 nm. \*\*  $\lambda_{exc}$  351 nm, amplitude average lifetime  $\tau^{aver} = \sum A_i \tau_i$  was calculated according to published method. [159] Lifetimes and quantum yields for **3CN** were not measured due to the low emission intensity.

Upon cooling powders to 77 K (Figure 31b) the luminescence becomes brighter, and better vibronic resolution is clearly visible. The progressional spacings from the

highest energy emission band are ca. 810, 1097, 1536, 2062  $\text{cm}^{-1}$  for **1P[OTf]** and 1423, 1348  $\text{cm}^{-1}$  for **2P[OTf]** and **nP[OTf]**, respectively. Similar values were reported for Pt(II) trans-aryalkynyl complexes in frozen glasses [183,184], and represent the  $\delta(\text{C-H})$ , aromatic ring deformation, and  $\nu(\text{C}\equiv\text{C})$  vibrational modes. Considering these facts, we attribute the nature of the luminescence to the mainly  $^3\text{LC}$  excited state.

We have also compared **P[OTf]** compounds to the previously **NN[BArF]** *cis*-series. It is interesting to see how the *trans*-position of alkynylphosphonium ligand enhances the  $^3\text{LC}$  solid-state phosphorescence due to the efficient hybridization between the metal  $d\pi$  orbitals and the  $p\pi$  orbitals of the alkynyl ligand. Additionally, for the *cis*-complexes **NN[BArF]**, aggregation effects rule the solid-state emission, and the MMLCT excited states with some admixture of  $^3\text{LC}$  states realize. As for the *trans*-compounds **P[OTf]**, the bulky  $\text{PPh}_3$  ligands are hampering aggregation almost completely and the  $^3\text{LC}$  emission in the solid state is dominant.

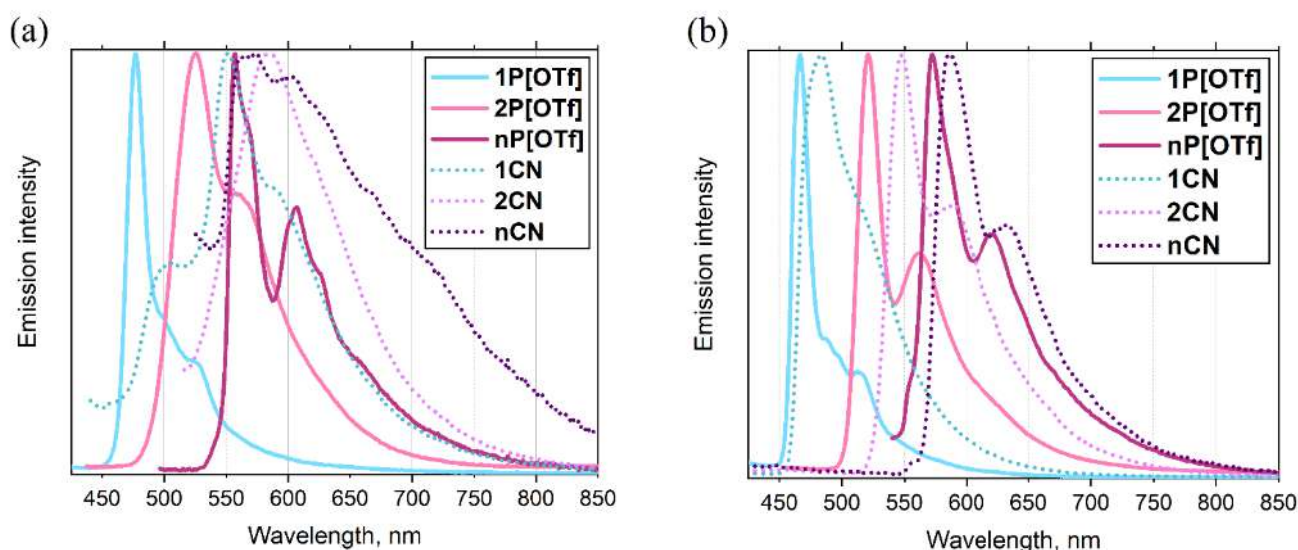


Figure 31. Normalized solid-state emission spectra of **P[OTf]** and **CN** series at (a) r.t., (b) 77 K;  $\lambda_{\text{ex}}$  365 nm

The substitution of neutral  $\text{PPh}_3$  ligands with anionic  $\text{CN}^-$  again completely changes the game. In contrast to the first series, cyanide complexes are weakly luminescent in the solid state at room temperature (Figure 31a). However, at 77 K the luminescence intensity is distinctly enhanced (Figure 31b). The emission spectrum of

**2CN** at 298 K demonstrates a structureless band, which is more typical for the charge-transfer transitions. Upon cooling to 77 K, this band exhibits blue shift and vibronic coupling. This fact suggests  $^3\text{MLCT}$  or mixed  $^3\text{MLCT}/^3\text{ILCT}$  assignment of the excited state at room temperature and “temperature switching” to  $^3\text{LC}$  at 77 K.

Complex **1CN** demonstrates more complicated behavior. Surprisingly, its emission spectrum at room temperature strongly resembles that of heterometallic {[trans-Pt(C≡CTol)<sub>2</sub>(CN)<sub>2</sub>][(PbTp)(acetone)]<sub>2</sub>} (Tp = trispyrazolylborate), described by Berenguer [139]. In the spectrum of complex **1CN** two bands appear: high energy one at 503 nm and low energy one at 526 nm. The latter completely disappears at 77 K, whereas the former is hypsochromically shifted and enhanced. Still, no clear vibronic structuration is observed for the high energy band. Also, this complex possesses a strikingly long excited state lifetime of 0.28 ms, whereas for **2CN** it is in order of magnitude lower. Complex **nCN** is nearly non-luminescent at room temperature in the solid state, but upon cooling, the strong  $^3\text{LC}$  emission is visible.

The study of photophysical properties of double-charged and neutral bis-alkynylphosphonium complexes of platinum(II) in *trans*- configuration has shown that the geometrical arrangement of ligands in different positions can fundamentally change the character of luminescence in the solid state. If in the case of the **P[OTf]** series the absence of Pt-Pt interactions was easily explained by the presence of a bulk triphenylphosphine ligand, then in the case of the **CN** series we see that even a small volume ligand still hampers metallophilic interactions in *trans*-coordinated systems, in contrast to the **NN[Cl]** and **NN[BArF]** series discussed in the previous subsection. Probably, the negative electrostatic charge localized on the central fragment of the complex molecule plays not the least role in this. The controllability of emission by changing the length or aromaticity of the linker, however, can be also traced in *trans*-systems, which makes the design of phosphors with a given wavelength possible. The introduction of a phosphonium fragment at the periphery of the ligand environment leads both to the appearance of double emission in some systems and to the appearance of bright  $^3\text{LC}$  emission in the **P[OTf]** series. This series is the first example of *trans*-alkynyl platinum(II) complexes with an additional PPh<sub>3</sub> ligand exhibiting triplet emission in the

solid state. Changing the charge of the *trans*-alkynylphosphonium system by substituting the phosphine ligand with a cyanide ligand leads to a simultaneous increase in the stability of the systems in solution and a decrease in the quantum yield in the solid state.

The obtained results were published in the first quartile journal Chemistry – A European Journal [8].

### 2.3.3. Mono-alkynyl Pt(II) complexes with ancillary C<sup>N</sup>N and N<sup>N</sup>N ligands

Charged mono-alkynylphosphonium Pt(II) complexes **1N[Cl]**–**nN[Cl]** and **1C[Cl]**–**nC[Cl]** will be considered together for the sake of comparison. These complexes, being different only in charge of the cationic part and one atom in the lateral aromatic ring, possess sufficiently similar UV-vis spectra in MeCN solutions (Figure 32).

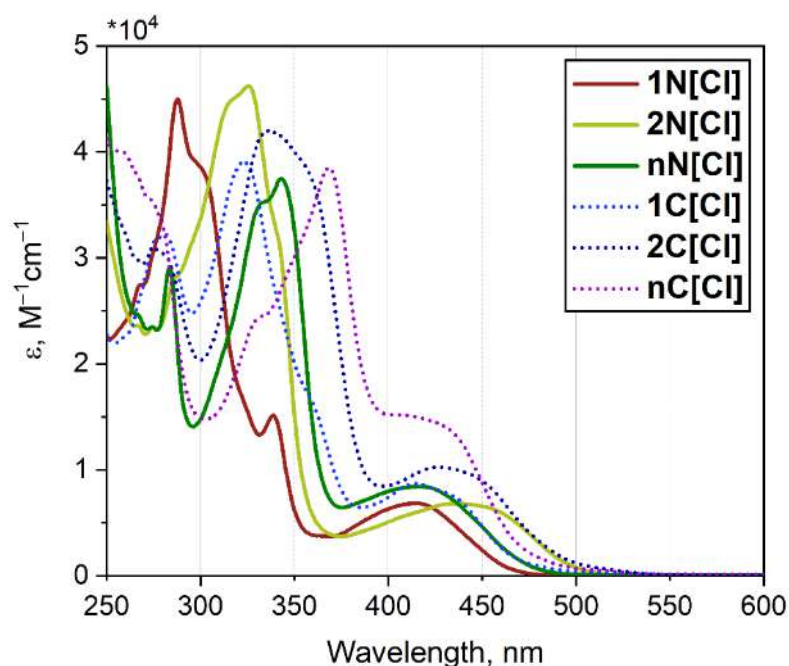


Figure 32. UV-vis spectra of **N[Cl]** and **C[Cl]** series, MeCN, r.t.

All of them consist of two absorption bands that were assigned with the reference to published literature [109,150,185–188]. The higher energy ones, lying in the region of 250–375 nm for **1N[Cl]**–**nN[Cl]** and 300–400 nm for **1C[Cl]**–**nC[Cl]** can be attributed to the spin-allowed intraligand  $\pi\pi^*$  transitions of the corresponding tridentate and alkynylphosphonium ligands. As for the lower energy bands, they predominately arise

due to the mixed metal-to-ligand charge transfer (MLCT) transitions from  $d\pi(\text{Pt})$  to  $\pi^*$  orbitals of the respective tridentate/alkynylphosphonium ligands and ligand-to-ligand charge transfer (LLCT) from alkynylphosphonium moiety to the tridentate ligand. The latter statement is confirmed by the TD-DFT calculations. As well as in previous series, the absorbance spectra of **1N[Cl]**–**nN[Cl]** and **1C[Cl]**–**nC[Cl]** are close to studied in the literature, but have more complex nature because of alkynylphosphonium fragment [92,145,189–192]. The change of counterion does not affect the shape of the **1N[X]** and **1C[X]** absorption spectra (Figure S52). All optical and photophysical properties of studied compounds in solution are summarized in the Table 5.

Despite the similarity of absorption properties, the emission behavior of **terpy**-containing and **phbpy**-containing series is different. Thus, complexes **2N[Cl]** and **nN[Cl]** possess low quantum yields, and are nearly non-emissive in aerated MeCN solutions. Moreover, the emission of **1N[Cl]** is non-detectable neither by the naked eye, nor by spectral equipment. This, as we believe, is due to the polar solvent quenching, already reported for terpyridyl Pt(II) complexes in MeCN solutions [21]. As none of the **N[Cl]** series dissolve in 1,2-DCE, we have compared the MeCN and 1,2-DCE solutions of the complex **1N[BArF]**. Upon changing the solvent from the former to the latter, we observe an increase of quantum yield from <1% in deaerated MeCN, up to 19.4% in deaerated 1,2-DCE solution of **1N[BArF]** (Table 5).

On the contrary, the luminescence of the **C[Cl]** series is visible by the naked eye. Upon excitation at 365 nm, complexes of **C[Cl]** series and some representatives of the **N** series, emit yellow-orange color. Solution luminescence spectra of **1N[BArF]**, **2N[Cl]**, **1C[Cl]** and **2C[Cl]** feature broad, structureless bands (Figure 33), that are typical for charge transfer (CT) transitions [150,187,188,193,194]. According to the TD-DFT calculations (*vide infra*), their nature is complicated, and involves not only MLCT, but also LLCT and ILCT. The excited state lifetimes along with luminescence quantum yields both for aerated and Ar-purged solutions, were measured for all Pt(II) complexes excluding **1N[Cl]**. The increase of all reported values upon deaeration along with significant Stokes shift suggest the triplet origin of the emissive state.

Table 5. Optical and photophysical characteristics of N and C series in 1,2-DCE solutions, r.t.

Complex	$\lambda_{\text{abs}}$ , nm	$\lambda_{\text{em}}$ , nm	$\tau$ , ** ns		QY, * %	
			aerated	deaerated	aerated	deaerated
<b>1N[Cl]</b>	288, 339, 414	–	–	–	<<1	<<1
<b>1N[BArF]</b>	287, 339, 415	545	875	2053	<<1 6***	<1 19***
<b>2N[Cl]</b>	325, 440	621	165	464	<<1	4
<b>nN[Cl]</b>	284, 343, 417	566	293	1178	<<1	1
<b>1C[Cl]</b>	323, 417	576	87	240	<1	3
<b>2C[Cl]</b>	337, 428	590	80	413	<1	4
<b>nC[Cl]</b>	368, 414	575	325	7279	<1	5

\*  $\lambda_{\text{exct}}$  365 nm. \*\*  $\lambda_{\text{exct}}$  351 nm. \*\*\* 1,2-DCE solutions.

The emission maximum of **2N[Cl]**, possessing longer linker, is shifted bathochromically with the respect to **1N[BArF]**. Biphenylene linker moiety, that is more electron-rich than phenylene, rises the  $d\pi(\text{Pt})$  orbital energy, causing a lower energy  $^3\text{MLCT}$  emission. This effect is also visible for **1C[Cl]** and **2C[Cl]**, but it is less pronounced [109]. The similar trend was present in **NN[BArF]**, **P[OTf]** and **CN** series, described before.

The emission spectrum of **nN[Cl]** and **nC[Cl]** differs from the first two representatives of these series. It features pronounced vibronic spacing (ca.  $1280\text{ cm}^{-1}$ ), that is characteristic of naphthalene fragment, present in the linker structure [182]. This fact, together with experimental evidence of bis-alkynylphosphonium Pt(II) complexes, described before, and obvious similarity of **nN[Cl]** and **nC[Cl]** spectra, indicates the ligand-centered ( $^3\text{LC}$ ) nature of the emission band. Moreover, this fact proves our hypothesis about the determinative factor of naphthyl-linked alkynylphosphonium ligand in the emission nature, regardless of the other ancillary ligands.

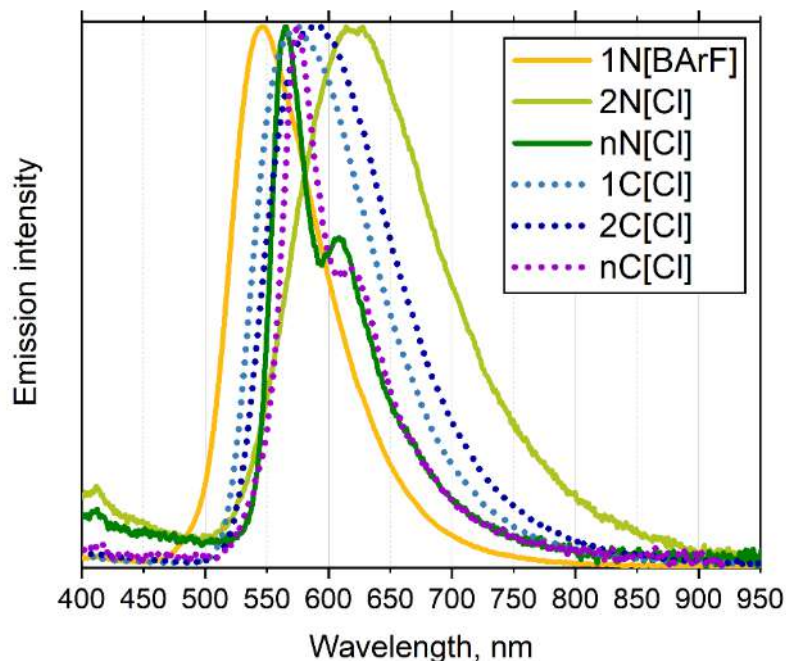


Figure 33. Normalized emission spectra of **2N[Cl]**, **nN[Cl]** in MeCN solution, and **1N[BArF]**, **1C[Cl]**–**nC[Cl]** in 1,2-DCE solutions,  $\lambda_{\text{ex}}$  365 nm.

To determine the influence of phosphonium fragment on the photophysical properties, we compared luminescence spectra of complexes **1N[BArF]**, **2N[Cl]** and **1C[Cl]**, **2C[Cl]** to their respective arylalkynyl analogues [41,194–196]. The emission spectra of compounds  $[\text{Pt}(\text{tBu}_3\text{terpy})(\text{C}\equiv\text{CPh})]\text{Cl}$  and  $[\text{Pt}(\text{terpy})(\text{C}\equiv\text{CPh}_2)]\text{Cl}$  are bathochromically shifted collated to the studied alkynylphosphonium compounds. According to the literature data, the HOMO in  $[\text{Pt}(\text{terpy})(\text{C}\equiv\text{CAr})]^+$  complexes is delocalized over the arylacetylide ligand [41,192]. Therefore, the introduction of electron-accepting moiety in the para-position of aryl results in the lowering the HOMO energy, and the emission shifts hypsochromically. This seems to be the reason for the difference between  $[\text{Pt}(\text{terpy})(\text{C}\equiv\text{CPh}_2)]\text{Cl}$  and **2N[Cl]**. As for the **1N[Cl]**, the quantum chemical calculations reveal the mixed  $d\pi(\text{Pt})$ -based and terpy-localized HOMO (*vide infra*), and the difference between **1N[Cl]** and its arylalkynyl analogue could be explained by the different emission origin. The same shift is present for the **C** series and their arylalkynyl analogues, but it is again less pronounced.

Both **N** and **C** series are emissive in the solid state. They exhibit orange to near-infrared emission, and the emission maxima are bathochromically shifted compared to those in solution. The spectra are shown in Figure 34, and solid-state emission characteristics are given in the Table 6.

Table 6. Solid-state photophysical properties of the **N** and **C** series

Complex	$\lambda_{em},^* \text{ nm}$		$\tau_{RT},^{**} \text{ ns}$	QY, %
	77 K	r.t.		
<b>1N[X]</b>	X = Cl: 877	X = Cl: 823	X = Cl: 111	X = Cl: 3
	X = BF <sub>4</sub> : 855	X = BF <sub>4</sub> : 799	X = BF <sub>4</sub> : 171	X = BF <sub>4</sub> : 2
	X = OTf: 811	X = OTf: 752	X = OTf: 259	X = OTf: 4
	X = BArF: 724	X = BArF: 681	X = BArF: 892	X = BArF: 15
<b>2N[Cl]</b>	837	829	86	1
<b>nN[Cl]</b>	870	840	106	1
<b>1C[X]</b>	X = Cl: 779	X = Cl: 773	X = Cl: 189	X = Cl: 2
	X = BF <sub>4</sub> : 797	X = BF <sub>4</sub> : 780	X = BF <sub>4</sub> : 118	X = BF <sub>4</sub> : 2
	X = OTf: 818	X = OTf: 773	X = OTf: –	X = OTf: –
	X = BArF: 803	X = BArF: 788	X = BArF: 117	X = BArF: 1
<b>2C[Cl]</b>	586	603	456	3
<b>nC[Cl]</b>	592	597	25, 120 ( $\tau_{aver} = 51$ )	–

\*  $\lambda_{ex}$  365 nm. \*\*  $\lambda_{ex}$  351 nm.

Amplitude average lifetime  $\tau_{aver} = \sum A_i \tau_i$  was calculated according to published method [159].

Unlike the luminescence in solution, the solid-state emission of the **N[Cl]** and **C[Cl]** series is drastically different. This fact can be rationalized by the different charge state of the **N[Cl]** and **C[Cl]** series: di- and monocationic respectively. In the **N[Cl]** series, the luminescence spectra of all compounds feature broad structureless bands with very close emission maxima (823, 829 and 840 nm for **1N[Cl]**, **2N[Cl]** and **nN[Cl]** correspondingly, Figure 34a). Upon cooling to 77 K, they are bathochromically shifted

and retain the spectrum shape. However, based on the lifetime values and the value of the red shift, we observe different emission states for the **1/n** and the **2** representatives of the series. The larger bathochromic shift with the same half-width of the band upon cooling along with near-infrared emission wavelengths suggests the metal/metal-to-ligand charge transfer (<sup>3</sup>MMLCT) origin of the excited state in the complexes **1N[Cl]** and **nN[Cl]**. It results from the metallophilic Pt–Pt interactions in the solid state, and the emission red shift emerges because of the low-temperature crystal lattice contraction. Referring to the previous studies of Pt(II) terpyridyl systems, we assume, that the degree of aggregation in the solid state is very high, similar to that in the dark green form of [Pt(terpy)(C≡CC≡CH)]OTf [58,197].

On the contrary, the bathochromic shift is less for **2N[Cl]**, and is apparently coming from the half-width decrease. This is more characteristic for <sup>3</sup>MC excited state, and the shortest lifetime value among this series confirms this statement [19]. Alternatively, this emission could originate from excited state, based on the  $\pi$ -stacked dimer aggregates without Pt···Pt metallophilic interactions. For the solid state, we were not able to directly compare the emission of the **N[Cl]** series to their arylalkynyl analogues, as we did for the solutions. The reason for that is the strong dependence of luminescence on the crystal packing.

The solid-state emission spectra of the **C[Cl]** series are markedly different from the **N[Cl]** series (Figure 34). Turning to the solid state from solution, **1C[Cl]** is significantly red-shifted (ca. 190 nm), while **2C[Cl]** and **nC[Cl]** remain nearly in the same range as solution emission maxima (red-shift 13 and 21 nm correspondingly). The behavior of the **1C[Cl]** resembles this of **2N[Cl]**: upon cooling, the solid-state emission maximum exhibits very small bathochromic shift, caused mainly by narrowing of the emission band, whereas the shape on the spectrum retains. The spectral attribution of this compound is again a debatable issue, and we can possibly attribute it to either the excited state, based on the  $\pi$ -stacked dimer aggregates, or <sup>3</sup>MC emission, similar to the “yellow form” of [Pt(bpy)Cl<sub>2</sub>] [27].

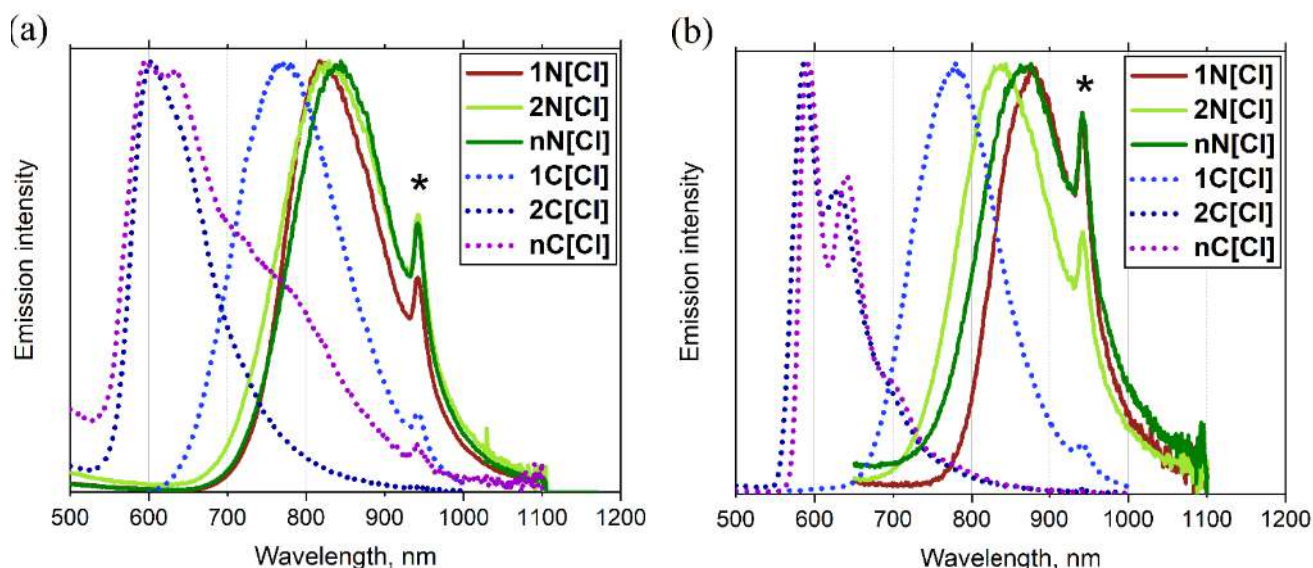


Figure 34. Normalized solid-state emission spectra of **N[Cl]** and **C[Cl]** series, (a) at r.t.; (b) at 77 K;  $\lambda_{\text{ex}}$  365 nm. An asterisk denotes an artifact of optical system.

At room temperature, luminescence spectrum of **2C[Cl]** consists of structureless emission band. Cooled to 77 K, complex **2C[Cl]** exhibits sharp, structured emission band with vibronic coupling of  $1140\text{ cm}^{-1}$ , which is characteristic for **phbpy** [198]. According to the literature data [27], this band is attributed to the  $^3\text{MLCT}$  emission of “monomeric” Pt(II) species, probably with some admixture of  $^3\text{LC}$  state.

The luminescence of **nC[Cl]** is somewhat more complicated. The room-temperature spectrum features high-energy band with broad vibronic structure, and the additional red-shifted band. At 77 K, the former band sharpens, showing a distinct vibronic structure with  $1267\text{ cm}^{-1}$  spacing, characteristic of naphthalene moiety. Its intensity increases, and the low-energy band becomes invisible. Based on these facts and the literature data [7,55,187,190,199,200], we assign the intensive band to the  $^3\text{LC}$  excited state, and the low-energy band of **nC[Cl]** to the excited state, based on the  $\pi$ -stacked dimer aggregates. However, the former band might also possess some  $^3\text{MLCT}$  character, as it has slightly reduced lifetimes value and poor vibronic resolution at 298 K [201]. The presence of two different excited states in **nC[Cl]** is also confirmed by the biexponential decay of the emission lifetimes.

The solid-state luminescence of Pt(II) complexes can depend on the nature of the counterion, as it was shown in a few publications [72,202,203]. The first example of comprehensive solid-state photophysical investigation of structure-property relationship in terpyridine-containing Pt(II) complexes was made for [Pt(terpy)Cl]X, where X = Cl<sup>-</sup>, ClO<sub>4</sub><sup>-</sup>, OTf<sup>-</sup>, PF<sub>6</sub><sup>-</sup> [204]. Later research concerning emission properties of [Pt(terpy)(C≡CR)]<sup>+</sup> complexes, was mostly focused on the description of polymorphs and aggregation in solution, and no dependence of solid-state luminescence properties on anion size was investigated [58,193,197,205]. In this work, we are filling this gap, showing a nice example of how the emission maxima of cationic Pt(II) complexes are nearly linearly dependent on the size of counterion.

To perform this experiment, the **1N[X]** complexes were synthesized, where X = Cl<sup>-</sup>, BF<sub>4</sub><sup>-</sup>, OTf<sup>-</sup> and BArF<sup>-</sup>. These counterions were chosen based on their bulkiness, as we believed they should prevent (the case of BArF<sup>-</sup>) or favor (the case of Cl<sup>-</sup>) the formation of Pt–Pt aggregates in the solid state. The absorption studies revealed that the shape of UV-vis spectrum is independent of counterion (Figure S52). Compounds **1N[BF<sub>4</sub>]** and **1N[OTf]** were weakly luminescent in MeCN solution, with the same emission maximum, as for **1N[BArF]**. The solid-state emission spectra of obtained compounds are shown in Figure 35, their properties are listed in the Table 6.

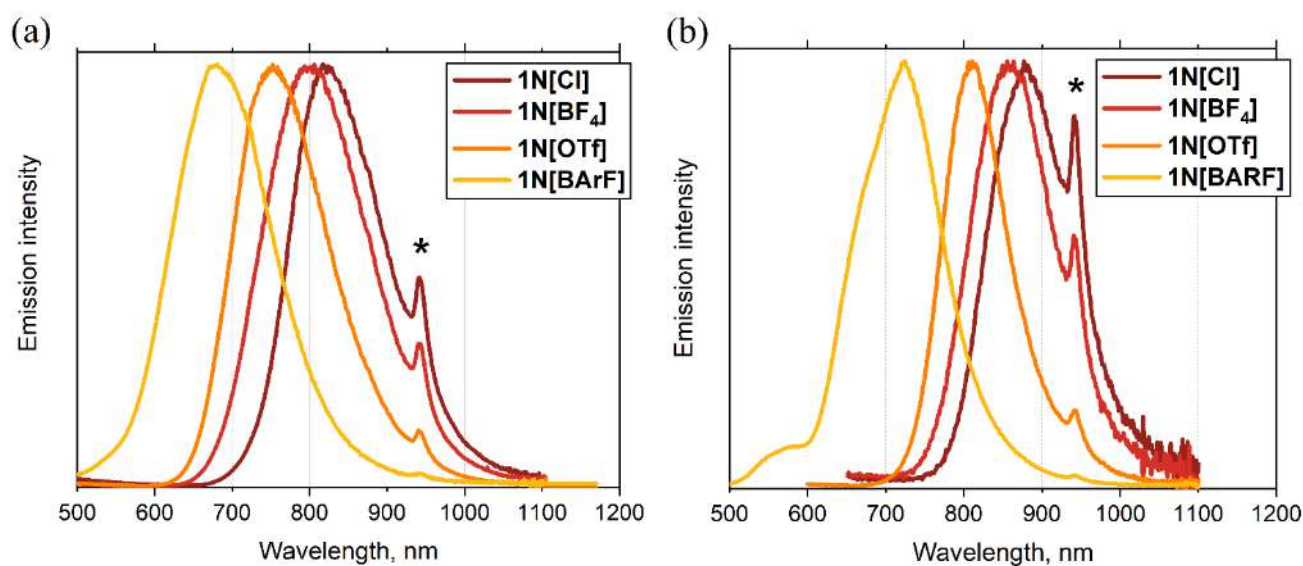


Figure 35. Normalized solid-state emission spectra of **1N[X]** (a) at r.t. and (b) 77 K,  $\lambda_{\text{ex}}$  365 nm. An asterisk denotes an artifact of the optical system.

The room-temperature luminescence spectra of all compounds **1N[X]** are dominated by one structureless band. Upon change of the counterion from  $\text{Cl}^-$  to  $\text{BArF}^-$ , the emission energy increases along with the size of counterion. The overall  $\lambda_{\text{em}}$  shift in this series is 142 nm, from near-infrared **1N[Cl]** (823 nm) to the orange **1N[BArF]** (681 nm). Measuring the emission spectra of **1N[X]** at 77 K, we have found that all compounds exhibit bathochromic shift from 49 nm ( $\text{BArF}^-$ ) to 59 nm ( $\text{OTf}^-$ ). This can be the characteristic feature of both  $^3\text{MMLCT}$  emission and emission of  $\pi$ -stacked oligomers, as it was discussed earlier. Thus, the rational choice of counterion allows fine-tuning of the solid-state emission characteristics, achieving 877 nm emission at 77 K. As it was stated before, we could not perform single-crystal XRD studies to gain insight into the packing and interactions therein. Nevertheless, further information about the molecular structure of these assemblies was provided by computational analyses [9].

Inspired by these results, we have investigated the **1C[X]** series with the same set of counterions. Both absorption and emission in the MeCN solution were independent of the counterion (Figure S52). However, we did not see the correlation between the size of counterion and solid-state emission. All complexes of **1C[X]** series demonstrate structureless emission bands. The nature of the excited state, expected from the luminescence change upon cooling, is different for all complexes. **1C[Cl]**, **1C[BF<sub>4</sub>]** and **1C[BArF]** presumably have  $^3\text{MC}$  emission, while **1C[OTf]** possesses  $^3\text{MMLCT}$  excited state. We assume that the difference between **1N[X]** and **1C[X]** series is caused by the different charge state of the complexes. Thus, in dicationic series **1N[X]** two counterions have more profound effect on the packing than in monocationic series **1C[X]**.

Thus, herein for the first time we have shown the possibility of controlling the luminescence of mono-alkynylphosphonium complexes of platinum(II) with an additional terpyridine ligand in the solid state by changing the size of the counterion. The charged mono-alkynylphosphonium systems of the **N** and **C** series also obey the general trend for a bathochromic emission shift in solution with increasing linker length, but to a lesser extent than the bis-alkynylphosphonium derivatives of the **NN[BArF]**, **P[OTf]** and **CN** series. It is also an important finding that packing and metallophilic interactions in the solid state play a crucial role in determining the luminescence character of these

systems. The obtained results were published in the first quartile journal ACS Inorganic Chemistry [9].

### 2.3.4. Mono-alkynyl Pt(II) complexes with C<sup>N</sup>C ancillary ligand

Neutral bis-cyclometallated complexes of CNC series are considered separately, as having significantly less effective luminescence compared to the rest of the tridentate compounds. DMSO solutions of complexes **1CNC** and **2CNC** absorb in the visible range, and the UV-vis electronic spectra were measured for them. Absorption wavelengths are summarized in the Table 7, and the corresponding spectra are depicted in the Figure 36.

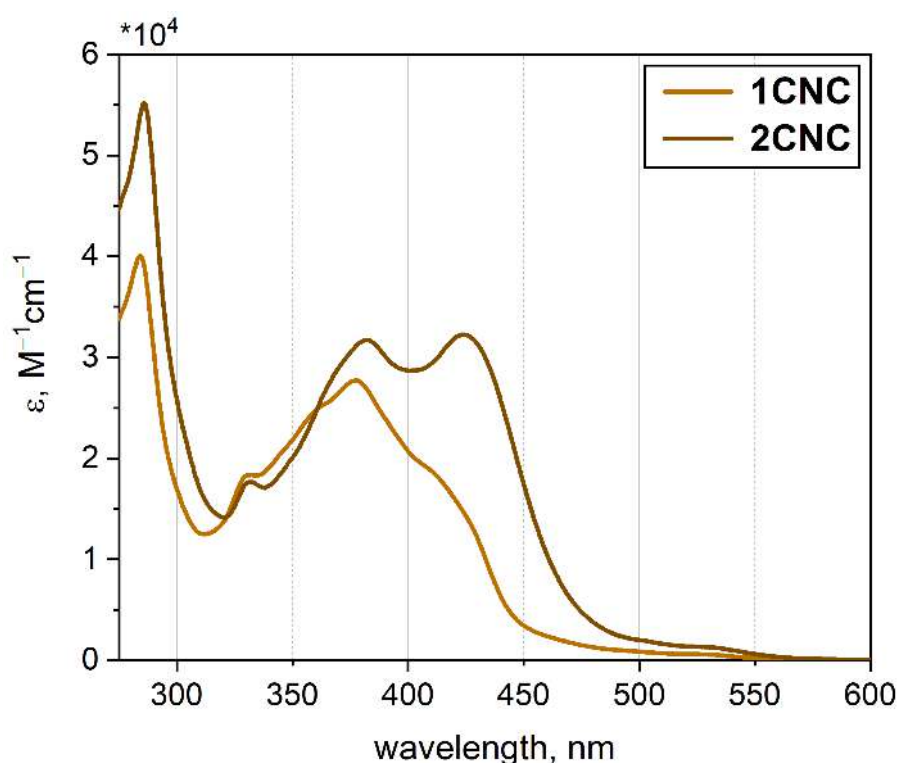


Figure 36. UV-vis spectra of **1CNC** and **2CNC** in DMSO solution, r.t.

Similar to the literature data [97,206–211], the studied Pt(II) complexes exhibit strong absorption bands in high-energetic (<300 nm) and low-energetic (350 – 450 nm) parts of the spectrum. With the reference of abovementioned studies, the former ones were assigned to the <sup>1</sup>IL transitions, localized both at CNC and alkynylphosphonium ligands. Weaker red-shifted bands arise from the mixed <sup>1</sup>MLCT ( $d\pi(\text{Pt}) \rightarrow \text{CNC}$ ) and <sup>1</sup>LLCT (alkynyl  $\rightarrow$  CNC). We presume that the bands with  $\lambda_{\text{abs}} = 378$  and 381 for **1CNC** and **2CNC** respectively have more <sup>1</sup>MLCT character, as they are nearly independent from

the alkynylphosphonium substituent. On the contrary, the absorption bands at ~410 nm (**1CNC**) and 423 nm (**2CNC**) are not so close, corresponding to the different alkynylphosphonium ligands structures. Thus, the extended  $\pi$ -conjugated linker in the ligand P2 brings additional  $\pi$ -donating ability, not only bathochromically shifting the corresponding absorption band, but also enhancing the extinction coefficient, as the <sup>1</sup>LLCT becomes more efficient.

Careful readers will also note the presence of the additional band in the 500 – 550 nm region of the UV-vis spectrum (Figure S53). It could not be attributed to the d-d transitions because of the CNC and alkynylphosphonium ligands' strong  $\sigma$ -donating nature. In addition, these transitions are unlikely observed at such low energies. Similar low intensity red-shifted absorption bands are examined in the contributions by Che and Yam [206,207] and with this in mind, we ascribe this band to a spin-forbidden <sup>3</sup>LC transition. It becomes possible due to the large spin-orbit coupling, caused by the presence of Pt atom as the metal center.

Table 7. Optical and photophysical properties of **1CNC** and **2CNC** in solution and solid state.

Complex	$\lambda_{\text{abs}}$ , nm	$\lambda_{\text{em}}$ ,* nm		$\tau_{\text{RT}}$ ,** ns		QY, %	
		DMSO	77 K	r.t.	DMSO		TB
<b>1CNC</b>	284, 332, 378, ~410, 522	521	710	692	89.0 (aer) 146.7 (deaer)	2.0	<0.1
<b>2CNC</b>	286, 332, 381, 423, 525	–	710	694	–	22.7	<0.1

\*  $\lambda_{\text{exct}}$  365 nm. \*\*  $\lambda_{\text{exct}}$  351 nm. Amplitude average lifetime  $\tau^{\text{aver}} = \sum A_i \tau_i$  was calculated according to published method [159].

As it was stated before, the emissive properties of **CNC** series differ significantly from charged mono-alkynyl systems of **N** and **C** series. Upon excitation at 365 nm, deaerated DMSO solution of complex **1CNC** surprisingly demonstrates green emission.

This is in sharp contrast with the reported isostructural analogue without phosphonium fragment [97], and that means that introduction of a charged acceptor fragment “turns on” the luminescence in this case. Based on the excited-state lifetime values and the rise of emission intensity upon deaeration, we state its phosphorescent nature. We assume that this emission is of mixed  $^3\text{MLCT}$  and  $^3\text{LC}$  nature, because upon freezing the solution, this band demonstrates hypsochromic shift and becomes vibronically structured (Figure 37). Besides, we see an additional band in the red part of the spectrum, apparently, arising because of the low solubility of **1CNC**. Solution of complex **2CNC** decomposes under the UV irradiation.

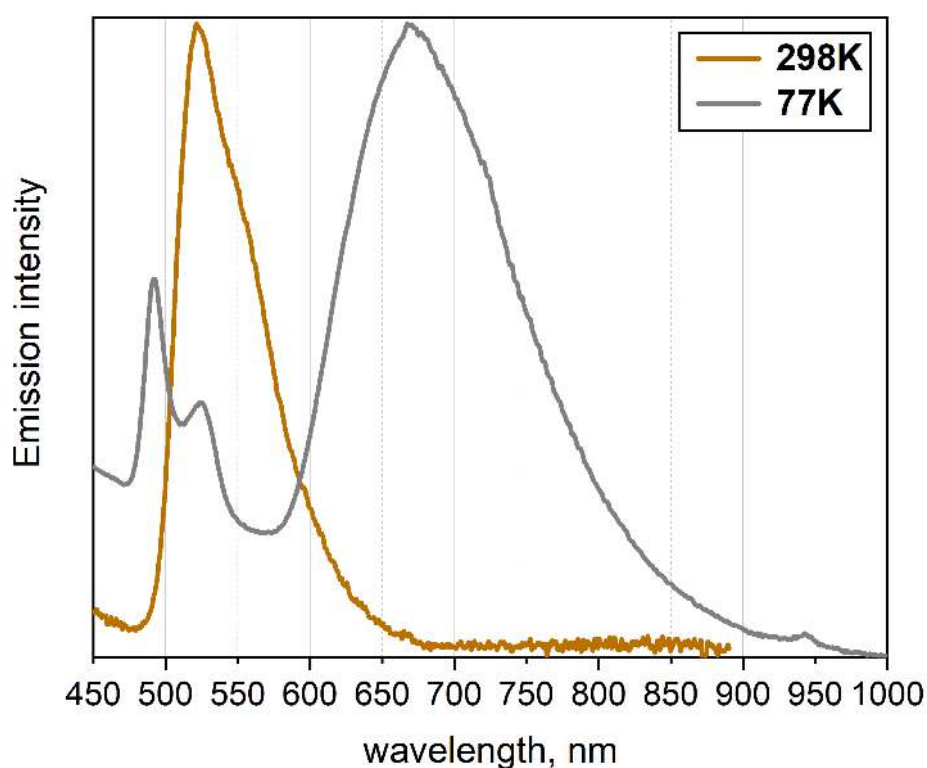


Figure 37. Normalized emission spectra of complex **1CNC** in DMSO solution at r.t. and 77 K;  $\lambda_{\text{ex}}$  365 nm.

Complexes of **CNC** series are also luminescent in the solid state, both at room temperature and at 77 K. Their emission spectra at 298 K show broad structureless bands with  $\lambda_{\text{em}}$  at ca. 700 nm. It is interesting to note that the spectra of studied compounds are almost identical both at room and low temperature, thus implying similar emission state. Upon cooling, the emission demonstrates small bathochromic shift and intensifies, which

is characteristic for triplet character. We assume that this emission could be attributed to either  $^3\text{MC}$  or “ $\pi$ -dimeric” luminescence, similar to **1C[Cl]** and **2N[Cl]**, discussed earlier.

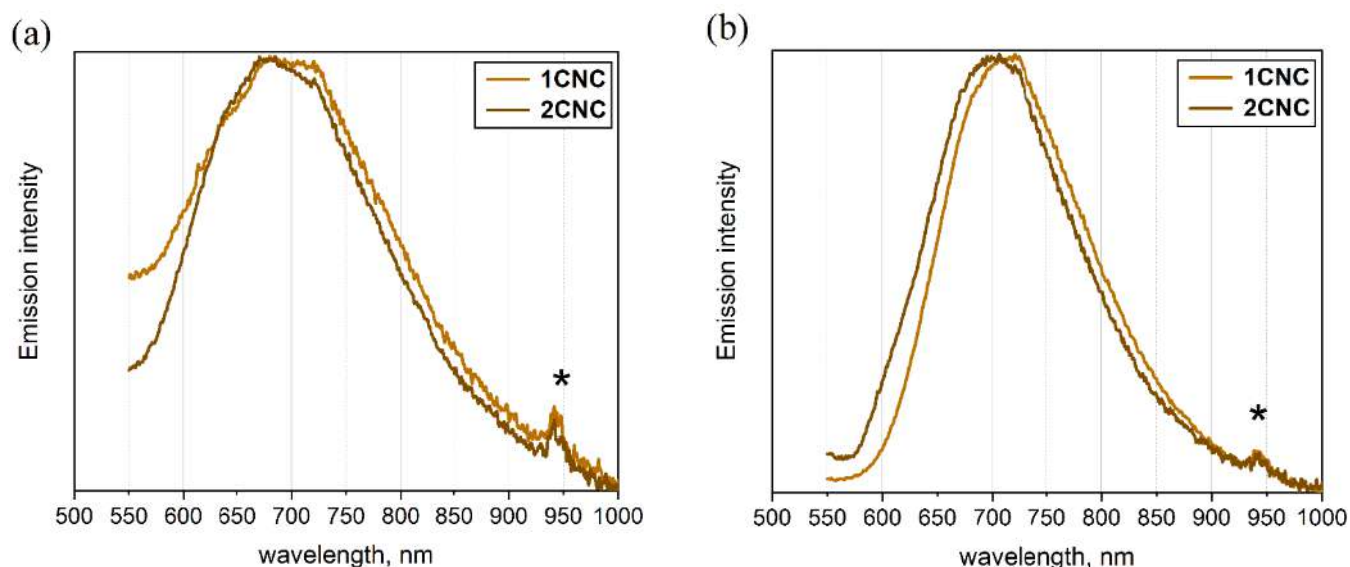


Figure 38. Normalized solid-state emission spectra of **CNC** series at (a) r.t. and (b) 77 K;  $\lambda_{\text{ex}}$  365 nm.

Based on the results on photophysical properties of **CNC** series, we state that the introduction of charge transfer systems as ligands allowed to “turn on” luminescence in these systems. Thus, the presence of emission in solution and solid state at room temperature for such compounds was shown for the first time. Unfortunately, it seems that the leading role in the quenching of phosphorescence in  $\text{C}^{\wedge}\text{N}^{\wedge}\text{C}$  systems is played by distortions of the structure during excitation, which does not allow us to obtain effective emission. Also, these systems are the only exception to the general trend in bathochromic shift: having similar excited states, they have almost identical emission within the series.

The results of this work are presently being prepared for publication in the journal RSC Dalton Transactions.

## CHAPTER 3. EXPERIMENTAL SECTION

### 3.1. Materials and instruments

Alkynylphosphonium salts  $P_1-P_n$  [6] and Pt(II)-containing precursors [Pt(dtbpy)Cl<sub>2</sub>] [212], *cis*-[Pt(PPh<sub>3</sub>)<sub>2</sub>Cl<sub>2</sub>] [213], [Pt(terpy)Cl]Cl [187], Pt(phbpy)Cl [214] and [Pt(CNC)dmsol] [215] were synthesized according to the literature methods. CuI (Merck), NaBARF (ABCR), NaOTf (Merck), NaCN (ABCR), NaBF<sub>4</sub> (Merck), AgOTf (Alpha Aesar), TEACl (Sigma Aldrich), TMACl (Sigma Aldrich), *n*-BuLi (BLD Pharm), DMSO-d<sub>6</sub> (ROTH), CDCl<sub>3</sub> (ROTH), acetone-d<sub>6</sub> (ROTH), CD<sub>3</sub>CN (ROTH), CD<sub>3</sub>OD (ROTH) were purchased from commercial suppliers and used without further purification. For column chromatography, silica gel (Macherey-Nagel, 0.04–0.063 mm, 230–400 mesh) or neutral alumina (Acros Organics, Brockmann I, 50–200 μm, 60A) were used. Thin-layer chromatography was performed on Macherey–Nagel Xtra Sil G/UV<sub>254</sub> or Sorbfil UV 254 plates with UV detection. All organic solvents, used in this study, were purchased from Vecton and purified according to the standard methods [216].

Spectral and crystallographic data for synthesized compounds were obtained on the St Petersburg University Research Park equipment, using “Magnetic Resonance Research Centre”, “Centre for X-ray Diffraction Studies”, “Chemical Analysis and Materials Research Centre” and “Centre for Optical and Laser Materials Research”.

<sup>1</sup>H, <sup>31</sup>P, <sup>19</sup>F, and <sup>1</sup>H<sup>1</sup>H COSY spectra were recorded on a Bruker Avance DPX 400 and Bruker Avance III 500 (400 or 500, 162, 376 MHz for <sup>1</sup>H, <sup>31</sup>P{H}, <sup>19</sup>F{H} spectra respectively). The obtained data was processed using MestReNova (v 11.0). The coupling constants in <sup>1</sup>H spectra (Hz) are measured in the first-order approximation. The multiplicity of signals is given according to the following abbreviations: s = singlet, d = doublet, t = triplet, q = quartet, dd = doublet of doublets, td = triplet of doublets, m = multiplet. Mass spectra were recorded on a MaXis Bruker Daltonik GmbH (Germany) electrospray ionization (ESI) instrument in positive mode. Elemental analysis was carried out in the Laboratory of Microanalysis of the Institute of Organoelement Compounds named after A.N. Nesmeyanov. Nesmeyanov Institute of Organoelement Compounds of

the Russian Academy of Sciences on a vario MICRO cube CHNS analyzer (Elementar, Germany).

The crystal structures of **1NN[Cl]**, **2NN[Cl]**, **1P[OTf]**, **nP[OTf]**, **2C[Cl]**, **nC[Cl]**, **1CNC** determined by the means of single crystal XRD analysis using Rigaku Oxford Diffraction diffractometer for the data collection at a temperature of ca. 100K. Diffraction data were processed in *CrysAlisPro* program [217]. The structures were solved by dual-space algorithm and refined using the *SHELX* programs [218], incorporated in the *OLEX2* program package Olex2 [219]. Supplementary crystallographic data for **1NN[Cl]**, **2NN[Cl]**, **1P[OTf]**, **nP[OTf]**, **nC[Cl]**, **1CNC** have been deposited at Cambridge Crystallographic Data Centre ([www.ccdc.cam.ac.uk/structures/](http://www.ccdc.cam.ac.uk/structures/)), № 2269523, 2269524, 2360483, 2360484, 2352281, 2383597. Several structures contained disordered solvent molecules which have been treated as a diffuse contribution to the overall scattering without specific atom positions by *SQUEEZE/PLATON* [220].

The UV-vis absorption spectra were registered on a Shimadzu UV-1800 spectrophotometer in a 1 cm quartz cuvette. The concentrations of complexes' solutions were ca.  $10^{-5}$  M and were chosen to have optical density of 0.3–0.5 at 365 nm.

The emission spectra for solid samples and solutions at room temperature and 77 K were recorded using Fluoromax-4, Horiba Jobin Yvon, and Avantes AvaSpec-2048×64 (Avantes, Apeldoorn, Netherlands).

The Avantes integration sphere (Avantes, Apeldoorn, Netherlands) was used to measure the solid-state emission quantum yield. The absolute emission quantum yield was determined in solution by a comparative method [221]. LED (365 nm) was applied for pumping and  $[\text{Ru}(\text{bpy})_3][\text{PF}_6]_2$  water solution ( $\Phi = 0.040$  air-saturated, 0.063 Ar-saturated) was used as a reference.

The pulse laser DTL-399QT 'Laser-export Co. Ltd' (wavelength 351 nm, pulse energy 50  $\mu\text{J}$ , pulse width 6 ns, repetition rate 0.01–1 kHz), an Ocean Optics monochromator Monoscan-2000 (interval of wavelengths 1 nm; Ocean Optics, Largo, FL, USA), photon counting head H10682 (Hamamatsu), and multiple-event time digitizer

P7887 (FAST ComTec GmbH) were used for solid-state and solution lifetime measurements.

A femtosecond laser system manufactured by Coherent was used to measure nonlinear optical properties in this work. The system includes: two Mira Optima 900D lasers, providing flexibility in the choice of pulse durations (in the pico- and femtosecond range); two Verdi V10 pump lasers; two Pulse Switch acousto-optical modulators to thin the pulse repetition rate of femtosecond lasers; two Mira SPO-I prism compressors for dispersive compression of femtosecond laser pulses in terms of duration; two SHG second harmonic generators for conversion of femtosecond pulse radiation on a nonlinear optical crystal; two Mira OPO optical parametric converters for wavelength conversion of the laser source and its smooth tuning; SynchroLock AP synchronizer for mutual synchronization of two femtosecond lasers and their synchronization with an external radio frequency source in the range of laser generation frequencies.

### 3.2. Synthesis of bis-alkynyl Pt(II) complexes with ancillary N<sup>N</sup> ligand

Pt(II) complexes of NN series were synthesized according to the general procedure. 1 eq of [Pt(dtbp)<sub>2</sub>Cl<sub>2</sub>] and 2 eq of corresponding phosphonium salt were added to the flask and dissolved in DCM. Argon was purged through the resulting solution for approx. 5 minutes. Then, 11 mol.% of CuI were added under argon, followed by trimethylamine in volumetric ratio 2:7 to DCM. The resulting reaction mixture was purged with argon for additional 10 minutes, sealed with septum and stirred overnight. After that, the reaction mixture was evaporated, redissolved in DCM, and purified with two-step column chromatography (1: silica, CH<sub>2</sub>Cl<sub>2</sub> → acetone → CH<sub>2</sub>Cl<sub>2</sub> + 30% MeOH; 2: alumina, CH<sub>2</sub>Cl<sub>2</sub> + 50% acetone → CH<sub>2</sub>Cl<sub>2</sub> + 4% MeOH). The resulting solutions were evaporated to minimal volume, precipitated with Et<sub>2</sub>O and dried in vacuo, yielding complexes with the general name NN[Cl].

Second stage included metathesis of obtained compounds with NaBARF. 1 eq of complex NN[Cl] was dissolved in DCM, and a minimal volume of diethyl ether solution of 1eq NaBARF was added. The reaction mixture was stirred for half an hour at room

temperature and then filtered through a pad of Celite to remove NaCl. The resulting mixture was purified by column chromatography (silica, CH<sub>2</sub>Cl<sub>2</sub>) and evaporated *in vacuo* until the dry foam of complexes **NN[BArF]** formed.

**[Pt(dtbpv)(P<sub>1</sub>)<sub>2</sub>]Cl<sub>2</sub>, 1NN[Cl]**. Yellow powder, yield 82%. <sup>1</sup>H NMR (400 MHz, CDCl<sub>3</sub>) δ 9.52 (d, *J* = 6.0 Hz, 2H, dtbpv), 8.09 (m, 2H, dtbpv), 7.73 (m, 2H, dtbpv), 7.83–7.66 (m, 24H, P<sub>1</sub>), 7.61 (m, 4H, P<sub>1</sub>), 3.30 (d, *J* = 13.3 Hz, 6H, Me(P<sub>1</sub>)), 1.49 (s, 18H, tBu(dtbpv)). <sup>31</sup>P NMR (162 MHz, CD<sub>2</sub>Cl<sub>2</sub>) δ 20.72 (s, 2P, P(P<sub>1</sub>)). ESI HRMS (*m/z*): calcd for [M]<sup>2+</sup>: 531.6858; found: 531.6856. Single crystals of **1NN[Cl]** were obtained by the slow diffusion of solvents through a gas phase at room temperature (CH<sub>2</sub>Cl<sub>2</sub>/Et<sub>2</sub>O). **1NN[Cl]**: *P*-1 (2), *a* = 12.22580(10), *b* = 15.0341(2), *c* = 19.24880(10) Å; α = 89.8380(10), β = 73.6110(10), γ = 69.2840(10) °; *V* = 3156.20(6) Å<sup>3</sup>; *Z* = 2; *R*<sub>1</sub> = 4.09%; CCDC 2269523).

**[Pt(dtbpv)(P<sub>1</sub>)<sub>2</sub>]BArF<sub>2</sub>, 1NN[BArF]**. Orange powder, yield 78%. <sup>1</sup>H NMR (400 MHz, Acetone-*d*<sub>6</sub>) δ 9.58 (d, *J* = 6.0 Hz, 2H, dtbpv), 8.77 (m, 2H, dtbpv), 8.00–7.88 (m, 12H, P<sub>1</sub>), 7.90 (m, 2H, dtbpv), 7.84 (m, 8H, P<sub>1</sub>), 7.81 (m, 16H, BArF), 7.78–7.71 (m, 8H, P<sub>1</sub>), 7.68 (m, 8H, BArF), 3.22 (d, *J* = 14.2 Hz, 6H, Me(P<sub>1</sub>)), 1.49 (s, 18H, tBu(dtbpv)). <sup>31</sup>P NMR (162 MHz, Acetone-*d*<sub>6</sub>) δ 20.82 (s, 2P, P(P<sub>1</sub>)). <sup>19</sup>F NMR (376 MHz, Acetone-*d*<sub>6</sub>) δ –63.28 (s, 48F, BArF).

ESI HRMS (*m/z*): calcd for [M]<sup>2+</sup>: 531.6858; found: 531.6869. Anal. calcd for C<sub>124</sub>H<sub>82</sub>B<sub>2</sub>F<sub>48</sub>N<sub>2</sub>P<sub>2</sub>Pt: C, 53.37; H, 2.96; N, 1.00%. Found: C, 53.66; H, 3.19; N, 1.25%. FTIR (KBr): 2109 cm<sup>-1</sup> (C≡C vibration).

**[Pt(dtbpv)(P<sub>2</sub>)<sub>2</sub>]Cl<sub>2</sub>, 2NN[Cl]**. Yellow powder, yield 76%. <sup>1</sup>H NMR (400 MHz, CDCl<sub>3</sub>) δ 9.70 (d, *J* = 5.9 Hz, 2H, dtbpv), 8.04 (m, 2H, dtbpv), 7.88 (m, 4H, P<sub>2</sub>), 7.86–7.77 (m, 16H, P<sub>2</sub>), 7.72 (m, 8H, P<sub>2</sub>), 7.65 (dd, *J*<sub>1</sub> = 5.9 Hz, *J*<sub>2</sub> = 1.6 Hz, 2H, dtbpv), 7.59 (m, 4H, P<sub>2</sub>), 7.53 (m, 4H, P<sub>2</sub>), 3.40 (d, *J* = 13.3 Hz, 6H, Me(P<sub>2</sub>)), 1.49 (s, 18H, tBu(dtbpv)). <sup>31</sup>P NMR (162 MHz, CDCl<sub>3</sub>) δ 21.66 (s, 2P, P(P<sub>2</sub>)).

ESI HRMS (*m/z*): calcd for [M]<sup>2+</sup>: 608.2181, found: 608.2166. Single crystals of **2NN[Cl]** were obtained by the slow diffusion of solvents through a gas phase at room temperature (CH<sub>2</sub>Cl<sub>2</sub>/Et<sub>2</sub>O). **2NN[Cl]**: (*P*bcn (60), *a* = 26.5050(5), *b* = 15.4826(3), *c* =

17.1901(4) Å;  $\alpha = 90$ ,  $\beta = 90$ ,  $\gamma = 90$  °;  $V = 7054.2(3)$  Å<sup>3</sup>;  $Z = 4$ ;  $R_1 = 4.80\%$ ; CCDC 2269524.

**[Pt(dtbpy)(P<sub>2</sub>)<sub>2</sub>]BArF<sub>2</sub>, 2NN[BArF]**. Orange powder, yield 77%. <sup>1</sup>H NMR (400 MHz, Acetone-*d*<sub>6</sub>)  $\delta$  9.70 (d,  $J = 6.0$  Hz, 2H, dtbpy), 8.72 (m, 2H, dtbpy), 8.12 (m, 4H, P<sub>2</sub>), 8.01–7.90 (m, 16H, P<sub>2</sub>), 7.92 (m, 2H, dtbpy), 7.89–7.77 (m, 24H, P<sub>2</sub>, BArF), 7.75 (m, 4H, P<sub>2</sub>), 7.69 (m, 8H, BArF), 7.57 (m, 4H, P<sub>2</sub>), 3.27 (d,  $J = 14.2$  Hz, 6H, Me(P<sub>2</sub>)), 1.50 (s, 18H, tBu(dtbpy)). <sup>31</sup>P NMR (162 MHz, Acetone-*d*<sub>6</sub>)  $\delta$  20.47 (s, 2P, P(P<sub>2</sub>)). <sup>19</sup>F NMR (376 MHz, Acetone-*d*<sub>6</sub>)  $\delta$  –62.35 (s, 48F, BArF).

ESI HRMS ( $m/z$ ): calcd for [M]<sup>2+</sup>: 608.2181, found: 608.2181. Anal. calcd for C<sub>136</sub>H<sub>90</sub>B<sub>2</sub>F<sub>48</sub>N<sub>2</sub>P<sub>2</sub>Pt: C, 55.51; H, 3.08; N, 0.95%. Found: C, 55.43; H, 3.20; N, 1.12%. FTIR (KBr): 2113 cm<sup>-1</sup> (C≡C vibration).

**[Pt(dtbpy)(P<sub>3</sub>)<sub>2</sub>]Cl<sub>2</sub>, 3NN[Cl]**. Yellow powder, yield 57%. <sup>1</sup>H NMR (400 MHz, CDCl<sub>3</sub>)  $\delta$  9.74 (d,  $J = 6.0$  Hz, 2H, dtbpy), 8.04 (m, 2H, dtbpy), 7.93 (m, 4H, P<sub>3</sub>), 7.86–7.78 (m, 16H, P<sub>3</sub>), 7.76–7.66 (m, 16H, P<sub>3</sub>), 7.64 (m, 2H, dtbpy), 7.54 (m, 8H, P<sub>3</sub>), 3.39 (d,  $J = 13.3$  Hz, 6H, Me(P<sub>3</sub>)), 1.49 (s, 18H, tBu(dtbpy)). <sup>31</sup>P NMR (162 MHz, CDCl<sub>3</sub>)  $\delta$  21.72 (s, 2P, P(P<sub>3</sub>)).

ESI HRMS ( $m/z$ ): calcd for [M]<sup>2+</sup>: 684.2495, found: 684.2487.

**[Pt(dtbpy)(P<sub>3</sub>)<sub>2</sub>]BArF<sub>2</sub>, 3NN[BArF]**. Orange powder, yield 54%. <sup>1</sup>H NMR (400 MHz, Acetone-*d*<sub>6</sub>)  $\delta$  9.74 (d,  $J = 6.0$  Hz, 2H, dtbpy), 8.70 (d,  $J = 2.1$  Hz, 2H, dtbpy), 8.18 (dd,  $J = 8.5, 3.0$  Hz, 4H, P<sub>3</sub>), 8.04–7.78 (m, 50H, P<sub>3</sub>, BArF), 7.92 (m, 2H, dtbpy), 7.75 (m, 4H, P<sub>3</sub>), 7.69 (m, 8H, BArF), 7.4 (m, 4H, P<sub>3</sub>), 3.29 (d,  $J = 14.0$  Hz, 6H, Me(P<sub>3</sub>)), 1.51 (s, 18H, tBu(dtbpy)). <sup>31</sup>P NMR (162 MHz, Acetone-*d*<sub>6</sub>)  $\delta$  21.97 (s, 2P, P(P<sub>3</sub>)). <sup>19</sup>F NMR (376 MHz, Acetone-*d*<sub>6</sub>)  $\delta$  –63.27 (s, 48F, BArF).

ESI HRMS ( $m/z$ ): calcd for [M]<sup>2+</sup>: 684.2495, found: 684.2500. Anal. calcd for C<sub>148</sub>H<sub>98</sub>B<sub>2</sub>F<sub>48</sub>N<sub>2</sub>P<sub>2</sub>Pt: C, 57.44; H, 3.19; N, 0.91%. Found: C, 57.40; H, 3.28; N, 1.13%. FTIR (KBr): 2110 cm<sup>-1</sup> (C≡C vibration).

**[Pt(dtbpy)(P<sub>n</sub>)<sub>2</sub>]Cl<sub>2</sub>, nNN[Cl]**. Yellow powder, yield 58%. <sup>1</sup>H NMR (400 MHz, CDCl<sub>3</sub>)  $\delta$  9.62 (d,  $J = 6.0$  Hz, 2H, dtbpy), 9.08 (m, 2H, P<sub>n</sub>), 8.13 (m, 2H, dtbpy), 7.94–7.84 (m, 8H, P<sub>n</sub>), 7.84–7.75 (m, 6H, P<sub>n</sub>), 7.75–7.61 (m, 10H, P<sub>n</sub>), 7.72 (m, 2H, dtbpy), 7.56–7.39 (m, 6H, P<sub>n</sub>), 3.43 (d,  $J = 12.7$  Hz, 6H, Me(P<sub>n</sub>)), 1.50 (s, 18H, tBu(dtbpy)). <sup>31</sup>P

NMR (162 MHz,  $\text{CDCl}_3$ )  $\delta$  21.12 (s, 2P, P( $\text{P}_n$ )). ESI HRMS (m/z): calcd for  $[\text{M}]^{2+}$ : 582.2024, found: 582.2017.

**[Pt(dtbpv)( $\text{P}_n$ )<sub>2</sub>][BArF<sub>2</sub>, nNN][BArF]**. Orange powder, yield 73%. <sup>1</sup>H NMR (400 MHz, Acetone-*d*<sub>6</sub>)  $\delta$  9.69 (d,  $J = 6.0$  Hz, 2H, dtbpv), 9.13 (m, 2H,  $\text{P}_n$ ), 8.80 (d,  $J = 2.1$  Hz, 2H, dtbpv), 8.03–7.94 (m, 12H,  $\text{P}_n$ ), 7.95 (m, 2H, dtbpv), 7.89–7.78 (m, 28H,  $\text{P}_n$ , BArF), 7.71–7.52 (m, 14H, BArF,  $\text{P}_n$ ), 3.35 (d,  $J = 13.6$  Hz, 6H, Me( $\text{P}_n$ )), 1.51 (s, 18H, tBu(dtbpv)). <sup>31</sup>P NMR (162 MHz, Acetone-*d*<sub>6</sub>)  $\delta$  21.32 (s, 2P, P( $\text{P}_n$ )). <sup>19</sup>F NMR (376 MHz, Acetone-*d*<sub>6</sub>)  $\delta$  –63.28 (s, 48F, BArF).

ESI HRMS (m/z): calcd for  $[\text{M}]^{2+}$ : 582.2024, found: 582.2023. Anal. calcd for  $\text{C}_{132}\text{H}_{86}\text{B}_2\text{F}_{48}\text{N}_2\text{P}_2\text{Pt}$ : C, 54.85; H, 3.00; N, 0.97%. Found: C, 54.89; H, 3.22; N, 1.08%. FTIR (KBr): 2102  $\text{cm}^{-1}$  ( $\text{C}\equiv\text{C}$  vibration).

### 3.3. Synthesis of bis-alkynyl Pt(II) complexes with ancillary phosphine and cyanide ligands

Complexes of **P[OTf]** series were synthesized according to the modified literature method [134]. One equivalent of  $[\text{Pt}(\text{PPh}_3)_2\text{Cl}_2]$  and two equivalents of the corresponding alkynylphosphonium ligand were dissolved in the minimal volume of chloroform and purged with argon for 10 minutes. Along with deaerating, CuI (5 mol.%) and Et<sub>3</sub>N (2:7 v/v to  $\text{CHCl}_3$ ) were added to the reaction mixture. The flask was sealed with septum and stirred at 35°C for 24 hours. The resulting solution was evaporated, and the crude powder was re-dissolved in dichloromethane. 4 equivalents of NaOTf acetone solution were added, and the reaction mixture was stirred for 30 minutes, followed by evaporation. The resulting powder was again dissolved in dichloromethane, filtered through celites to remove excess NaOTf and NaCl and precipitated using diethyl ether.

**[Pt(PPh<sub>3</sub>)<sub>2</sub>( $\text{P}_1$ )<sub>2</sub>][OTf<sub>2</sub>, 1P[OTf]**. Off-white powder, yield 70%. <sup>1</sup>H NMR (500 MHz,  $\text{CDCl}_3$ )  $\delta$  7.78 (m, 16H, ortho-H ( $\text{PPh}_3$ ), para-H ( $\text{P}_1$ )), 7.66 (td,  $J = 8.1, 3.5$  Hz, 8H, meta-H ( $\text{P}_1$ )), 7.57 (m, 8H, ortho-H ( $\text{P}_1$ )), 7.47 (t,  $J = 7.3$  Hz, 6H, para-H ( $\text{PPh}_3$ )), 7.41 (m, 12H, meta-H ( $\text{PPh}_3$ )), 7.15 (dd,  $J = 13.1, 8.2$  Hz, 4H,  $\text{P}_1$ ), 6.44 (d,  $J = 7.6$  Hz, 4H,  $\text{P}_1$ ),

2.85 (d,  $J = 13.2$  Hz, 6H, Me ( $P_1$ )).  $^{31}\text{P}$  NMR (202 MHz,  $\text{CDCl}_3$ )  $\delta$  20.92 (s, 2P,  $P_1$ ), 18.93 (s,  $J_{\text{P-Pt}} = 2584.6$  Hz, 2P,  $\text{PPh}_3$ ).  $^{19}\text{F}$  NMR (376 MHz,  $\text{DMSO-}d_6$ )  $\delta$  -78.35 (s, 6F, OTf).

ESI HRMS (m/z): calcd for  $[\text{M}]^{2+}$ : 660.1812; found: 660.1810. Anal. calcd for  $\text{C}_{80}\text{H}_{64}\text{F}_6\text{O}_6\text{P}_4\text{PtS}_2 + 1.4\text{CHCl}_3$ : C, 54.75; H, 3.69 %. Found: C, 54.53; H, 3.83%. FTIR (KBr):  $2107\text{ cm}^{-1}$  ( $\text{C}\equiv\text{C}$  vibration). Single crystals of **1P[OTf]** ( $P\bar{1}$  (2),  $a = 9.27050(10)$ ,  $b = 14.1404(2)$ ,  $c = 14.58660(10)$  Å;  $\alpha = 85.9460(10)$ ,  $\beta = 79.6510(10)$ ,  $\gamma = 88.9410(10)$  °;  $V = 1876.29(4)$  Å<sup>3</sup>;  $Z = 1$ ;  $R_1 = 3.82\%$ ; CCDC 2360483).

**[Pt(PPh<sub>3</sub>)<sub>2</sub>(P<sub>2</sub>)<sub>2</sub>][OTf]<sub>2</sub>, 2P[OTf]**. Yellowish powder, yield 88%.  $^1\text{H}$  NMR (500 MHz,  $\text{CDCl}_3$ )  $\delta$  7.84 (m, 16H, ortho-H ( $\text{PPh}_3$ ), para-H ( $P_2$ )), 7.78 (m, 4H,  $P_2$ ), 7.69 (m, 20H,  $P_2$ ), 7.43 (m, 18H, para-H ( $\text{PPh}_3$ ), meta-H ( $\text{PPh}_3$ )), 7.22 (d,  $J = 8.0$  Hz, 4H,  $P_2$ ), 6.39 (d,  $J = 8.0$  Hz, 4H,  $P_2$ ), 2.99 (d,  $J = 13.3$  Hz, 6H, Me ( $P_2$ )).  $^{31}\text{P}$  NMR (202 MHz,  $\text{CDCl}_3$ )  $\delta$  21.23 (s, 2P,  $P_2$ ), 18.76 (s,  $J_{\text{P-Pt}} = 2624.6$  Hz, 2P,  $\text{PPh}_3$ ).  $^{19}\text{F}$  NMR (376 MHz,  $\text{DMSO-}d_6$ )  $\delta$  -78.44 (s, 6F, OTf).

ESI HRMS (m/z): calcd for  $[\text{M}]^{2+}$ : 736.2125; found: 736.2132. Anal. calcd for  $\text{C}_{92}\text{H}_{72}\text{F}_6\text{O}_6\text{P}_4\text{PtS}_2 + 0.8\text{CHCl}_3$ : C, 59.73; H, 3.93 %. Found: C, 59.74; H, 3.98 %. FTIR (KBr):  $2104.4\text{ cm}^{-1}$  ( $\text{C}\equiv\text{C}$  vibration).

**[Pt(PPh<sub>3</sub>)<sub>2</sub>(P<sub>n</sub>)<sub>2</sub>][OTf]<sub>2</sub>, nP[OTf]**. Yellow-orange powder, yield 85%.  $^1\text{H}$  NMR (500 MHz, Chloroform-*d*)  $\delta$  7.85 (12H, ortho-H ( $\text{PPh}_3$ )), 7.79 (m, 4H, para-H ( $P_n$ )), 7.67 (m, 16H,  $P_n$ ), 7.42 (m, 4H,  $P_n$ ), 7.35 (m, 18H, para-H ( $\text{PPh}_3$ ), meta-H ( $\text{PPh}_3$ )), 7.29 (m, 2H,  $P_n$ ), 7.17 (dd,  $J = 17.1, 7.8$  Hz, 2H,  $P_n$ ), 7.09 (m, 2H,  $P_n$ ), 6.48 (dd,  $J = 7.8, 2.7$  Hz, 2H,  $P_n$ ), 2.99 (d,  $J = 12.8$  Hz, 6H, Me ( $P_n$ )).  $^{31}\text{P}$  NMR (202 MHz,  $\text{CDCl}_3$ )  $\delta$  20.24 (s, 2P,  $P_3$ ), 18.91 (s,  $J_{\text{P-Pt}} = 2581.2$  Hz, 2P,  $\text{PPh}_3$ ).  $^{19}\text{F}$  NMR (376 MHz,  $\text{DMSO-}d_6$ )  $\delta$  -77.75 (s, 6F, OTf).

ESI HRMS (m/z): calcd for  $[\text{M}]^{2+}$ : 710.1968; found: 710.1988. Anal. calcd for  $\text{C}_{88}\text{H}_{68}\text{F}_6\text{O}_6\text{P}_4\text{PtS}_2 + 0.5\text{CHCl}_3$ : C, 59.78; H, 3.88 %. Found: C, 59.77; H, 4.10 %. FTIR (KBr):  $2087.1\text{ cm}^{-1}$  ( $\text{C}\equiv\text{C}$  vibration). Single crystals of **3P** were obtained by the slow diffusion of solvents through a gas phase at room temperature ( $\text{CH}_2\text{Cl}_2$ /pentane).

**nP[OTf]** ( $P\bar{1}$  (2),  $a = 9.5089(2)$ ,  $b = 11.4039(2)$ ,  $c = 19.8310(3)$  Å;  $\alpha = 77.297(2)$ ,  $\beta = 78.273(2)$ ,  $\gamma = 66.447(2)$  °;  $V = 1906.97(7)$  Å<sup>3</sup>;  $Z = 1$ ;  $R_1 = 4.15\%$ ; CCDC 2360484).

Second series of Pt(II) complexes with general formula **[Pt(CN)<sub>2</sub>(P<sub>i</sub>)<sub>2</sub>]** was obtained using optimized literature method [136]. Methanol solution of 4 eq NaCN was added to the stirred solution of complexes **P[OTf]** in dichloromethane. The off-white powders of complexes **1CN** and **2CN** started to form immediately, and the reaction mixture was stirred for 1 hour. The formation of **nCN** lasted for 24 hours. The resulting suspensions were centrifuged, washed with methanol (2 times), acetone (2 times), dichloromethane (2 times), diethyl ether (2 times) and dried *in vacuo*.

**[Pt(CN)<sub>2</sub>(P<sub>1</sub>)<sub>2</sub>], 1CN.** Off-white powder, yield 92%. <sup>1</sup>H NMR (500 MHz, DMSO-*d*<sub>6</sub>)  $\delta$  7.86 (dd,  $J = 8.7, 4.8$  Hz, 4H, p-Ph), 7.77–7.70 (m, 16H, o-Ph, m-Ph), 7.53 (dd,  $J = 12.9, 8.5$  Hz, 4H, linker-H), 7.44 (dd,  $J = 8.5, 3.2$  Hz, 4H, linker-H), 3.06 (d,  $J = 14.5$  Hz, 6H, Me(P<sub>1</sub>)). <sup>31</sup>P NMR (202 MHz, DMSO-*d*<sub>6</sub>)  $\delta$  21.86 (s, 2P, P<sub>1</sub>).

Anal. calcd. for C<sub>44</sub>H<sub>34</sub>N<sub>2</sub>P<sub>2</sub>Pt + 0.7CH<sub>2</sub>Cl<sub>2</sub>: C, 59.18; H, 3.93; N, 3.09 %. Found: C, 59.22; H, 4.13, N 2.14 %. ATR-FTIR: 2109 cm<sup>-1</sup> (C≡N vibration); 2097 cm<sup>-1</sup> (C≡C vibration).

**[Pt(CN)<sub>2</sub>(P<sub>2</sub>)<sub>2</sub>], 2CN.** Off-white powder, yield 91%. <sup>1</sup>H NMR (500 MHz, DMSO-*d*<sub>6</sub>)  $\delta$  8.09–8.03 (m, 4H, linker-H), 7.89 (m, 4H, o-Ph), 7.83–7.73 (m, 20H, p-Ph, m-Ph, linker-H), 7.67 (d,  $J = 8.4$  Hz, 4H, linker-H), 7.27 (d,  $J = 8.4$  Hz, 4H, linker-H), 3.14 (d,  $J = 14.5$  Hz, 6H, Me(P<sub>2</sub>)). <sup>31</sup>P NMR (202 MHz, DMSO-*d*<sub>6</sub>)  $\delta$  22.07 (s, 2P, P<sub>2</sub>).

ESI HRMS (m/z): calcd for [M+2H+MeOH]<sup>2+</sup>: 516.6442; found: 516.6439. Anal. calcd. for C<sub>56</sub>H<sub>42</sub>N<sub>2</sub>P<sub>2</sub>Pt + 0.5 CH<sub>2</sub>Cl<sub>2</sub> + 0.2 Et<sub>2</sub>O: C, 64.42; H, 5.07; N, 2.64 %. Found: C, 64.59; H, 4.82; N, 1.51%. ATR-FTIR: 2104 cm<sup>-1</sup> (C≡N vibration); 2087 cm<sup>-1</sup> (C≡C vibration).

**[Pt(CN)<sub>2</sub>(P<sub>n</sub>)<sub>2</sub>], nCN.** Light yellow powder, yield 71%. <sup>1</sup>H NMR (500 MHz, DMSO-*d*<sub>6</sub>)  $\delta$  8.88 (d,  $J = 8.4$  Hz, 2H, linker-H), 7.88 (m, 4H, p-Ph), 7.81 (m, 8H, m-H), 7.75 (td,  $J = 7.8, 3.5$  Hz, 8H, o-H), 7.67 (m, 2H, linker-H), 7.61 (d,  $J = 8.4$  Hz, 2H, linker-

H), 7.56–7.48 (m, 4H, linker-H), 7.44 (dd,  $J = 16.9, 7.8$  Hz, 2H, linker-H), 3.21 (d,  $J = 13.9$  Hz, 6H, Me (P<sub>n</sub>)). <sup>31</sup>P NMR (202 MHz, DMSO-*d*<sub>6</sub>)  $\delta$  21.18 (s, 2P, P<sub>n</sub>).

ESI HRMS (m/z): calcd for [M+2H]<sup>2+</sup>: 474.6154; found: 474.6164. Anal. calcd. for C<sub>52</sub>H<sub>38</sub>N<sub>2</sub>P<sub>2</sub>Pt + 0.6CH<sub>2</sub>Cl<sub>2</sub> + 0.1Et<sub>2</sub>O: C, 62.91; H, 4.44; N, 2.78 %. Found: C, 63.10; H, 4.64; N 1.71%. ATR-FTIR: 2114 cm<sup>-1</sup> (C≡N vibration); 2076 cm<sup>-1</sup> (C≡C vibration).

### 3.4. Synthesis of mono-alkynyl Pt(II) complexes with ancillary C<sup>^</sup>N<sup>^</sup>N ligand

The series of Pt(II) complexes, **1C[X]–nC[X]** based on **phbpy**, were synthesized according to the general method. To the argon-purged dichloromethane solution of [Pt(phbpy)Cl] and alkynylphosphonium salt, 5 mol.% CuI and Et<sub>3</sub>N (2:7 v:v to DCM) were added, the reaction mixture was additionally purged with argon for 10 minutes and stirred overnight at room temperature. After evaporation, it was purified by column chromatography (silica, DCM → acetone → DCM + 20% MeOH), yielding separate fractions for chloride and triflate complexes.

Tetrafluoroborate and BArF derivatives were prepared as follows. To the solution of **1C[Cl]** in dichloromethane diethyl ether solution of 1 eq NaBArF or methanol solution of 5 eq NaBF<sub>4</sub> were added, respectively. The reaction mixtures were stirred for 1 hour at room temperature, filtered through celite, then evaporated, washed with hexane and dried *in vacuo*.

**Pt(phbpy)(P<sub>1</sub>)Cl, 1C[Cl]**. Orange powder, yield 63%. <sup>1</sup>H NMR (400 MHz, Methanol-*d*<sub>4</sub>)  $\delta$  8.91 (m, 1H, phbpy), 8.13 (m, 2H, phbpy), 7.94–7.83 (m, 4H, P<sub>1</sub>), 7.83–7.75 (m, 8H, P<sub>1</sub>), 7.74–7.58 (m, 2H, P<sub>1</sub>), 7.63 (m, 4H, phbpy), 7.61 (m, 1H, phbpy), 7.41 (m, 1H, phbpy), 7.05 (m, 2H, phbpy), 2.98 (d,  $J = 14.0$  Hz, 3H, P<sub>1</sub>). <sup>31</sup>P NMR (162 MHz, Acetone-*d*<sub>6</sub>)  $\delta$  21.70 (s, 1P, P<sub>1</sub>).

ESI HRMS (m/z): calcd for [M]<sup>2+</sup>: 726.1636; found: 726.1668. Anal. calcd for C<sub>37</sub>H<sub>28</sub>ClN<sub>2</sub>PPt + 0.5CH<sub>2</sub>Cl<sub>2</sub> + 0.2n-pentane: C, 56.46; H, 3.86; N, 3.42%. Found: C, 56.29; H, 4.02; N, 3.63%. FTIR (KBr): 2091 cm<sup>-1</sup> (C≡C vibration).

**Pt(phbpy)(P<sub>1</sub>)BF<sub>4</sub>, 1C[BF<sub>4</sub>]**. Orange powder, yield 87%. <sup>1</sup>H NMR (400 MHz, Acetone-d<sub>6</sub>) δ 9.15 (m, 1H, phbpy), 8.47 (m, 1H, phbpy), 8.38 (td, J = 7.9, 1.7 Hz, 1H, phbpy), 8.19–8.12 (m, 2H, phbpy), 8.00–7.88 (m, 7H, P<sub>1</sub>, phbpy), 7.89–7.80 (m, 6H, P<sub>1</sub>), 7.73 (m, 4H, P<sub>1</sub>), 7.62 (m, 1H, phbpy), 7.11 (dtd, J = 16.5, 7.9, 1.7 Hz, 2H, phbpy), 3.19 (d, J = 14.0 Hz, 3H, Me(P<sub>1</sub>)). <sup>31</sup>P NMR (162 MHz, Acetone-d<sub>6</sub>, 1P, P<sub>1</sub>) δ 21.64 (s, 1P, P<sub>1</sub>). <sup>19</sup>F NMR (376 MHz, Acetone-d<sub>6</sub>) δ -151.8, -151.9 (<sup>10</sup>B and <sup>11</sup>B respectively, m, 4F, BF<sub>4</sub>).

Anal. calcd for C<sub>37</sub>H<sub>28</sub>BF<sub>4</sub>N<sub>2</sub>PPt + 0.25 CH<sub>2</sub>Cl<sub>2</sub> + 0.1 MeCN: C, 53.62; H, 3.46; N, 3.51%. Found: C, 53.60; H, 3.39; N, 3.46%.

**Pt(phbpy)(P<sub>1</sub>)OTf, 1C[OTf]**. Dark-green powder, yield 34%. <sup>1</sup>H NMR (400 MHz, DMSO-d<sub>6</sub>) δ 9.00 (d, J = 5.5 Hz, 1H, phbpy), 8.55 (m, 1H, phbpy), 8.38 (m, 1H, phbpy), 8.27 (d<sub>AB</sub>, J = 7.9 Hz, 1H, phbpy), 8.17 (m, 1H, phbpy), 8.05 (d<sub>AB</sub>, J = 7.9 Hz, 1H, phbpy), 7.88 (m, 4H, P<sub>1</sub>), 7.83–7.73 (m, 10H, P<sub>1</sub>), 7.73–7.59 (m, 6H, P<sub>1</sub>, phbpy), 7.11 (m, 2H, phbpy), 3.12 (d, J = 14.5 Hz, 3H, Me(P<sub>1</sub>)). <sup>31</sup>P NMR (162 MHz, Acetone-d<sub>6</sub>) δ 21.65 (s, 1P, P<sub>1</sub>). <sup>19</sup>F NMR (376 MHz, Acetone-d<sub>6</sub>) δ -78.84 (s, 3F, OTf).

Anal. calcd for C<sub>38</sub>H<sub>28</sub>F<sub>3</sub>N<sub>2</sub>O<sub>3</sub>PPtS+2.1 CHCl<sub>3</sub>: C, 42.76; H, 2.69; N, 2.49%. Found: C, 42.87; H, 2.80; N, 2.67%.

**Pt(phbpy)(P<sub>1</sub>)BArF, 1C[BArF]**. Brown powder, yield 83%. <sup>1</sup>H NMR (400 MHz, Acetone-d<sub>6</sub>) δ 9.17 (m, 1H, phbpy), 8.49 (m, 1H, phbpy), 8.40 (td, J = 7.8, 1.7 Hz, 1H, phbpy), 8.21–8.14 (m, 2H, phbpy), 8.02–7.91 (m, 6H, P<sub>1</sub>, phbpy), 7.91–7.82 (m, 7H, P<sub>1</sub>), 7.82–7.78 (m, 8H, BArF), 7.77–7.71 (m, 4H, P<sub>1</sub>), 7.69 (s, 4H, BArF), 7.63 (dd, J = 7.8, 1.7 Hz, 1H, phbpy), 7.11 (m, 2H, phbpy), 3.20 (d, J = 14.1 Hz, 3H, Me(P<sub>1</sub>)). <sup>31</sup>P NMR (162 MHz, Acetone-d<sub>6</sub>) δ 21.64 (s, 1P, P<sub>1</sub>). <sup>19</sup>F NMR (376 MHz, Acetone-d<sub>6</sub>) δ -63.28 (s, 24F, BArF).

Anal. calcd for C<sub>69</sub>H<sub>40</sub>BF<sub>24</sub>N<sub>2</sub>PPt: C, 52.13; H, 2.54; N, 1.76%. Found: C, 52.19; H, 2.59; N, 1.81%.

**Pt(phbpy)(P<sub>2</sub>)Cl, 2C[Cl]**. Orange powder, yield 77%. <sup>1</sup>H NMR (400 MHz, Methanol-d<sub>4</sub>) δ 9.03 (m, 1H, phbpy), 8.09 (m, 2H, phbpy), 8.04 (m, 2H, P<sub>2</sub>), 7.90–7.63 (m, 14H, P<sub>2</sub>), 7.68 (m, 4H, phbpy), 7.59 (d, J = 8.4 Hz, 2H, P<sub>2</sub>), 7.52 (m, 1H, phbpy), 7.39 (m, 1H, phbpy), 7.06 (s, 2H, phbpy), 2.96 (d, J = 14.0 Hz, 3H, Me(P<sub>2</sub>)). <sup>31</sup>P NMR (162 MHz, DMSO-d<sub>6</sub>) δ 22.41 (s, 1P, P<sub>2</sub>).

ESI HRMS ( $m/z$ ): calcd for  $[M]^{2+}$ : 802.1931; found: 802.1957. Anal. calcd for  $C_{43}H_{32}ClN_2PPt + 0.6 CH_2Cl_2$ : C, 58.89; H, 3.76; N, 3.15%. Found: C, 58.80; H, 3.93; N, 3.21%. FTIR (KBr):  $2101\text{ cm}^{-1}$  ( $C\equiv C$  vibration). Single crystals of **2C[Cl]** were obtained by the slow diffusion of solvents through a gas phase at room temperature (MeOH/pentane).

**Pt(phbpy)(P<sub>n</sub>)Cl, nC[Cl]**. Orange powder, yield 35%. <sup>1</sup>H NMR (400 MHz, Methanol-*d*<sub>4</sub>)  $\delta$  9.09 (d,  $J = 5.5$  Hz, 1H, phbpy), 9.01 (d,  $J = 8.4$  Hz, 1H, P<sub>n</sub>), 8.28 (m, 1H, phbpy), 8.21 (td,  $J = 7.8, 1.6$  Hz, 1H, phbpy), 8.00 (m, 2H, P<sub>n</sub>), 7.95–7.66 (m, 11H, P<sub>n</sub>), 7.78 (m, 1H, phbpy), 7.69 (m, 4H, phbpy), 7.57 (m, 2H, P<sub>3</sub>), 7.52 (m, 1H, phbpy), 7.09 (m, 2H, phbpy), 3.14 (d,  $J = 13.5$  Hz, 3H, Me(P<sub>n</sub>)). <sup>31</sup>P NMR (162 MHz, Methanol-*d*<sub>4</sub>)  $\delta$  20.96 (s, 1P, P<sub>n</sub>). ESI HRMS ( $m/z$ ): calcd for  $[M]^{2+}$ : 776.1806; found: 776.1791. Anal. calcd for  $C_{41}H_{30}ClN_2PPt + 0.5 CH_2Cl_2 + 0.2 MeOH$ : C, 58.17; H, 3.72; N, 3.25%. Found: C, 58.00; H, 4.05; N, 3.43%. FTIR (KBr):  $2083\text{ cm}^{-1}$  ( $C\equiv C$  vibration). Single crystals of **nC[Cl]** were obtained by the slow diffusion of solvents through a gas phase at room temperature (MeOH/pentane). **nC[Cl]**: ( $P\bar{1}$  (2),  $a = 8.8549(4)$ ,  $b = 14.5893(4)$ ,  $c = 15.8516(6)$  Å;  $\alpha = 97.417(3)$ ,  $\beta = 103.085(4)$ ,  $\gamma = 100.285(3)$  °;  $V = 1931.65(13)$  Å<sup>3</sup>;  $Z = 2$ ;  $R_1 = 6.48\%$ ; CCDC 2352281).

### 3.5. Synthesis of Pt(II) mono-alkynyl complexes with ancillary N<sup>^</sup>N<sup>^</sup>N ligand

The series of complexes **1N[X]–nN[X]**, based on **terpy**, were synthesized according to the similar method. Equimolar amounts of  $[Pt(terpy)Cl]Cl$  and corresponding alkynylphosponium ligand were dissolved in MeOH and purged with argon for 5 minutes. Then, under argon, 5 mol.% of CuI were added, followed by trimethylamine (2:7 v:v to methanol). The resulting mixture was bubbled with argon for additional 10 minutes, sealed with septum and stirred for 60h at 55°C. Then it was cooled on an ice bath and 2,3 equivalents of AgOTf were added, followed by stirring for 1 hour. The resulting dark suspension was centrifuged, dissolved in acetone:MeOH (3:1 v:v) mixture and filtered through celites. Evaporation in vacuo and precipitation with Et<sub>2</sub>O gave the dark powders of **N[OTf]**.

To synthesize pure chloride derivatives  $\mathbf{N[Cl]}$ , the powders of  $\mathbf{N[OTf]}$  were dissolved in acetone, and 5 eq of tetraethylammonium chloride were added. The reaction was stirred at room temperature for 24 hours, the resulting suspension was centrifuged, washed with acetone, dissolved in 2 ml of the DCM:MeOH 9:1 mixture and passed through the pad with silica to remove tetraethylammonium salts. Addition of  $\text{Et}_2\text{O}$  gave dark powders of complexes  $\mathbf{1N[Cl]-nN[Cl]}$ .

Tetrafluoroborate derivative was synthesized by dissolving  $\mathbf{1N[OTf]}$  with 5 eq of  $\text{NaBF}_4$  in acetone/methanol solution and stirring this mixture for 24 hours. The resulting dark-green suspension was washed with water, acetone, diethyl ether and dried.

**Pt(terpy)(P<sub>1</sub>)Cl<sub>2</sub>, 1N[Cl]**. Dark-red powder, yield 63%.  $^1\text{H}$  NMR (400 MHz,  $\text{DMSO-}d_6$ )  $\delta$  9.18 (d,  $J = 4.7$  Hz, 2H, terpy), 8.73 (m, 4H, terpy), 8.65 (m, 1H, terpy), 8.55 (t,  $J = 7.3$  Hz, 2H, terpy), 7.94 (m, 2H, terpy), 7.93 (m, 2H, P<sub>1</sub>), 7.86 (dd,  $J = 8.3, 3.0$  Hz, 2H, P<sub>1</sub>), 7.83–7.76 (m, 8H, P<sub>1</sub>), 7.72 (m, 2H, P<sub>1</sub>), 3.16 (d,  $J = 14.6$  Hz, 3H, Me(P<sub>1</sub>)).  $^{31}\text{P}$  NMR (162 MHz,  $\text{DMSO-}d_6$ )  $\delta$  22.53 (s, 1P, P<sub>1</sub>).

ESI HRMS ( $m/z$ ): calcd for  $[\text{M}]^{2+}$ : 364.0823; found: 364.0830. Anal. calcd for  $\text{C}_{36}\text{H}_{28}\text{Cl}_2\text{N}_3\text{PPt} + 1.2\text{CH}_2\text{Cl}_2 + 1.1\text{MeOH}$ : C, 49.11; H, 3.74; N, 4.49%. Found: C, 49.04; H, 4.09; N, 4.79%. FTIR (KBr):  $2120\text{ cm}^{-1}$  ( $\text{C}\equiv\text{C}$  vibration).

**Pt(terpy)(P<sub>1</sub>)(BF<sub>4</sub>)<sub>2</sub>, 1N[BF<sub>4</sub>]**. Dark-green powder, yield 83%.  $^1\text{H}$  NMR (400 MHz,  $\text{DMSO-}d_6$ )  $\delta$  9.18 (m, 2H, terpy), 8.72 (m, 4H, terpy), 8.65 (m, 1H, terpy), 8.55 (td,  $J = 8.0, 7.7, 1.4$  Hz, 2H, terpy), 7.94 (m, 2H, terpy), 7.93 (m, 2H, P<sub>1</sub>), 7.86 (dd,  $J = 8.3, 3.0$  Hz, 2H, P<sub>1</sub>), 7.79 (m, 8H, P<sub>1</sub>), 7.72 (dd,  $J = 12.9, 8.4$  Hz, 2H, P<sub>1</sub>), 3.16 (d,  $J = 14.6$  Hz, 3H, Me(P<sub>1</sub>)).  $^{31}\text{P}$  NMR (162 MHz,  $\text{DMSO-}d_6$ )  $\delta$  22.53 (s, 1P, P<sub>1</sub>).  $^{19}\text{F}$  NMR (376 MHz,  $\text{DMSO-}d_6$ )  $\delta$  -148.27, -148.32 ( $^{10}\text{B}$  and  $^{11}\text{B}$  respectively, m, 8F,  $\text{BF}_4$ ).

Anal. calcd for  $\text{C}_{36}\text{H}_{28}\text{B}_2\text{F}_8\text{N}_3\text{PPt} + 0.5\text{CH}_2\text{Cl}_2$ : C, 46.40; H, 3.09; N, 4.45%. Found: C, 46.60; H, 3.05; N, 4.49%.

**Pt(terpy)(P<sub>1</sub>)(OTf)<sub>2</sub>, 1N[OTf]**. Dark-green powder, yield 88%.  $^1\text{H}$  NMR (400 MHz,  $\text{DMSO-}d_6$ )  $\delta$  9.19 (d,  $J = 4.9$  Hz, 2H, terpy), 8.72 (m, 4H, terpy), 8.66 (m, 1H, terpy), 8.55 (td,  $J = 7.9, 1.3$  Hz, 2H, terpy), 7.94 (m, 2H, terpy), 7.93 (m, 2H, P<sub>1</sub>), 7.86 (dd,  $J = 8.5, 3.0$  Hz, 2H, P<sub>1</sub>), 7.79 (m, 8H, P<sub>1</sub>), 7.72 (m, 2H, P<sub>1</sub>), 3.16 (d,  $J = 14.6$  Hz, 3H,

Me(P<sub>1</sub>)). <sup>31</sup>P NMR (162 MHz, DMSO-*d*<sub>6</sub>) δ 22.53 (s, 1P, P<sub>1</sub>). <sup>19</sup>F NMR (376 MHz, DMSO-*d*<sub>6</sub>) δ -77.74 (s, 3F, OTf).

Anal. calcd for C<sub>38</sub>H<sub>28</sub>F<sub>6</sub>N<sub>3</sub>O<sub>6</sub>PPTs<sub>2</sub>+0.5CH<sub>2</sub>Cl<sub>2</sub>: C, 43.25; H, 2.73; N, 3.93%. Found: C, 43.01; H, 2.81; N, 4.00%.

**Pt(terpy)(P<sub>1</sub>)(BArF)<sub>2</sub>, 1N[BArF]**. Red powder, yield 81%. <sup>1</sup>H NMR (400 MHz, DMSO-*d*<sub>6</sub>) δ 9.19 (d, *J* = 5.4 Hz, 2H, terpy), 8.72 (t, *J* = 8.2 Hz, 4H, terpy), 8.65 (m, 1H, terpy), 8.55 (m, 2H, terpy), 7.94 (m, 2H, terpy), 7.93 (m, 2H, P<sub>1</sub>), 7.86 (dd, *J* = 8.5, 3.0 Hz, 2H, P<sub>1</sub>), 7.79 (m, 8H, P<sub>1</sub>), 7.74 (s, 8H, BArF), 7.72 (m, 2H, P<sub>1</sub>), 7.63 (m, 16H, BArF), 3.16 (d, *J* = 14.6 Hz, 3H, Me(P<sub>1</sub>)). <sup>31</sup>P NMR (162 MHz, DMSO-*d*<sub>6</sub>) δ 22.53 (s, 1P, P<sub>1</sub>). <sup>19</sup>F NMR (376 MHz, DMSO-*d*<sub>6</sub>) δ -61.57 (s, 48F, BArF).

Anal. calcd for C<sub>100</sub>H<sub>52</sub>B<sub>2</sub>F<sub>48</sub>N<sub>3</sub>PPT: C, 48.92; H, 2.13; N, 1.71%. Found: C, 49.21; H, 2.60; N, 1.90%.

**Pt(terpy)(P<sub>2</sub>)Cl<sub>2</sub>, 2N[Cl]**. Dark-red powder, yield 62%. <sup>1</sup>H NMR (400 MHz, DMSO-*d*<sub>6</sub>) δ 9.23 (d, *J* = 4.7 Hz, 2H, terpy), 8.73 (m, 4H, terpy), 8.64 (m, 1H, terpy), 8.55 (td, *J* = 8.0, 1.3 Hz, 2H, terpy), 8.12 (dd, *J* = 8.4, 2.7 Hz, 2H, P<sub>2</sub>), 7.97 (m, 2H, terpy), 7.94–7.89 (m, 2H, P<sub>2</sub>), 7.88–7.75 (m, 12H, P<sub>2</sub>), 7.69 (m, 2H, P<sub>2</sub>), 3.21 (s, 3H, P<sub>2</sub>). <sup>31</sup>P NMR (162 MHz, DMSO-*d*<sub>6</sub>) δ 22.52 (s, 1P, P<sub>2</sub>).

ESI HRMS (*m/z*): calcd for [M]<sup>2+</sup>: 402.0980; found: 402.0987 Anal. calcd for C<sub>42</sub>H<sub>32</sub>Cl<sub>2</sub>N<sub>3</sub>PPT + 1.3CH<sub>2</sub>Cl<sub>2</sub> + 1MeOH: C, 52.26; H, 3.82; N, 4.13%. Found: C, 52.16; H, 4.06; N, 4.40%. FTIR (KBr): 2118 cm<sup>-1</sup> (C≡C vibration).

**Pt(terpy)(P<sub>n</sub>)Cl<sub>2</sub>, nN[Cl]**. Dark-green powder, yield 78%. <sup>1</sup>H NMR (400 MHz, DMSO-*d*<sub>6</sub>) δ 9.21 (d, *J* = 4.7 Hz, 2H, terpy), 8.80 (m, 1H, P<sub>n</sub>), 8.76 (m, 4H, terpy), 8.68 (m, 1H, terpy), 8.57 (td, *J* = 7.4, 1.0 Hz, 2H, terpy), 7.96 (m, 2H, terpy), 8.01–7.73 (m, 13H, P<sub>n</sub>), 7.62 (t, *J* = 8.1 Hz, 1H, P<sub>n</sub>), 7.55 (dd, *J* = 16.9, 7.7 Hz, 1H, P<sub>n</sub>), 3.29 (s, 3H, Me(P<sub>n</sub>)). <sup>31</sup>P NMR (162 MHz, DMSO-*d*<sub>6</sub>) δ 22.07 (s, 1P, P<sub>n</sub>).

ESI HRMS (*m/z*): calcd for [M]<sup>2+</sup>: 389.0909; found: 389.0884. Anal. calcd for C<sub>40</sub>H<sub>30</sub>Cl<sub>2</sub>N<sub>3</sub>PPT + 1.3CH<sub>2</sub>Cl<sub>2</sub> + 1MeOH: C, 51.21; H, 3.72; N, 4.24%. Found: C, 51.22; H, 4.00; N, 4.61%. FTIR (KBr): 2107 cm<sup>-1</sup> (C≡C vibration).

### 3.6. Synthesis of Pt(II) mono-alkynyl complexes with ancillary N<sup>^</sup>N<sup>^</sup>N<sup>^</sup> ligand

The synthesis of **CNC** complexes was carried out according to the modified literature method [97]. At the first step, 0.28 mmol (2 eq) of corresponding alkynylphosphonium ligand P<sub>i</sub> was dissolved in 10 ml of freshly distilled THF, degassed and cooled to -50°C. Then, 10% excess of 2.5M nBuLi hexanes solution was added (ca. 0.1 ml). The resulting yellow solution was stirred for half an hour. After that, 0.14 mmol (1 eq) of [Pt(CNC)dmsol] was added under argon and the reaction mixture was left to stir overnight, slowly coming to the room temperature. The resulting suspension was centrifuged. The orange precipitate was washed with DCM (4 times), methanol (1 time), diethyl ether (1 time) and dried *in vacuo*.

**[Pt(CNC)(P<sub>1</sub>)], 1CNC.** Orange powder, yield 56%. <sup>1</sup>H NMR (400 MHz, DMSO-*d*<sub>6</sub>) δ 7.87 (m, 2H, P<sub>1</sub>), 7.77 (m, 8H, P<sub>1</sub>), 7.76 (m, 2H, CNC), 7.66 (t, *J* = 7.9 Hz, 1H, CNC), 7.50 (m, 6H, P<sub>1</sub>), 7.49 (m, 2H, CNC), 7.03 (m, 2H, CNC), 6.92 (m, 2H, CNC), 3.06 (d, *J* = 14.3 Hz, 3H, Me(P<sub>1</sub>)). <sup>31</sup>P NMR (162 MHz, DMSO-*d*<sub>6</sub>) δ 21.74 (s, 1P, P<sub>1</sub>).

ESI HRMS (*m/z*): calcd for [M+H]<sup>+</sup>: 725.1687; found: 725.1689. FTIR (KBr): 2068 cm<sup>-1</sup> (C≡C vibration). Single crystals of **1CNC** were obtained by the slow evaporation of diluted acetone solution. **1CNC**: (I2/c (15), *a* = 24.9558(8), *b* = 12.2843(3), *c* = 21.9034(7) Å; α = 90, β = 115.373(4), γ = 90 °; *V* = 6067.1(4) Å<sup>3</sup>; *Z* = 4; *R*<sub>1</sub> = 4.82%; CCDC 2383597).

**[Pt(CNC)(P<sub>2</sub>)], 2CNC.** Orange powder, yield 66%. <sup>1</sup>H NMR (400 MHz, DMSO-*d*<sub>6</sub>) δ 8.07 (dd, *J* = 8.5, 2.8 Hz, 2H, P<sub>2</sub>), 7.90 (m, 2H, P<sub>2</sub>), 7.84 (m, 2H, CNC), 7.77 (m, 10H, P<sub>2</sub>), 7.70 (d, *J* = 8.5 Hz, 2H, P<sub>2</sub>), 7.65 (t, *J* = 7.9 Hz, 1H, CNC), 7.48 (d, *J* = 7.9 Hz, 2H, CNC), 7.38 (d, *J* = 24.3, 8.4 Hz, 4H, P<sub>2</sub>), 7.06 (m, 2H, CNC), 6.93 (m, 2H, CNC), 3.13 (s, 3H, P<sub>2</sub>). <sup>31</sup>P NMR (162 MHz, DMSO-*d*<sub>6</sub>) δ 22.21 (s, 1P, P<sub>2</sub>).

ESI HRMS (*m/z*): calcd for [M+H]<sup>+</sup>: 801.2004; found: 801.2001. FTIR (KBr): 2073 cm<sup>-1</sup> (C≡C vibration).

**[Pt(CNC)(P<sub>n</sub>)], nCNC.** Dark-brown powder, yield 8%. ESI HRMS (m/z): calcd for [M+H]<sup>+</sup>: 775.1845; found: 775.1840. FTIR (KBr): 2053 cm<sup>-1</sup> (C≡C vibration).

## CONCLUSION

### In this work, the following results were obtained:

1. A set of alkynylphosphonium salts, D- $\pi$ -A type compounds with different linkers that can act as ligand due to the C $\equiv$ C donor site (4 compounds in total) have been synthesized.
2. Six series of platinum(II) alkynylphosphonium complexes (29 compounds in total) were synthesized, among them:
  - (1) Bis-alkynylphosphonium complexes based on 4,4'-di-tertbutyl-2,2'-bipyridine in *cis*-configuration (8 compounds);
  - (2) Bis-alkynylphosphonium complexes with additional triphenylphosphine and cyanide ligands in *trans*-configuration (6 compounds);
  - (3) Mono-alkynylphosphonium complexes based on tridentate N<sup>N</sup>N 2,2':6',2''-terpyridine and cyclometallating C<sup>N</sup>N and C<sup>N</sup>C ligands 6-phenyl-2,2'-bipyridine and 2,6-diphenylpyridine (15 compounds).
3. The influence of charged phosphonium group in alkynylphosphonium ligand on copper-catalyzed chloride to alkyne substitution reactions was investigated. The optimization of the corresponding synthesis methods was carried out.
4. The obtained complexes were characterized by a full set of modern physicochemical analysis methods, including polynuclear (<sup>1</sup>H, <sup>31</sup>P{<sup>1</sup>H}, <sup>19</sup>F{<sup>1</sup>H}) NMR spectroscopy and two-dimensional <sup>1</sup>H<sup>1</sup>H COSY NMR spectroscopy; high-resolution electrospray ionization mass spectrometry in positive mode (ESI+), IR spectroscopy and elemental analysis. The structures of seven compounds were established by X-ray single crystal analysis.
5. Optical and photophysical properties of all obtained platinum (II) complexes were characterized using absorption spectroscopy in solution and luminescence spectroscopy both in solution and in solid state. The lifetime of excited states and luminescence quantum yields were measured both in aerated and deaerated solution and in solid state, and the *stimuli-responsive* and nonlinear optical properties of the obtained compounds were investigated.

**Based on the results obtained, the following conclusions can be drawn:**

1. For bis-alkynylphosphonium complexes of platinum(II) in the *cis*-configuration of NN[CI] and NN[BArF] series, the luminescence depends not only on the structure of alkynylphosphonium ligands, but also on aggregation effects. Increasing the length of the linker leads to a bathochromic shift in luminescence in solution, allowing structure-property correlation and using this to obtain emitters with desired photophysical characteristics. Introduction of alkynylphosphonium fragment along with bulk tert-butyl groups in the diimine ligand leads to the appearance of stimuli-responsive properties and enhancement of nonlinear-optical (two-photon absorption and emission) properties of the obtained complex compounds.

2. The geometrical arrangement of alkynylphosphonium ligands in different positions around the metal is able to fundamentally change the character of luminescence in the solid state. The *trans*- positioning of alkynylphosphonium ligands improves the conjugation between them, leading to dominant ligand-centered emission. The controllability of emission by varying the length of the linker, however, is also seen in *trans*- systems, allowing the design of phosphors with a given emission wavelength. The introduction of a phosphonium fragment at the periphery of the ligand environment leads both to the appearance of double emission in some systems and to the appearance of bright <sup>3</sup>LC emission in the P[OTf] series. This series is the first example of *trans*-alkynyl complexes of platinum(II) with additional aryl phosphine ligand possessing triplet emission in solid state.

3. Mono-alkynylphosphonium complexes of platinum(II) with additional N<sup>^</sup>N<sup>^</sup>N and C<sup>^</sup>N<sup>^</sup>N ligands also obey the general trend for the bathochromic shift of emission in solution with increasing linker length, but to a lesser extent than bis-alkynylphosphonium derivatives. The luminescence character of these systems in the solid state is determined by packing and metallophilic interactions. Also in this work it was shown for the first time that the increase of the anion size can increase the emission energy in the solid state.

4. The introduction of charge transfer systems as ligands into the coordination environment allows to “turn on” the luminescence of monoalkynylphosphonium

complexes of platinum(II) based on C<sup>N</sup>C ligands. It was shown for the first time the presence of emission in solution and solid state at room temperature for such compounds. Unfortunately, it seems that the leading role in phosphorescence quenching in C<sup>N</sup>C systems is played by distortions of the structure under excitation, which does not allow to obtain effective luminescence.

5. The presence of a naphthyl linker in an alkynylphosphonium ligand is a determinant of the nature of alkynylphosphonium complexes' luminescence in solution, regardless of the ancillary ligands.

**LIST OF ABBREVIATIONS**

1,2-DCE	–	1,2-dichloroethane
$^{19}\text{F}\{\text{H}\}$	–	$^{19}\text{F}$ without spin-spin interaction of $^{19}\text{F}$ and $^1\text{H}$
BODIPY	–	boron-dipyrromethene
COSY	–	correlation spectroscopy
DCM	–	dicloromethane
DMF	–	N,N-dimethylformamide
DMSO	–	dimethylsulphoxide
dpbz	–	2,6-dipyridylbenzene
dphpy	–	2,6-diphenylpyridine
dtbpy	–	4,4'-ditertbutyl-2,2'-bipyridine
ESI+	–	positive-mode electrospray ionisation
ILCT	–	intra-ligand charge-transfer
IR	–	infrared
LC	–	ligand-centered
LLCT	–	ligand-to-ligand charge-transfer
LUMO	–	lowest unoccupied molecular orbital
MC	–	metal-centered
MLCT	–	metal-to-ligand charge-transfer
MMLCT	–	metal/metal-to-ligand charge transfer
MTHF	–	2-methyltetrahydrofuran
NHC	–	N-heterocyclic carbene
NMR	–	nuclear magnetic resonance
OFET	–	organic field-effect transistor
OLED	–	organic light-emitting diodes
phbpy	–	6-phenyl-2,2'-bipyridine
PMMA	–	polymethylmetacrylate
$R_f$	–	retardation factor

SSI	–	spin-spin interaction
TD-DFT	–	time-dependent density functional theory
TEACl	–	tetraethylammonium chloride
terpy	–	2,2':6',2''-terpyridine
THF	–	tetrahydrofuran
TMACl	–	tetramethylammonium chloride
XRD		X-Ray diffraction analysis
HOMO	–	highest occupied molecular orbital
MO	–	molecular orbital

## ACKNOWLEDGEMENTS

This work would not have been possible without many people. First, I would like to thank my supervisor, Elena Valerievna Gracheva, for the belief in me, interesting tasks, answers to my questions, and productive discussions. Thank you for accepting me into our group in the Master's program, despite my irrelevant experience!

Speaking about the research group, I would like to express my sincere gratitude to the entire LMCO Group team, and especially to Maxim Luginin, Evgeniya Abramova and Dmitry Snetkov. Scientific or not, discussions with you gave me a lot of pleasure! Thank you also for maintaining an easy atmosphere in the lab. I also thank my colleagues from the friendly scientific group of S.P. Tunik: Yulia Shakirova, Ilya Kritchenkov and Anastasia Solomatina, and a former colleague of our group, Stanislav Petrovsky. Your consultations on the measurement of photophysical properties and synthetic problems helped me a lot.

The staff of the SPSU Research Park from centers “Magnetic Resonance Research Methods”, “X-ray Diffraction Research Methods”, “Optical and Laser Methods of Matter Research”, and “Methods of Matter Composition Analysis” provided great support. Special thanks go to A. Y. Ivanov, S. N. Smirnov, S. S. Shayakhmedov and I. E. Kolesnikov, as well as A. S. Melnikov (SPbSPU “Polytech”). For quantum-chemical calculations I thank Sofia Slavova and Anastasia Sizova.

My special “thank you” to my school chemistry teacher, Kopnina Olga, who made me fall in love with this beautiful science. Thank you for spending your free time preparing me for chemical olympiads.

Finally, I thank my mom, Tatiana Paderina, and my husband, Alexei Chupikov, for their love, support, and readiness to listen to my long stories about my chemistry.

## REFERENCES

1. Highly Efficient OLEDs with Phosphorescent Materials / ed. Yersin H. Wiley, 2007.
2. Belyaev A., Chou P., Koshevoy I.O. Cationic Organophosphorus Chromophores: A Diamond in the Rough among Ionic Dyes // *Chem. – A Eur. J.* 2021. Vol. 27, № 2. P. 537–552.
3. Kondrasenko I. et al. Ambipolar Phosphine Derivatives to Attain True Blue OLEDs with 6.5% EQE // *ACS Appl. Mater. Interfaces.* 2016. Vol. 8, № 17. P. 10968–10976.
4. Lee C.-H. et al. Highly luminescent phosphine oxide-containing bipolar alkynylgold(III) complexes for solution-processable organic light-emitting devices with small efficiency roll-offs // *Chem. Sci.* 2018. Vol. 9, № 29. P. 6228–6232.
5. Yam V.W.-W., Law A.S.-Y. Luminescent d8 metal complexes of platinum(II) and gold(III): From photophysics to photofunctional materials and probes // *Coord. Chem. Rev.* 2020. Vol. 414. P. 213298.
6. Petrovskii S. et al. Homoleptic Alkynylphosphonium Au(I) Complexes as Push–Pull Phosphorescent Emitters // *Inorg. Chem.* 2023. Vol. 62, № 13. P. 5123–5133.
7. Paderina A. et al. Alkynylphosphonium Pt(II) Complexes: Synthesis, Characterization, and Features of Photophysical Properties in Solution and in the Solid State // *Inorg. Chem.* 2023. Vol. 62, № 44. P. 18056–18068.
8. Grachova E., Paderina A., Sizova A. Cationic or Neutral: Dependence of Photophysical Properties of Bis-alkynylphosphonium Pt(II) Complexes on Ancillary Ligand // *Chem. – A Eur. J.* 2024, P. e202402242.
9. Paderina A. et al. Aggregation Game: Changing Solid-State Emission Using Different Counterions in Monoalkynylphosphonium Pt(II) Complexes // *Inorg. Chem.* 2024. Vol. 63, № 38, P. 17548–17560.
10. Mauro M. et al. When self-assembly meets biology: Luminescent platinum complexes for imaging applications // *Chem. Soc. Rev.* 2014. Vol. 43, № 12. P. 4144–4166.

11. Yang X., Yao C., Zhou G. Highly efficient phosphorescent materials based on platinum complexes and their application in organic light-emitting devices (OLEDs) // *Platin. Met. Rev.* 2013. Vol. 57, № 1. P. 2–16.
12. Tang M.C. et al. Platinum and Gold Complexes for OLEDs // *Top. Curr. Chem.* 2016. Vol. 374, № 4. P. 46.
13. Fuertes S. et al. Green light-emitting electrochemical cells based on platinum(ii) complexes with a carbazole-appended carbene ligand // *J. Mater. Chem. C.* 2022. Vol. 10, № 41. P. 15491–15500.
14. Sinn S. et al. A Ratiometric Luminescent Switch Based on Platinum Complexes Tethered to a Crown-Ether Scaffold // *ChemPhysChem.* 2016. Vol. 17, № 12. P. 1829–1834.
15. Colombo A. et al. An excursion in the second-order nonlinear optical properties of platinum complexes // *Coord. Chem. Rev.* 2021. Vol. 446. P. 214113.
16. Zhu S. et al. AIPE-active Pt(ii) complexes with a tunable triplet excited state: Design, mechanochromism and application in anti-counterfeiting // *Inorg. Chem. Front.* 2020. Vol. 7, № 23. P. 4677–4686.
17. Pang C. et al. An Excellent Platinum Piezoresistive Pressure Sensor Using Adhesive Bonding with SU-8 // *Adv. Mater. Res.* 2009. Vol. 60–61. P. 68–73.
18. Chan A.K.W. et al. Synthesis and Characterization of Luminescent Cyclometalated Platinum(II) Complexes with Tunable Emissive Colors and Studies of Their Application in Organic Memories and Organic Light-Emitting Devices // *J. Am. Chem. Soc.* 2017. Vol. 139, № 31. P. 10750–10761.
19. Williams J.A.G. Photochemistry and Photophysics of Coordination Compounds: Platinum // *Photochemistry and Photophysics of Coordination Compounds II.* Berlin, Heidelberg, Heidelberg: Springer Berlin Heidelberg, 2007. Vol. 281. P. 205–268.
20. Fleeman W.L., Connick W.B. Self-quenching and Cross-quenching Reactions of Excited Platinum(II) Diimine Complexes // *Comments Inorg. Chem.* 2002. Vol. 23, № 3. P. 205–230.
21. Castellano F.N. et al. Photophysics in bipyridyl and terpyridyl platinum(II)

- acetylides // *Coord. Chem. Rev.* 2006. Vol. 250, № 13–14. P. 1819–1828.
22. Chi Y., Chou P.-T. Transition-metal phosphors with cyclometalating ligands: fundamentals and applications // *Chem. Soc. Rev.* 2010. Vol. 39, № 2. P. 638–655.
  23. Lazzaro D.P., McGuire R., McMillin D.R. Regiospecific Quenching of a Photoexcited Platinum(II) Complex at Acidic and Basic Sites // *Inorg. Chem.* 2011. Vol. 50, № 10. P. 4437–4444.
  24. Catherine E. Housecroft; Alan G. Sharpe. *Inorganic chemistry*. 4th ed. Pearson, 2012.
  25. Preston D.M. et al. Unusual spectroscopic features in the emission and absorption spectra of single-crystal potassium tetrachloroplatinate(II) ( $K_2[PtCl_4]$ ) caused by multiple-mode excited-state distortions // *J. Am. Chem. Soc.* 1988. Vol. 110, № 17. P. 5628–5633.
  26. Miskowski V.M., Houlding V.H. Electronic Spectra and Photophysics of Platinum(II) Complexes with  $\alpha$ -Diimine Ligands. Solid-State Effects. 1. Monomers and Ligand  $\pi$  Dimers // *Inorg. Chem.* 1989. Vol. 28, № 8. P. 1529–1533.
  27. Miskowski V.M. et al. Electronic spectra and photophysics of platinum(II) complexes with  $\alpha$ -diimine ligands. Mixed complexes with halide ligands // *Inorg. Chem.* 1993. Vol. 32, № 11. P. 2518–2524.
  28. Yersin H. et al. Franck-Condon analysis of transition-metal complexes // *J. Am. Chem. Soc.* 1980. Vol. 102, № 3. P. 951–955.
  29. Vogler A., Kunkely H. Luminescent Metal Complexes: Diversity of Excited States // *Transition Metal and Rare Earth Compounds* / ed. Yersin H. Springer, Berlin, Heidelberg, 2001. P. 143–182.
  30. Wang X., Del Guerso A., Schmehl R.H. Photophysical behavior of transition metal complexes having interacting ligand localized and metal-to-ligand charge transfer states // *J. Photochem. Photobiol. C Photochem. Rev.* 2004. Vol. 5, № 1. P. 55–77.
  31. Endicott J.F., Chen Y.-J. Charge transfer-excited state emission spectra of mono-

- and bi-metallic coordination complexes: Band shapes, reorganizational energies and lifetimes // *Coord. Chem. Rev.* 2007. Vol. 251, № 3–4. P. 328–350.
32. Nigam S., Rutan S. Principles and Applications of Solvatochromism // *Appl. Spectrosc.* 2001. Vol. 55, № 11. P. 362A-370A.
  33. Rijavec T., Bračko S. Smart dyes for medical and other textiles // *Smart Textiles for Medicine and Healthcare.* Elsevier, 2007. P. 123–149.
  34. Kalyanasundaram K. Luminescence and redox reactions of the metal-to-ligand charge-transfer excited state of tricarbonylchloro-(polypyridyl)rhenium(I) complexes // *J. Chem. Soc. Faraday Trans. 2.* 1986. Vol. 82, № 12. P. 2401.
  35. Wong K.M.C., Yam V.W.W. Luminescence platinum(II) terpyridyl complexes- From fundamental studies to sensory functions // *Coord. Chem. Rev.* 2007. Vol. 251, № 17–20. P. 2477–2488.
  36. Aldridge T.K., Stacy E.M., McMillin D.R. Studies of the Room-Temperature Absorption and Emission Spectra of [Pt(trpy)X]<sup>+</sup> Systems // *Inorg. Chem.* 1994. Vol. 33, № 4. P. 722–727.
  37. Whittle C.E. et al. Photophysics of diimine platinum(II) bis-acetylide complexes // *Inorg. Chem.* 2001. Vol. 40, № 16. P. 4053–4062.
  38. Poveda D. et al. Luminescent Platinum(II) Complexes with Terdentate NACAC Ligands // *Inorg. Chem.* 2023. Vol. 62, № 51. P. 20987–21002.
  39. Vogler A., Kunkely H. Charge Transfer Excitation of Coordination Compounds. Generation of Reactive Intermediates. 1993. P. 71–111.
  40. Cummings S.D., Eisenberg R. Tuning the Excited-State Properties of Platinum(II) Diimine Dithiolate Complexes // *J. Am. Chem. Soc.* 1996. Vol. 118, № 8. P. 1949–1960.
  41. Tong G.S.M. et al. Ligand-to-Ligand Charge-Transfer Transitions of Platinum(II) Complexes with Arylacetylide Ligands with Different Chain Lengths: Spectroscopic Characterization, Effect of Molecular Conformations, and Density Functional Theory Calculations // *Chem. - A Eur. J.* 2010. Vol. 16, № 22. P. 6540–6554.
  42. Shiotsuka M. et al. Photoluminescence of platinum(II) diethynylphenanthroline

- organometallic complexes with bis-arylethynyl derivatives in solution and solid state // *J. Organomet. Chem.* 2019. Vol. 880. P. 116–123.
43. Nolan D. et al. Propellers and Planes: Phosphorescent Pt II  $\sigma$ -Acetylides from Polyaromatic Ligands // *Eur. J. Inorg. Chem.* 2011. Vol. 2011, № 21. P. 3248–3256.
  44. Wu W. et al. Red-light excitable fluorescent platinum(ii) bis(aryleneethynylene) bis(trialkylphosphine) complexes showing long-lived triplet excited states as triplet photosensitizers for triplet-triplet annihilation upconversion // *J. Mater. Chem. C.* 2013. Vol. 1, № 4. P. 705–716.
  45. Prusakova V., McCusker C.E., Castellano F.N. Ligand-Localized Triplet-State Photophysics in a Platinum(II) Terpyridyl Perylenediimideacetylide // *Inorg. Chem.* 2012. Vol. 51, № 15. P. 8589–8598.
  46. Pomestchenko I.E. et al. Room Temperature Phosphorescence from a Platinum(II) Diimine Bis(pyrenylacetylide) Complex // *Inorg. Chem.* 2003. Vol. 42, № 5. P. 1394–1396.
  47. Pomestchenko I.E., Castellano F.N. Solvent Switching between Charge Transfer and Intraligand Excited States in a Multichromophoric Platinum(II) Complex // *J. Phys. Chem. A.* 2004. Vol. 108, № 16. P. 3485–3492.
  48. Jackel A. et al. Turning-On of Coumarin Phosphorescence in Acetylacetonato Platinum Complexes of Cyclometalated Pyridyl-Substituted Coumarins // *Inorganics.* 2015. Vol. 3, № 2. P. 55–81.
  49. He R. et al. High-Purity and Saturated Deep-Blue Luminescence from trans -NHC Platinum(II) Butadiyne Complexes: Properties and Organic Light Emitting Diode Application // *ACS Appl. Mater. Interfaces.* 2021. Vol. 13, № 4. P. 5327–5337.
  50. Farley S.J. et al. Controlling Emission Energy, Self-Quenching, and Excimer Formation in Highly Luminescent NACAN-Coordinated Platinum(II) Complexes // *Inorg. Chem.* 2005. Vol. 44, № 26. P. 9690–9703.
  51. Liao K.-Y. et al. Pt(II) Metal Complexes Tailored with a Newly Designed Spiro-Arranged Tetradentate Ligand; Harnessing of Charge-Transfer Phosphorescence and Fabrication of Sky Blue and White OLEDs // *Inorg. Chem.* 2015. Vol. 54, №

8. P. 4029–4038.
52. Kozina D.O. et al. Unusual Reactivity and Photophysical Properties of Platinum(II) Pincer Complexes Containing 6,6'-Diphenyl-2,2'-bipyridine Ligands // *Eur. J. Inorg. Chem.* 2021. Vol. 2021, № 2. P. 117–125.
53. Houlding V.H., Miskowski V.M. The effect of linear chain structure on the electronic structure of Pt(II) diimine complexes // *Coord. Chem. Rev.* 1991. Vol. 111. P. 145–152.
54. Bailey J.A., Miskowski V.M., Gray H.B. Spectroscopic and structural properties of binuclear platinum-terpyridine complexes // *Inorg. Chem.* 1993. Vol. 32, № 4. P. 369–370.
55. Büchner R. et al. Luminescence properties of salts of the [Pt(4'Ph-terpy)Cl]<sup>+</sup> chromophore: crystal structure of the red form of [Pt(4'Ph-terpy)Cl]BF<sub>4</sub> (4'Ph-terpy = 4'-phenyl-2,2':6',2''-terpyridine) // *J. Chem. Soc. Dalt. Trans.* 1999. № 5. P. 711–718.
56. Yersin H., Gliemann G. SPECTROSCOPIC STUDIES OF M<sub>x</sub> [Pt(CN)<sub>4</sub>] · yH<sub>2</sub>O // *Ann. N. Y. Acad. Sci.* 1978. Vol. 313, № 1. P. 539–559.
57. Connick W.B. et al. Emission Spectroscopic Properties of the Red Form of Dichloro(2,2'-bipyridine)platinum(II). Role of Intermolecular Stacking Interactions // *Inorg. Chem.* 1996. Vol. 35, № 21. P. 6261–6265.
58. Yam V.W.-W., Wong K.M.-C., Zhu N. Solvent-Induced Aggregation through Metal···Metal/ $\pi$ ··· $\pi$  Interactions: Large Solvatochromism of Luminescent Organoplatinum(II) Terpyridyl Complexes // *J. Am. Chem. Soc.* 2002. Vol. 124, № 23. P. 6506–6507.
59. Strassert C.A., Mauro M., De Cola L. Photophysics of soft and hard molecular assemblies based on luminescent complexes. 2011. P. 47–103.
60. Lai S.-W. et al. Probing d<sub>8</sub>–d<sub>8</sub> Interactions in Luminescent Mono- and Binuclear Cyclometalated Platinum(II) Complexes of 6-Phenyl-2,2'-bipyridines // *Inorg. Chem.* 1999. Vol. 38, № 18. P. 4046–4055.
61. Lu W. et al. Structural and Spectroscopic Studies on Pt···Pt and  $\pi$ – $\pi$  Interactions in Luminescent Multinuclear Cyclometalated Platinum(II) Homologues Tethered

- by Oligophosphine Auxiliaries // *J. Am. Chem. Soc.* 2004. Vol. 126, № 24. P. 7639–7651.
62. Leung S.Y.-L. et al. Synthesis, Structural Characterization, and Photophysical Study of Luminescent Face-to-Face Dinuclear Platinum(II) Alkynyl Phosphine Complexes and Their Tetranuclear Mixed-Metal Platinum(II)–Silver(I) and –Copper(I) Complexes // *Organometallics*. 2010. Vol. 29, № 21. P. 5558–5569.
63. Hudson Z.M. et al. Probing the structural origins of vapochromism of a triarylboron- functionalized platinum(II) acetylide by optical and multinuclear solid-state NMR spectroscopy // *Inorg. Chem.* 2011. Vol. 50, № 8. P. 3447–3457.
64. Wenger O.S. Vapochromism in organometallic and coordination complexes: Chemical sensors for volatile organic compounds // *Chem. Rev.* 2013. Vol. 113, № 5. P. 3686–3733.
65. Sivchik V. V. et al. Solid-State and Solution Metallophilic Aggregation of a Cationic [Pt(NCN)L] + Cyclometalated Complex // *Inorg. Chem.* 2016. Vol. 55, № 7. P. 3351–3363.
66. Cuerva C. et al. Multi-Stimuli-Responsive Properties of Aggregation-Enhanced Emission-Active Unsymmetrical Pt II Metallomesogens through Self-Assembly // *Chem. – A Eur. J.* 2019. Vol. 25, № 52. P. 12046–12051.
67. Soto M.A., Kandel R., MacLachlan M.J. Chromic Platinum Complexes Containing Multidentate Ligands // *Eur. J. Inorg. Chem.* 2021. Vol. 2021, № 10. P. 894–906.
68. Martínez-Junquera M., Lalinde E., Moreno M.T. Multistimuli-Responsive Properties of Aggregated Isocyanide Cycloplatinated(II) Complexes // *Inorg. Chem.* 2022. Vol. 61, № 28. P. 10898–10914.
69. Mei J. et al. Aggregation-Induced Emission: Together We Shine, United We Soar! // *Chem. Rev.* 2015. Vol. 115, № 21. P. 11718–11940.
70. Yoshida M., Kato M. Regulation of metal–metal interactions and chromic phenomena of multi-decker platinum complexes having  $\pi$ -systems // *Coord. Chem. Rev.* 2018. Vol. 355. P. 101–115.
71. Li B. et al. Visual self-assembly and stimuli-responsive materials based on recent

- phosphorescent platinum(II) complexes // *Mol. Syst. Des. Eng.* 2020. Vol. 5, № 10. P. 1578–1605.
72. Yam V.W.-W., Au V.K.-M., Leung S.Y.-L. Light-Emitting Self-Assembled Materials Based on d 8 and d 10 Transition Metal Complexes // *Chem. Rev.* 2015. Vol. 115, № 15. P. 7589–7728.
73. Muro M.L. et al. Platinum II Acetylide Photophysics. 2009. P. 1–35.
74. Li Y. et al. Synthesis of Unsymmetric Bipyridine–Pt II –Alkynyl Complexes through Post-Click Reaction with Emission Enhancement Characteristics and Their Applications as Phosphorescent Organic Light-Emitting Diodes // *Chem. – A Eur. J.* 2014. Vol. 20, № 42. P. 13710–13715.
75. Petrovskii S. et al. Post-Functionalization of Organometallic Complexes via Click-Reaction // *Molecules.* 2022. Vol. 27, № 19. P. 6494.
76. Chan C.W., Cheng L.K., Che C.M. Luminescent donor-acceptor platinum(ii) complexes // *Coord. Chem. Rev.* 1994. Vol. 132, № C. P. 87–97.
77. Berenguer J.R., Lalinde E., Teresa Moreno M. An overview of the chemistry of homo and heteropolynuclear platinum complexes containing bridging acetylide ( $\mu\text{-C}\equiv\text{CR}$ ) ligands // *Coord. Chem. Rev.* 2010. Vol. 254, № 7–8. P. 832–875.
78. Berenguer J.R. et al. Self-Assembly of Luminescent Alkynyl-Based Platinum–Cadmium Complexes Containing Auxiliary Diimine or Terpyridine Ligands. // *Inorg. Chem.* 2009. Vol. 48, № 12. P. 5250–5262.
79. Wei Q.-H. et al. Luminescent heterohexanuclear complexes with platinum alkynyl and silver diphosphine as components // *Chem. Commun.* 2003. № 17. P. 2188.
80. Cebrián C., Mauro M. Recent advances in phosphorescent platinum complexes for organic light-emitting diodes // *Beilstein J. Org. Chem.* 2018. Vol. 14. P. 1459–1481.
81. Bullock J.D. et al. In Search of Deeper Blues: Trans -N-Heterocyclic Carbene Platinum Phenylacetylide as a Dopant for Phosphorescent OLEDs // *ACS Appl. Mater. Interfaces.* 2017. Vol. 9, № 47. P. 41111–41114.
82. Maganti T., Venkatesan K. The Search for Efficient True Blue and Deep Blue Emitters: An Overview of Platinum Carbene Acetylide Complexes //

- Chempluschem. 2022. Vol. 87, № 5.
83. Yam V.W.-W., Cheng Y.-H. Stimuli-Responsive and Switchable Platinum(II) Complexes and Their Applications in Memory Storage // *Bull. Chem. Soc. Jpn.* 2022. Vol. 95, № 6. P. 846–854.
  84. Lee J.K.-W. et al. A Photochromic Platinum(II) Bis(alkynyl) Complex Containing a Versatile 5,6-Dithienyl-1,10-phenanthroline // *Organometallics*. 2007. Vol. 26, № 1. P. 12–15.
  85. Wong H.L. et al. Photochromic alkynes as versatile building blocks for metal alkynyl systems: Design, synthesis, and photochromic studies of diarylethene-containing platinum(II) phosphine alkynyl complexes // *Inorg. Chem.* 2011. Vol. 50, № 2. P. 471–481.
  86. Yam V.W.-W. et al. Synthesis, Luminescence, Electrochemistry, and Ion-Binding Studies of Platinum(II) Terpyridyl Acetylide Complexes // *Organometallics*. 2001. Vol. 20, № 22. P. 4476–4482.
  87. Yu C. et al. Polymer-Induced Self-Assembly of Alkynylplatinum(II) Terpyridyl Complexes by Metal···Metal/ $\pi$ ··· $\pi$  Interactions // *Angew. Chemie Int. Ed.* 2005. Vol. 44, № 5. P. 791–794.
  88. Tam A.Y.-Y. et al. Luminescent metallogels of platinum(II) terpyridyl complexes: interplay of metal···metal,  $\pi$ - $\pi$  and hydrophobic–hydrophobic interactions on gel formation // *Chem. Commun.* 2007. № 20. P. 2028–2030.
  89. Yang Q. et al. Switch of the Lowest Excited-States of Terpyridylplatinum(II) Acetylide Complexes Bearing Amino or Azacrown Moieties by Proton and Cations // *Eur. J. Inorg. Chem.* 2004. Vol. 2004, № 9. P. 1948–1954.
  90. Wong K.M.-C. et al. Functionalized Platinum(II) Terpyridyl Alkynyl Complexes as Colorimetric and Luminescence pH Sensors // *Inorg. Chem.* 2005. Vol. 44, № 5. P. 1492–1498.
  91. Tang W.-S. et al. Synthesis, photophysics and binding studies of Pt(II) alkynyl terpyridine complexes with crown ether pendant. Potential luminescent sensors for metal ions // *J. Mater. Chem.* 2005. Vol. 15, № 27–28. P. 2714.

92. Han X. et al. Switching between Ligand-to-Ligand Charge-Transfer, Intraligand Charge-Transfer, and Metal-to-Ligand Charge-Transfer Excited States in Platinum(II) Terpyridyl Acetylide Complexes Induced by pH Change and Metal Ions // *Chem. – A Eur. J.* 2007. Vol. 13, № 4. P. 1231–1239.
93. Chan C.W.-T., Chan K., Yam V.W.-W. Induced Self-Assembly and Disassembly of Alkynylplatinum(II) 2,6-Bis(benzimidazol-2'-yl)pyridine Complexes with Charge Reversal Properties: “Proof-of-Principle” Demonstration of Ratiometric Förster Resonance Energy Transfer Sensing of pH // *ACS Appl. Mater. Interfaces.* 2023. Vol. 15, № 21. P. 25122–25133.
94. Lam Y.Y. et al. Organometallic d6, d8 and d10 metal complexes for biosensing and imaging, cancer therapy and theranosis // *J. Organomet. Chem.* 2024. Vol. 1005. P. 122982.
95. Chan M.H.Y., Yam V.W.W. Toward the Design and Construction of Supramolecular Functional Molecular Materials Based on Metal-Metal Interactions // *J. Am. Chem. Soc.* 2022. Vol. 144, № 50. P. 22805–22825.
96. Haque A. et al. Cyclometallated tridentate platinum(ii) arylacetylide complexes: Old wine in new bottles // *Chem. Soc. Rev.* 2019. Vol. 48, № 23. P. 5547–5563.
97. Berenguer J.R., Lalinde E., Torroba J. Synthesis, Characterization and Photophysics of a New Series of Anionic C,N,C Cyclometalated Platinum Complexes // *Inorg. Chem.* 2007. Vol. 46, № 23. P. 9919–9930.
98. Tong G.S., Che C. Emissive or Nonemissive? A Theoretical Analysis of the Phosphorescence Efficiencies of Cyclometalated Platinum(II) Complexes // *Chem. – A Eur. J.* 2009. Vol. 15, № 29. P. 7225–7237.
99. Cocchi M. et al. Highly efficient near-infrared organic excimer electrophosphorescent diodes // *Appl. Phys. Lett.* 2007. Vol. 90, № 2. P. 023506.
100. Cocchi M. et al. Single-dopant organic white electrophosphorescent diodes with very high efficiency and its reduced current density roll-off // *Appl. Phys. Lett.* 2007. Vol. 90, № 16. P. 163508.
101. Chen Y. et al. Photoresponsive Supramolecular Organometallic Nanosheets Induced by Pt II  $\cdots$  Pt II and C-H $\cdots$  $\pi$  Interactions // *Angew. Chemie Int. Ed.* 2009.

- Vol. 48, № 52. P. 9909–9913.
102. Sato S. et al. Coassembly-Directed Fabrication of an Exfoliated Form of Alternating Multilayers Composed of a Self-assembled Organoplatinum(II) Complex–Fullerene Dyad // *Inorg. Chem.* 2015. Vol. 54, № 24. P. 11581–11583.
  103. Shao P. et al. Cyclometalated Platinum(II) 6-Phenyl-4-(9,9-dihexylfluoren-2-yl)-2,2'-bipyridine Complexes: Synthesis, Photophysics, and Nonlinear Absorption // *Inorg. Chem.* 2010. Vol. 49, № 10. P. 4507–4517.
  104. Zhang B. et al. Synthesis, Structural Characterization, Photophysics, and Broadband Nonlinear Absorption of a Platinum(II) Complex with the 6-(7-Benzothiazol-2'-yl-9,9-diethyl-9 H -fluoren-2-yl)-2,2'-bipyridinyl Ligand // *Chem. – A Eur. J.* 2012. Vol. 18, № 15. P. 4593–4606.
  105. Rossi E. et al. Tuning the Dipolar Second-Order Nonlinear Optical Properties of Cyclometalated Platinum(II) Complexes with Tridentate N<sup>C</sup>N Binding Ligands // *Chem. – A Eur. J.* 2013. Vol. 19, № 30. P. 9875–9883.
  106. Wu W. et al. Long-Lived Room-Temperature Near-IR Phosphorescence of BODIPY in a Visible-Light-Harvesting N<sup>C</sup>N Pt II –Acetylide Complex with a Directly Metalated BODIPY Chromophore // *Chem. – A Eur. J.* 2012. Vol. 18, № 7. P. 1961–1968.
  107. Wu W. et al. Tridentate cyclometalated platinum(II) complexes with strong absorption of visible light and long-lived triplet excited states as photosensitizers for triplet–triplet annihilation upconversion // *Dye. Pigment.* 2013. Vol. 96, № 1. P. 220–231.
  108. Yang Q.-Z. et al. A Luminescent Chemosensor with Specific Response for Mg<sup>2+</sup> // *Inorg. Chem.* 2004. Vol. 43, № 17. P. 5195–5197.
  109. Lanoë P.H. et al. Cyclometallated platinum(II) complexes incorporating ethynyl-flavone ligands: Switching between triplet and singlet emission induced by selective binding of Pb<sup>2+</sup> ions // *Chem. Commun.* 2008. № 36. P. 4333–4335.
  110. Zhang L.-K. et al. A highly selective and sensitive luminescent chemosensor for Zn<sup>2+</sup> ions based on cyclometalated platinum(II) complexes // *Dalt. Trans.* 2013. Vol. 42, № 12. P. 4244.

111. Bureš F. Fundamental aspects of property tuning in push-pull molecules // RSC Adv. 2014. Vol. 4, № 102. P. 58826–58851.
112. Ching K.C. et al. A new zwitterionic salt for non-linear optics: {4'-[methyl(diphenyl)phosphonio]biphenyl-4-yl}triphenylborate // J. Chem. Soc., Faraday Trans. 1991. Vol. 87, № 14. P. 2225–2228.
113. Allen D.W., Li X. Solvatochromic and halochromic properties of some phosphonioarylimino- and phosphonioarylazo-phenolate betaine dyes // J. Chem. Soc. Perkin Trans. 2. 1997. № 6. P. 1099–1104.
114. Lambert C. et al. Synthesis and nonlinear optical properties of three-dimensional phosphonium ion chromophores // Chem. - A Eur. J. 1998. Vol. 4, № 3. P. 512–521.
115. Allen D.W., Mifflin J.P., Skabara P.J. Synthesis and solvatochromism of some dipolar aryl-phosphonium and -phosphine oxide systems // J. Organomet. Chem. 2000. Vol. 601, № 2. P. 293–298.
116. Lee M.H. et al. Fluoride ion complexation by a cationic borane in aqueous solution // Chem. Commun. 2007. № 11. P. 1133.
117. Kim Y., Gabbai F.P. Cationic Boranes for the Complexation of Fluoride Ions in Water below the 4 ppm Maximum Contaminant Level // J. Am. Chem. Soc. 2009. Vol. 131, № 9. P. 3363–3369.
118. Li Y. et al. A Dual-Emissive Phosphine–Borane Lewis Pair with a U-Shaped Linker: Impact of Methylation and Complexation on Fluoride Binding Affinity // Organometallics. 2014. Vol. 33, № 4. P. 964–973.
119. Belyaev A. et al. A Facile Molecular Machine: Optically Triggered Counterion Migration by Charge Transfer of Linear Donor- $\pi$ -Acceptor Phosphonium Fluorophores // Angew. Chemie Int. Ed. 2019. Vol. 58, № 38. P. 13456–13465.
120. Partanen I. et al. From Terminal to Spiro-Phosphonium Acceptors, Remarkable Moieties to Develop Polyaromatic NIR Dyes // Chem. – A Eur. J. 2023. Vol. 29, № 44.
121. Zielonka J. et al. Mitochondria-Targeted Triphenylphosphonium-Based Compounds: Syntheses, Mechanisms of Action, and Therapeutic and Diagnostic

- Applications // Chem. Rev. 2017. Vol. 117, № 15. P. 10043–10120.
122. Nigam S. et al. Structurally optimised BODIPY derivatives for imaging of mitochondrial dysfunction in cancer and heart cells // Chem. Commun. 2016. Vol. 52, № 44. P. 7114–7117.
123. Adams C.J. et al. Synthesis and characterisation of new platinum-acetylide complexes containing diimine ligands // J. Chem. Soc. Dalt. Trans. 2000. P. 63–67.
124. Melekhova A.A. et al. Synthesis, characterization, luminescence and non-linear optical properties of diimine platinum(II) complexes with arylacetylene ligands // J. Organomet. Chem. 2014. Vol. 763–764. P. 1–5.
125. Partanen I. et al. Fast and Tunable Phosphorescence from Organic Ionic Crystals // Angew. Chemie Int. Ed. 2023. Vol. 62, № 36.
126. NIST Chemistry WebBook [Electronic resource]. 2022. URL: <https://webbook.nist.gov/chemistry/>.
127. Siu P.K.M. et al. A diiminoplatinum(II) complex of 4-ethynylbenzo-15-crown-5 as a luminescent sensor for divalent metal ions // Eur. J. Inorg. Chem. 2003. Vol. 2003, № 15. P. 2749–2752.
128. Lu W. et al. Structural Basis for Vapoluminescent Organoplatinum Materials Derived from Noncovalent Interactions as Recognition Components // Chem. - A Eur. J. 2003. Vol. 9, № 24. P. 6155–6166.
129. Al-Rasbi N.K. et al. Bimetallic Pt(II)-bipyridyl-diacetylide/Ln(III) tris-diketonate adducts based on a combination of coordinate bonding and hydrogen bonding between the metal fragments: Syntheses, structures and photophysical properties // Polyhedron. Elsevier Ltd, 2009. Vol. 28, № 2. P. 227–232.
130. Yu B. et al. Synthesis and characterization of a luminescence metallosupramolecular hyperbranched polymer // Chem. Commun. 2013. Vol. 49, № 32. P. 3333–3335.
131. Bastien G. et al. C 60 Recognition from Extended Tetrathiafulvalene Bis - acetylide Platinum(II) Complexes // Org. Lett. 2016. Vol. 18, № 22. P. 5856–5859.

132. Haskins-Glusac K. et al. Photophysics and Photochemistry of Stilbene-Containing Platinum Acetylides // *J. Phys. Chem. B*. 2004. Vol. 108, № 16. P. 4969–4978.
133. Saha R. et al. A new series of luminescent phosphine stabilised platinum ethynyl complexes // *Dalt. Trans.* 2005. № 16. P. 2760.
134. Campbell K. et al. Using ligand exchange reactions to control the coordination environment of Pt(II) acetylide complexes: applications to conjugated metallacyclines // *J. Organomet. Chem.* 2003. Vol. 683, № 2. P. 379–387.
135. Lang H., Villar A. de., Walfort B. {trans-(Ph<sub>3</sub>P)<sub>2</sub> Pt[(μ-σ,η 2-CCPh)AgOTf]<sub>2</sub>}<sub>n</sub>: a novel coordination polymer with Pt(CCPh)<sub>2</sub> and Ag[μ-OS(O)(CF<sub>3</sub>)O]<sub>2</sub>Ag linkages // *Inorg. Chem. Commun.* 2004. Vol. 7, № 5. P. 694–697.
136. Berenguer J.R. et al. New trans-configured acetylide-cyanide platinum(II) anions: Spectroscopic and optical studies // *Organometallics*. 2013. Vol. 32, № 3. P. 835–845.
137. Grim S.O., Keiter R.L., McFarlane W. A phosphorus-31 nuclear magnetic resonance study of tertiary phosphine complexes of platinum(II) // *Inorg. Chem.* 1967. Vol. 6, № 6. P. 1133–1137.
138. Rahman M.M., Younus M., Ogawa A. Synthesis of the First Example of Selenium-Containing Platinum(II)–Alkenylaryalkynyl Complexes // *Eur. J. Inorg. Chem.* 2015. Vol. 2015, № 8. P. 1340–1344.
139. Berenguer J.R. et al. Novel mixed anion [trans-Pt(C≡CTol)<sub>2</sub>(CN)<sub>2</sub>]<sub>2</sub><sup>-</sup> as a building block of new luminescent PtII–TII and PtII–PbII coordination polymers // *Chem. Commun.* 2012. Vol. 48, № 51. P. 6384–6386.
140. Lara R., Lalinde E., Moreno M.T. Phosphorescent platinum(II) alkynyls end-capped with benzothiazole units // *Dalt. Trans.* 2017. Vol. 46, № 14. P. 4628–4641.
141. Sadowy A.L. et al. Chiral cis -Platinum Acetylide Complexes via Diphosphine Ligand Exchange: Effect of the Ligand // *Organometallics*. 2008. Vol. 27, № 23. P. 6321–6325.
142. Mukhopadhyay S. et al. Activation of C–CN bond of propionitrile: An alternative route to the syntheses of 5-substituted-1H-tetrazoles and dicyano-platinum(II)

- species // *Polyhedron*. 2008. Vol. 27, № 13. P. 2883–2888.
143. Khairul W.M. et al. Transition metal alkynyl complexes by transmetalation from Au(C≡CAr)(PPh<sub>3</sub>) (Ar = C<sub>6</sub>H<sub>5</sub> or C<sub>6</sub>H<sub>4</sub>Me-4) // *Dalt. Trans.* 2009. № 4. P. 610–620.
144. Miyagi Y. et al. Ligand Exchange Reaction for Controlling the Conformation of Platinum-Containing Polymers // *Macromolecules*. 2018. Vol. 51, № 3. P. 815–824.
145. Schneider J. et al. Cyclometalated 6-Phenyl-2,2'-bipyridyl (CNN) Platinum(II) Acetylide Complexes: Structure, Electrochemistry, Photophysics, and Oxidative- and Reductive-Quenching Studies // *Inorg. Chem.* 2009. Vol. 48, № 10. P. 4306–4316.
146. Hans Reich's Collection. NMR Spectroscopy. [Electronic resource]. URL: [https://organicchemistrydata.org/hansreich/resources/nmr/?index=nmr\\_index%2F31P\\_shift](https://organicchemistrydata.org/hansreich/resources/nmr/?index=nmr_index%2F31P_shift).
147. McCarthy J.S. et al. Role of the Trifluoropropynyl Ligand in Blue-Shifting Charge-Transfer States in Emissive Pt Diimine Complexes and an Investigation into the PMMA-Imposed Rigidoluminescence and Rigidochromism // *Inorg. Chem.* 2022. Vol. 61, № 29. P. 11366–11376.
148. Chan S.C. et al. Organic light-emitting materials based on bis(arylacetylide)platinum(II) complexes bearing substituted bipyridine and phenanthroline ligands: Photo- and electroluminescence from 3MLCT excited states // *Chem. - A Eur. J.* 2001. Vol. 7, № 19. P. 4180–4190.
149. Clark M.L. et al. Spectroscopic properties of orthometalated platinum(II) bipyridine complexes containing various ethynylaryl groups // *Chem. - A Eur. J.* 2008. Vol. 14, № 24. P. 7168–7179.
150. Lu W. et al. Light-Emitting Tridentate Cyclometalated Platinum(II) Complexes Containing  $\sigma$ -Alkynyl Auxiliaries: Tuning of Photo- and Electrophosphorescence // *J. Am. Chem. Soc.* 2004. Vol. 126, № 15. P. 4958–4971.
151. Kang J. et al. Facile and Equipment-Free Data Encryption and Decryption by Self-Encrypting Pt(II) Complex // *ACS Appl. Mater. Interfaces*. 2019. Vol. 11, № 14.

- P. 13350–13358.
152. Ni J. et al. A new sensor for detection of CH<sub>3</sub>CN and ClCH<sub>2</sub>CN vapors based on vapoluminescent platinum(ii) complex // *J. Chem. Soc. Dalt. Trans. Chemistry College, Dalian University of Technology, Dalian 116024, China, 2013. Vol. 42, № 36. P. 13092–13100.*
  153. Ni J. et al. Vapor-and mechanical-grinding-triggered color and luminescence switches for Bis( $\theta$ -fluorophenylacetylde) platinum(II) complexes // *Chem. - A Eur. J. State Key Laboratory of Structural Chemistry, Fujian Institute of Research on the Structure of Matter, Chinese Academy of Sciences, 155 Yangqiao Road West, Fuzhou, Fujian 350002, China, 2011. Vol. 17, № 4. P. 1171–1183.*
  154. Kang J. et al. 1-D “platinum Wire” Stacking Structure Built of Platinum(II) Diimine Bis( $\sigma$ -acetylde) Units with Luminescence in the NIR Region // *Inorg. Chem. 2016. Vol. 55, № 20. P. 10208–10217.*
  155. Ni J. et al. Luminescence Vapochromism of a Platinum(II) Complex for Detection of Low Molecular Weight Halohydrocarbon // *Inorg. Chem. State Key Laboratory of Structural Chemistry, Fujian Institute of Research on the Structure of Matter, Chinese Academy of Sciences, Fuzhou, Fujian 350002, China, 2009. Vol. 48, № 21. P. 10202–10210.*
  156. Zhang X. et al. Vapochromic and Mechanochromic Phosphorescence Materials Based on a Platinum(II) Complex with 4-Trifluoromethylphenylacetylde // *Inorg. Chem. State Key Laboratory of Structural Chemistry, Fujian Institute of Research on the Structure of Matter, Chinese Academy of Sciences, Fuzhou, Fujian 350002, China, 2012. Vol. 51, № 10. P. 5569–5579.*
  157. Giordano P.J., Wrighton M.S. The Nature of the Lowest Excited State in fac-Tricarbonylhalobis(4-phenylpyridine)rhenium(I) and fac-Tricarbonylhalobis(4, 4'-bipyridine)rhenium(I): Emissive Organometallic Complexes in Fluid Solution // *J. Am. Chem. Soc. 1979. Vol. 101, № 11. P. 2888–2897.*
  158. Guo H. et al. Naphthalimide phosphorescence finally exposed in a platinum(II) diimine complex // *Inorg. Chem. 2010. Vol. 49, № 15. P. 6802–6804.*
  159. Sillen A., Engelborghs Y. The Correct Use of “Average” Fluorescence Parameters

- // Photochem. Photobiol. 1998. Vol. 67, № 5. P. 475–486.
160. Joseph R. Lakowicz. Solvent and Environmental Effects // Principles of Fluorescence Spectroscopy. Boston, MA: Springer US, 2006. P. 205–235.
  161. Lees A.J. The Luminescence Rigidochromic Effect Exhibited by Organometallic Complexes: Rationale and Applications // Comments Inorg. Chem. 1995. Vol. 17, № 6. P. 319–346.
  162. Hua F. et al. Luminescent charge-transfer platinum(II) metallacycle // Inorg. Chem. 2007. Vol. 46, № 21. P. 8771–8783.
  163. Koo C.K. et al. A bioaccumulative cyclometalated platinum(II) complex with two-photon-induced emission for live cell imaging // Inorg. Chem. 2009. Vol. 48, № 3. P. 872–878.
  164. Melnikov A.S. et al. Two-photon absorption cross section for Coumarins 102, 153 and 307 // J. Phys. Conf. Ser. 2017. Vol. 917, № 6. P. 062029.
  165. Botchway S.W. et al. Time-resolved and two-photon emission imaging microscopy of live cells with inert platinum complexes // Proc. Natl. Acad. Sci. 2008. Vol. 105, № 42. P. 16071–16076.
  166. Yao X. et al. Turning on two-photon activity over  $\text{N}\wedge\text{N}\wedge\text{N}$  cyclometalated Pt(II) complex by introducing flexible chains // Dye. Pigment. 2021. Vol. 184. P. 108788.
  167. Rozhkov A. V. et al. Reverse Arene Sandwich Structures Based upon  $\pi$ -Hole-[MII] ( $d8$  M = Pt, Pd) Interactions, where Positively Charged Metal Centers Play the Role of a Nucleophile // Angew. Chemie Int. Ed. 2019. Vol. 58, № 13. P. 4164–4168.
  168. Rozhkov A. V. et al. Hole $\cdots$   $d_{z^2}$ [PtII] Interactions with Electron-Deficient Arenes Enhance the Phosphorescence of PtII-Based Luminophores // Inorg. Chem. 2020. Vol. 59, № 13. P. 9308–9314.
  169. Rawashdeh-Omary M.A. et al. Chemistry and optoelectronic properties of stacked supramolecular entities of trinuclear gold(I) complexes sandwiching small organic acids [9] // J. Am. Chem. Soc. 2001. Vol. 123, № 39. P. 9689–9691.
  170. Ni J. et al. Thermo- and mechanical-grinding-triggered color and luminescence

- switches of the diimine-platinum(ii) complex with 4-bromo-2,2'-bipyridine // *Dalt. Trans.* 2014. Vol. 43, № 1. P. 352–360.
171. Ni J. et al. Mechanochromic luminescence switch of platinum(II) complexes with 5-trimethylsilylethynyl-2,2'-bipyridine // *Inorg. Chem.* 2011. Vol. 50, № 18. P. 9090–9096.
172. Perry M. et al. Effect of hexafluorobenzene on the photophysics of pyrene // *J. Phys. Chem. A.* 2007. Vol. 111, № 23. P. 4884–4889.
173. Lu J. et al. “ $\pi$ -Hole- $\pi$ ” Interaction Promoted Photocatalytic Hydrodefluorination via Inner-Sphere Electron Transfer // *J. Am. Chem. Soc.* 2016. Vol. 138, № 49. P. 15805–15808.
174. Faizullin B.A. et al. pH-responsive composite nanomaterial engineered from silica nanoparticles and luminescent mitochondrion-targeted Pt(II) complex as anticancer agent // *J. Mol. Liq.* 2024. Vol. 399. P. 124381.
175. Russo M. et al. Synthesis of highly ethynylated mono and dinuclear Pt(II) tethers bearing the 4,4'-bis(ethynyl)biphenyl (debp) unit as central core // *J. Organomet. Chem.* 2001. Vol. 619, № 1–2. P. 49–61.
176. Sina A.A.I. et al. Synthesis, Structures and Properties of Novel Platinum(II) Acetylide Complexes and Polymers with Tri(tolyl)phosphine as the Auxiliary Ligand // *J. Inorg. Organomet. Polym. Mater.* 2015. Vol. 25, № 3. P. 427–436.
177. Miyagi Y. et al. Effect of phosphine ligand on the optical absorption/emission properties of platinum-containing conjugated polymers // *Polym. Chem.* 2018. Vol. 9, № 14. P. 1772–1779.
178. Tao C.-H., Yam V.W.-W. Branched carbon-rich luminescent multinuclear platinum(II) and palladium(II) alkynyl complexes with phosphine ligands // *J. Photochem. Photobiol. C Photochem. Rev.* 2009. Vol. 10, № 3. P. 130–140.
179. Chan C.K.M. et al. Design, synthesis, characterization, luminescence and non-linear optical (NLO) properties of multinuclear platinum(ii) alkynyl complexes // *Dalt. Trans.* 2011. Vol. 40, № 40. P. 10670–10685.
180. D'Amato R. et al. Synthesis, characterisation and optical properties of symmetrical and unsymmetrical Pt(II) and Pd(II) bis-acetylides. Crystal structure

- of trans-[Pt(PPh<sub>3</sub>)<sub>2</sub>(CC-C<sub>6</sub>H<sub>5</sub>)(CC-C<sub>6</sub>H<sub>4</sub>NO<sub>2</sub>)] // *J. Organomet. Chem.* 2001. Vol. 627, № 1. P. 13–22.
181. Ogilby P.R. Singlet oxygen: there is indeed something new under the sun // *Chem. Soc. Rev.* 2010. Vol. 39, № 8. P. 3181.
182. The National Institute of Advanced Industrial Science and Technology (AIST). Spectral Database for Organic Compounds SDBS [Electronic resource]. URL: [https://sdb.db.aist.go.jp/sdb/cgi-bin/cre\\_index.cgi](https://sdb.db.aist.go.jp/sdb/cgi-bin/cre_index.cgi).
183. Yam V.W.-W. et al. Synthesis, Structural Characterization, and Luminescence Properties of Branched Palladium(II) and Platinum(II) Acetylide Complexes // *Organometallics*. 2001. Vol. 20, № 3. P. 453–459.
184. Emmert L.A. et al. The Excited-State Symmetry Characteristics of Platinum Phenylacetylene Compounds // *J. Phys. Chem. A*. 2003. Vol. 107, № 51. P. 11340–11346.
185. Hebenbrock M. et al. Phosphorescent Pt(ii) complexes bearing a monoanionic C<sup>^</sup>N<sup>^</sup>N luminophore and tunable ancillary ligands // *Dalt. Trans.* 2017. Vol. 46, № 10. P. 3160–3169.
186. Chung C.Y.-S., Yam V.W.-W. Induced Self-Assembly and Förster Resonance Energy Transfer Studies of Alkynylplatinum(II) Terpyridine Complex Through Interaction With Water-Soluble Poly(phenylene ethynylene sulfonate) and the Proof-of-Principle Demonstration of this Two-Component Ensem // *J. Am. Chem. Soc.* 2011. Vol. 133, № 46. P. 18775–18784.
187. Po C. et al. Design, synthesis, luminescence and non-linear optical properties of 1,3,5-triethynylbenzene-based alkynylplatinum(II) terpyridine complexes // *J. Organomet. Chem.* 2019. Vol. 881. P. 13–18.
188. Wong K.M.-C. et al. Synthesis, Photophysical Properties, and Biomolecular Labeling Studies of Luminescent Platinum(II)-Terpyridyl Alkynyl Complexes // *Organometallics*. 2004. Vol. 23, № 14. P. 3459–3465.
189. Liu R. et al. The synthesis, crystal structure and photophysical properties of mononuclear platinum(II) 6-phenyl-[2,2']bipyridinyl acetylide complexes // *Dye. Pigment*. 2011. Vol. 88, № 1. P. 88–94.

190. Harris C.F. et al. Synthesis, Structure, Photophysics, and a DFT Study of Phosphorescent C\*N^N- and C^N^N-Coordinated Platinum Complexes // *Inorg. Chem.* 2013. Vol. 52, № 20. P. 11711–11722.
191. Yang Q.-Z. et al. Long-Lived Emission from Platinum(II) Terpyridyl Acetylide Complexes // *Inorg. Chem.* 2002. Vol. 41, № 22. P. 5653–5655.
192. Wang X. et al. Excited State Absorption Properties of Pt(II) Terpyridyl Complexes Bearing  $\pi$ -Conjugated Arylacetylides // *J. Phys. Chem. B.* 2010. Vol. 114, № 45. P. 14440–14449.
193. Yam V.W.-W. et al. Luminescent Platinum(II) Terpyridyl Complexes: Effect of Counter Ions on Solvent-Induced Aggregation and Color Changes // *Chem. - A Eur. J.* 2005. Vol. 11, № 15. P. 4535–4543.
194. Lu W. et al. [(C<sub>*λ*</sub>N<sub>*λ*</sub>N)Pt(C-C)*n*R] (HC<sub>*λ*</sub>N<sub>*λ*</sub>N = 6-aryl-2,2'-bipyridine, *n* = 1–4, R = aryl, SiMe<sub>3</sub>) as a new class of light-emitting materials and their applications in electrophosphorescent devices // *Chem. Commun.* 2002. № 3. P. 206–207.
195. Wang J. et al. Organo- and hydrogelators based on luminescent monocationic terpyridyl platinum(II) complexes with biphenylacetylide ligands // *Chem. - An Asian J.* 2011. Vol. 6, № 11. P. 3011–3019.
196. Liu R. et al. Photophysics and Nonlinear Absorption of Cyclometalated 4,6-Diphenyl-2,2'-bipyridyl Platinum(II) Complexes with Different Acetylide Ligands // *J. Phys. Chem. A.* 2010. Vol. 114, № 48. P. 12639–12645.
197. Yam V.W.W. Luminescent metal alkynyls - From simple molecules to molecular rods and materials // *J. Organomet. Chem.* 2004. Vol. 689, № 8. P. 1393–1401.
198. Tobisu M., Hyodo I., Chatani N. Nickel-Catalyzed Reaction of Arylzinc Reagents with N-Aromatic Heterocycles: A Straightforward Approach to C–H Bond Arylation of Electron-Deficient Heteroaromatic Compounds // *J. Am. Chem. Soc.* 2009. Vol. 131, № 34. P. 12070–12071.
199. Eskelinen T. et al. Photophysics and Excited State Dynamics of Cyclometalated [M(Phbpy)(CN)] (M = Ni, Pd, Pt) Complexes: A Theoretical and Experimental Study // *Inorg. Chem.* 2021. Vol. 60, № 12. P. 8777–8789.
200. Mathew I., Sun W. Photophysics of Pt(II) 4,6-diphenyl-2,2'-bipyridyl complexes

- in solution and in LB film // *J. Organomet. Chem.* 2009. Vol. 694, № 17. P. 2750–2756.
201. Zi-Xin W. et al. Tuning the Excited-state Properties of Cyclometalated Platinum (II) Complexes of 6-Phenyl-2,2'-bipyridine by Ancillary Acetylide Ligand // *Chinese J. Chem.* 2003. Vol. 21, № 2. P. 196–199.
202. Taylor S.D. et al. Solid-state materials for anion sensing in aqueous solution: highly selective colorimetric and luminescence-based detection of perchlorate using a platinum(ii) salt // *Chem. Commun.* 2010. Vol. 46, № 7. P. 1070.
203. Muro M.L., Daws C.A., Castellano F.N. Microarray pattern recognition based on PtII terpyridyl chloride complexes: vapo-chromic and vapoluminescent response // *Chem. Commun.* 2008. № 46. P. 6134.
204. Liu H.Q. et al. Novel luminescent cyclometalated and terpyridine gold(III) complexes and DNA binding studies // *J. Chem. Soc. Chem. Commun.* 1995. № 17. P. 1787–1788.
205. Büchner R. et al. Synthesis, crystal structure and solid state photoluminescence of [Pt(trpy)(CCPh)]SbF<sub>6</sub> (trpy=2,2':6',2''-terpyridine) // *Inorganica Chim. Acta.* 2007. Vol. 360, № 5. P. 1633–1638.
206. Lu W. et al.  $\pi$ - $\pi$  interactions in organometallic systems. Crystal structures and spectroscopic properties of luminescent mono-, bi-, and trinuclear trans-cyclometalated platinum(II) complexes derived from 2,6-diphenylpyridine // *Organometallics.* 2001. Vol. 20, № 12. P. 2477–2486.
207. Yam V.W.W. et al. Syntheses, electronic absorption, emission, and ion-binding studies of platinum(II) C<sup>N</sup>C and terpyridyl complexes containing crown ether pendants // *Chem. - A Eur. J.* 2002. Vol. 8, № 17. P. 4066–4076.
208. Leung S.Y. et al. Luminescent Cyclometalated Alkynylplatinum(II) Complexes with a Tridentate Pyridine-Based N-Heterocyclic Carbene Ligand: Synthesis, Characterization, Electrochemistry, Photophysics, and Computational Studies // *Chem. – A Eur. J.* 2013. Vol. 19, № 31. P. 10360–10369.
209. Prokhorov A.M. et al. Brightly luminescent Pt(II) pincer complexes with a sterically demanding carboranyl-phenylpyridine ligand: A new material class for

- diverse optoelectronic applications // *J. Am. Chem. Soc.* 2014. Vol. 136, № 27. P. 9637–9642.
210. Fang B. et al. Series of C<sup>N</sup>C Cyclometalated Pt(II) Complexes: Synthesis, Crystal Structures, and Nonlinear Optical Properties in the Near-Infrared Region // *Inorg. Chem.* 2018. Vol. 57, № 22. P. 14134–14143.
211. Ogawa T. et al. Phosphorescence properties of anionic cyclometalated platinum(II) complexes with fluorine-substituted tridentate diphenylpyridine in the solid state // *Chem. Phys. Lett.* 2020. Vol. 739. P. 137024.
212. Stengel I. et al. Postfunctionalization of luminescent bipyridine Pt II bisacetylides by click chemistry // *Eur. J. Inorg. Chem.* 2012. Vol. 2012, № 11. P. 1795–1809.
213. Gao, C., Zhang, Z., Chen J. Synthetic method of cis-bis(triphenylphosphine)platinum(II) dichloride: pat. CN2016-10133853 USA. China, 2016.
214. Peng K., Moreth D., Schatzschneider U. C<sup>N</sup>N Coordination Accelerates the iClick Reaction of Square-Planar Palladium(II) and Platinum(II) Azido Complexes with Electron-Poor Alkynes and Enables Cycloaddition with Terminal Alkynes // *Organometallics*. 2021. Vol. 40, № 15. P. 2584–2593.
215. Cave G.W. V. et al. C–H Activation Induced by Water. Monocyclometalated to Dicyclicometalated: CANAC Tridentate Platinum Complexes // *Organometallics*. 2000. Vol. 19, № 7. P. 1355–1364.
216. Armareg W.L.F., Cha C. Purification of Laboratory Chemicals // Elsevier. Elsevier, 2013. 1–1002 p.
217. CrysAlisPro, Rigaku Oxford Diffraction: 1.171.39.35a // CrysAlisPro, Rigaku Oxford Diffraction. Yarnton, UK: Agilent Technologies, 2017. P. Version 1.171.39.35a, 2017.
218. Sheldrick G.M. SHELXT – Integrated space-group and crystal-structure determination // *Acta Crystallogr. Sect. A. International Union of Crystallography*, 2015. Vol. 71, № 1. P. 3–8.
219. Dolomanov O. V. et al. OLEX2 : a complete structure solution, refinement and analysis program // *J. Appl. Crystallogr. International Union of Crystallography*,

2009. Vol. 42, № 2. P. 339–341.
220. Spek A.L. PLATON SQUEEZE: a tool for the calculation of the disordered solvent contribution to the calculated structure factors // *Acta Crystallogr. Sect. C. International Union of Crystallography*, 2015. Vol. 71, № 1. P. 9–18.
221. Brouwer A.M. Standards for photoluminescence quantum yield measurements in solution (IUPAC technical report) // *Pure Appl. Chem.* 2011. Vol. 83, № 12. P. 2213–2228.

## SUPPLEMENTARY INFORMATION

- Figure S1. (A)  $^1\text{H}$  (top),  $^{31}\text{P}\{\text{H}\}$  (middle) and  $^{19}\text{F}$  (bottom) spectra in aromatic range of **1NN[Cl]**; (B)  $^1\text{H}^1\text{H}$  COSY spectrum in aromatic range of **1NN[Cl]**. ..... 137
- Figure S2. (A)  $^1\text{H}$  (top),  $^{31}\text{P}\{\text{H}\}$  (middle) and  $^{19}\text{F}$  (bottom) spectra in aromatic range of **2NN[Cl]**; (B)  $^1\text{H}^1\text{H}$  COSY spectrum in aromatic range of **2NN[Cl]**. ..... 138
- Figure S3. (A)  $^1\text{H}$  (top),  $^{31}\text{P}\{\text{H}\}$  (middle) and  $^{19}\text{F}$  (bottom) spectra in aromatic range of **3NN[Cl]**; (B)  $^1\text{H}^1\text{H}$  COSY spectrum in aromatic range of **3NN[Cl]**. ..... 139
- Figure S4. (A)  $^1\text{H}$  (top),  $^{31}\text{P}\{\text{H}\}$  (middle) and  $^{19}\text{F}$  (bottom) spectra in aromatic range of **nNN[Cl]**; (B)  $^1\text{H}^1\text{H}$  COSY spectrum in aromatic range of **nNN[Cl]**. ..... 140
- Figure S5. (A)  $^1\text{H}$  (top),  $^{31}\text{P}\{\text{H}\}$  (middle) and  $^{19}\text{F}$  (bottom) spectra in aromatic range of **1NN[BArF]**; (B)  $^1\text{H}^1\text{H}$  COSY spectrum in aromatic range of **1NN[BArF]**. ..... 141
- Figure S6. (A)  $^1\text{H}$  (top),  $^{31}\text{P}\{\text{H}\}$  (middle) and  $^{19}\text{F}$  (bottom) spectra in aromatic range of **2NN[BArF]**; (B)  $^1\text{H}^1\text{H}$  COSY spectrum in aromatic range of **2NN[BArF]**. ..... 142
- Figure S7. (A)  $^1\text{H}$  (top),  $^{31}\text{P}\{\text{H}\}$  (middle) and  $^{19}\text{F}$  (bottom) spectra in aromatic range of **3NN[BArF]**; (B)  $^1\text{H}^1\text{H}$  COSY spectrum in aromatic range of **3NN[BArF]**. ..... 143
- Figure S8. (A)  $^1\text{H}$  (top),  $^{31}\text{P}\{\text{H}\}$  (middle) and  $^{19}\text{F}$  (bottom) spectra in aromatic range of **nNN[BArF]**; (B)  $^1\text{H}^1\text{H}$  COSY spectrum in aromatic range of **nNN[BArF]**. ..... 144
- Figure S9. Experimental (gray) ESI<sup>+</sup> MS spectra of **NN[Cl]** series and simulated isotopic patterns of the  $[\text{M}]^{2+}$ . ..... 145
- Figure S10. Experimental (gray) ESI<sup>+</sup> MS spectra of **NN[BArF]** series and simulated isotopic patterns of the  $[\text{M}]^{2+}$ . ..... 146
- Figure S11. FTIR spectra of **NN[BArF]** in the region of  $\text{C}\equiv\text{C}$  vibration, KBr. .... 147
- Figure S12. ORTEP view of **2NN[Cl]** molecular structure, the thermal ellipsoids are set at a 50% probability level. Counterions are omitted for clarity. .... 147
- Figure S13. Fragment of crystal packing of **2NN[Cl]**. Counterions are omitted for clarity. .... 148

Figure S14. (A) $^1\text{H}$ (top), $^{31}\text{P}\{\text{H}\}$ (middle) and $^{19}\text{F}$ (bottom) spectra in aromatic range of <b>1P[OTf]</b> ; (B) $^1\text{H}^1\text{H}$ COSY spectrum in aromatic range of <b>1P[OTf]</b> . .....	149
Figure S15. (A) $^1\text{H}$ (top), $^{31}\text{P}\{\text{H}\}$ (middle) and $^{19}\text{F}$ (bottom) spectra in aromatic range of <b>2P[OTf]</b> ; (B) $^1\text{H}^1\text{H}$ COSY spectrum in aromatic range of <b>2P[OTf]</b> . .....	150
Figure S16. (A) $^1\text{H}$ (top), $^{31}\text{P}\{\text{H}\}$ (middle) and $^{19}\text{F}$ (bottom) spectra in aromatic range of <b>nP[OTf]</b> ; (B) $^1\text{H}^1\text{H}$ COSY spectrum in aromatic range of <b>nP[OTf]</b> . .....	151
Figure S17. $^1\text{H}$ (top), $^{31}\text{P}\{\text{H}\}$ (bottom) spectra in aromatic range of <b>1CN</b> . .....	152
Figure S18. $^1\text{H}$ (top), $^{31}\text{P}\{\text{H}\}$ (bottom) spectra in aromatic range of <b>2CN</b> . .....	153
Figure S19. $^1\text{H}$ (top), $^{31}\text{P}\{\text{H}\}$ (bottom) spectra in aromatic range of <b>nCN</b> . .....	154
Figure S20. Experimental (gray) ESI <sup>+</sup> MS spectra of <b>P[OTf]</b> series and simulated isotopic patterns of the $[\text{M}]^{2+}$ . .....	155
Figure S21. Experimental (gray) ESI <sup>+</sup> MS spectra of <b>CN</b> series and simulated isotopic patterns of the $[\text{M}]^{2+}$ . .....	156
Figure S22. FTIR spectra of <b>P[OTf]</b> and <b>CN</b> series in the region of $\text{C}\equiv\text{C}$ vibration, KBr. ....	157
Figure S23. (A) $^1\text{H}$ (top), $^{31}\text{P}\{\text{H}\}$ (middle) and $^{19}\text{F}$ (bottom) spectra in aromatic range of <b>1C[Cl]</b> ; (B) $^1\text{H}^1\text{H}$ COSY spectrum in aromatic range of <b>1C[Cl]</b> . .....	158
Figure S24. (A) $^1\text{H}$ (top), $^{31}\text{P}\{\text{H}\}$ (middle) and $^{19}\text{F}$ (bottom) spectra in aromatic range of <b>2C[Cl]</b> ; (B) $^1\text{H}^1\text{H}$ COSY spectrum in aromatic range of <b>2C[Cl]</b> . .....	159
Figure S25. $^1\text{H}$ (top), $^{31}\text{P}\{\text{H}\}$ (middle) and $^{19}\text{F}$ (bottom) spectra in aromatic range of <b>1C[Cl]</b> ; (B) $^1\text{H}^1\text{H}$ COSY spectrum in aromatic range of <b>1C[Cl]</b> . .....	160
Figure S26. $^1\text{H}$ (top) and $^{19}\text{F}$ (bottom) stacked spectra in aromatic range of <b>1C[X]</b> . Counterions are labeled on the corresponding spectra, measured in DMSO- $d_6$ . .....	161
Figure S27. Experimental (gray) ESI <sup>+</sup> MS spectra of <b>C[Cl]</b> series and simulated isotopic patterns of the $[\text{M}]^+$ . .....	162
Figure S28. FTIR spectra of <b>C[Cl]</b> series in the region of $\text{C}\equiv\text{C}$ vibration, KBr. ...	163

Figure S29. ORTEP view of <b>2C[Cl]</b> molecular structure, the thermal ellipsoids are set at a 50% probability level. ....	163
Figure S30. Fragment of crystal packing of <b>2NN[Cl]</b> . Counterions are omitted for clarity. ....	164
Figure S31. Schemes of unsuccessful syntheses for Pt(II) NCN complexes. <b>1</b> : MeOH, 1 eq. KOH, 18/48/72 h, or DCM:Et <sub>3</sub> N 7:2, 5 mol.% CuI, 24/48 h. <b>2</b> : MeCN, 1 eq. AgOTf. <b>3</b> : 2 eq. KOH, 24 h. ....	164
Figure S32. (A) <sup>1</sup> H (top), <sup>31</sup> P {H} (middle) and <sup>19</sup> F (bottom) NMR spectra in aromatic range of <b>1N[Cl]</b> ; (B) <sup>1</sup> H <sup>1</sup> H COSY spectrum in aromatic range of <b>1N[Cl]</b> . ....	165
Figure S33. (A) <sup>1</sup> H (top), <sup>31</sup> P {H} (middle) and <sup>19</sup> F (bottom) NMR spectra in aromatic range of <b>2N[Cl]</b> ; (B) <sup>1</sup> H <sup>1</sup> H COSY spectrum in aromatic range of <b>2N[Cl]</b> . ....	166
Figure S34. (A) <sup>1</sup> H (top), <sup>31</sup> P {H} (middle) and <sup>19</sup> F (bottom) NMR spectra in aromatic range of <b>nN[Cl]</b> ; (B) <sup>1</sup> H <sup>1</sup> H COSY spectrum in aromatic range of <b>nN[Cl]</b> . ....	167
Figure S35. <sup>1</sup> H (top) and <sup>19</sup> F (bottom) stacked spectra in aromatic range of <b>1N[X]</b> . Counterions are labeled on the corresponding spectra, measured in DMSO-d <sub>6</sub> . ....	168
Figure S36. Experimental (gray) ESI <sup>+</sup> MS spectra of <b>N[Cl]</b> series and simulated isotopic patterns of the [M] <sup>2+</sup> . ....	169
Figure S37. FTIR spectra of <b>N[Cl]</b> series in the region of C≡C vibration, KBr. ...	170
Figure S38. (A) <sup>1</sup> H (top), <sup>31</sup> P {H} (bottom) NMR spectra in aromatic range of <b>1CNC</b> ; (B) <sup>1</sup> H <sup>1</sup> H COSY spectrum in aromatic range of <b>1CNC</b> . ....	171
Figure S39. (A) <sup>1</sup> H (top), <sup>31</sup> P {H} (bottom) NMR spectra in aromatic range of <b>2CNC</b> ; (B) <sup>1</sup> H <sup>1</sup> H COSY spectrum in aromatic range of <b>2CNC</b> . ....	172
Figure S40. Experimental (gray) ESI <sup>+</sup> MS spectra of <b>CNC</b> series and simulated isotopic patterns of the [M] <sup>+</sup> . ....	173
Figure S41. FTIR spectra of <b>CNC</b> series in the region of C≡C vibration, KBr. ....	174
Figure S42. ORTEP view of <b>1CNC</b> molecular structure, the thermal ellipsoids are set at a 50% probability level. ....	174

Figure S43. Power dependence of the upconverted luminescence intensity of <b>NN[BArF]</b> series (MeCN, r.t.). R-factors of linear fits are indicated on diagram. ....	175
Figure S44. <i>Stimuli responsive</i> normalized emission spectra of <b>2NN[BArF]</b> – <b>nNN[BArF]</b> , r.t. ....	176
Figure S45. CIE 1931 coordinates for <b>NN[BArF]</b> series under different conditions. ....	177
Figure S46. Schematic representation of <i>stimuli responsive</i> properties of <b>3NN[BArF]</b> under UV light (365 nm).....	178
Figure S47. Schematic representation of <i>stimuli responsive</i> properties of <b>nNN[BArF]</b> under UV light (365 nm). ....	178
Figure S48. UV-vis absorption spectra of complex <b>2P[OTf]</b> before and after UV irradiation (365 nm).....	178
Figure S49. Ligands used in Ref. [43]. ....	179
Figure S50. UV-vis spectra of <b>C[X]</b> and <b>N[X]</b> series.....	179
Figure S51. The low-energy part of the <b>CNC series</b> UV-vis spectra. ....	180
Table S1. Crystallographic data for compounds of <b>NN[Cl]</b> series. ....	181
Table S2. Selected structural parameters of <b>NN[Cl]</b> series. ....	182
Table S3. Selected structural parameters of <b>P[OTf]</b> .....	182
Table S4. Crystallographic data for compounds of <b>P[OTf]</b> and <b>CNC</b> .....	183
Table S5. Selected structural parameters of <b>1CNC</b> . ....	184
Table S6. Optical and photophysical properties of <b>NN[BArF]</b> complexes in MeCN solution, r.t.....	184
Table S7. Photophysical properties of <b>NN[BArF]</b> complexes after mechanical grinding and after fuming with Et <sub>2</sub> O.....	185

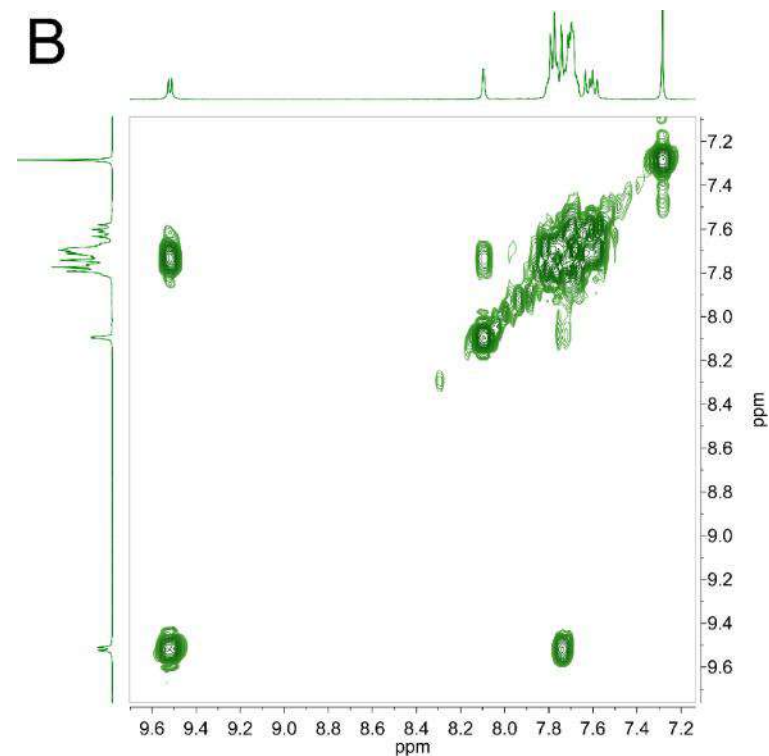
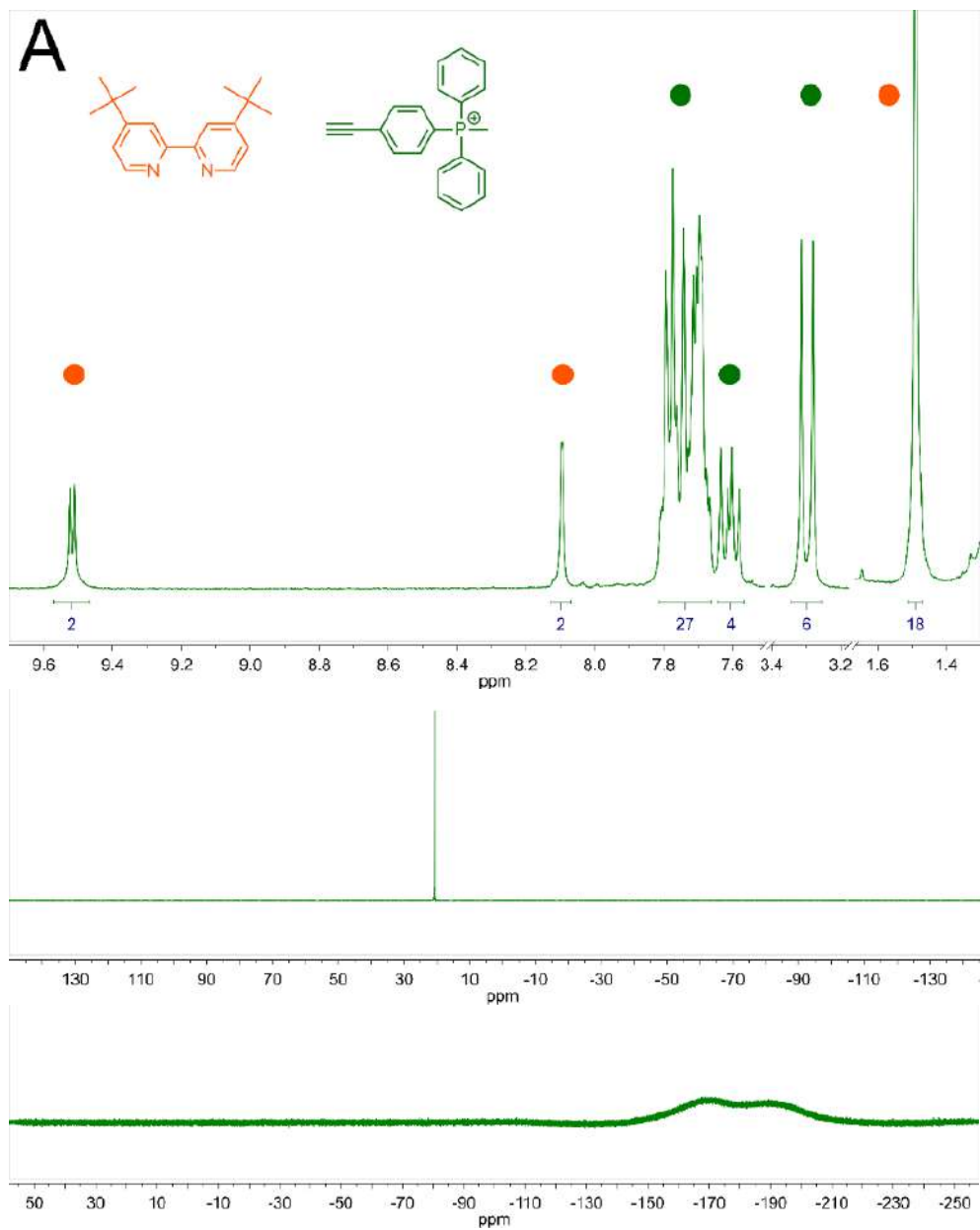


Figure S1. (A)  $^1\text{H}$  (top),  $^{31}\text{P}\{^1\text{H}\}$  (middle) and  $^{19}\text{F}$  (bottom) spectra in aromatic range of  $1\text{NN}[\text{Cl}]$ ; (B)  $^1\text{H}$ - $^1\text{H}$  COSY spectrum in aromatic range of  $1\text{NN}[\text{Cl}]$ .

$^1\text{H}$ ,  $^{19}\text{F}$  и  $^1\text{H}$ - $^1\text{H}$  COSY spectra were measured in  $\text{CDCl}_3$ ,  $^{31}\text{P}$  spectrum was measured in  $\text{CD}_2\text{Cl}_2$ , 298K.

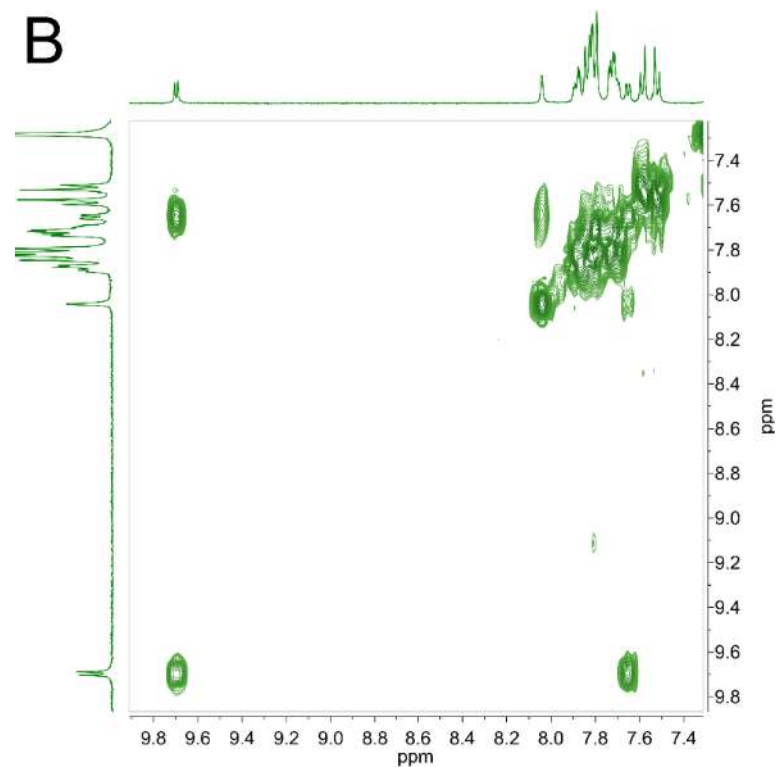
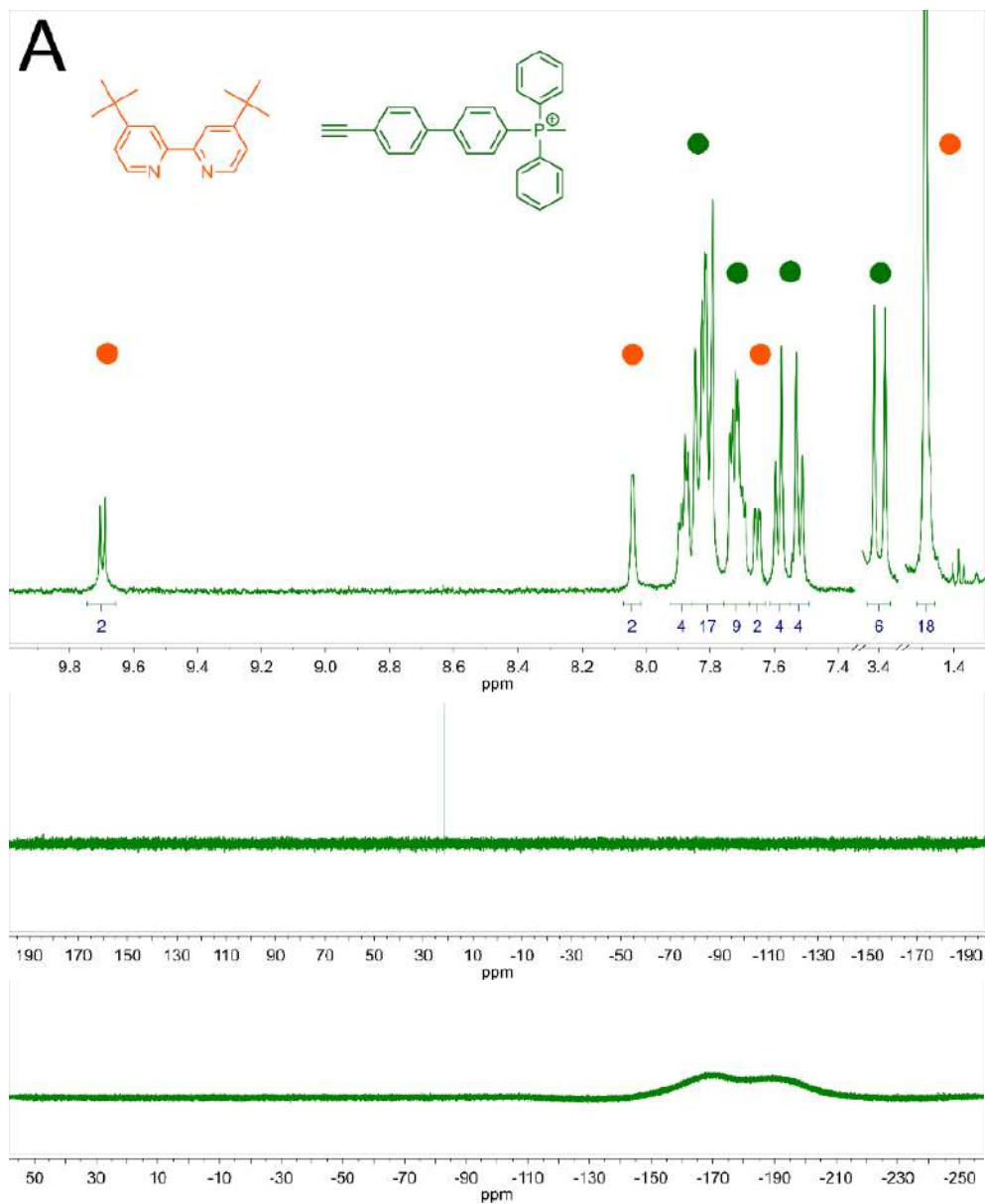


Figure S2. (A)  $^1\text{H}$  (top),  $^{31}\text{P}\{^1\text{H}\}$  (middle) and  $^{19}\text{F}$  (bottom) spectra in aromatic range of **2NN[Cl]**; (B)  $^1\text{H}$ - $^1\text{H}$  COSY spectrum in aromatic range of **2NN[Cl]**. All spectra were measured at 298K in  $\text{CDCl}_3$ .

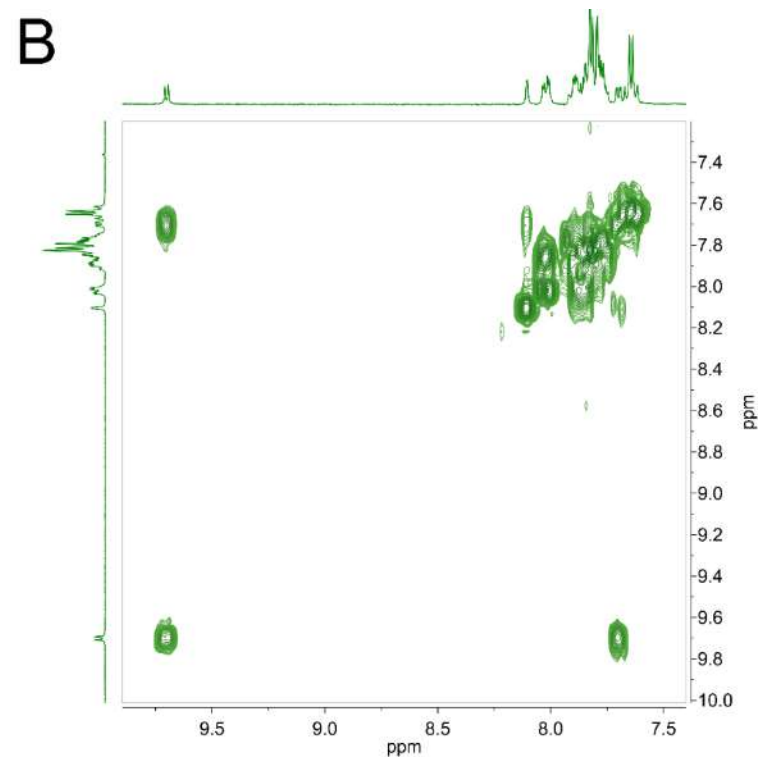
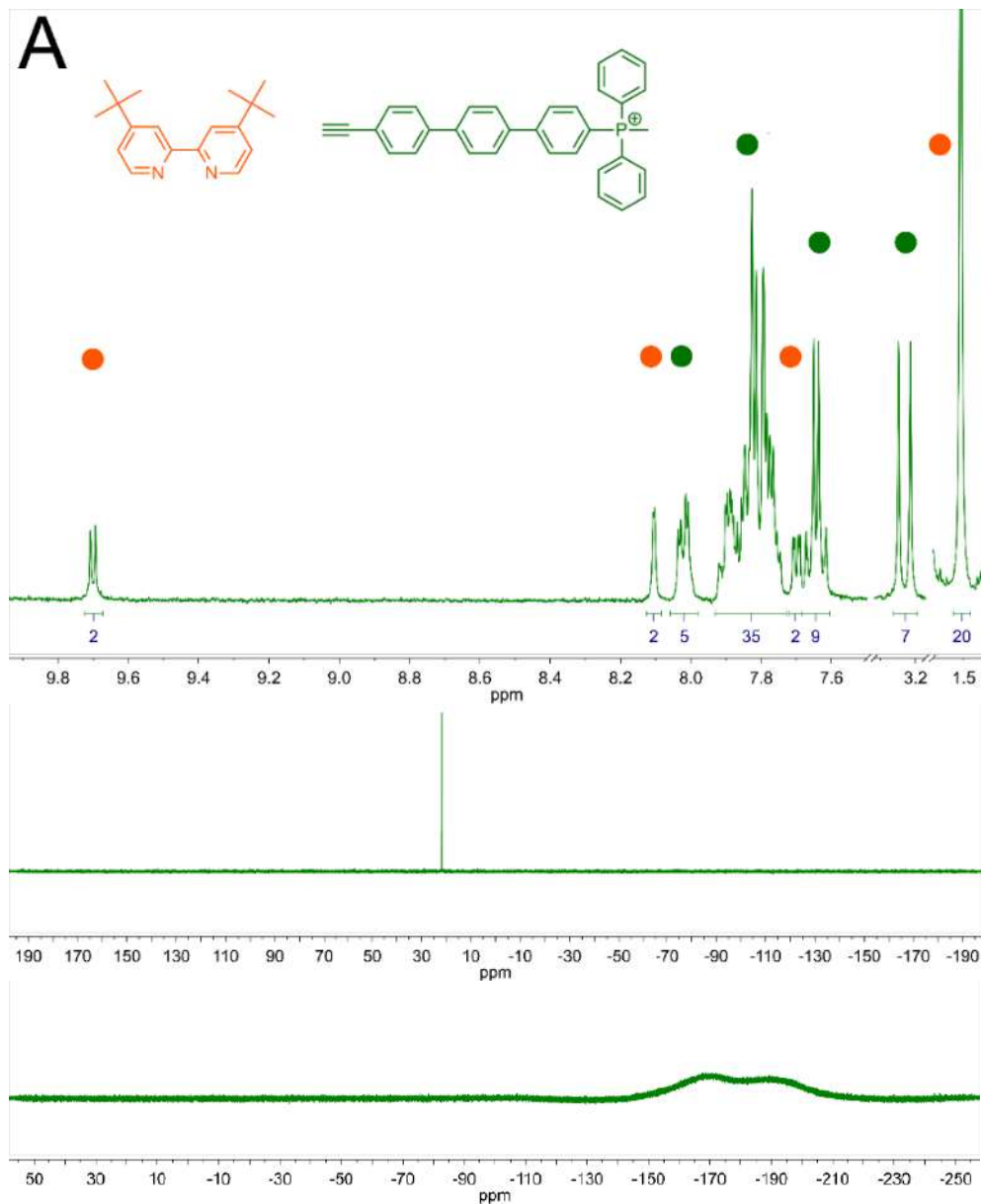


Figure S3. (A)  $^1\text{H}$  (top),  $^{31}\text{P}\{^1\text{H}\}$  (middle) and  $^{19}\text{F}$  (bottom) spectra in aromatic range of  $3\text{NN}[\text{Cl}]$ ; (B)  $^1\text{H}$ - $^1\text{H}$  COSY spectrum in aromatic range of  $3\text{NN}[\text{Cl}]$ .

$^1\text{H}$  and  $^1\text{H}$ - $^1\text{H}$  COSY spectra were measured in  $\text{CD}_2\text{Cl}_2$ .  $^{31}\text{P}\{^1\text{H}\}$  and  $^{19}\text{F}$  spectra were measured at 298K in  $\text{CDCl}_3$ .

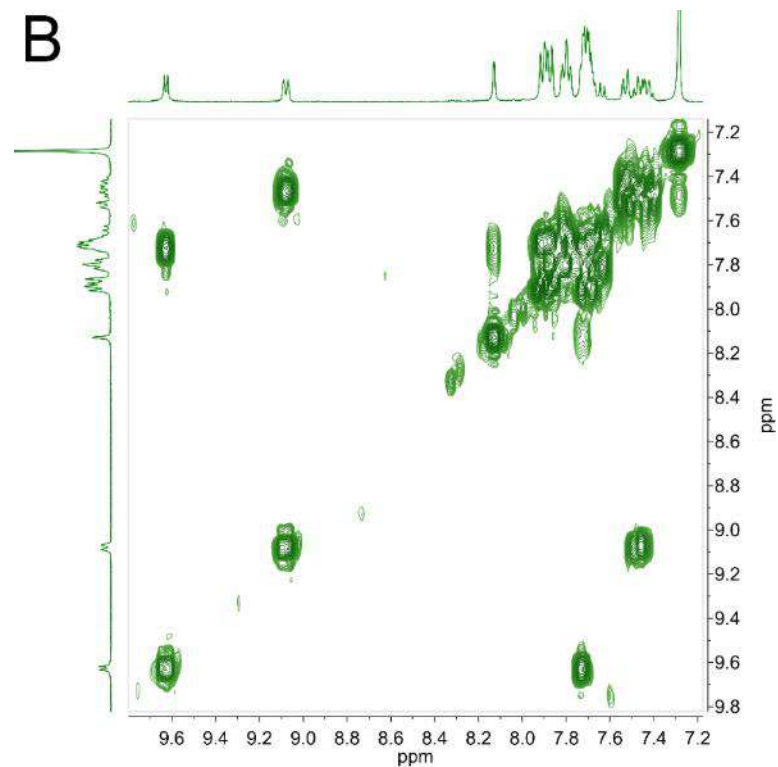
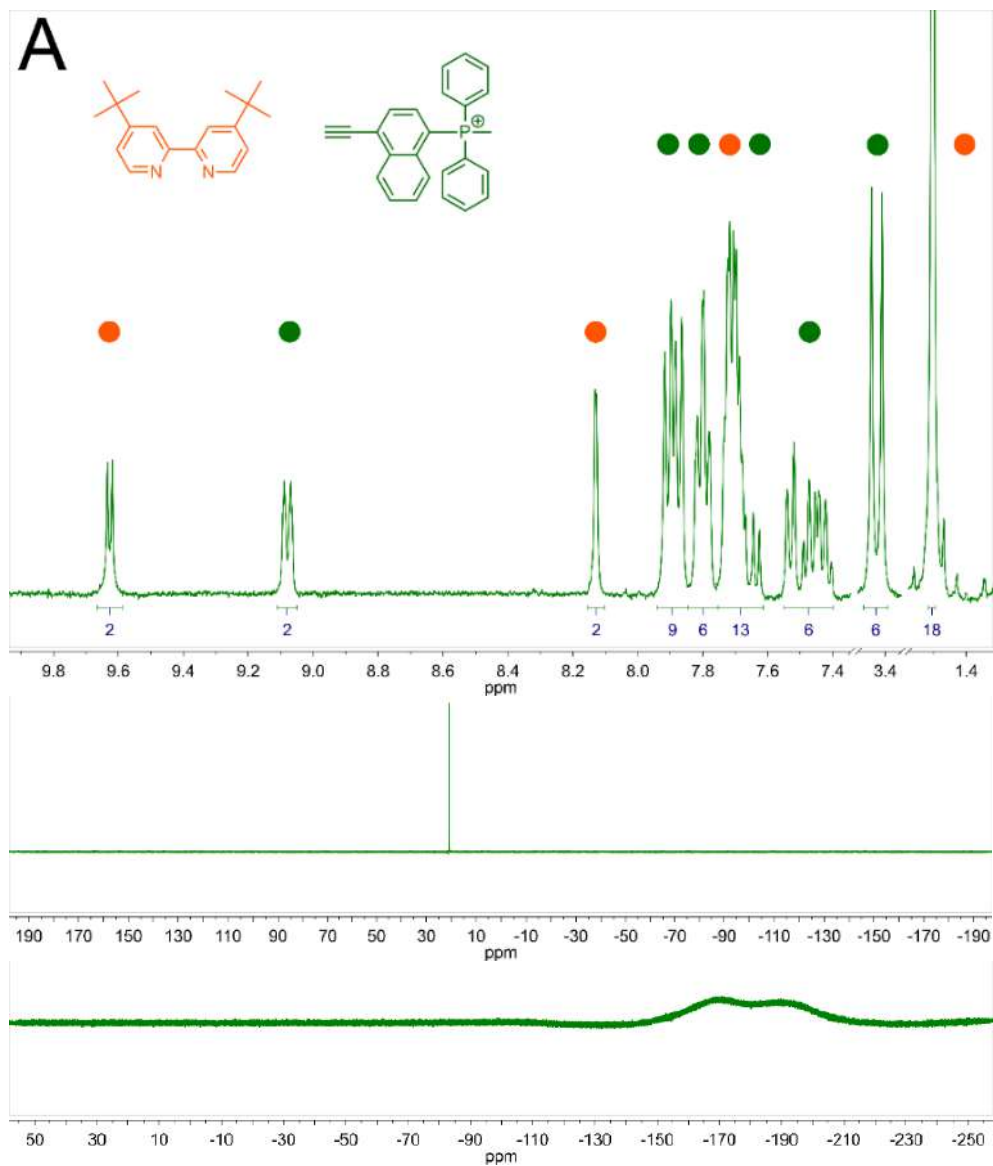


Figure S4. (A)  $^1\text{H}$  (top),  $^{31}\text{P}\{\text{H}\}$  (middle) and  $^{19}\text{F}$  (bottom) spectra in aromatic range of **nNN[Cl]**; (B)  $^1\text{H}$ - $^1\text{H}$  COSY spectrum in aromatic range of **nNN[Cl]**. All spectra were measured at 298K in  $\text{CDCl}_3$ .

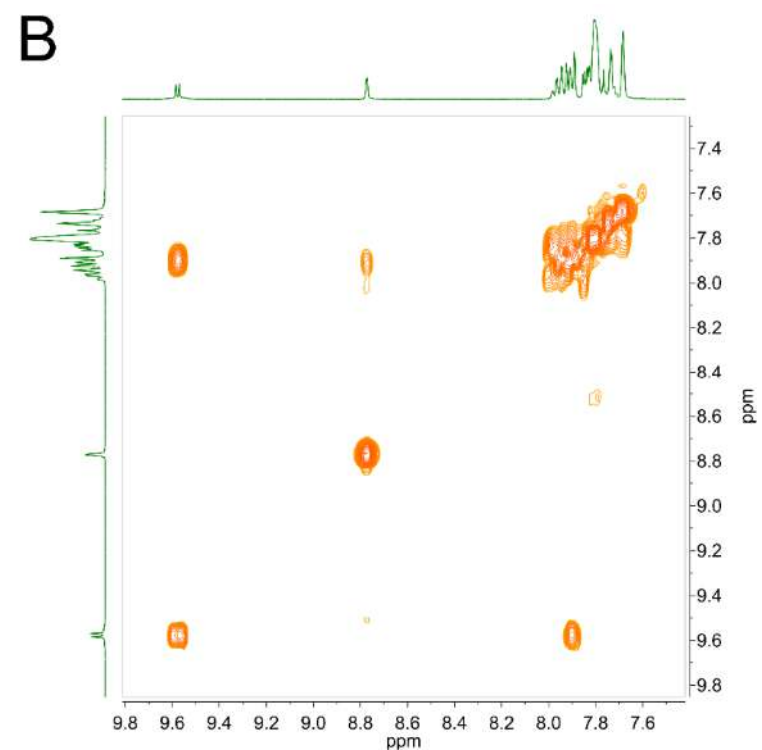
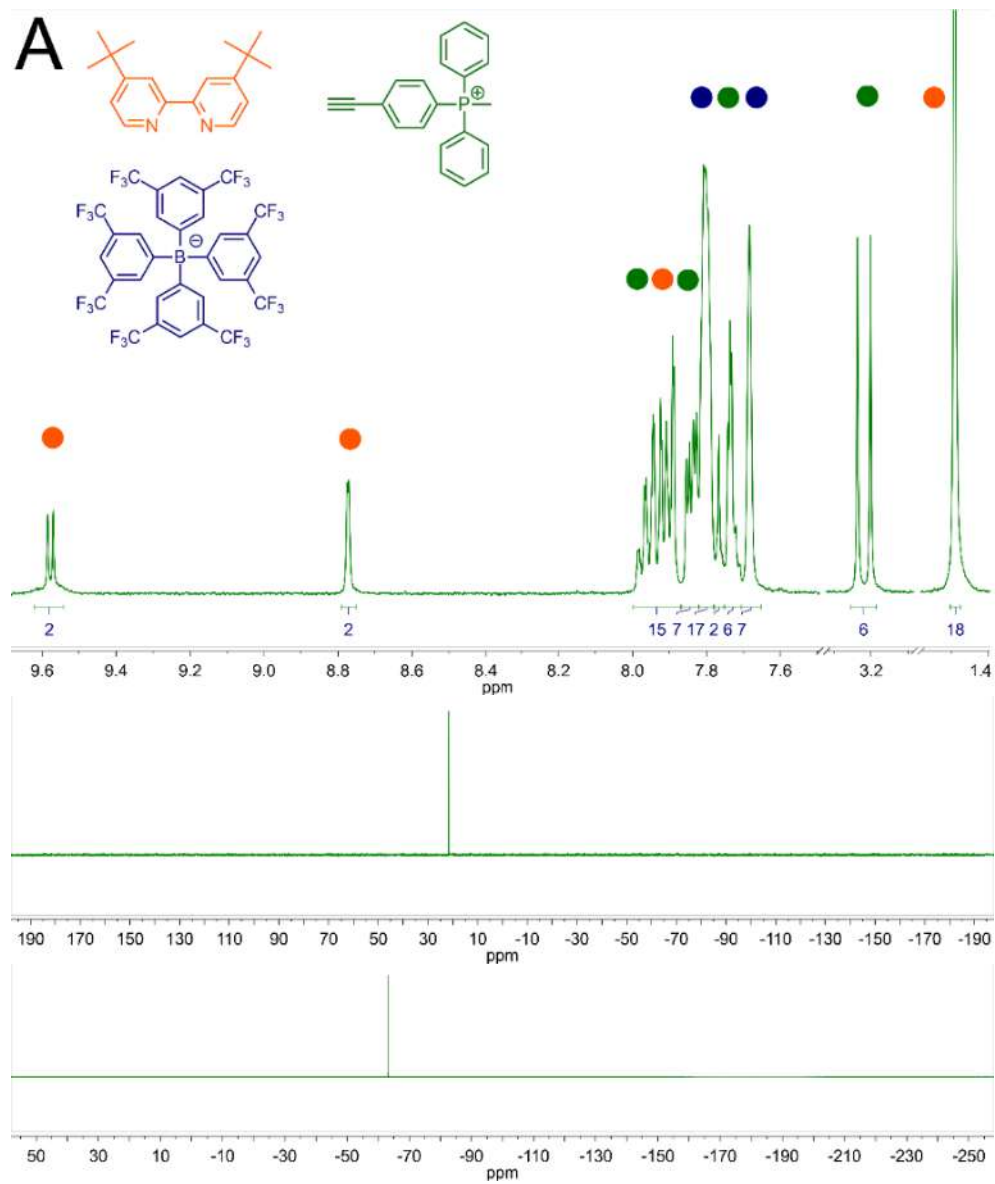


Figure S5. (A)  $^1\text{H}$  (top),  $^{31}\text{P}\{^1\text{H}\}$  (middle) and  $^{19}\text{F}$  (bottom) spectra in aromatic range of **1NN[BArF]**; (B)  $^1\text{H}$ - $^1\text{H}$  COSY spectrum in aromatic range of **1NN[BArF]**.

All spectra were measured at 298K in acetone- $\text{d}_6$ .

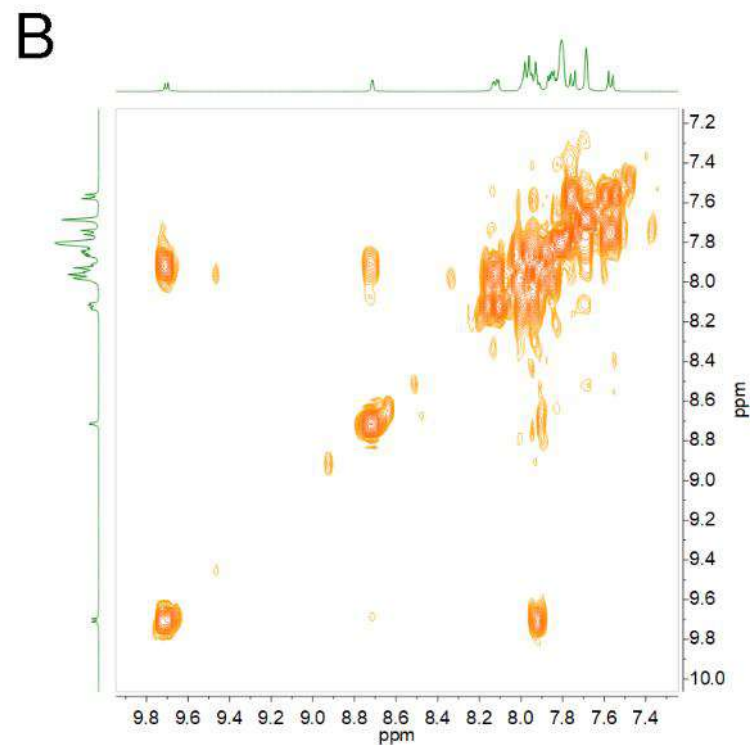
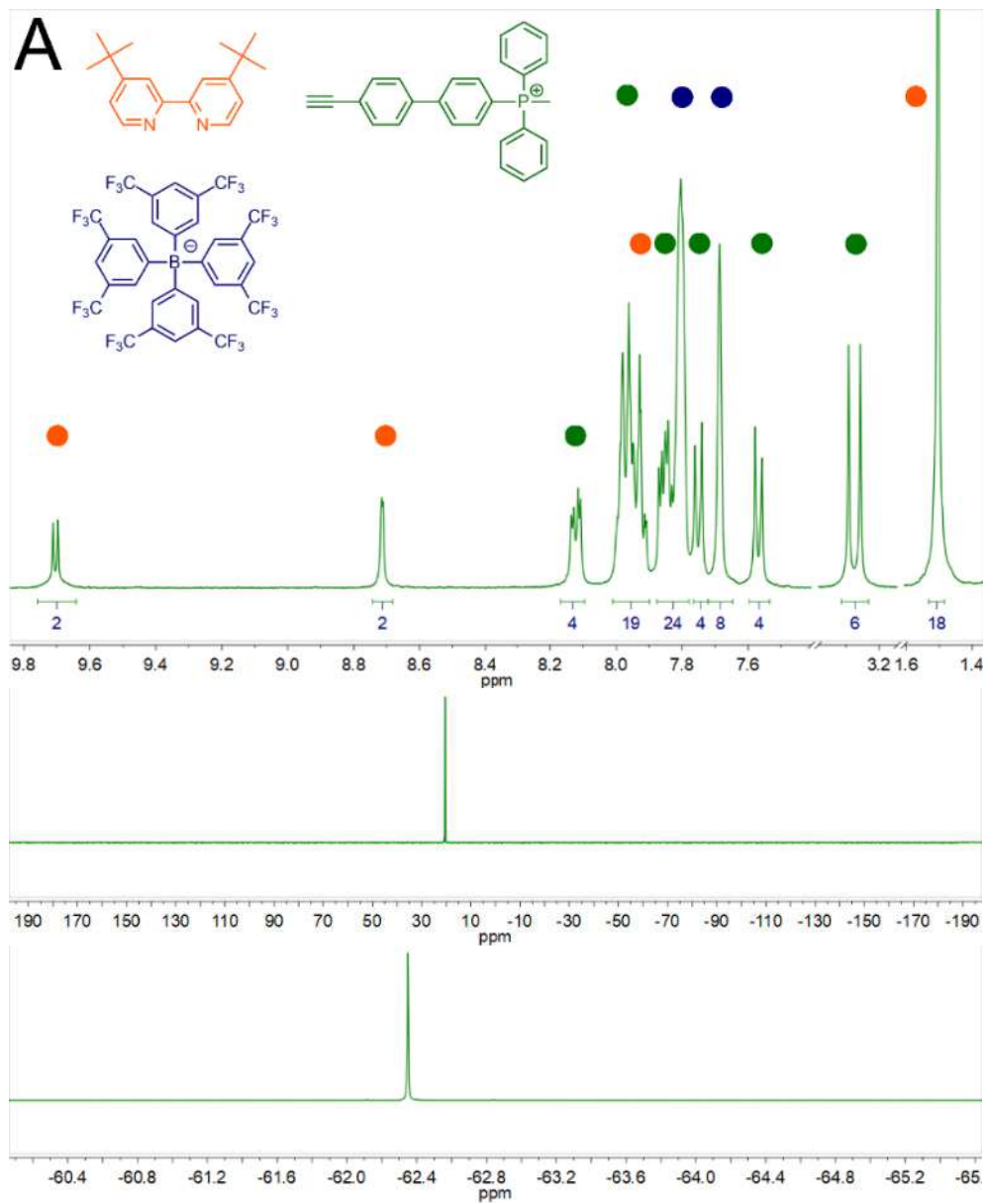


Figure S6. (A)  $^1\text{H}$  (top),  $^{31}\text{P}\{^1\text{H}\}$  (middle) and  $^{19}\text{F}$  (bottom) spectra in aromatic range of  $2\text{NN}[\text{BArF}]$ ; (B)  $^1\text{H}\text{-}^1\text{H}$  COSY spectrum in aromatic range of  $2\text{NN}[\text{BArF}]$ .

All spectra were measured at 298K in acetone- $\text{d}_6$ .

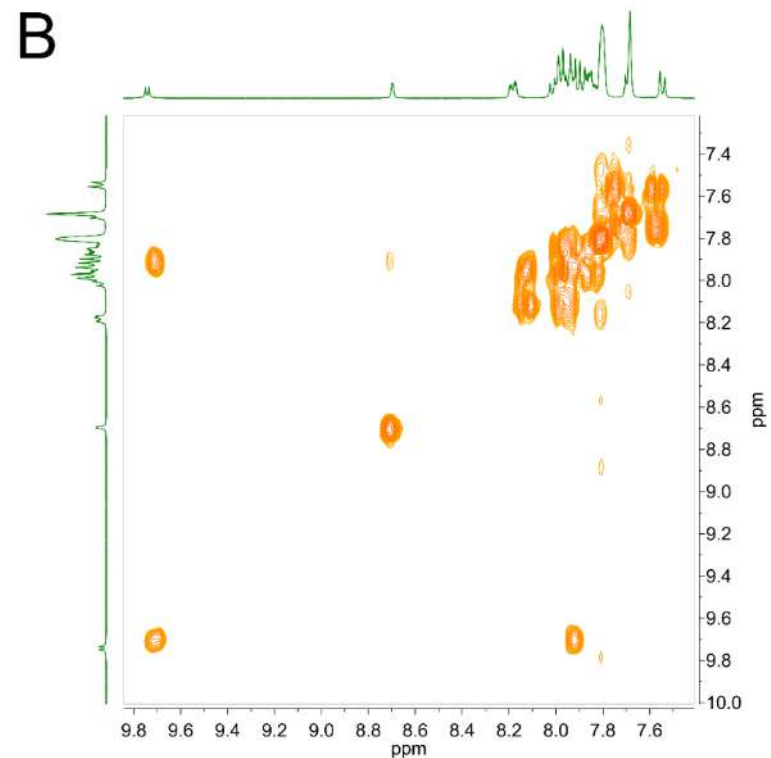
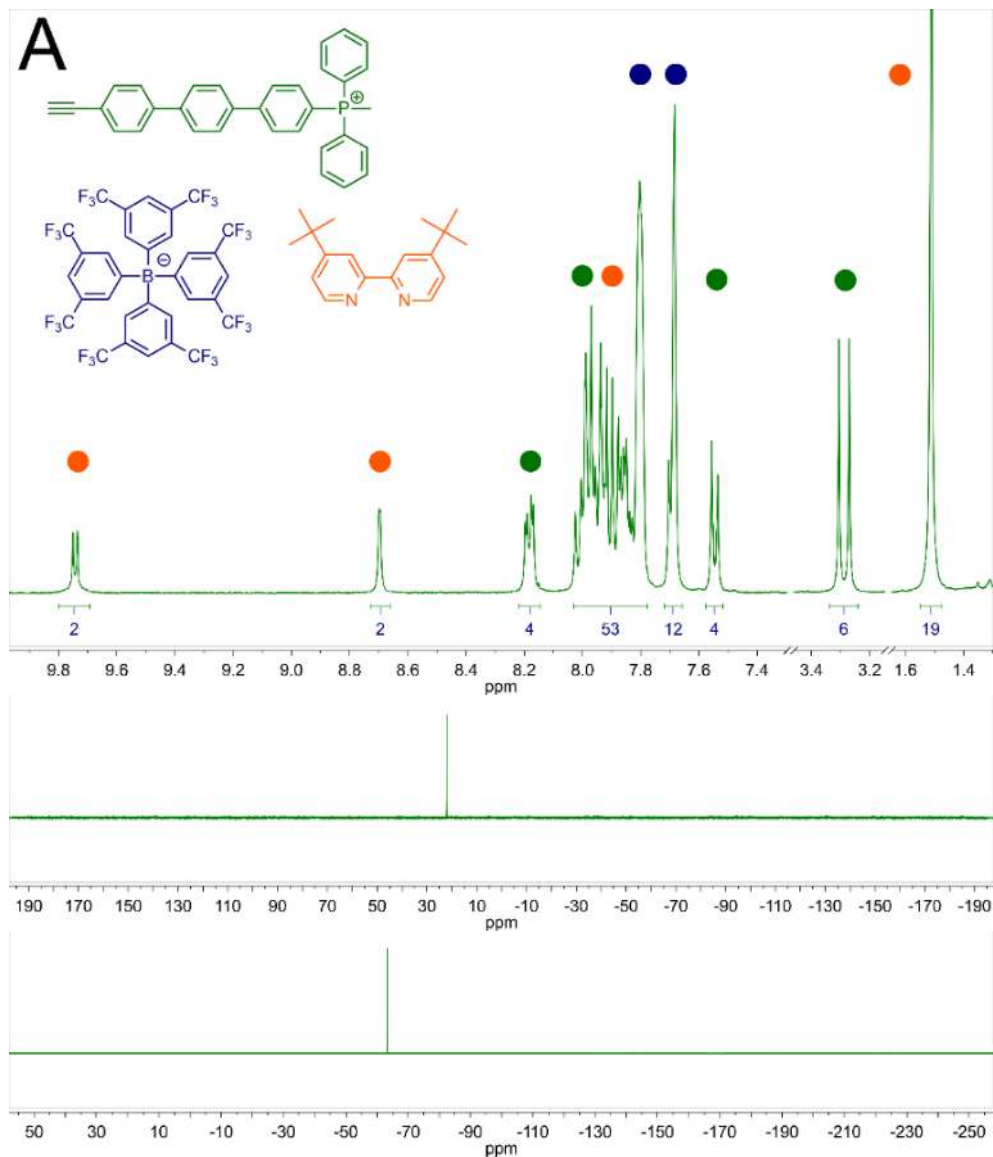


Figure S7. (A)  $^1\text{H}$  (top),  $^{31}\text{P}\{\text{H}\}$  (middle) and  $^{19}\text{F}$  (bottom) spectra in aromatic range of  $3\text{NN}[\text{BArF}]$ ; (B)  $^1\text{H}$  $^1\text{H}$  COSY spectrum in aromatic range of  $3\text{NN}[\text{BArF}]$ .

All spectra were measured at 298K in acetone- $\text{d}_6$ .

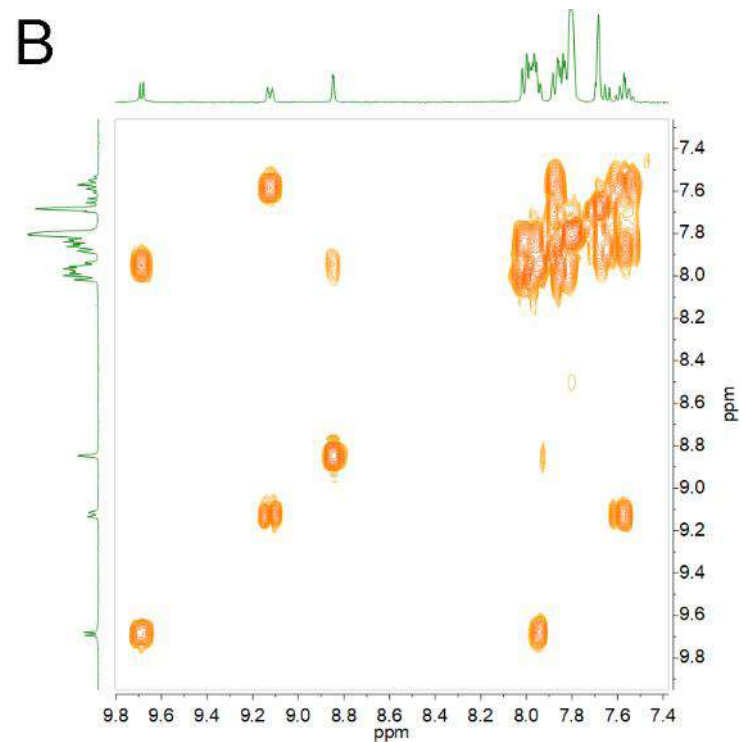
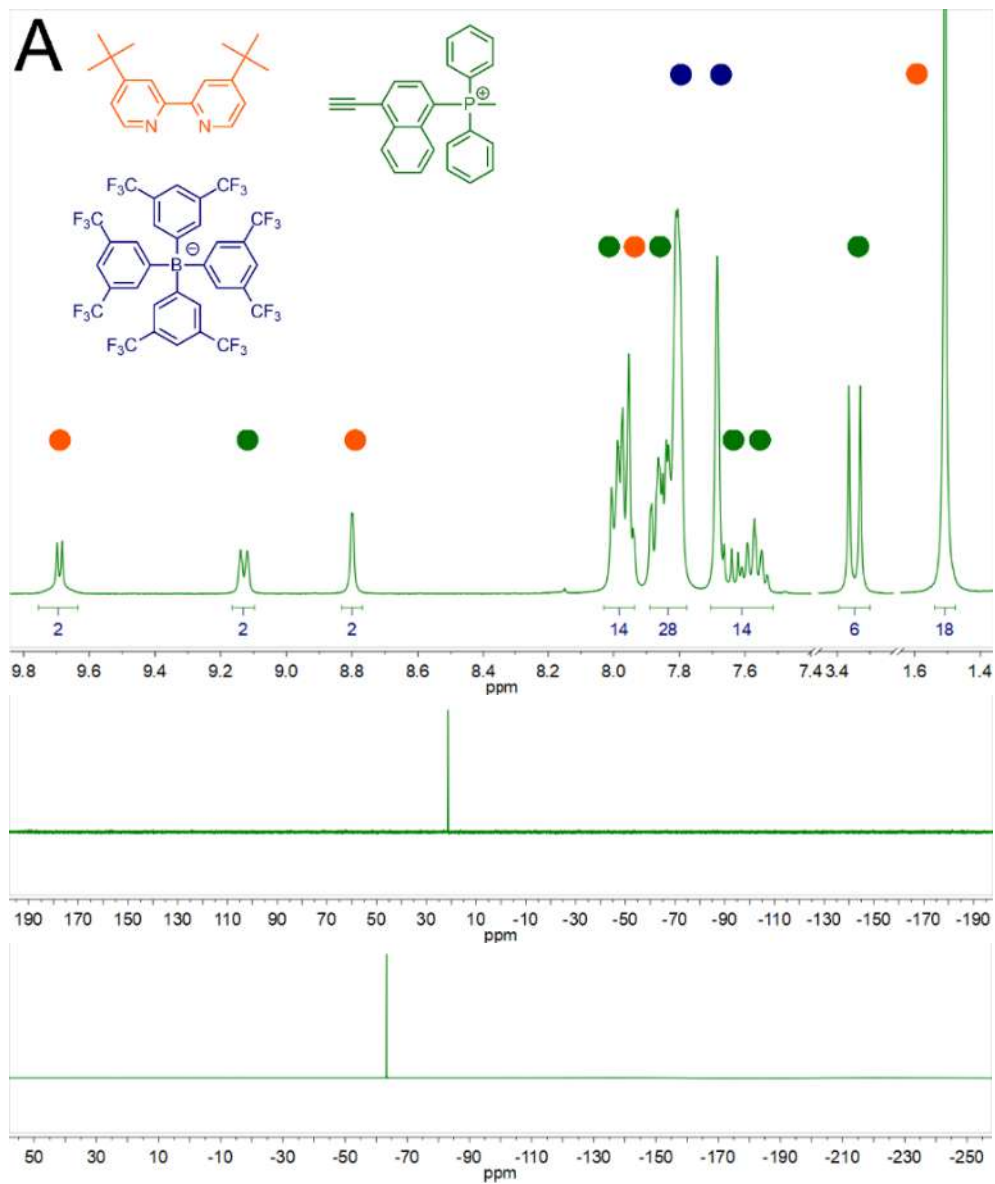


Figure S8. (A)  $^1\text{H}$  (top),  $^{31}\text{P}\{^1\text{H}\}$  (middle) and  $^{19}\text{F}$  (bottom) spectra in aromatic range of **nNN[BArF]**; (B)  $^1\text{H}$ - $^1\text{H}$  COSY spectrum in aromatic range of **nNN[BArF]**. All spectra were measured at 298K in  $\text{CDCl}_3$ .

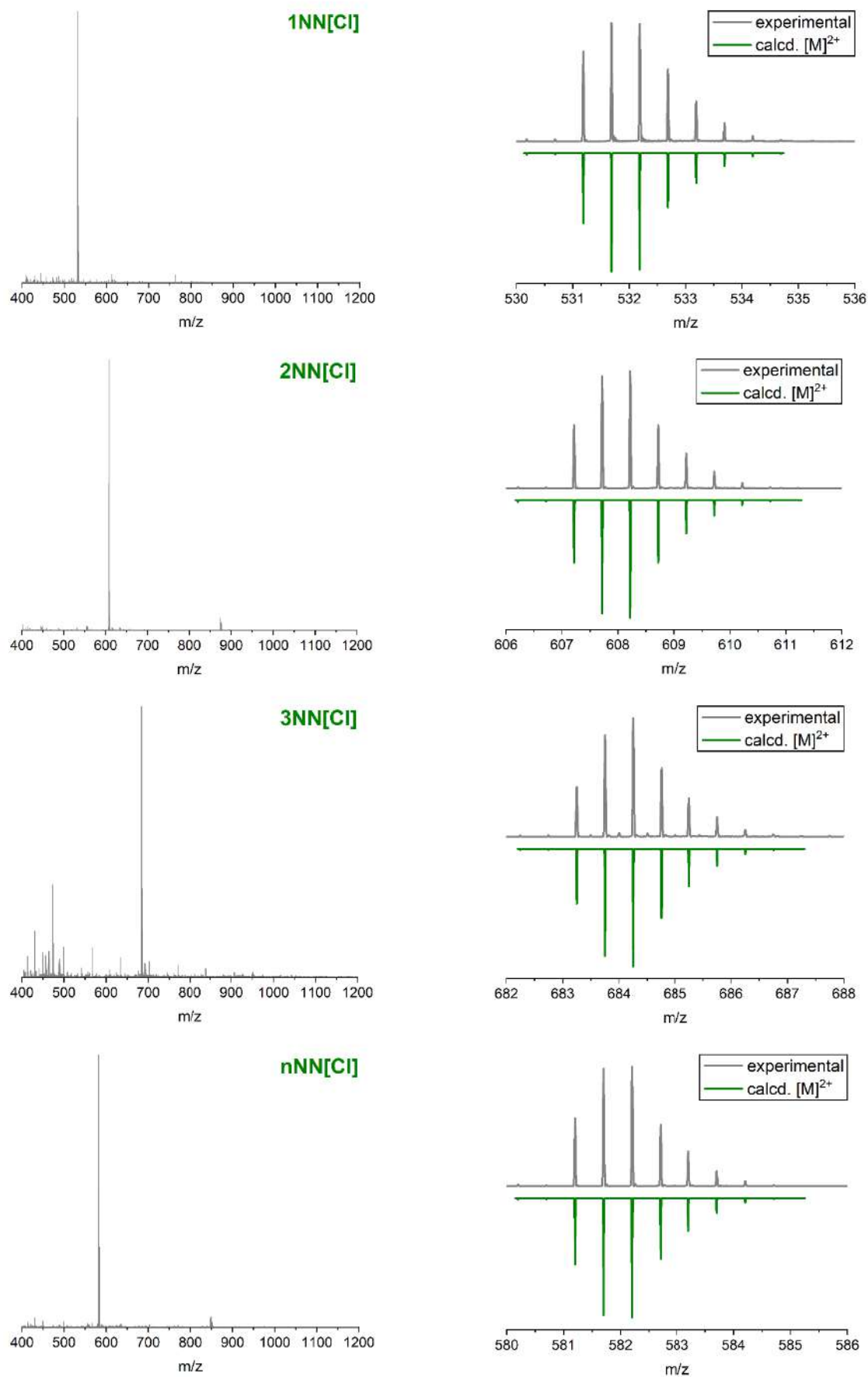


Figure S9. Experimental (gray) ESI<sup>+</sup> MS spectra of NN[Cl] series and simulated isotopic patterns of the [M]<sup>2+</sup>.

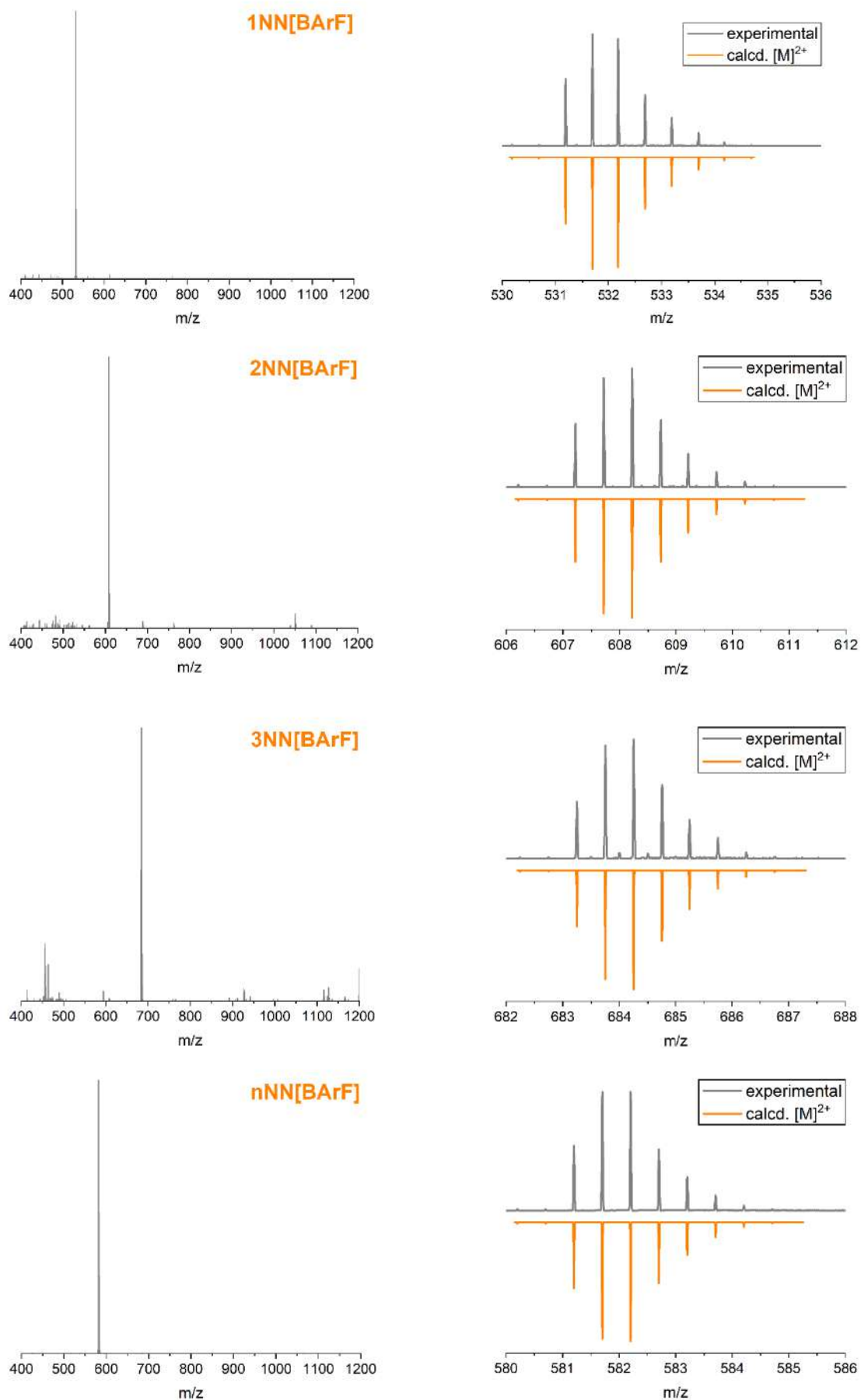


Figure S10. Experimental (gray) ESI<sup>+</sup> MS spectra of NN[BArF] series and simulated isotopic patterns of the  $[M]^{2+}$ .

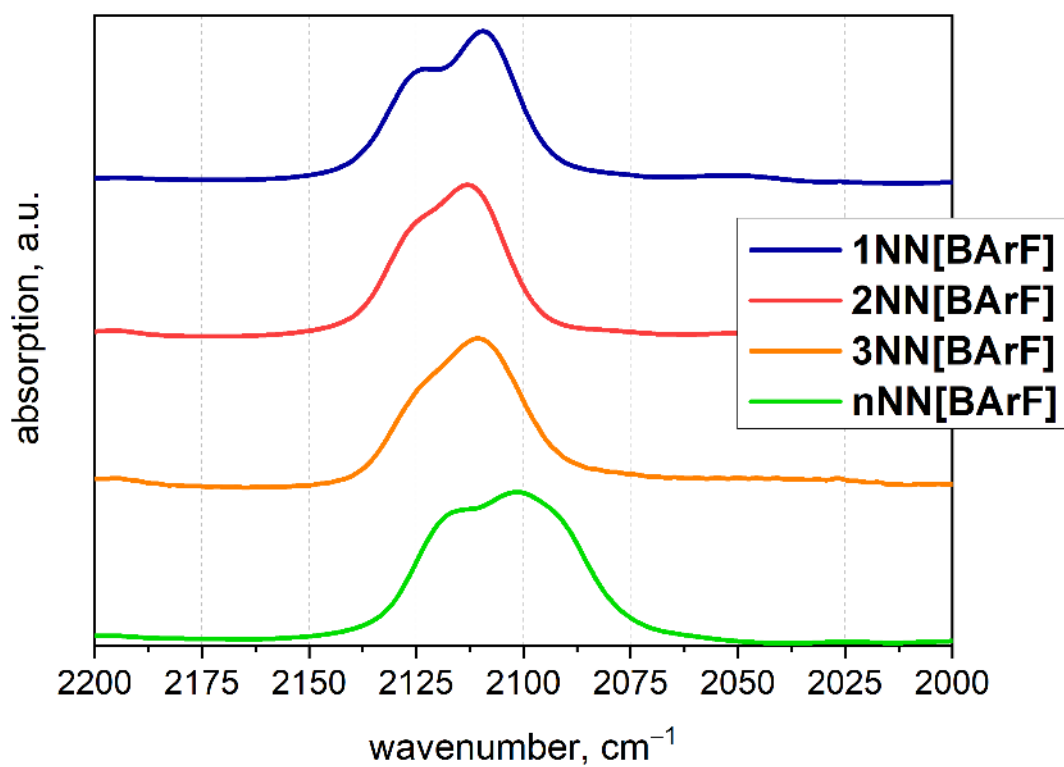


Figure S11. FTIR spectra of **NN[BArF]** in the region of C≡C vibration, KBr.

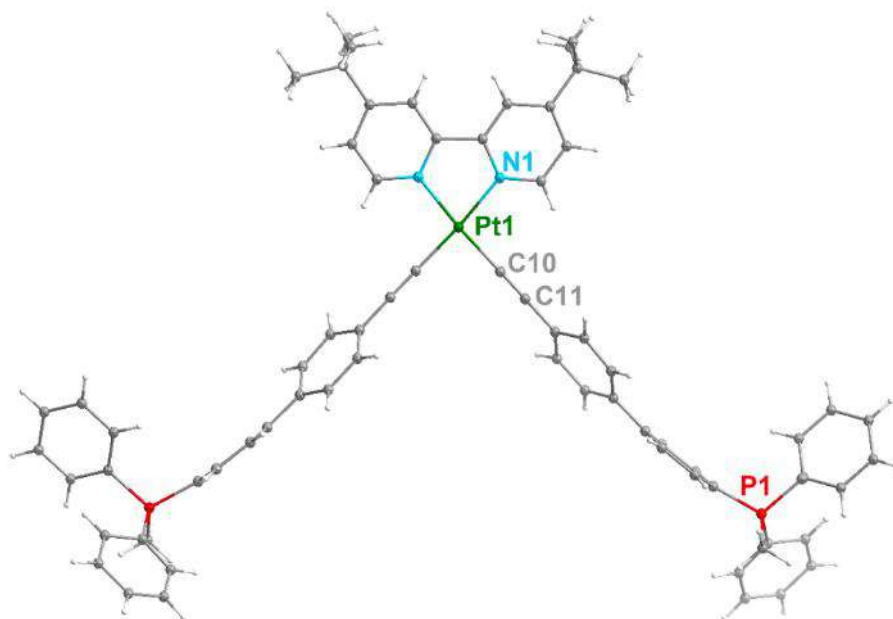


Figure S12. ORTEP view of **2NN[Cl]** molecular structure, the thermal ellipsoids are set at a 50% probability level. Counterions are omitted for clarity.

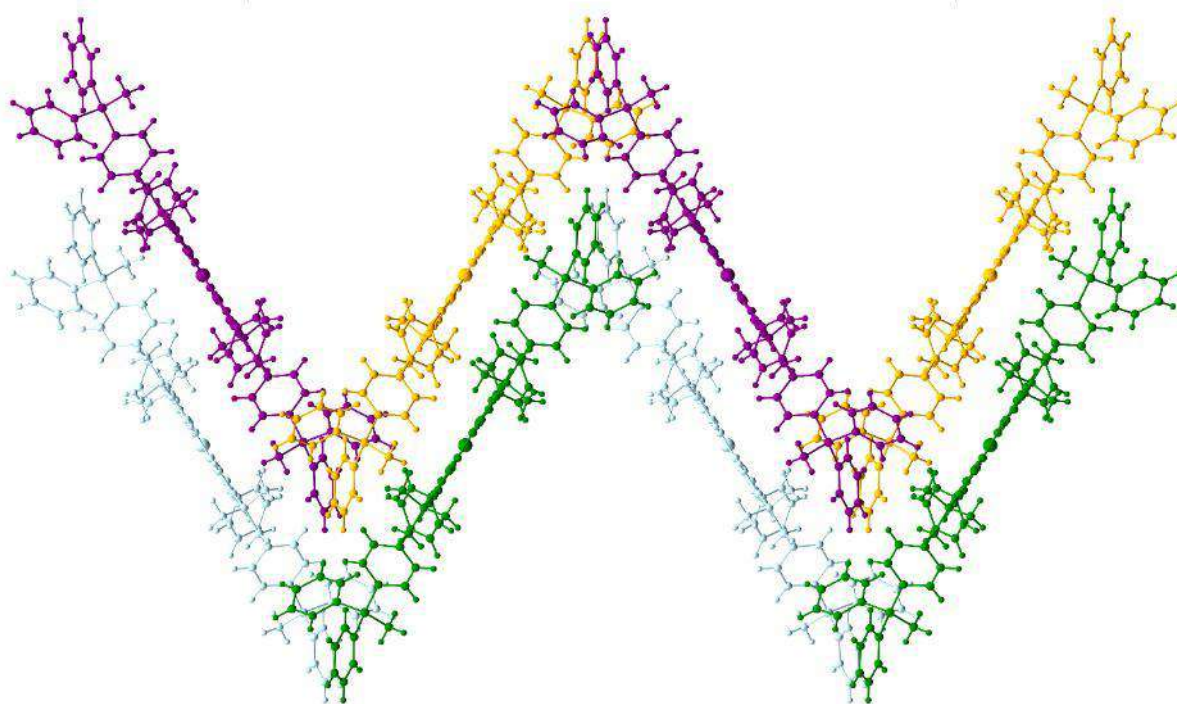


Figure S13. Fragment of crystal packing of **2NN[Cl]**. Counterions are omitted for clarity.

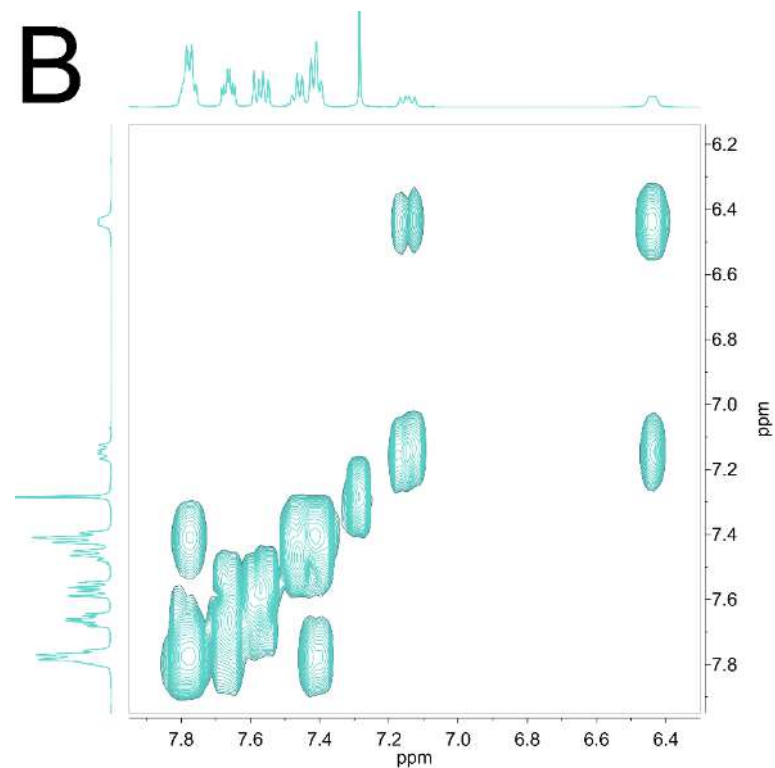
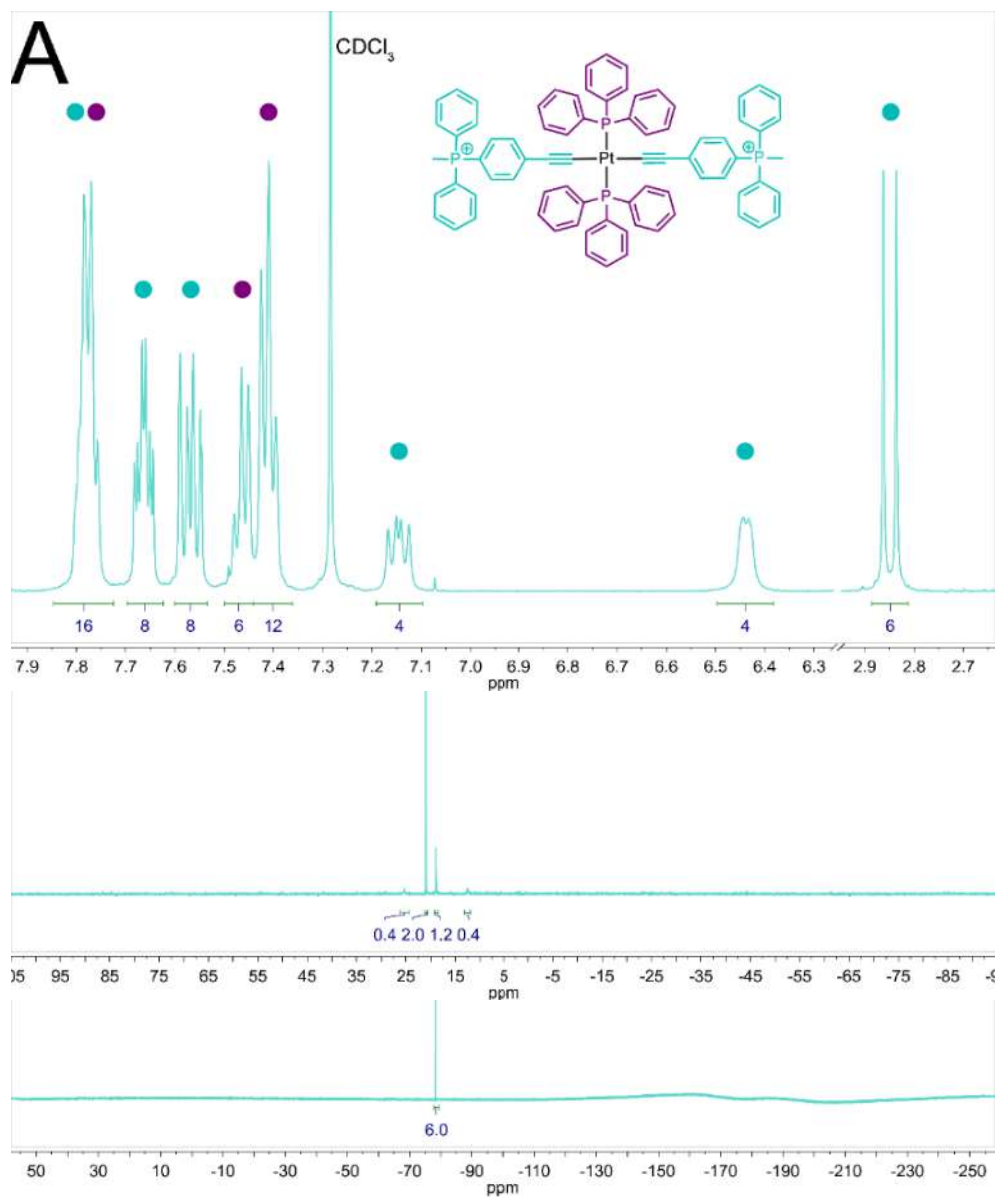


Figure S14. (A)  $^1\text{H}$  (top),  $^{31}\text{P}\{^1\text{H}\}$  (middle) and  $^{19}\text{F}$  (bottom) spectra in aromatic range of **1P[OTf]**; (B)  $^1\text{H}^1\text{H}$  COSY spectrum in aromatic range of **1P[OTf]**.

$^1\text{H}$ ,  $^{31}\text{P}\{^1\text{H}\}$  and  $^1\text{H}^1\text{H}$  COSY NMR spectra were measured in CDCl<sub>3</sub>,  $^{19}\text{F}$  spectrum – in DMSO-d<sub>6</sub>.

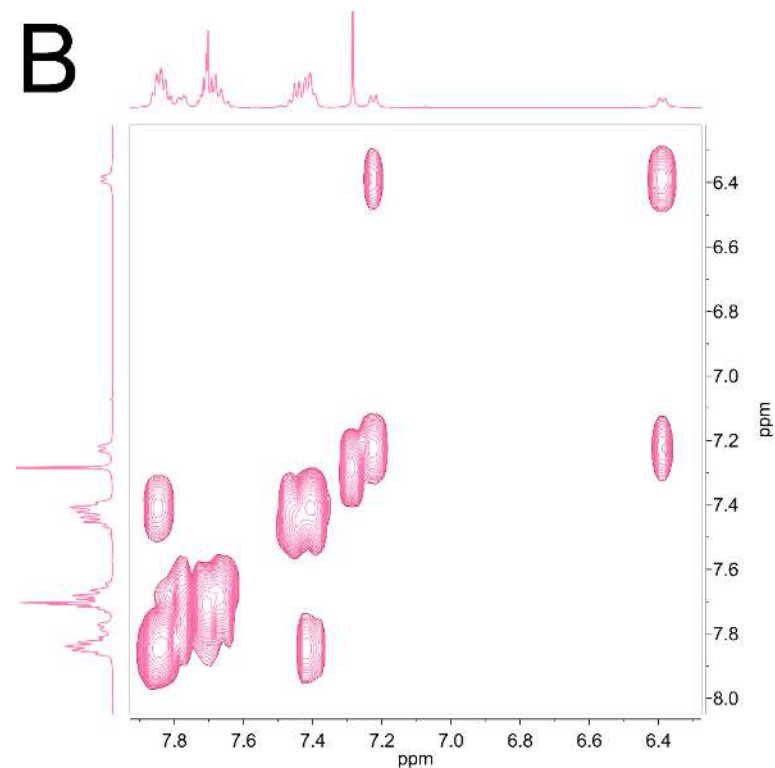
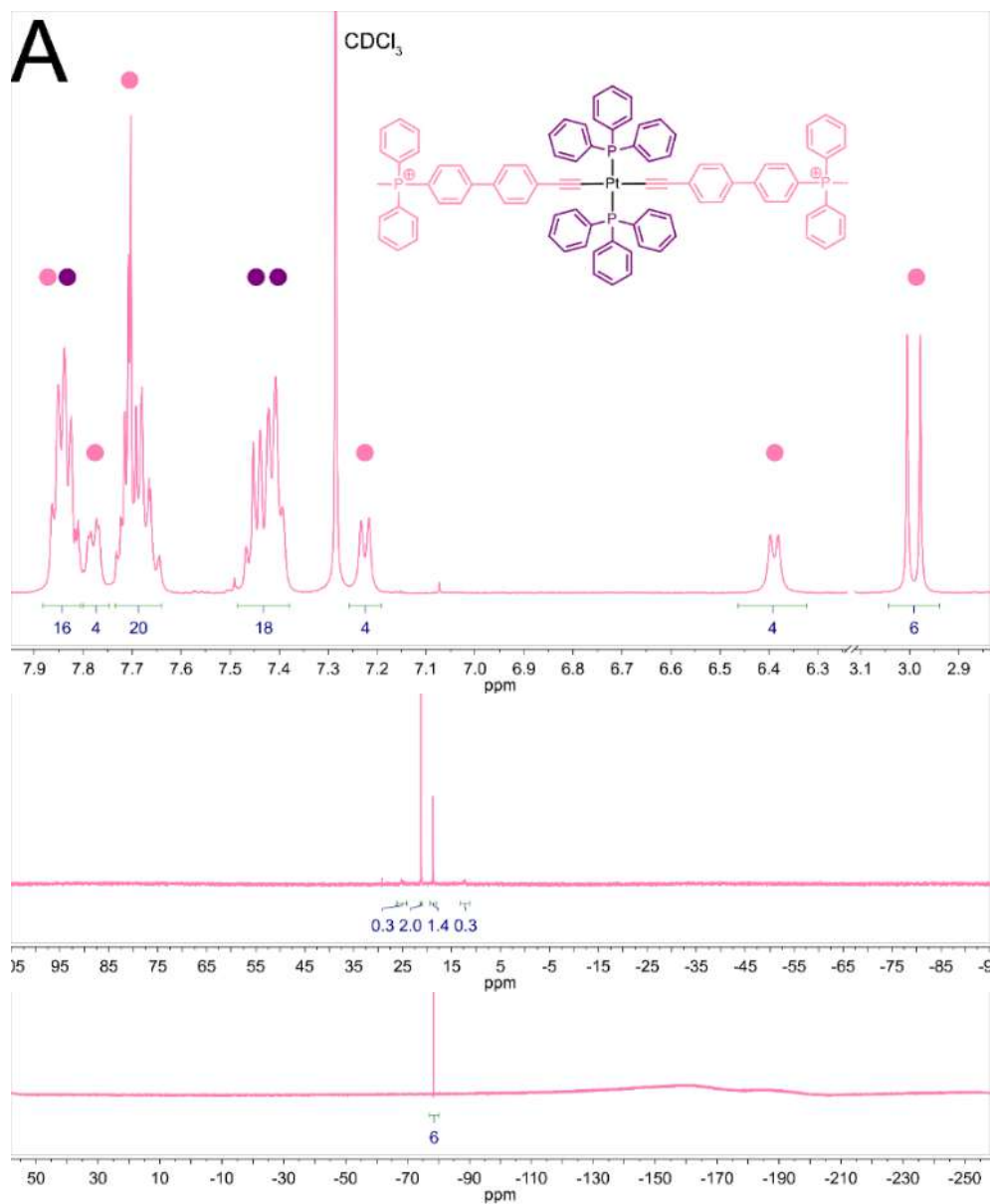


Figure S15. (A)  $^1\text{H}$  (top),  $^{31}\text{P}\{^1\text{H}\}$  (middle) and  $^{19}\text{F}$  (bottom) spectra in aromatic range of **2P[OTf]**; (B)  $^1\text{H}\{^1\text{H}\}$  COSY spectrum in aromatic range of **2P[OTf]**.  $^1\text{H}$ ,  $^{31}\text{P}\{^1\text{H}\}$  and  $^1\text{H}\{^1\text{H}\}$  COSY NMR spectra were measured in CDCl<sub>3</sub>,  $^{19}\text{F}$  spectrum – in DMSO-d<sub>6</sub>.

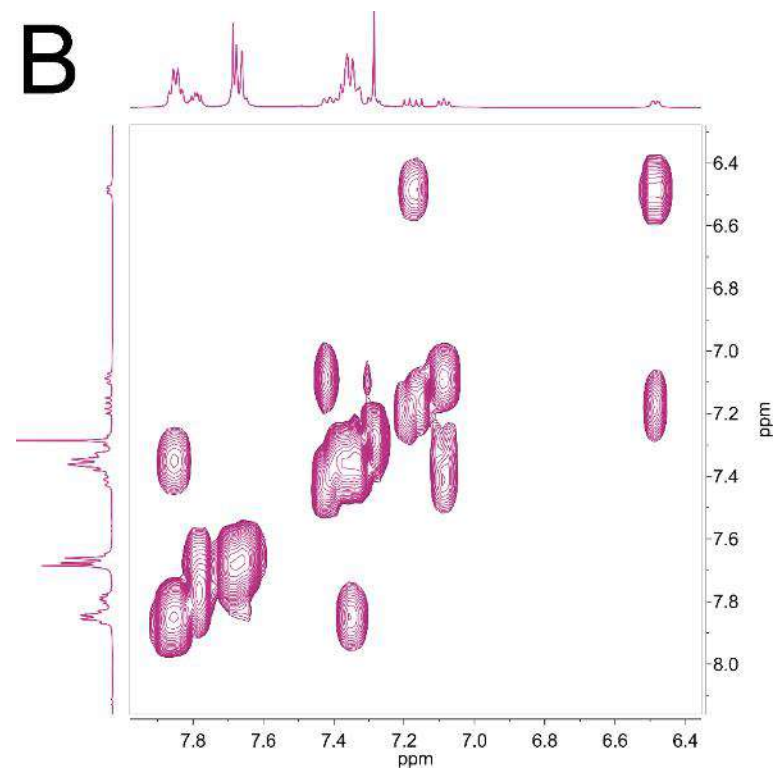
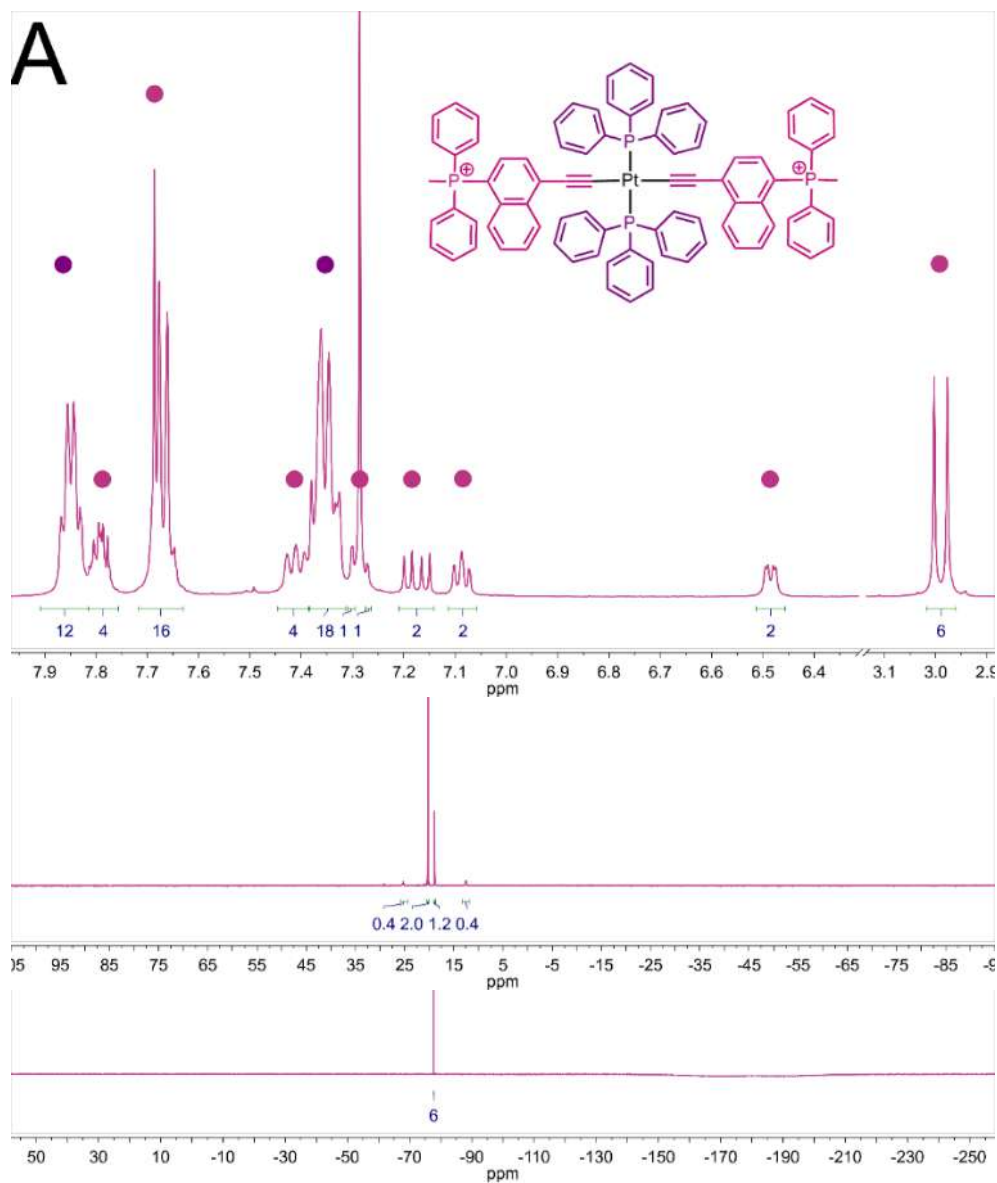


Figure S16. (A)  $^1\text{H}$  (top),  $^{31}\text{P}\{^1\text{H}\}$  (middle) and  $^{19}\text{F}$  (bottom) spectra in aromatic range of  $n\mathbf{P}[\mathbf{OTf}]$ ; (B)  $^1\text{H}\text{-}^1\text{H}$  COSY spectrum in aromatic range of  $n\mathbf{P}[\mathbf{OTf}]$ .  $^1\text{H}$ ,  $^{31}\text{P}\{^1\text{H}\}$  and  $^1\text{H}\text{-}^1\text{H}$  COSY NMR spectra were measured in  $\text{CDCl}_3$ ,  $^{19}\text{F}$  spectrum – in  $\text{DMSO-d}_6$ .

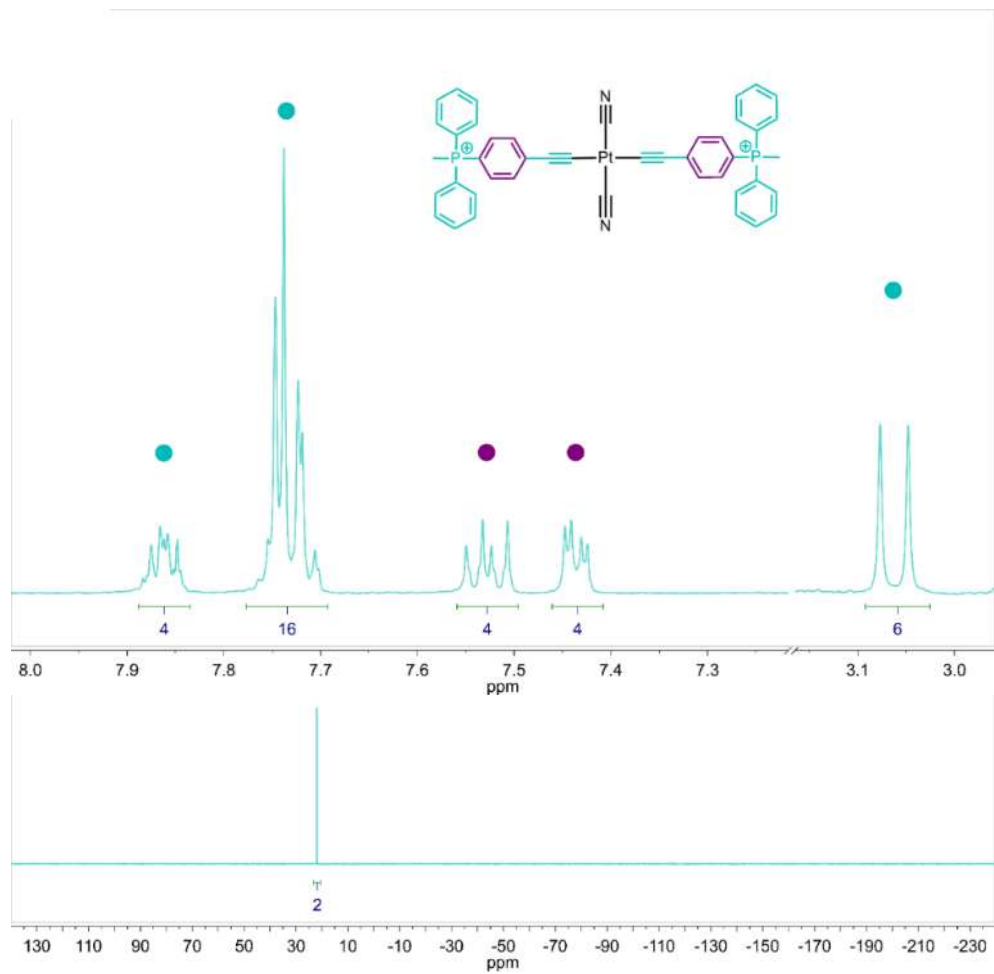


Figure S17.  $^1\text{H}$  (top),  $^{31}\text{P}\{^1\text{H}\}$  (bottom) spectra in aromatic range of **1CN**.

All NMR spectra were measured in  $\text{DMSO-d}_6$ .

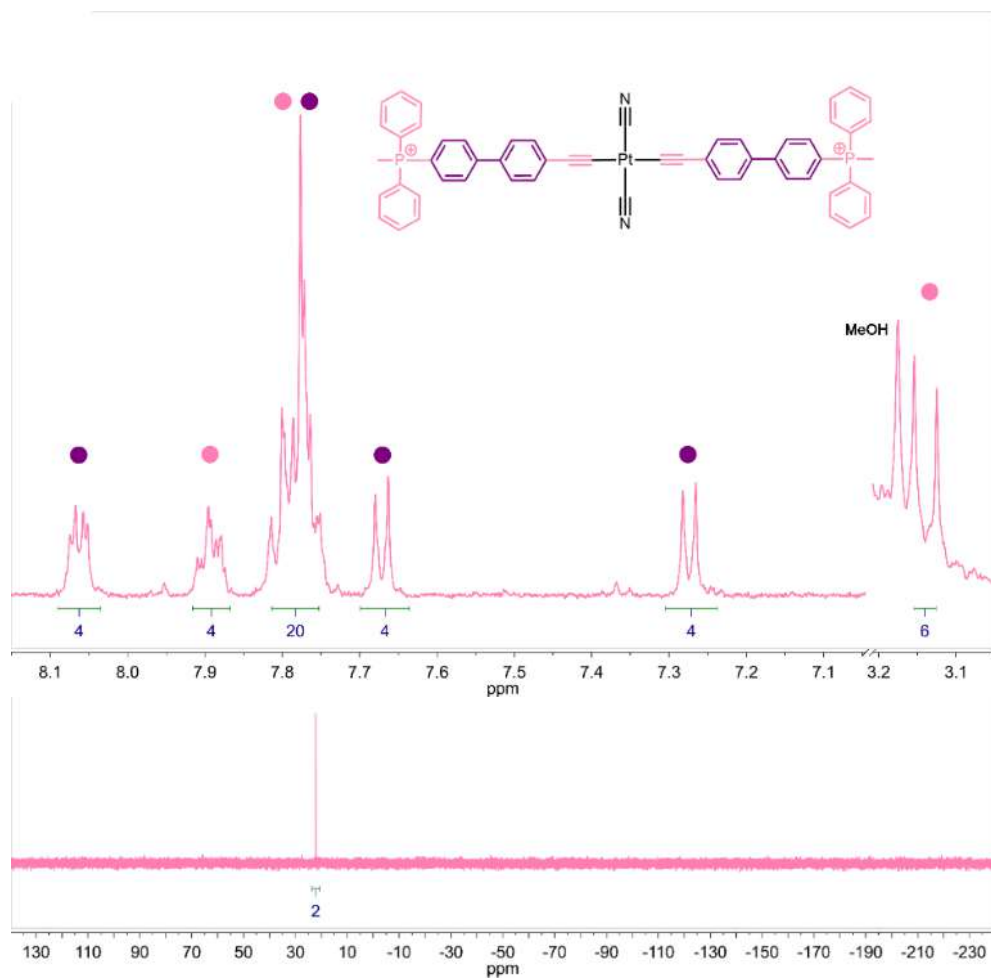


Figure S18.  $^1\text{H}$  (top),  $^{31}\text{P}\{^1\text{H}\}$  (bottom) spectra in aromatic range of **2CN**.

All NMR spectra were measured in  $\text{DMSO-d}_6$ .

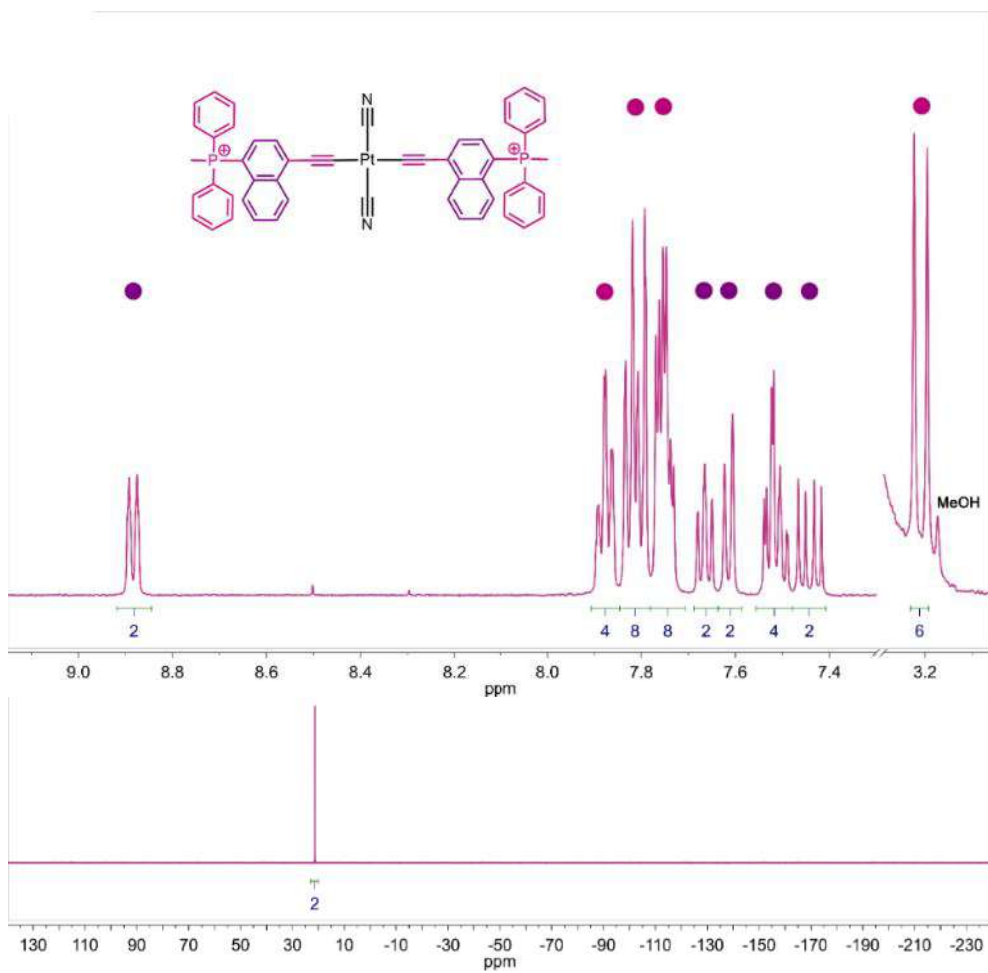


Figure S19. <sup>1</sup>H (top), <sup>31</sup>P{<sup>1</sup>H} (bottom) spectra in aromatic range of **nCN**.

All NMR spectra were measured in DMSO-d<sub>6</sub>.

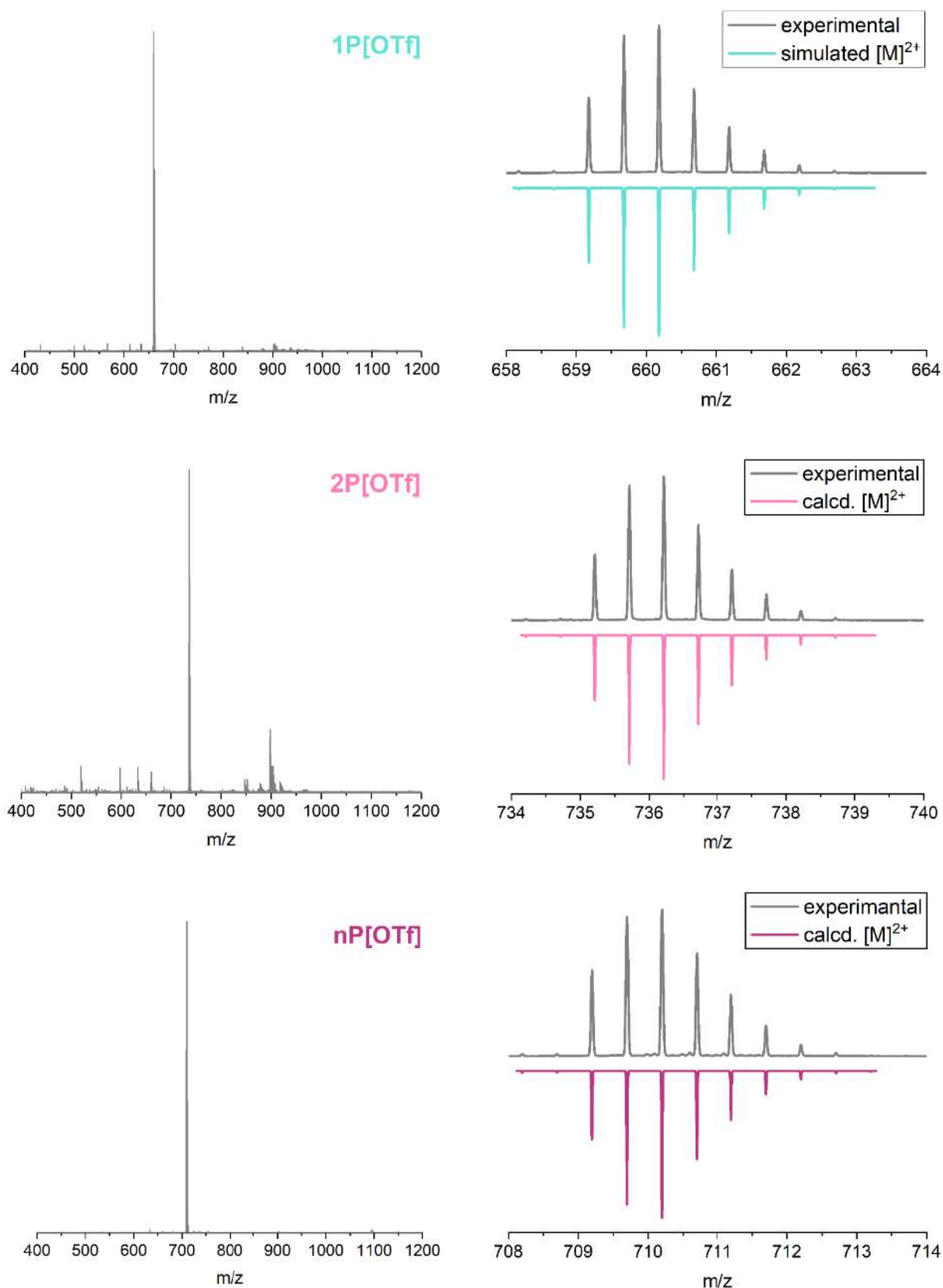


Figure S20. Experimental (gray) ESI<sup>+</sup> MS spectra of **P[OTf]** series and simulated isotopic patterns of the  $[M]^{2+}$ .

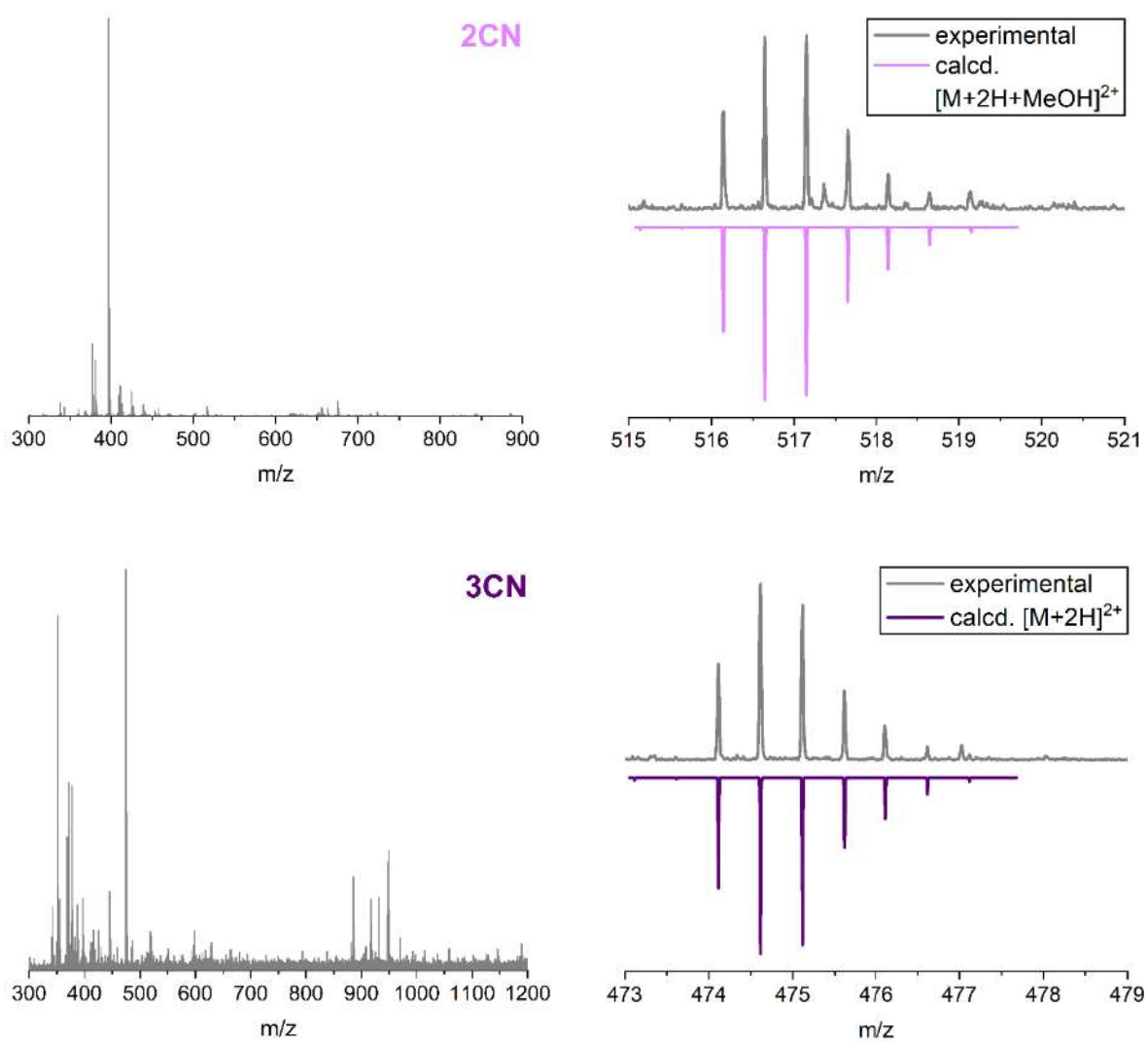


Figure S21. Experimental (gray) ESI+ MS spectra of CN series and simulated isotopic patterns of the  $[M]^{2+}$ .

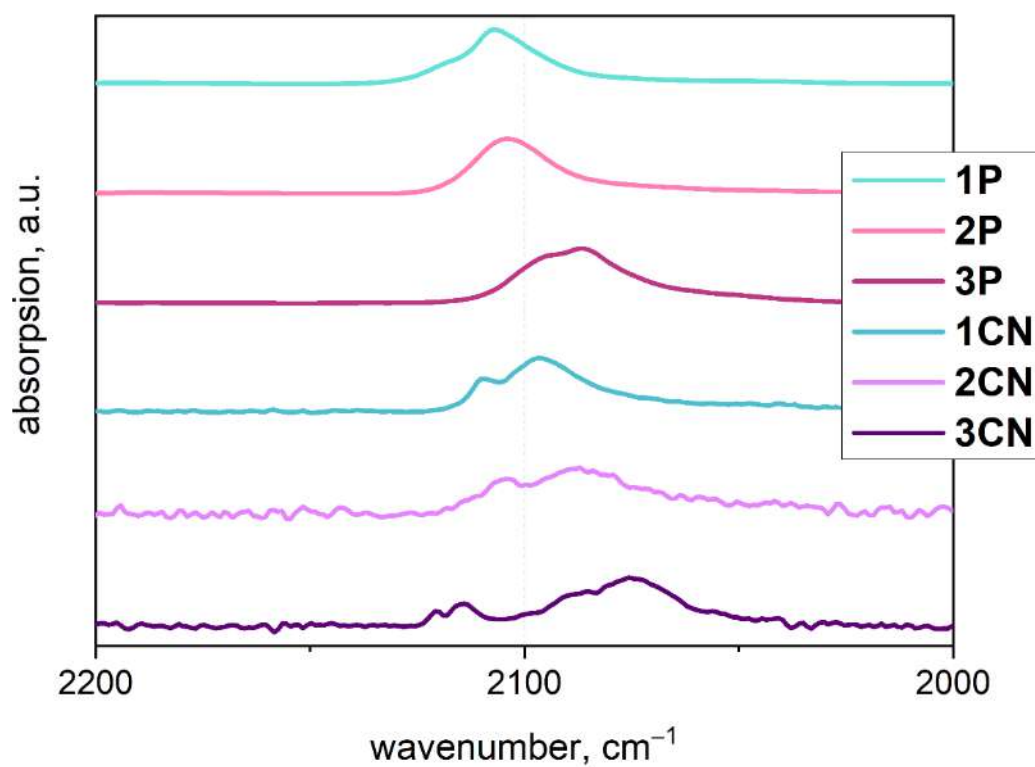


Figure S22. FTIR spectra of **P[OTf]** and **CN** series in the region of C≡C vibration, KBr.

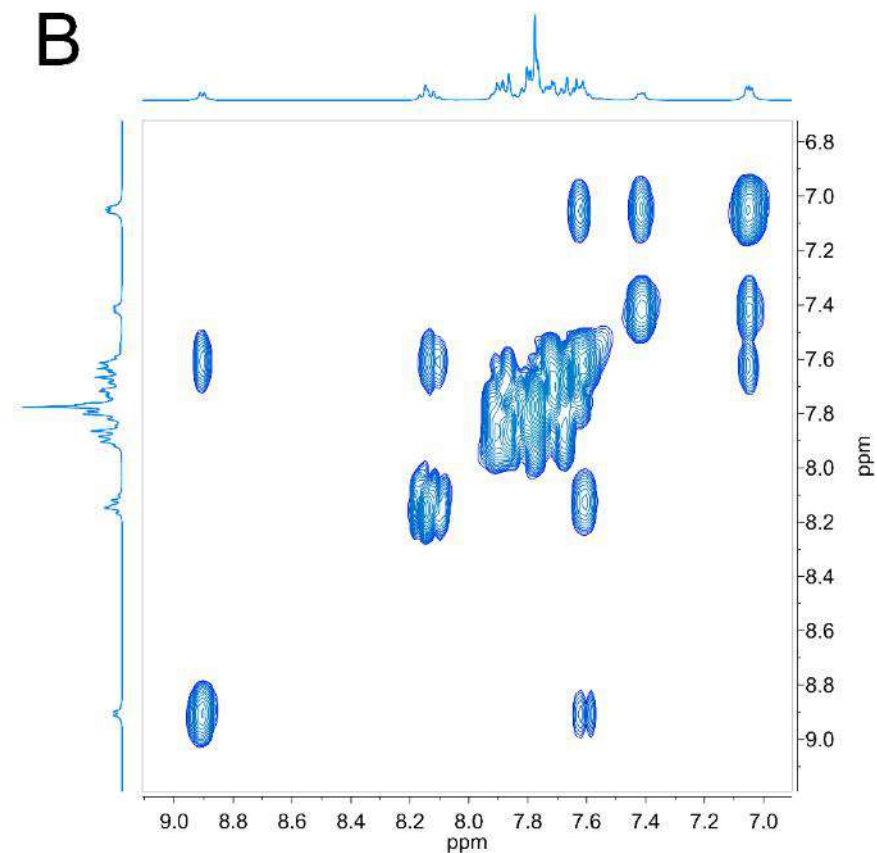
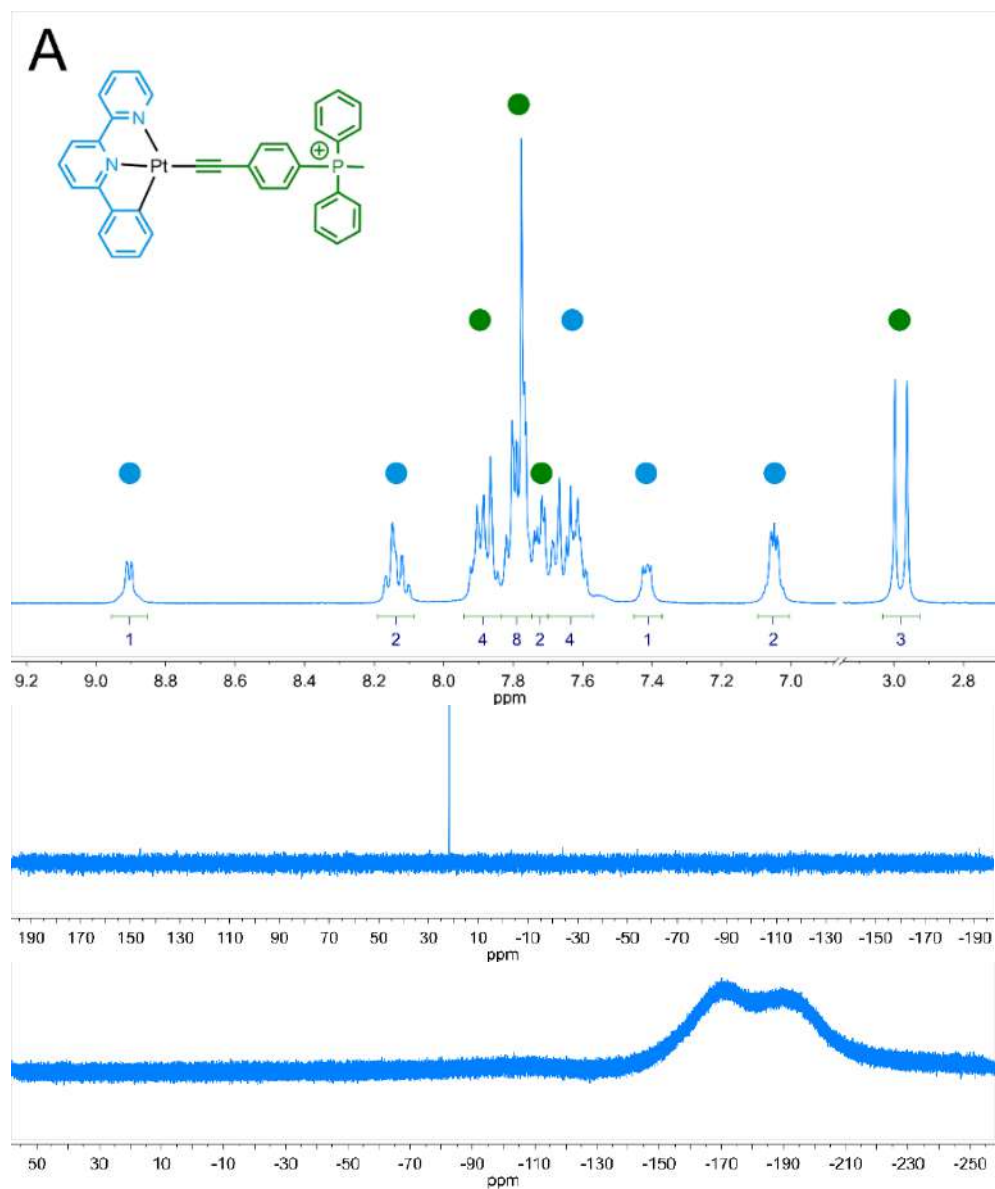


Figure S23. (A)  $^1\text{H}$  (top),  $^{31}\text{P}\{^1\text{H}\}$  (middle) and  $^{19}\text{F}$  (bottom) spectra in aromatic range of **1C[Cl]**; (B)  $^1\text{H}$ - $^1\text{H}$  COSY spectrum in aromatic range of **1C[Cl]**.  $^1\text{H}$  and  $^1\text{H}$ - $^1\text{H}$  COSY NMR spectra were measured in MeOD,  $^{31}\text{P}$  and  $^{19}\text{F}$  spectra – in acetone- $d_6$ .

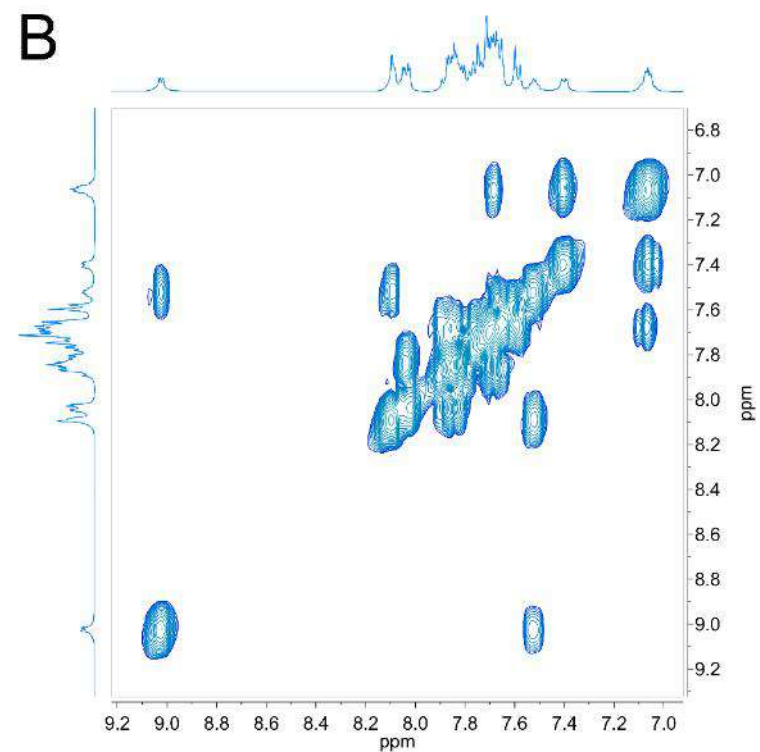
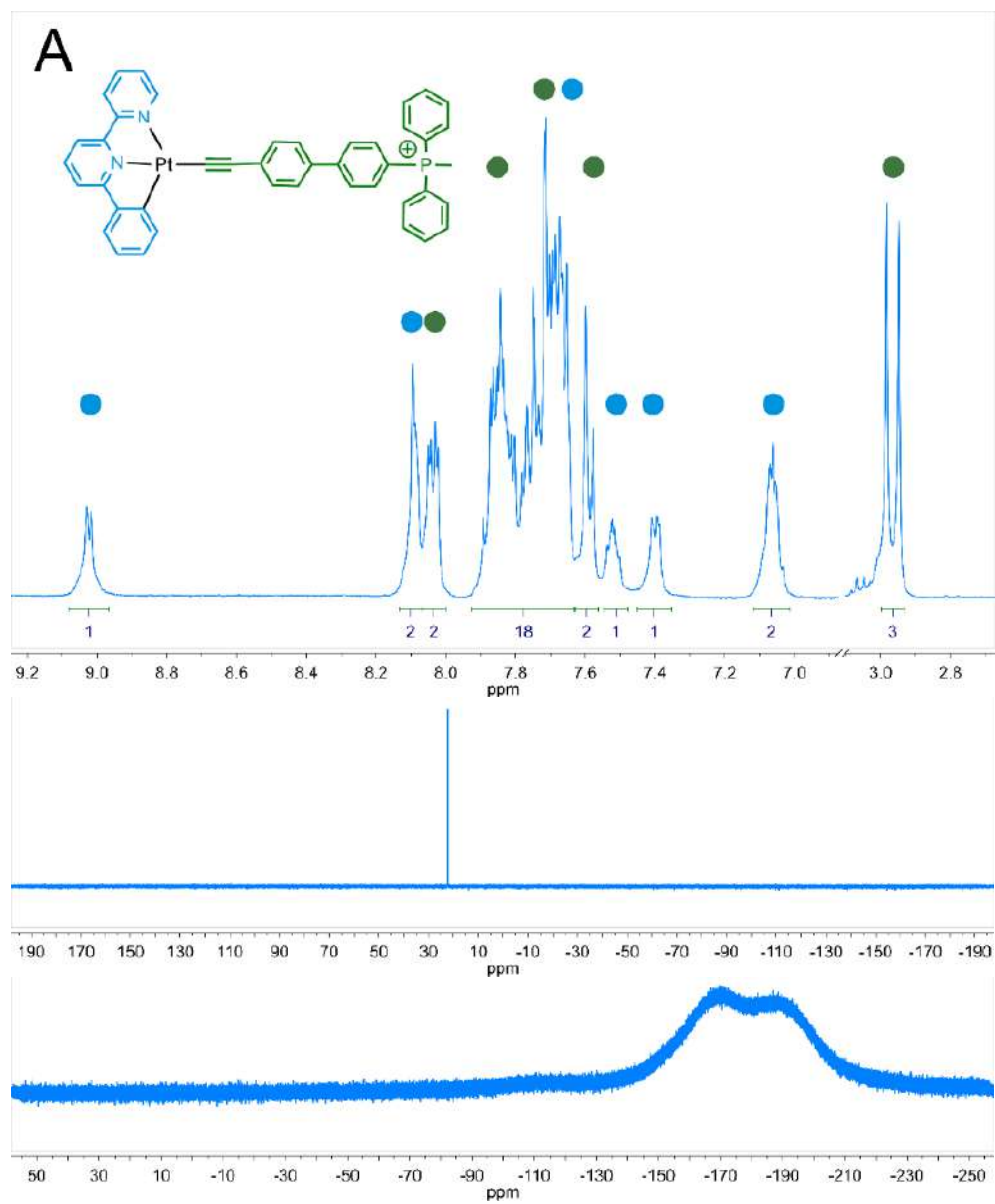


Figure S24. (A)  $^1\text{H}$  (top),  $^{31}\text{P}\{^1\text{H}\}$  (middle) and  $^{19}\text{F}$  (bottom) spectra in aromatic range of **2C[Cl]**; (B)  $^1\text{H}\text{-}^1\text{H}$  COSY spectrum in aromatic range of **2C[Cl]**.  $^1\text{H}$  and  $^1\text{H}\text{-}^1\text{H}$  COSY NMR spectra were measured in MeOD,  $^{31}\text{P}$  and  $^{19}\text{F}$  spectra – in DMSO- $d_6$ .

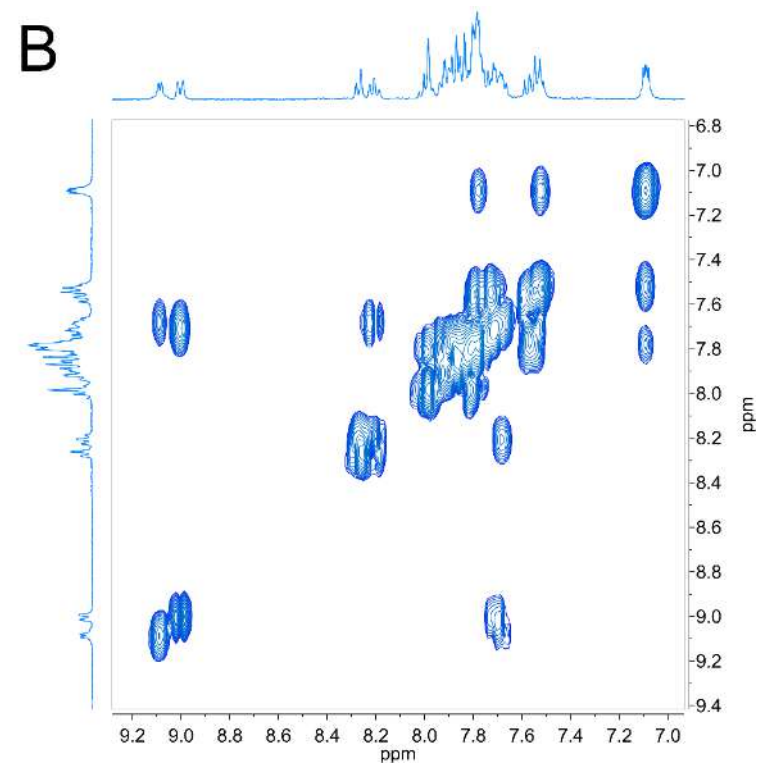
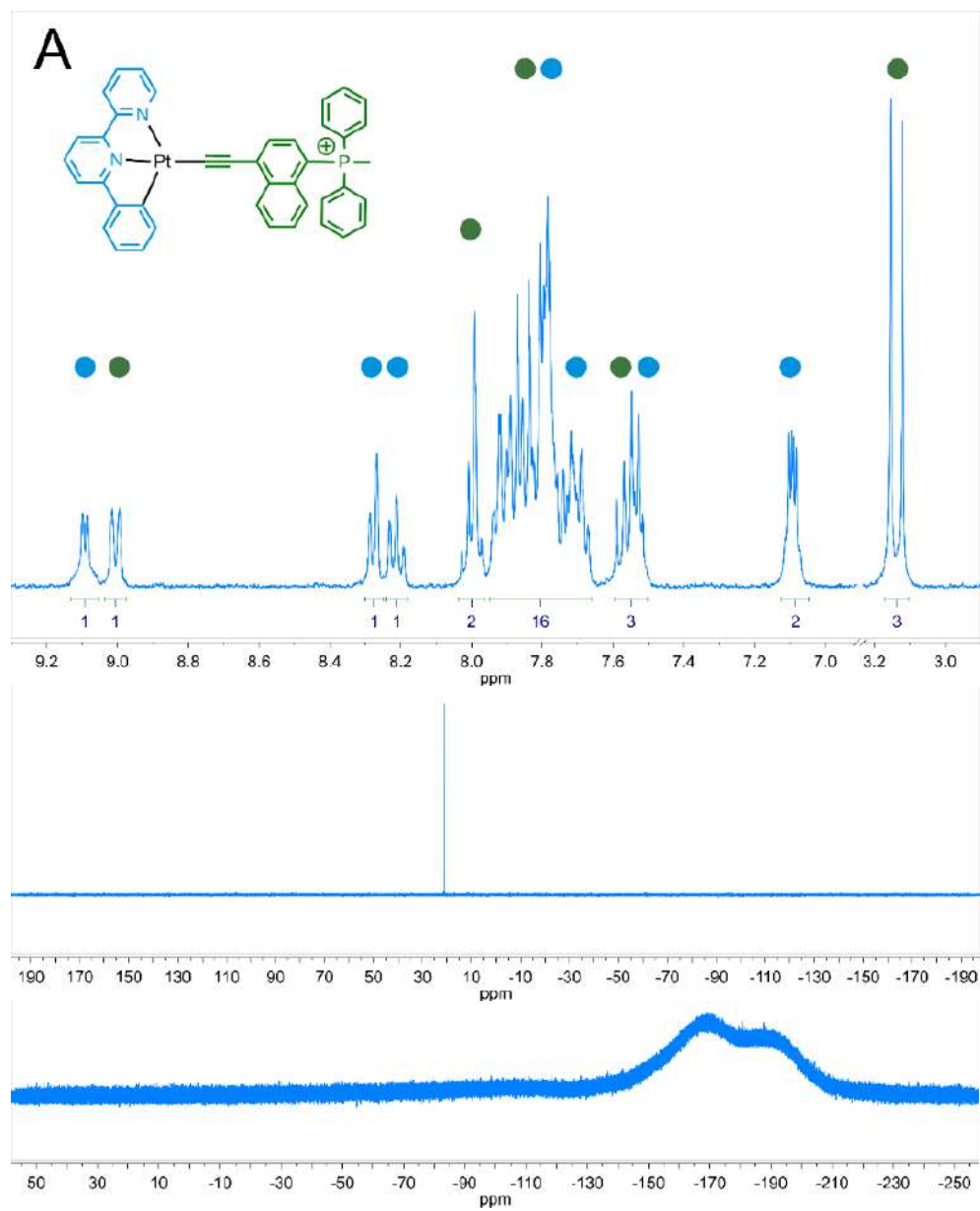


Figure S25.  $^1\text{H}$  (top),  $^{31}\text{P}\{^1\text{H}\}$  (middle) and  $^{19}\text{F}$  (bottom) spectra in aromatic range of **1C[Cl]**; (B)  $^1\text{H}$  $^1\text{H}$  COSY spectrum in aromatic range of **1C[Cl]**. All spectra were measured in acetone- $d_6$ .

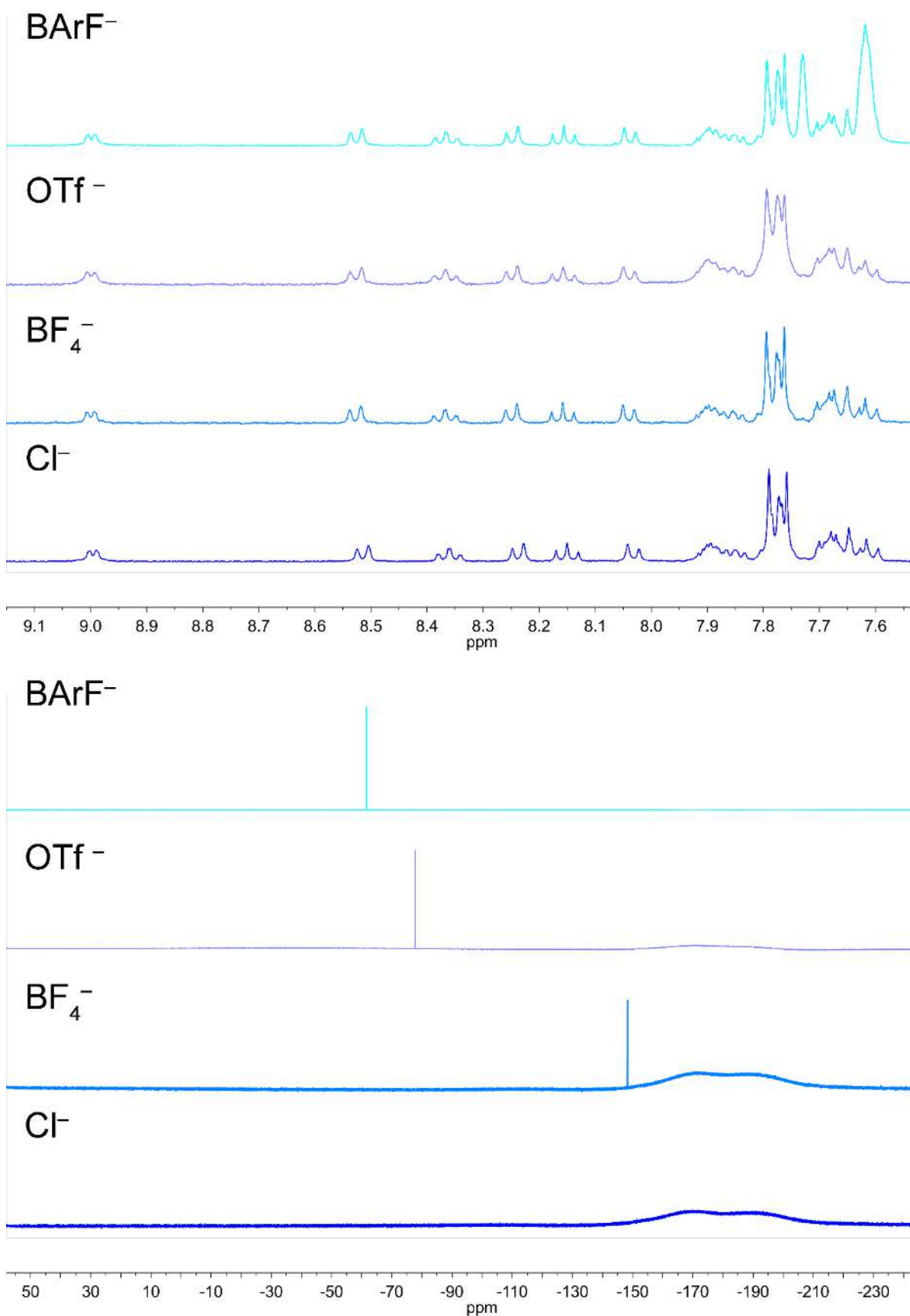


Figure S26. <sup>1</sup>H (top) and <sup>19</sup>F (bottom) stacked spectra in aromatic range of **1C[X]**. Counterions are labeled on the corresponding spectra, measured in DMSO-d<sub>6</sub>.

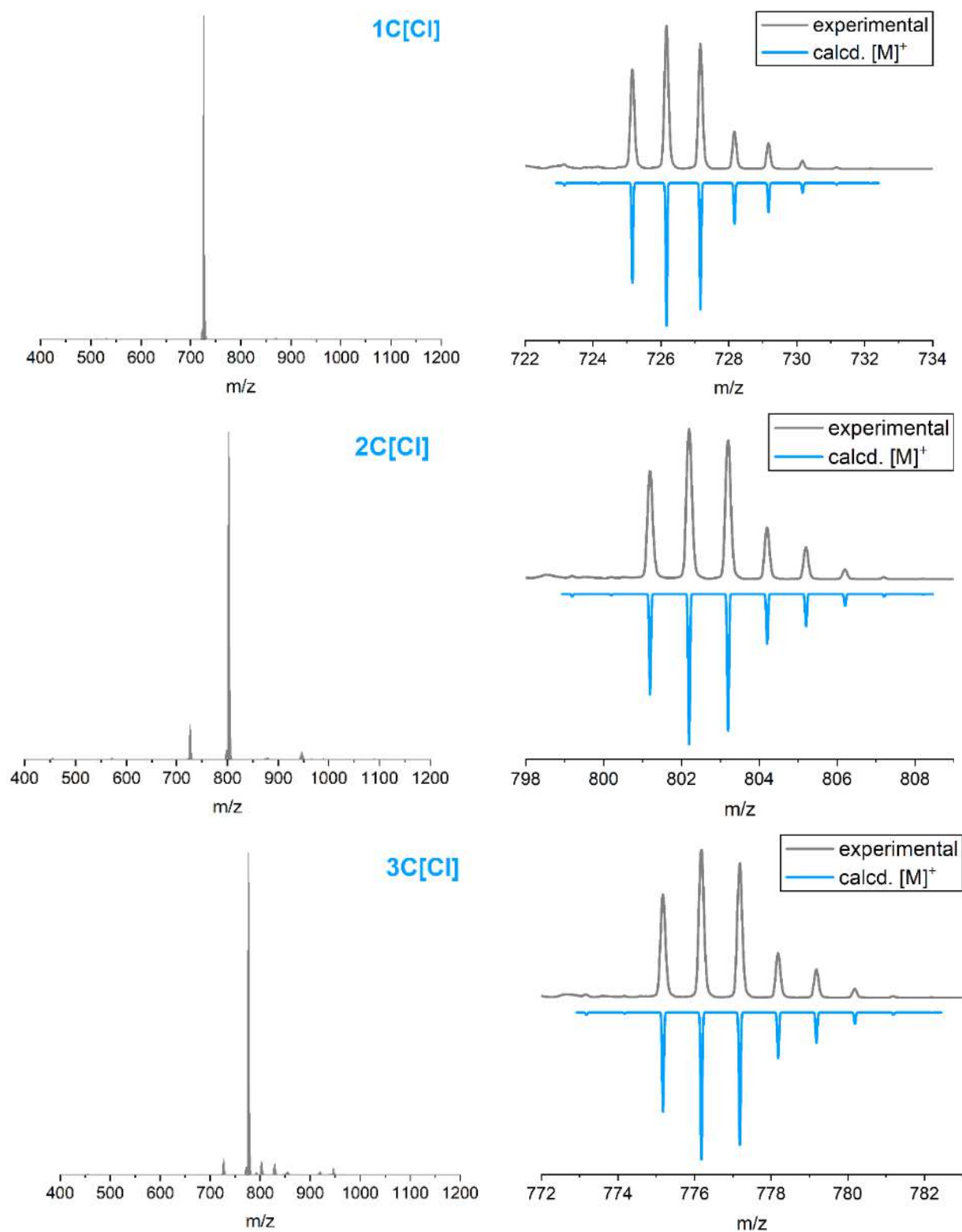


Figure S27. Experimental (gray) ESI<sup>+</sup> MS spectra of **C[Cl]** series and simulated isotopic patterns of the  $[M]^+$ .

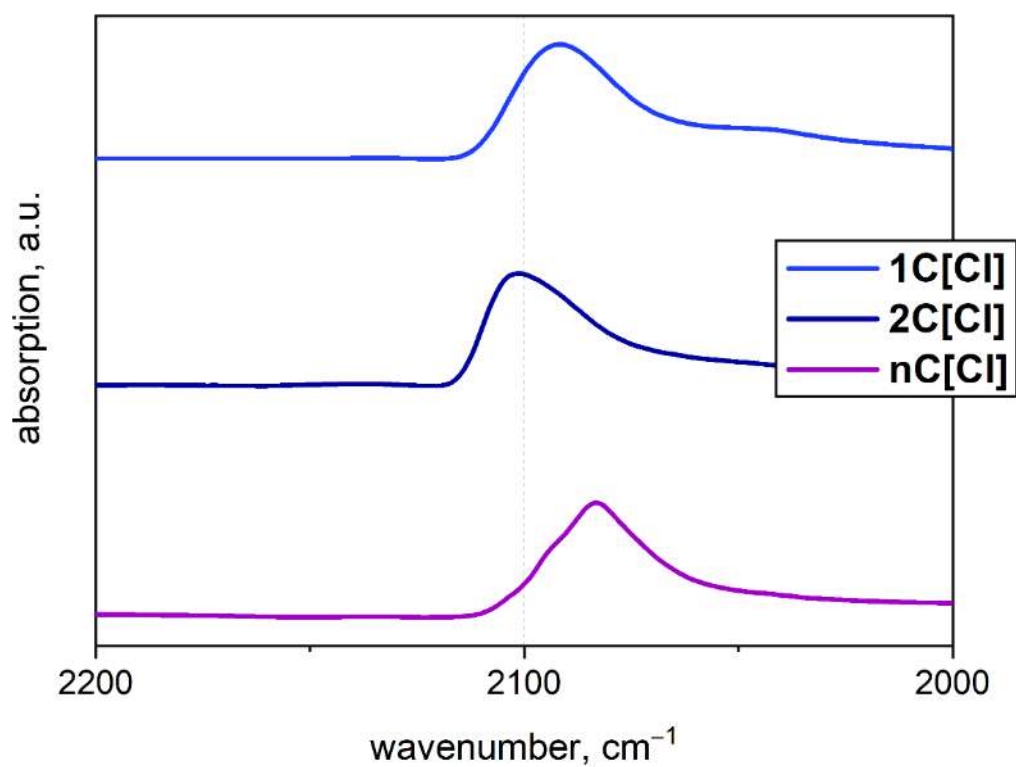


Figure S28. FTIR spectra of **C[Cl]** series in the region of C≡C vibration, KBr.

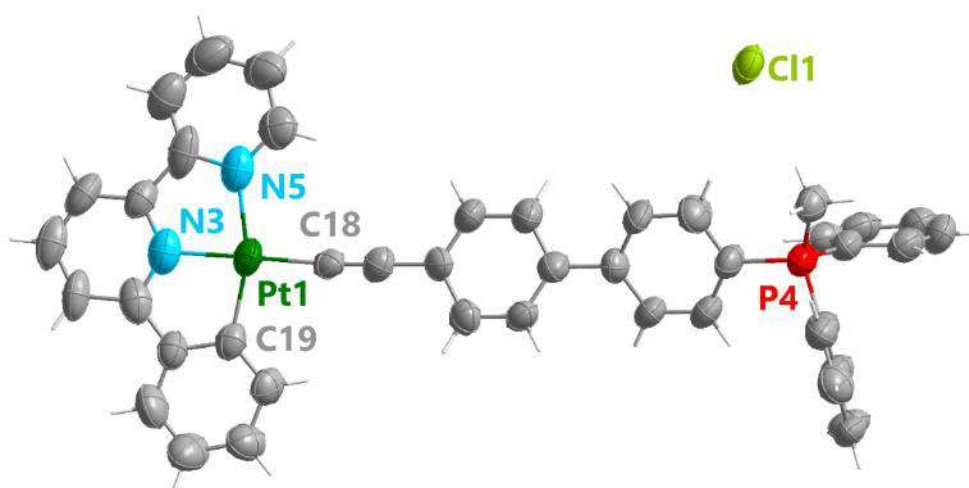


Figure S29. ORTEP view of **2C[Cl]** molecular structure, the thermal ellipsoids are set at a 50% probability level.

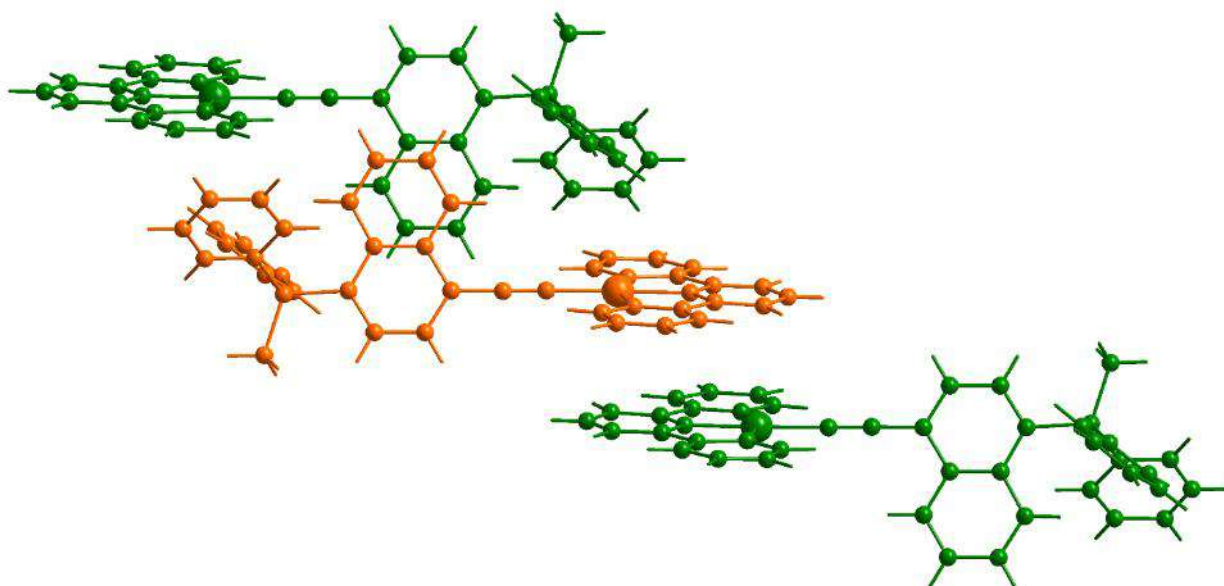


Figure S30. Fragment of crystal packing of **2NN[Cl]**. Counterions are omitted for clarity.

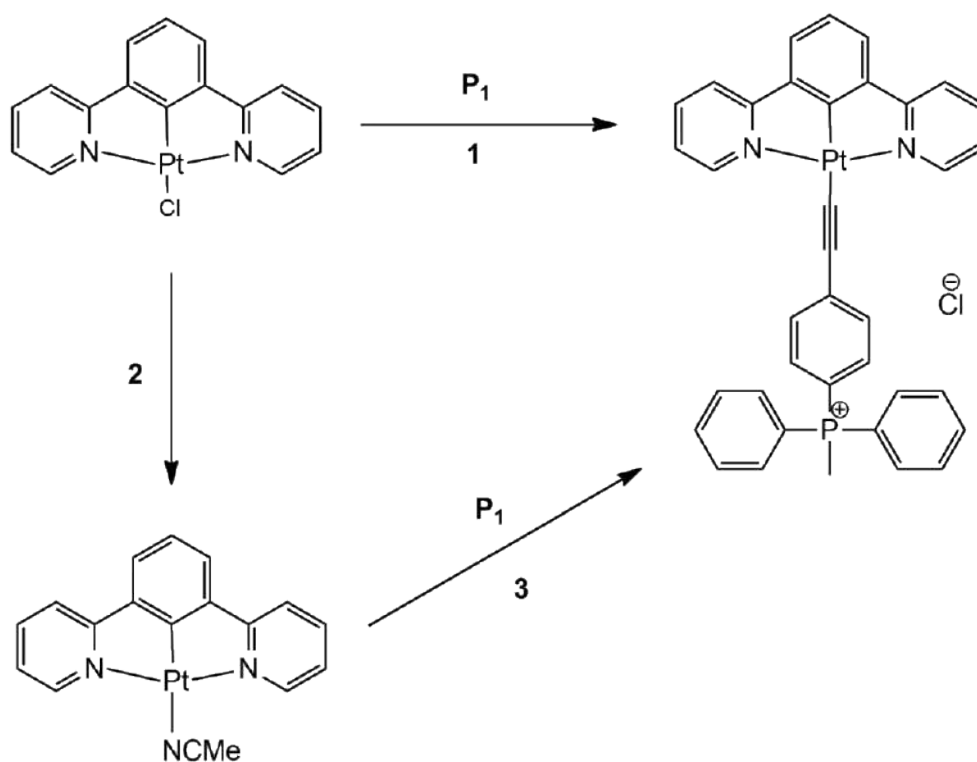


Figure S31. Schemes of unsuccessful syntheses for Pt(II) NCN complexes. **1**: MeOH, 1 eq. KOH, 18/48/72 h, or DCM:Et<sub>3</sub>N 7:2, 5 mol.% CuI, 24/48 h. **2**: MeCN, 1 eq. AgOTf. **3**: 2 eq. KOH, 24 h.

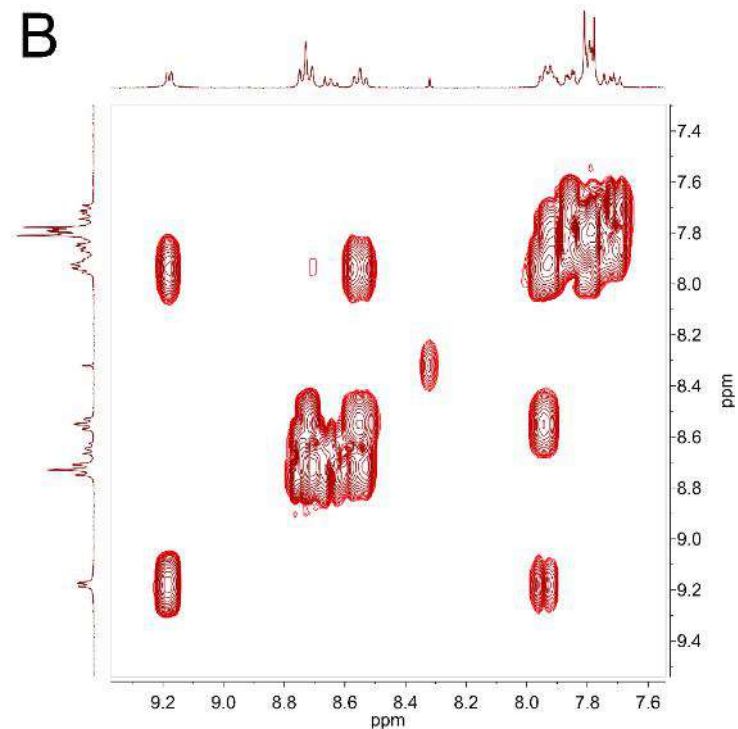
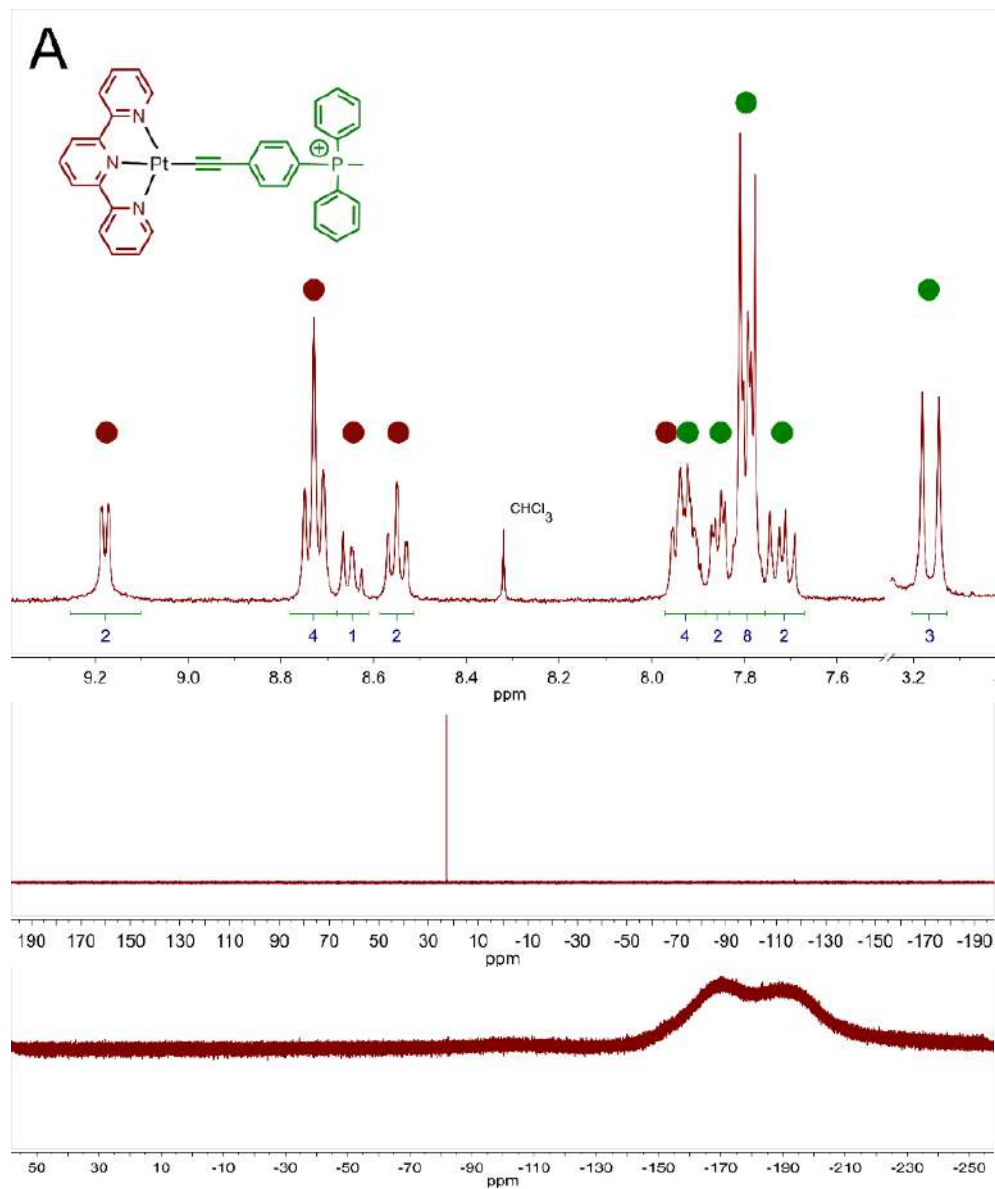


Figure S32. (A)  $^1\text{H}$  (top),  $^{31}\text{P}\{\text{H}\}$  (middle) and  $^{19}\text{F}$  (bottom) NMR spectra in aromatic range of **1N[Cl]**; (B)  $^1\text{H}$  $^1\text{H}$  COSY spectrum in aromatic range of **1N[Cl]**. All NMR spectra were measured in  $\text{DMSO-d}_6$ .

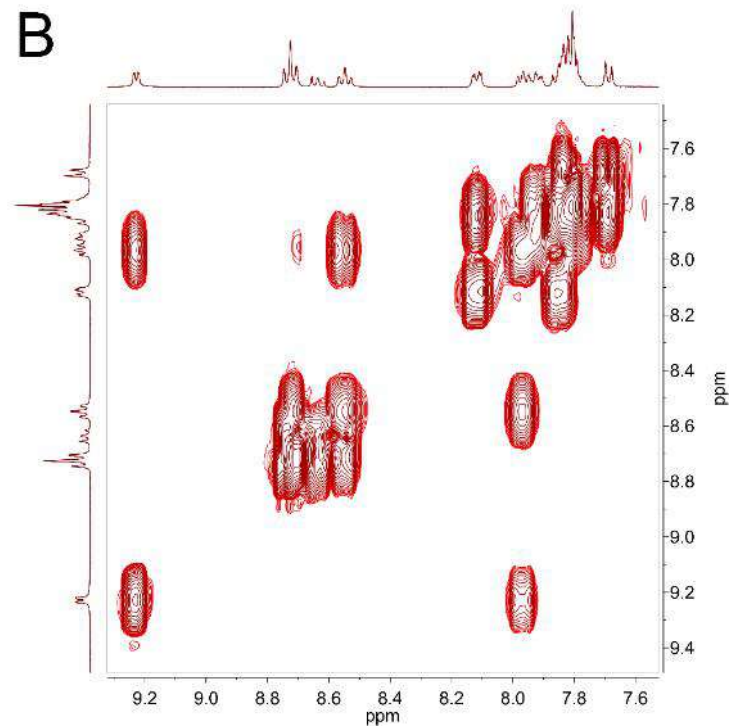
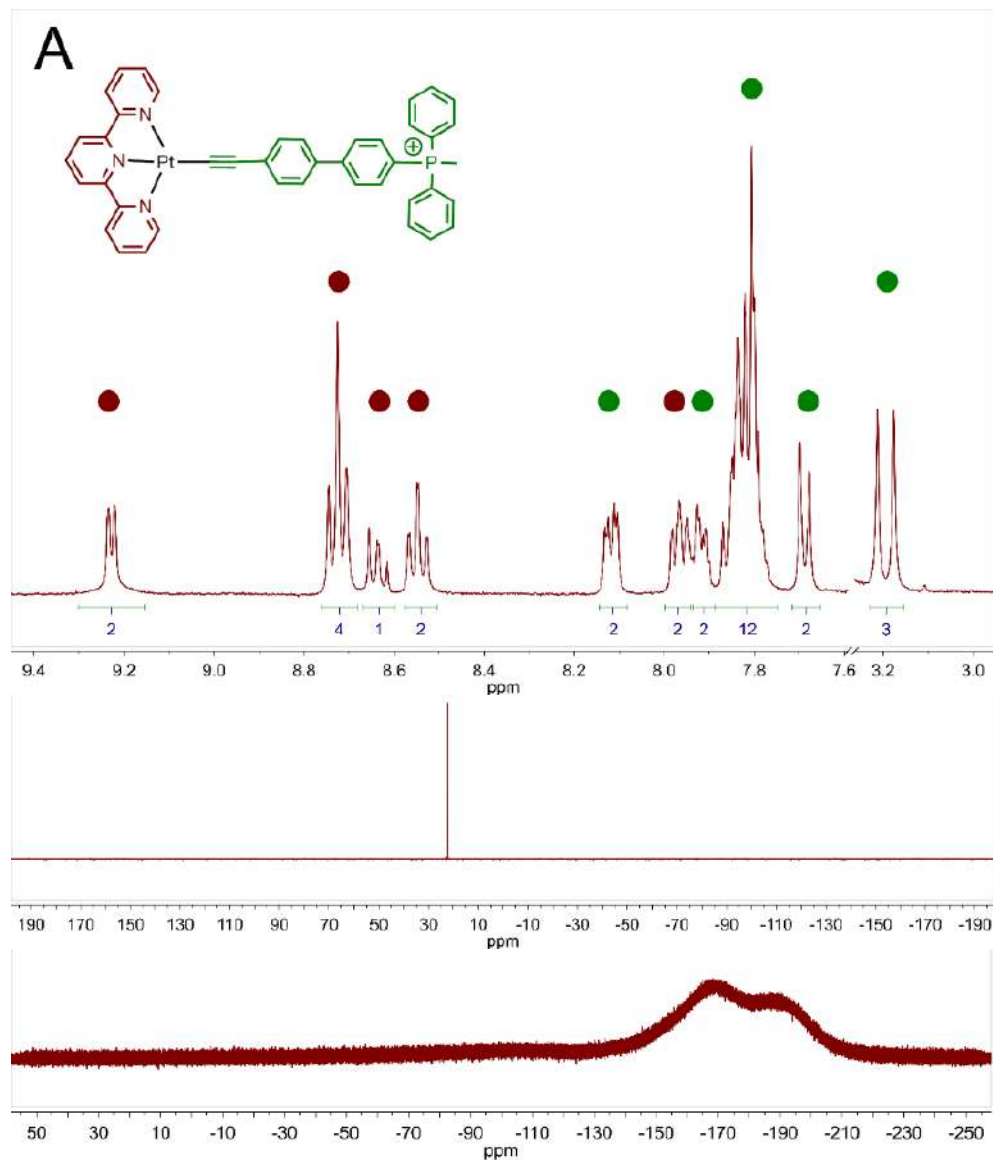


Figure S33. (A)  $^1H$  (top),  $^{31}P\{^1H\}$  (middle) and  $^{19}F$  (bottom) NMR spectra in aromatic range of  $2N[Cl]$ ; (B)  $^1H$ - $^1H$  COSY spectrum in aromatic range of  $2N[Cl]$ . All NMR spectra were measured in DMSO- $d_6$ .

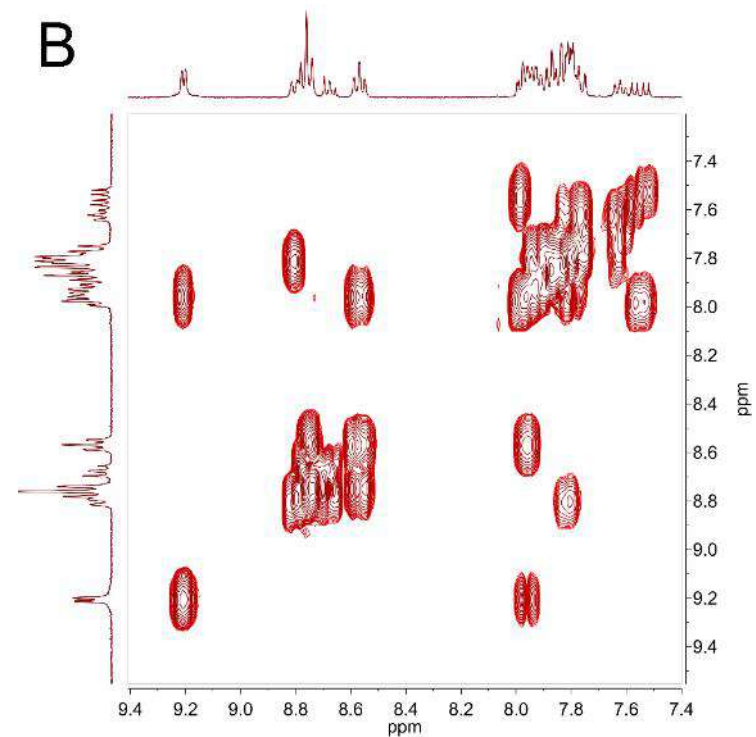
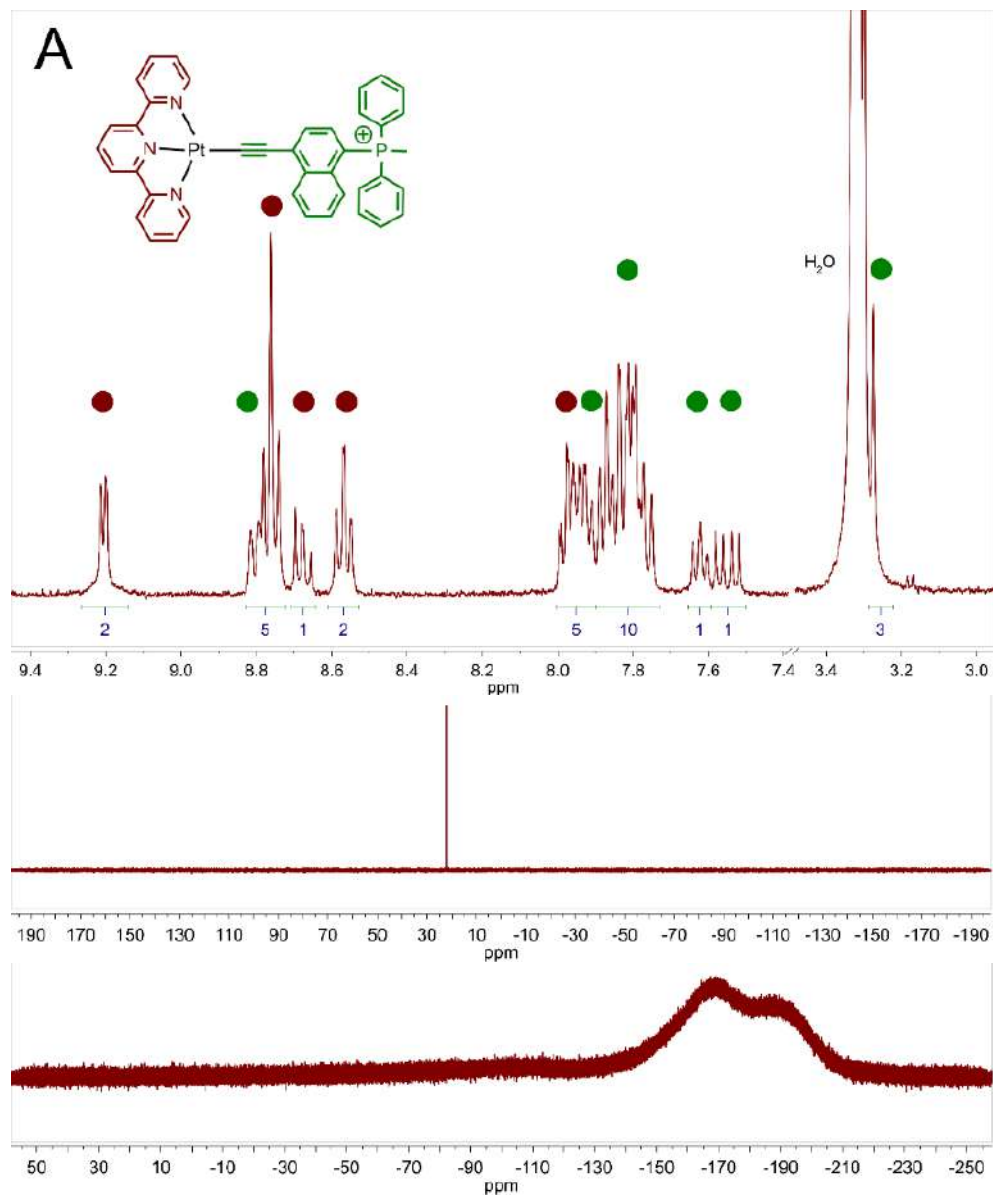


Figure S34. (A)  $^1\text{H}$  (top),  $^{31}\text{P}\{\text{H}\}$  (middle) and  $^{19}\text{F}$  (bottom) NMR spectra in aromatic range of **nN[Cl]**; (B)  $^1\text{H}\text{H}$  COSY spectrum in aromatic range of **nN[Cl]**. All NMR spectra were measured in DMSO- $d_6$ .

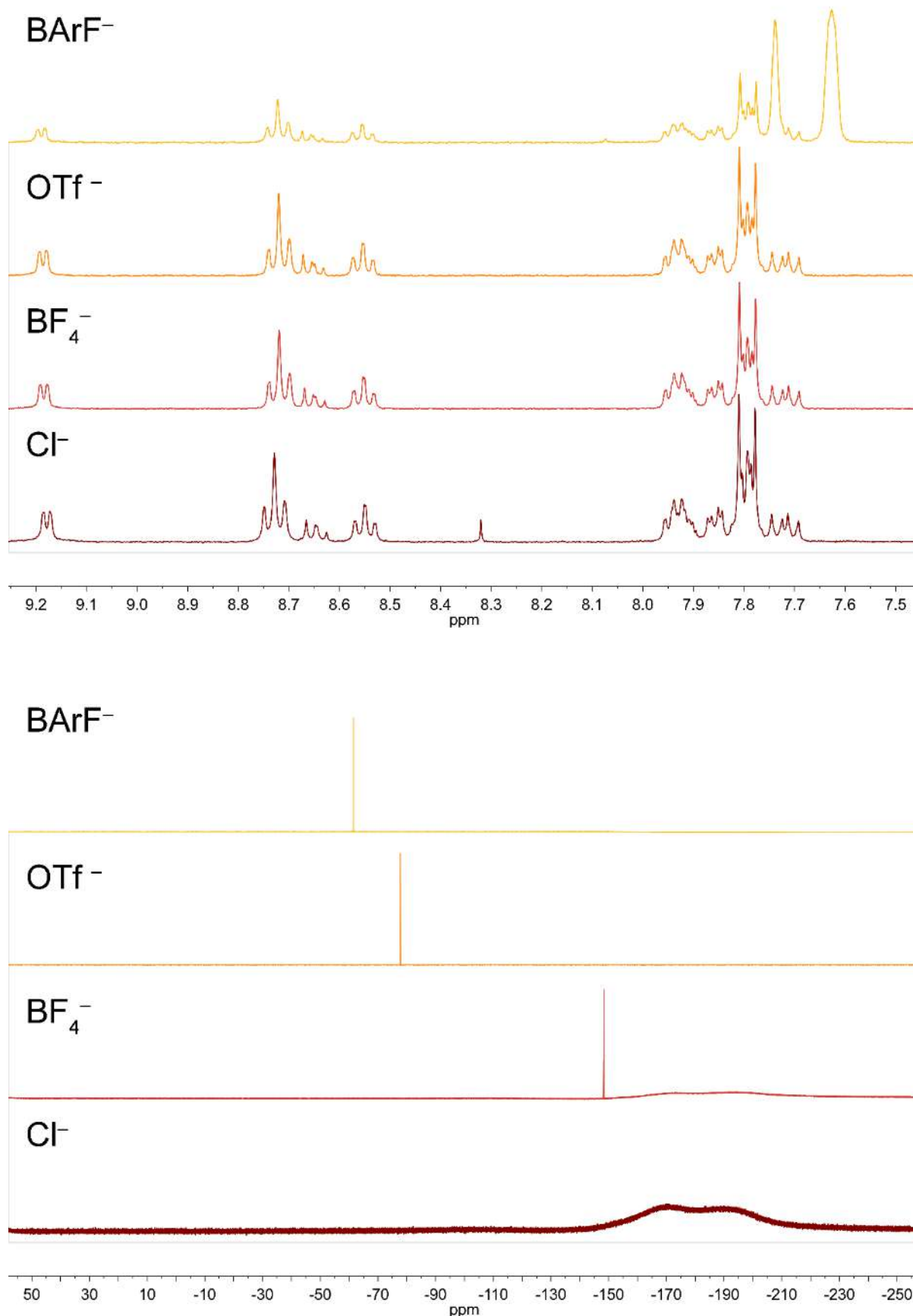


Figure S35.  $^1\text{H}$  (top) and  $^{19}\text{F}$  (bottom) stacked spectra in aromatic range of  $1\text{N}[\text{X}]$ . Counterions are labeled on the corresponding spectra, measured in  $\text{DMSO-d}_6$ .

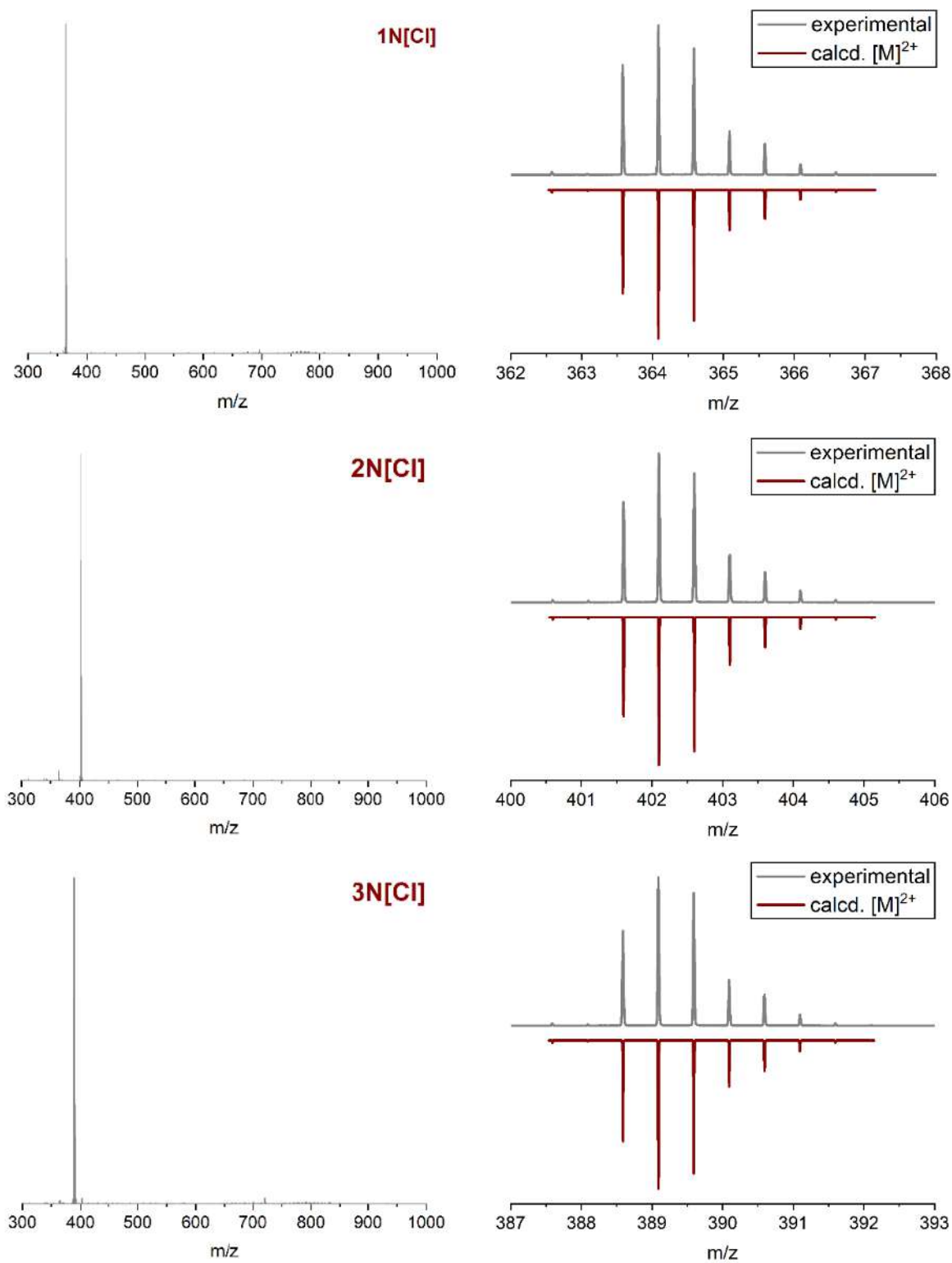


Figure S36. Experimental (gray) ESI<sup>+</sup> MS spectra of **N[Cl]** series and simulated isotopic patterns of the  $[M]^{2+}$ .

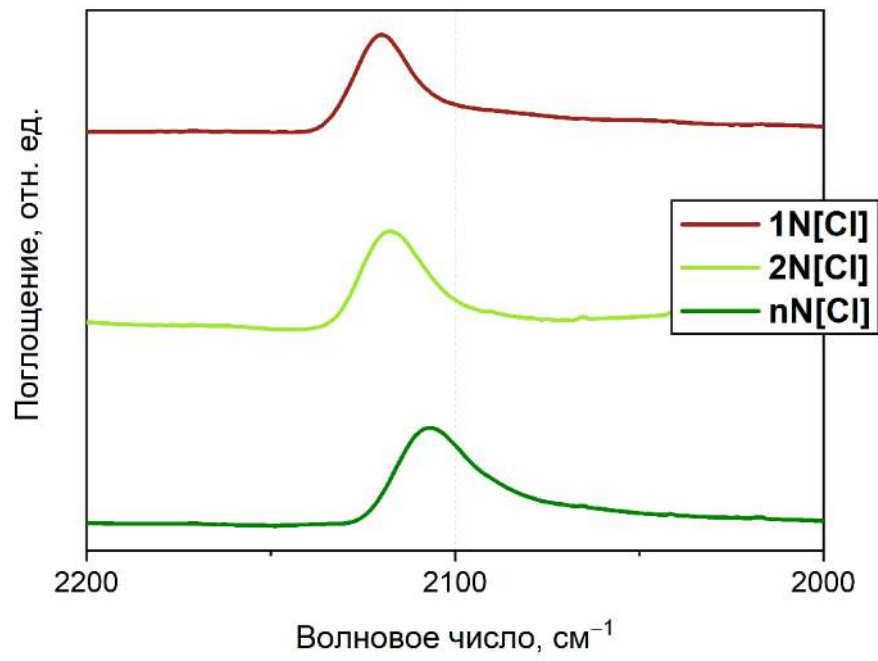


Figure S37. FTIR spectra of  $\text{N[Cl]}$  series in the region of C≡C vibration, KBr.

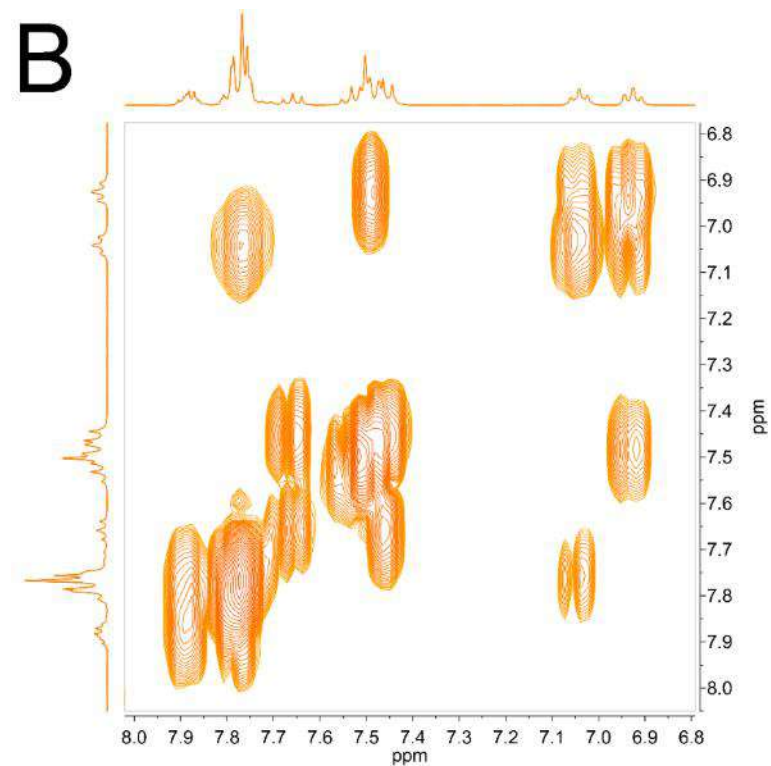
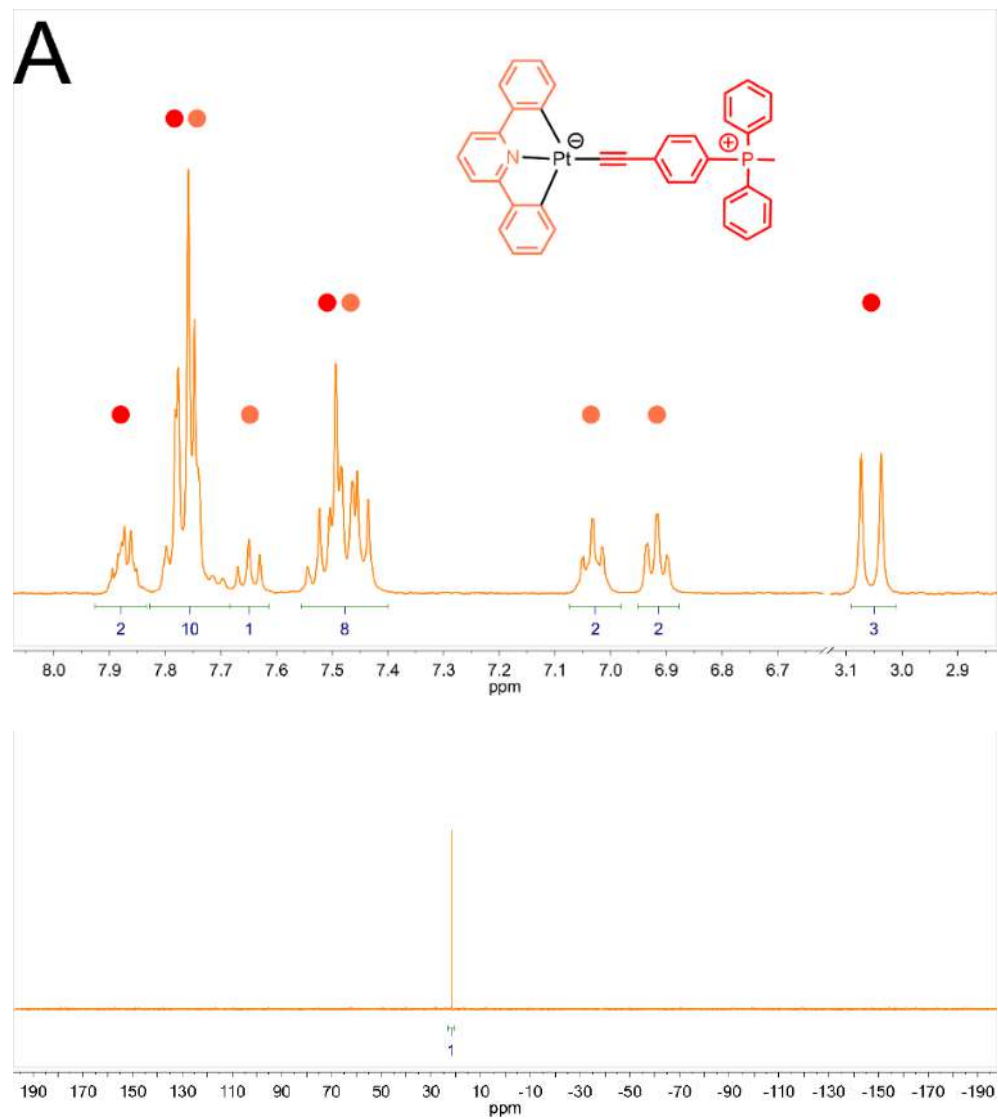


Figure S38. (A)  $^1\text{H}$  (top),  $^{31}\text{P}\{^1\text{H}\}$  (bottom) NMR spectra in aromatic range of **1CNC**; (B)  $^1\text{H}\text{-}^1\text{H}$  COSY spectrum in aromatic range of **1CNC**.

All NMR spectra were measured in  $\text{DMSO-d}_6$ .

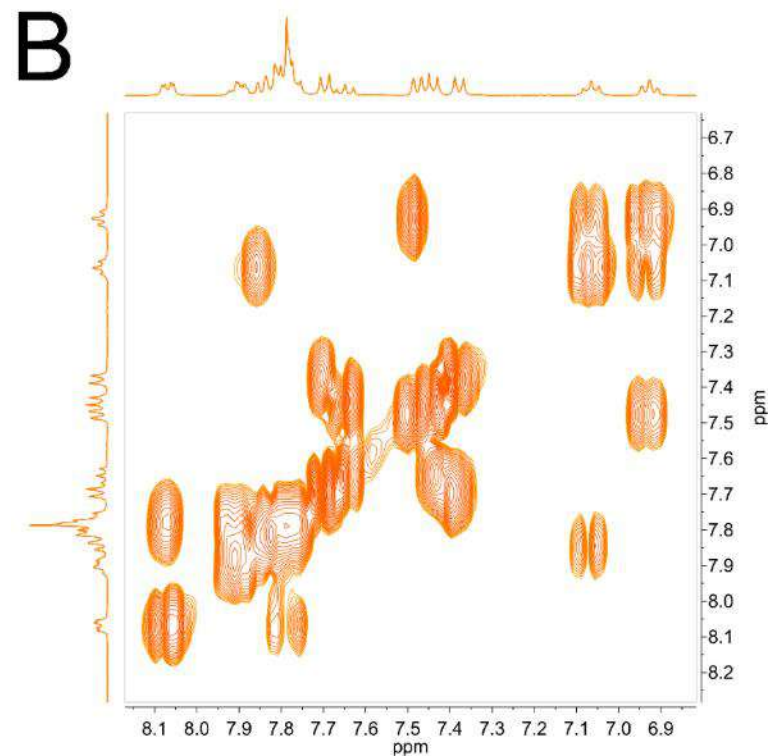
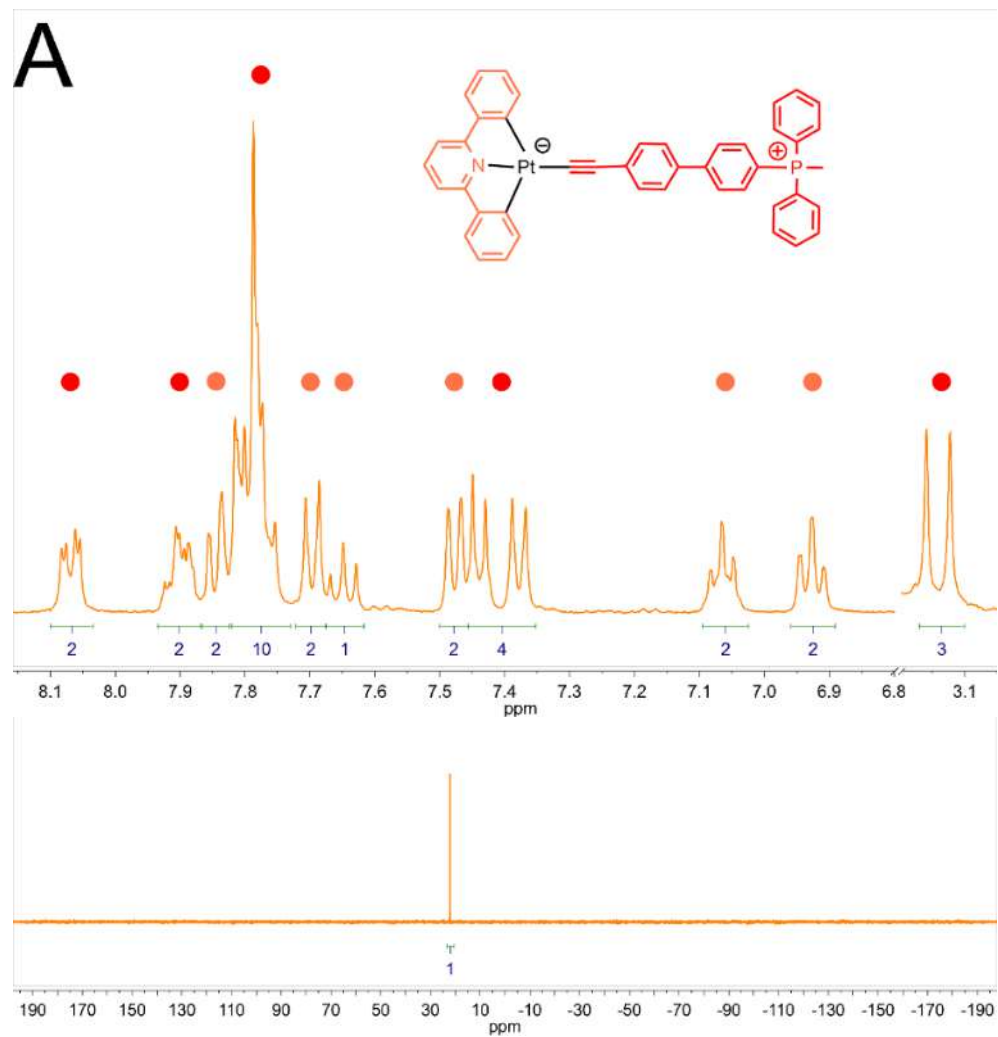


Figure S39. (A)  $^1\text{H}$  (top),  $^{31}\text{P}\{^1\text{H}\}$  (bottom) NMR spectra in aromatic range of **2CNC**; (B)  $^1\text{H}\text{-}^1\text{H}$  COSY spectrum in aromatic range of **2CNC**.

All NMR spectra were measured in  $\text{DMSO-d}_6$ .

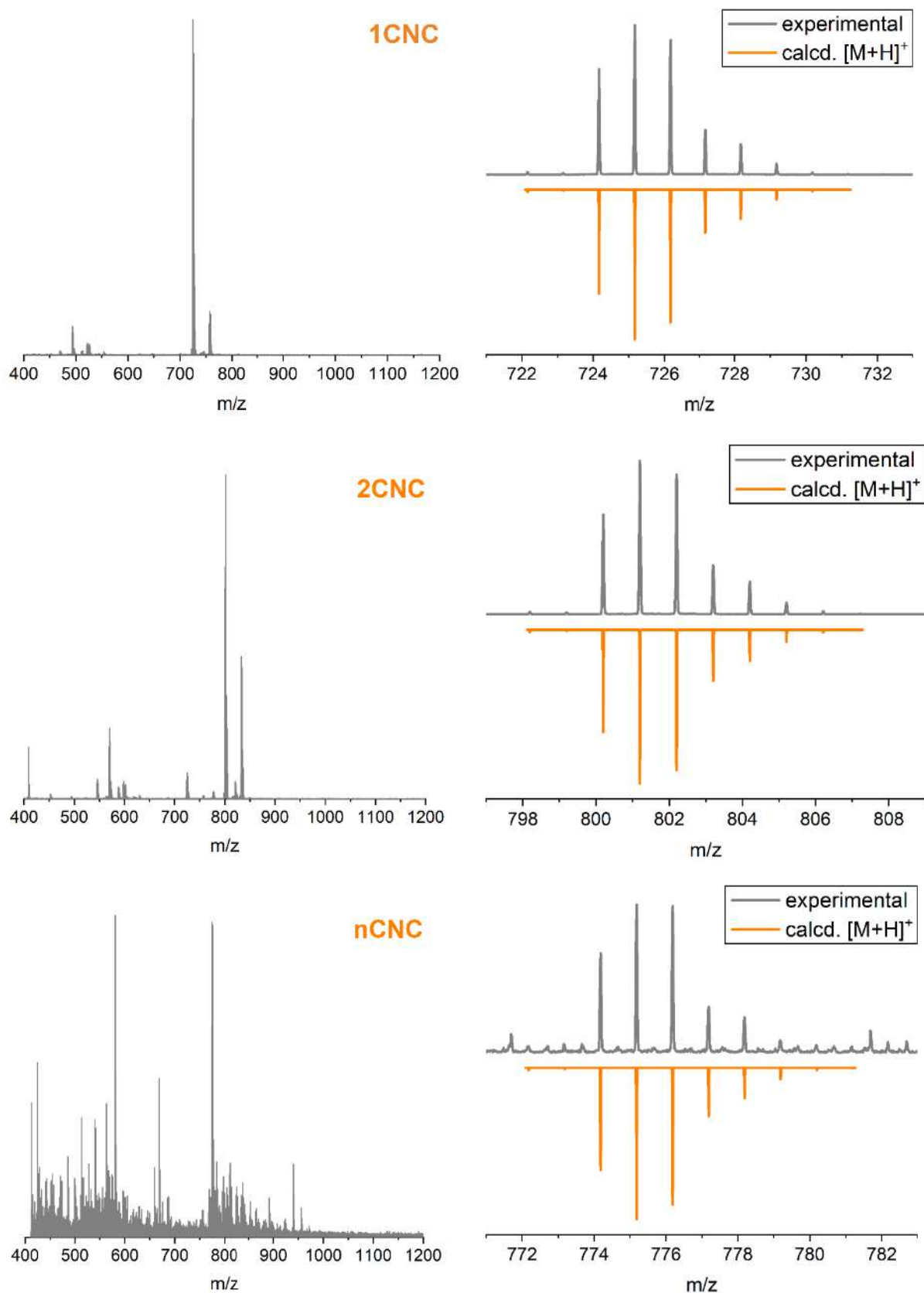


Figure S40. Experimental (gray) ESI<sup>+</sup> MS spectra of CNC series and simulated isotopic patterns of the  $[M]^+$ .

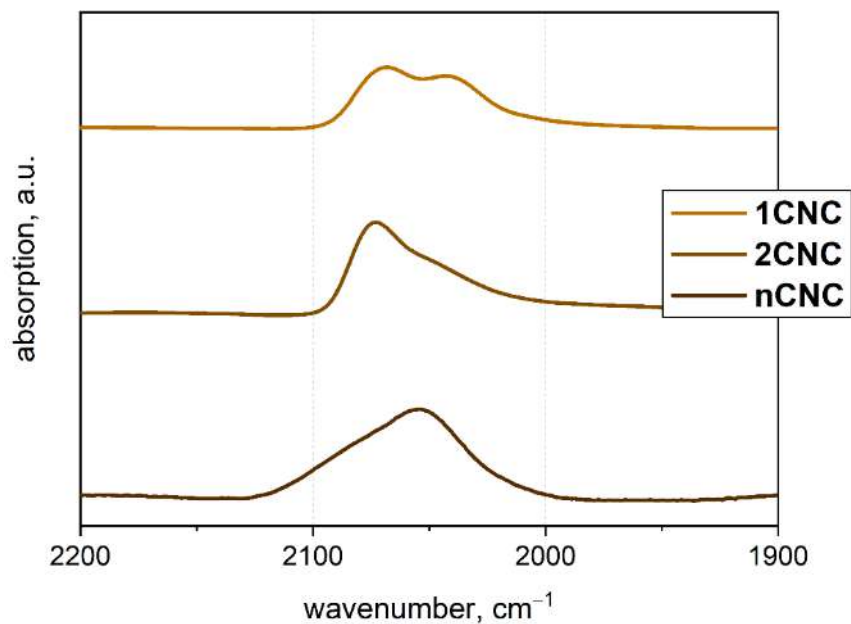


Figure S41. FTIR spectra of CNC series in the region of C≡C vibration, KBr.

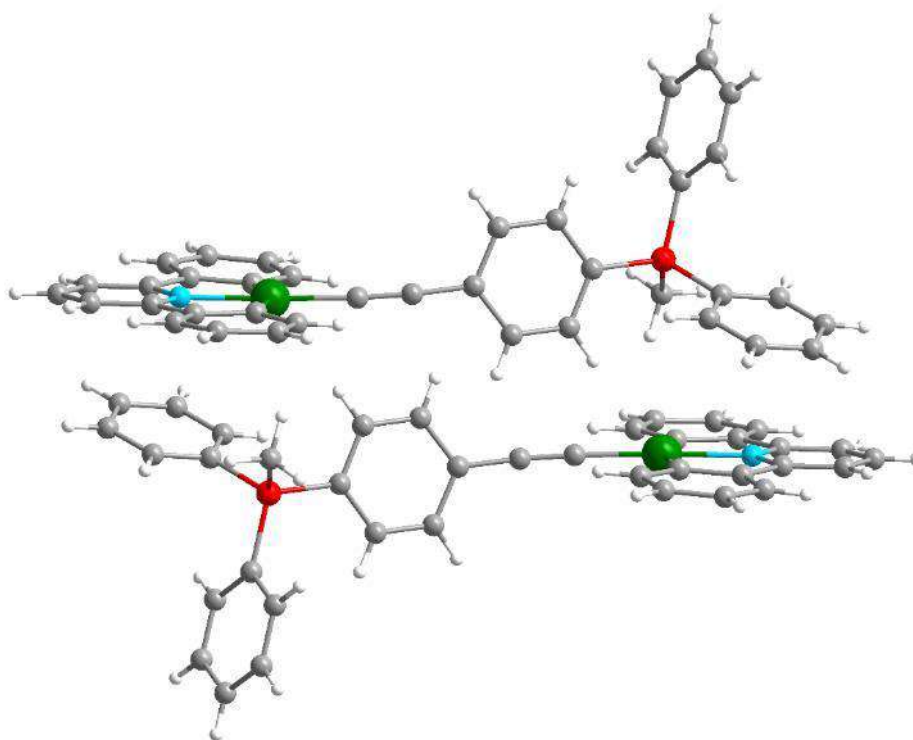


Figure S42. ORTEP view of **1CNC** molecular structure, the thermal ellipsoids are set at a 50% probability level.

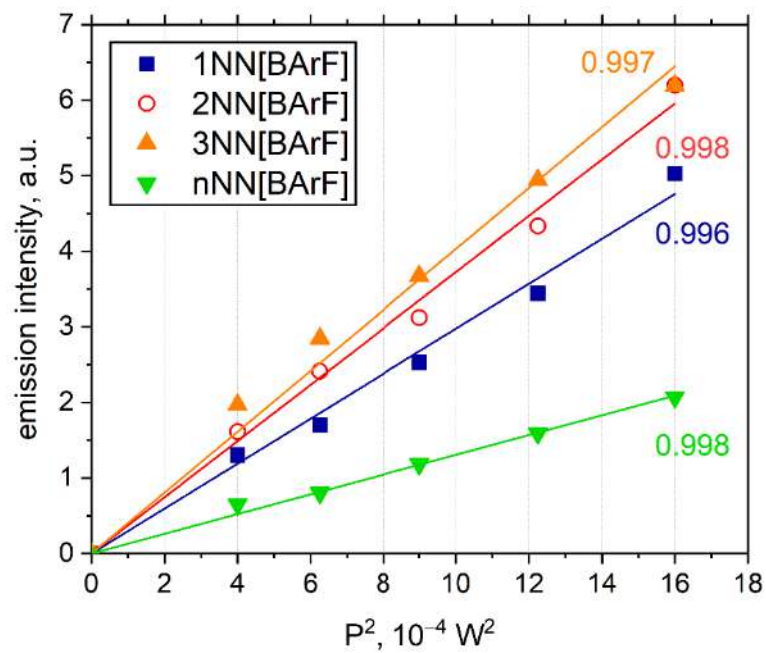


Figure S43. Power dependence of the upconverted luminescence intensity of NN[BArF] series (MeCN, r.t.). R-factors of linear fits are indicated on diagram.

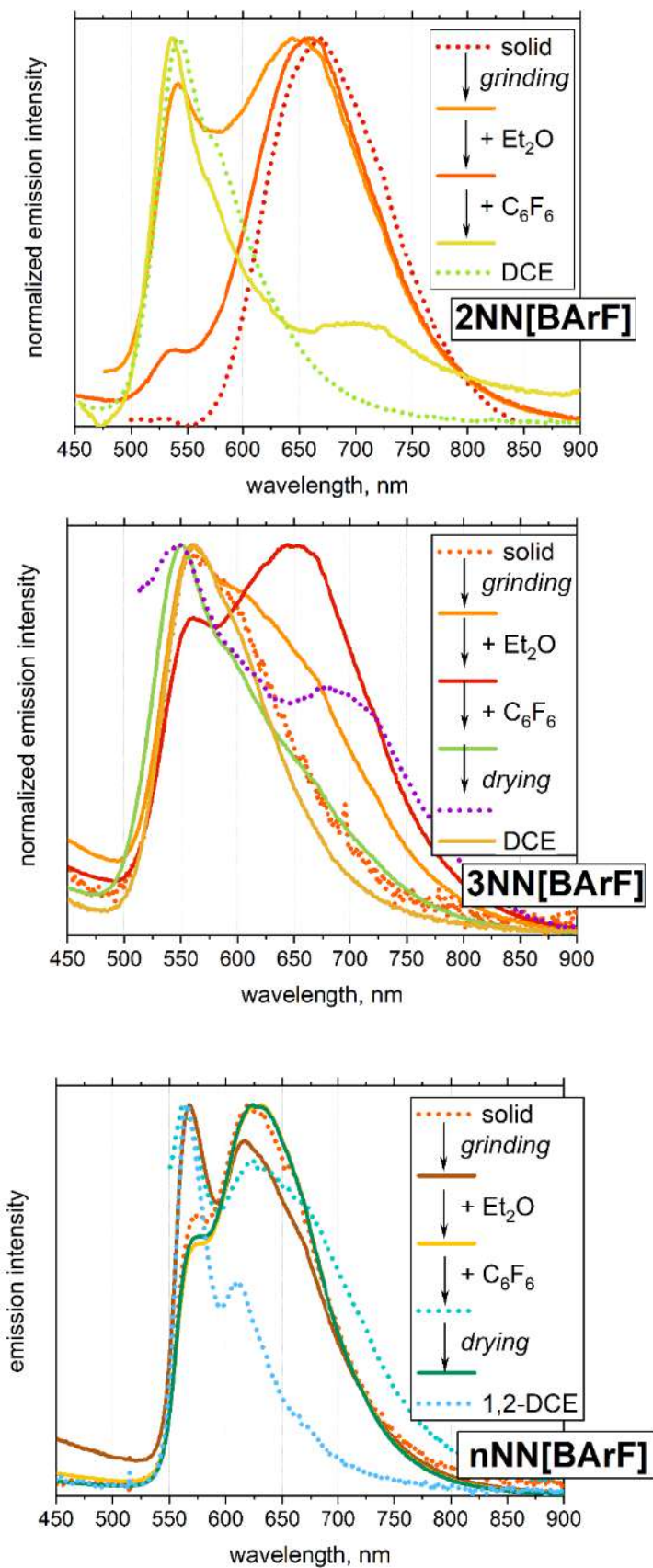


Figure S44. *Stimuli responsive* normalized emission spectra of **2NN[BArF]**–**nNN[BArF]**, r.t.

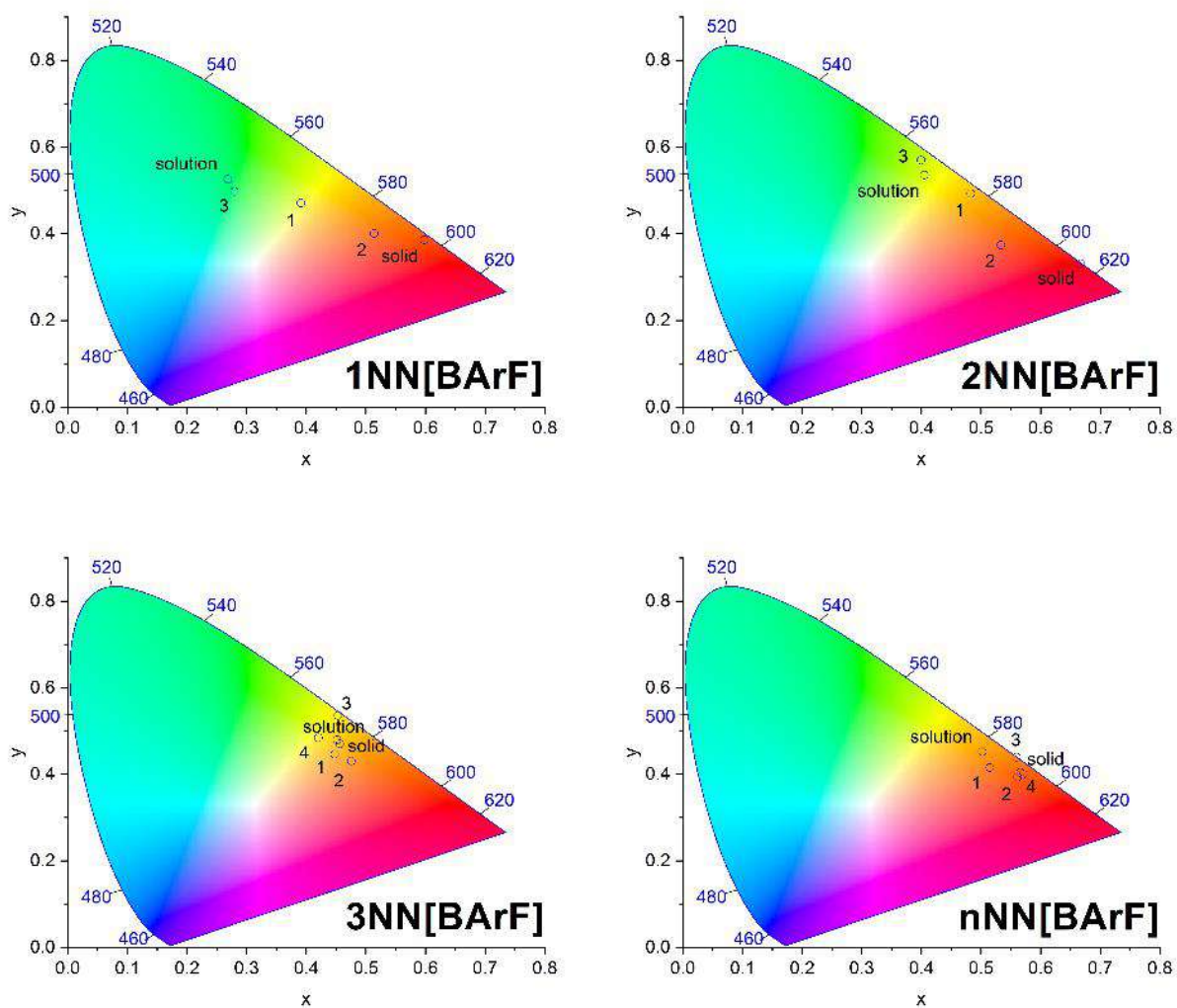


Figure S45. CIE 1931 coordinates for NN[BArF] series under different conditions.

*Legend:* **solution** [1,2-DCE,  $10^{-5}$  M, r.t.], **solid** ["as-obtained" powder, r.t.], **1** [powder after grinding]  $\rightarrow$  **2** [+ Et<sub>2</sub>O]  $\rightarrow$  **3** [+ C<sub>6</sub>F<sub>6</sub>]  $\rightarrow$  **4** [dried powder].

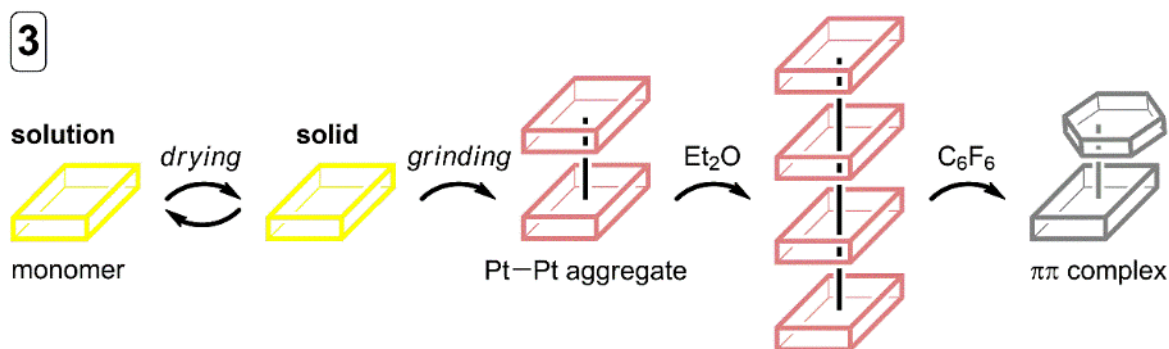


Figure S46. Schematic representation of *stimuli responsive* properties of **3NN[BArF]** under UV light (365 nm).

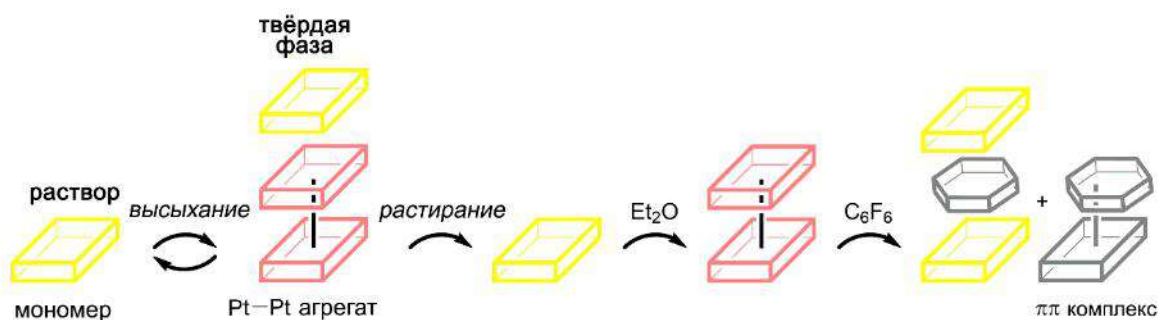


Figure S47. Schematic representation of *stimuli responsive* properties of **nNN[BArF]** under UV light (365 nm).

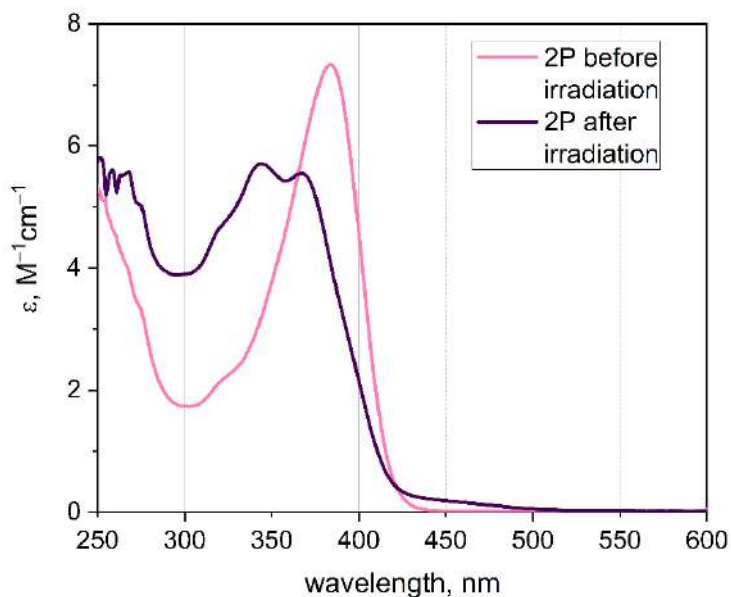


Figure S48. UV-vis absorption spectra of complex **2P[OTf]** before and after UV irradiation (365 nm).

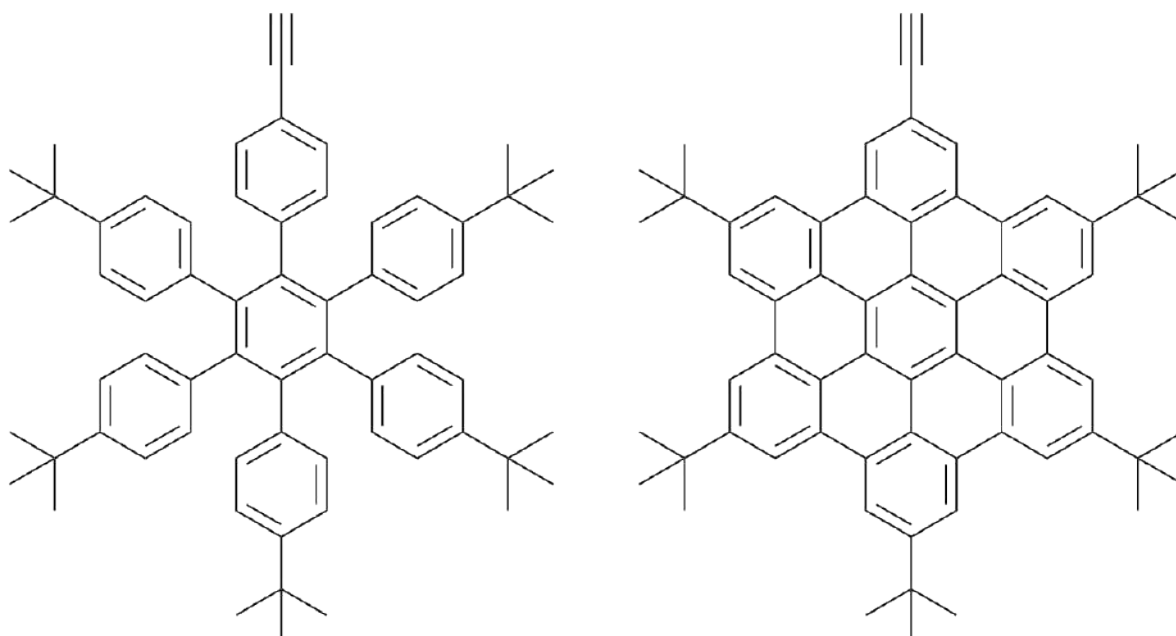


Figure S49. Ligands used in Ref. [43].

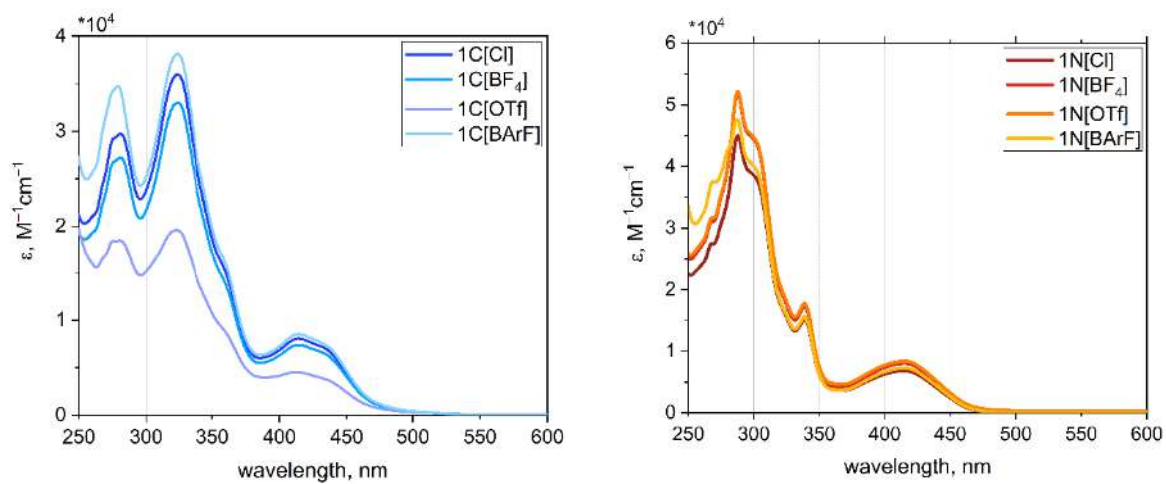


Figure S50. UV-vis spectra of **C[X]** and **N[X]** series.

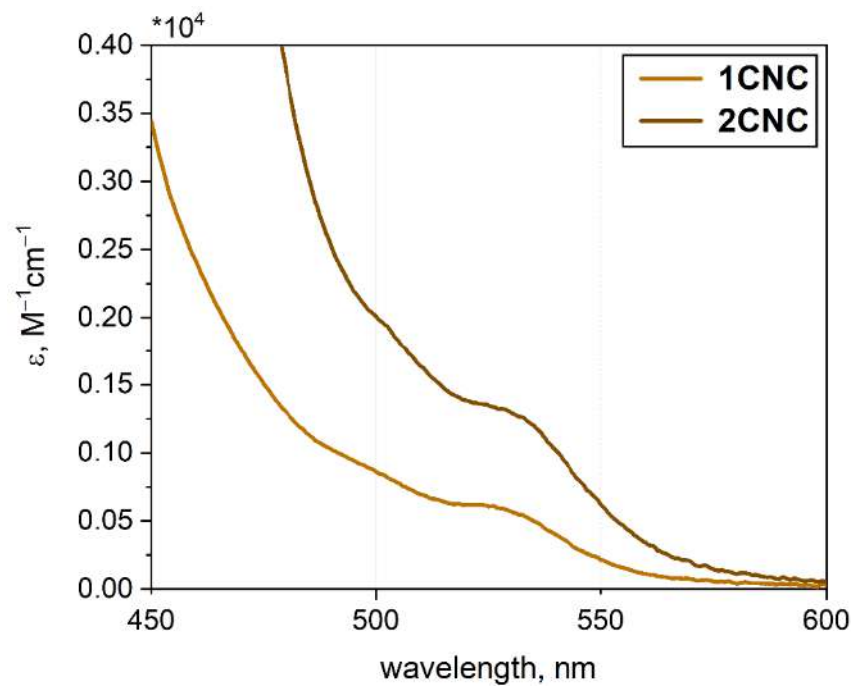


Figure S51. The low-energy part of the **CNC** series UV-vis spectra.

Table S1. Crystallographic data for compounds of NN[Cl] series.

Compound	1NN[Cl]	2NN[Cl]
Formula	C <sub>62</sub> H <sub>62</sub> Cl <sub>5</sub> N <sub>2</sub> P <sub>2</sub> Pt	C <sub>72</sub> H <sub>66</sub> Cl <sub>2</sub> N <sub>2</sub> P <sub>2</sub> Pt
Crystal system	triclinic	orthorhombic
<i>a</i> (Å)	12.22580(10)	26.5050(5)
<i>b</i> (Å)	15.0341(2)	15.4826(3)
<i>c</i> (Å)	19.24880(10)	17.1901(4)
$\alpha$ (°)	89.8380(10)	90
$\beta$ (°)	73.6110(10)	90
$\gamma$ (°)	69.2840(10)	90
<i>V</i> (Å <sup>3</sup> )	3156.20(6)	7054.2(3)
Molecular weight	1269.41	1287.19
Space group (number)	$P\bar{1}$ (2)	Pbcn (60)
$\mu$ (mm <sup>-1</sup> )	6.864	5.132
Temperature (K)	100.00(10)	99.9(3)
<i>Z</i>	2	4
$\rho_{\text{calc}}$ (g/cm <sup>-3</sup> )	1.336	1.212
Crystal size (mm <sup>3</sup> )	0.06×0.12×0.12	0.1×0.13×0.17
Diffractometer	SuperNova, Single source at offset/far, HyPix3000	SuperNova, Single source at offset/far, HyPix3000
Radiation	Cu <i>K</i> <sub>α</sub>	Cu <i>K</i> <sub>α</sub>
Total reflections	68717	25297
Unique reflections	11527	6504
Angle range 2 $\theta$ (°)	8.09 to 138.15 (0.83 Å)	6.61 to 138.80 (0.82 Å)
Reflections with $ F_o  \geq 4\sigma_F$	10954	4730
<i>R</i> <sub>int</sub>	0.0317	0.0324
<i>R</i> <sub>σ</sub>	0.0182	0.0261
<i>R</i> <sub>1</sub> ( $ F_o  \geq 4\sigma_F$ )	0.0409	0.0480
<i>wR</i> <sub>2</sub> ( $ F_o  \geq 4\sigma_F$ )	0.1116	0.1333
<i>R</i> <sub>1</sub> (all data)	0.0426	0.0621
<i>wR</i> <sub>2</sub> (all data)	0.1131	0.1527
Goodness-of-fit on <i>F</i> <sup>2</sup>	1.049	1.024
$\rho_{\text{max}}, \rho_{\text{min}}$ (e/Å <sup>3</sup> )	2.41/−1.27	1.30/−0.61
CCDC number	2269523	2269524
$R_1 = \Sigma  F_o  -  F_c  /\Sigma F_o $ ; $wR_2 = \{\Sigma[w(F_o^2 - F_c^2)^2]/\Sigma[w(F_o^2)^2]\}^{1/2}$ ; $w = 1/[\sigma^2(F_o^2) + (aP)^2 + bP]$ , where $P = (F_o^2 + 2F_c^2)/3$ ; $s = \{\Sigma[w(F_o^2 - F_c^2)]/(n - p)\}^{1/2}$ where <i>n</i> is the number of reflections and <i>p</i> is the number of refinement parameters.		

Table S2. Selected structural parameters of NN[Cl] series.

Bond lengths, Å			Literature range, Å
	1NN[Cl]	2NN[Cl]	
Pt1–N1	2.054(3)	2.064(4)	1.959–2.077
Pt1–N2	2.062(3)	2.064(4)	
Pt1–C19	1.951(4)	1.966(6)	1.932–1.994
Pt1–C40	1.968(4)	1.966(6)	
C19–C20	1.211(6)	1.189(7)	1.072–1.247
C40–C41	1.205(6)	1.189(7)	
Bond angles, °			Literature range, °
N1–Pt1–N2	78.88(13)	78.6(3)	76.81–79.27
C19–Pt1–C40	87.91(15)	87.4(3)	85.75–91.88

Table S3. Selected structural parameters of P[OTf].

Bond lengths, Å			Literature range, Å
	1P[OTf]	nP[OTf]	
Pt1–C1	2.020(3)	2.024(4)	1.981–2.053
Pt1–P2	2.3143(7)	2.3053(9)	2.286–2.325
C1–C2	1.195(5)	1.186(6)	1.188–1.223
Bond angles, °			Literature range, Å
C1–Pt1–C1'	180.0	180.0	179.68–180.0
P2–Pt1–P2'	180.0	180.0	179.68–180.0
C1–Pt1–P2	92.85(8)	92.16(11)	92.54–94.10
C1–Pt1–P2'	87.15(8)	87.84(11)	85.90–87.46

Table S4. Crystallographic data for compounds of **P[OTf]** and **CNC**.

Compound	<b>1P[OTf]</b>	<b>nP[OTf]</b>	<b>1CNC</b>
Formula	C <sub>86</sub> H <sub>76</sub> F <sub>6</sub> O <sub>8</sub> P <sub>4</sub> PtS <sub>2</sub>	C <sub>88</sub> H <sub>68</sub> F <sub>6</sub> O <sub>6</sub> P <sub>4</sub> PtS <sub>2</sub>	C <sub>79</sub> H <sub>62</sub> N <sub>2</sub> OP <sub>2</sub> Pt <sub>2</sub>
Crystal system	triclinic	triclinic	monoclinic
<i>a</i> (Å)	9.27050(10)	9.5089(2)	24.9558(8)
<i>b</i> (Å)	14.1404(2)	11.4039(2)	12.2843(3)
<i>c</i> (Å)	14.58660(10)	19.8310(3)	21.9034(7)
$\alpha$ (°)	85.9460(10)	77.297(2)	90
$\beta$ (°)	79.6510(10)	78.273(2)	115.373(4)
$\gamma$ (°)	88.9410(10)	66.447(2)	90
<i>V</i> (Å <sup>3</sup> )	1876.29(4)	1906.97(7)	6067.1(4)
Molecular weight	1734.55	1718.51	1507.42
Space group (number)	<i>P</i> $\bar{1}$ (2)	<i>P</i> $\bar{1}$ (2)	<i>I</i> 2/ <i>c</i> (15)
$\mu$ (mm <sup>-1</sup> )	5.440	5.329	9.385
Temperature (K)	99.99(10)	100.00(10)	100.00(10)
<i>Z</i>	1	1	4
$\rho_{\text{calc}}$ (g/cm <sup>-3</sup> )	1.535	1.496	1.650
Crystal size (mm <sup>3</sup> )	0.08×0.1×0.23	0.05×0.07×0.09	0.08×0.14×0.18
Diffractometer	SuperNova, Single source at offset/far, HyPix3000	SuperNova, Single source at offset/far, HyPix3000	SuperNova, Single source at offset/far, HyPix3000
Radiation	Cu <i>K</i> $\alpha$	Cu <i>K</i> $\alpha$	Cu <i>K</i> $\alpha$
Total reflections	36952	18463	5420
Unique reflections	6965	7051	5420
Angle range 2 $\theta$ (°)	6.17 to 138.46 (0.82 Å)	4.61 to 138.33 (0.82 Å)	7.84 to 138.18 (0.83 Å)
Reflections with $ F_o  \geq 4\sigma_F$	6772	6883	5196
<i>R</i> <sub>int</sub>	0.0859	0.0430	0.0395
<i>R</i> <sub><math>\sigma</math></sub>	0.0507	0.0492	0.0348
<i>R</i> <sub>1</sub> ( $ F_o  \geq 4\sigma_F$ )	0.0382	0.0415	0.0482
<i>wR</i> <sub>2</sub> ( $ F_o  \geq 4\sigma_F$ )	0.0914	0.1052	0.1425
<i>R</i> <sub>1</sub> (all data)	0.0397	0.0425	0.0494
<i>wR</i> <sub>2</sub> (all data)	0.0924	0.1063	0.1441
Goodness-of-fit on <i>F</i> <sup>2</sup>	1.037	1.064	1.074
$\rho_{\text{max}}, \rho_{\text{min}}$ (e/Å <sup>3</sup> )	2.35/-1.88	1.43/-1.58	3.83/-1.41
CCDC number	2360483	2360484	2383597
$R_1 = \Sigma  F_o  -  F_c  /\Sigma F_o $ ; $wR_2 = \{\Sigma[w(F_o^2 - F_c^2)^2]/\Sigma[w(F_o^2)^2]\}^{1/2}$ ; $w = 1/[\sigma^2(F_o^2) + (aP)^2 + bP]$ , where $P = (F_o^2 + 2F_c^2)/3$ ; $s = \{\Sigma[w(F_o^2 - F_c^2)]/(n - p)\}^{1/2}$ where <i>n</i> is the number of reflections and <i>p</i> is the number of refinement parameters.			

Table S5. Selected structural parameters of **1CNC**.

Bond lengths, Å		Bond angles, °	
Pt1–N1	2.016(6)	C1–Pt1–C17	160.5(3)
Pt1–C1	2.064(7)	N1–Pt1–C1	80.4(3)
Pt1–C17	2.063(7)	N1–Pt1–C17	80.1(3)
Pt1–C18	1.944(7)	C1–Pt1–C18	99.1(3)
C18–C19	1.228(10)	C17–Pt1–C18	100.3(3)

Table S6. Optical and photophysical properties of **NN[BArF]** complexes in MeCN solution, r.t.

Complex	$\lambda_{\text{abs}}$ , nm	$\lambda_{\text{em}}$ ,* nm	$\tau$ ,** ns		$\Phi$ ,* %
			aer.	deaer.	aer.
<b>1NN[BArF]</b>	307, 318, 372	510	20.1	20.8	<1
<b>2NN[BArF]</b>	266, 321, 339, 390	537	203.4	2533.7	<1
<b>3NN[BArF]</b>	273, 323, 336, 390	558	182.7	5026.9	<1
<b>nNN[BArF]</b>	320, 350, 386	563	377.8	21189.3	<1

\*  $\lambda_{\text{ex}}$  365 nm. \*\*  $\lambda_{\text{ex}}$  351 nm

Table S7. Photophysical properties of NN[BArF] complexes after mechanical grinding and after fuming with Et<sub>2</sub>O

Complex	$\lambda_{em}$ after grinding,* nm	$\lambda_{em}$ after fuming with Et <sub>2</sub> O,* nm	$\tau$ after grinding,** ns	$\tau$ after fuming with Et <sub>2</sub> O,** ns	QY after grinding,* %
1NN[BArF]	503, 634	500, 638	598 [503 nm] 904 [634 nm]	250 [500 nm] 713 [638 nm]	20.8
2NN[BArF]	541, 649	537***, 659	1010 [541 nm] 808 [649 nm]	529 [659 nm]	7.4
3NN[BArF]	560, ~648	562, 648	1026 [560 nm] 863 [648 nm]	850 [562 nm] 796 [648 nm]	3.5
4NN[BArF]	568, 617	574, 628	4247 [568 nm] 2601 [617 nm]	3110 [574 nm] 2222 [628 nm]	2.4

\*  $\lambda_{ex}$  365 nm. \*\*  $\lambda_{ex}$  351 nm. \*\*\* very low intensity